GENETIC DISRUPTION OF VIP SIGNALING ALTERS INTESTINAL MICROBIAL

STRUCTURE AND IMMUNITY

A Dissertation
Submitted to the Graduate Faculty
of the
North Dakota State University
of Agriculture and Applied Science

By

Manpreet Singh Bains

In Partial Fulfillment of the Requirements
for the Degree of
DOCTOR OF PHILOSOPHY

Major Program:
Molecular Pathogenesis

May 2018

Fargo, North Dakota

North Dakota State University
Graduate School

Title

Genetic disruption of VIP signaling alters intestinal microbial structure and
immunity

By

Manpreet Singh Bains

The Supervisory Committee certifies that this ***disquisition*** complies with North Dakota

State University's regulations and meets the accepted standards for the degree of

DOCTOR OF PHILOSOPHY

SUPERVISORY COMMITTEE:

Glenn Dorsam, PhD

Chair

John McEvoy, PhD

Eugene Berry, PhD

Lawrence Reynolds, PhD

Approved:

06/27/2018	John McEvoy, PhD
Date	Department Chair

ABSTRACT

Vasoactive intestinal peptide (VIP) regulates clock gene expression in the brain that synchronizes diurnal feeding behaviors in mammals. In the gastrointestinal (GI) tissues, VIP influences host nutrient absorption from ingested food, and regulates host metabolic functions. VIP signaling ensures efficient nutrient absorption by influencing ghrelin and leptin expression to balance caloric intake. Importantly, obese humans have elevated plasma VIP levels, supporting its association with fat mass accumulation. In contrast, VIP deficiency leads to weight loss and reduced adiposity, while disrupting epithelial cell nutrient absorption, tight junctions and mucus secretion. Moreover, VIP regulates host glucose metabolism as VIP knockout mice are pre-diabetic with elevated blood glucose and insulin levels. In addition to metabolism, VIP is anti-inflammatory and when knocked out, results in exacerbated inflammatory bowel disease (IBD) pathology. The GI track is also home to ≈40 trillion bacteria, called the gut microbiota, which unlock additional calories from fiber for the host. Microbiota dysbiosis is caused by dysfunction in biological systems downstream from VIP signaling, including dysregulated expression of host clock genes, metabolic hormones, immune-relevant mediators and metabolic and inflammatory disease states, like obesity and IBD. It is not known, however, whether the VIP signaling axis contributes to the maintenance of the gut microbiota structure and diversity. We hypothesized that VIP deficiency will cause gut dysbiosis, lower bacterial diversity and reduce its energy extraction potential. To this end, we isolated fecal samples from VIP knockout mice (VIP-/-) and employed 16S rRNA sequencing. VIP deficiency (VIP-/- and VIP-/+) resulted in marked gut microbial compositional changes and reduced bacterial diversity compared to male and female VIP+/+ littermates (n=48). Increased abundance of Bacteroides, Parabacteroides and Helicobacter genera (gram-negative, GN), with reductions of Lachnospiraceae NK4A136,

Oscillibacter and Ruminiclostridium genera (gram-positive, GP), were the driving force for the observed increase in the GN/GP ratio. A predicted algorithm program, called PICRUSt, showed changes in microbial metabolism consistent with elevated lipopolysaccharide metabolism and reduced intake of fiber in VIP-/- mice. These data support that VIP regulates intestinal homeostasis by maintaining microbiota balance, diversity and energy harvesting potential, while upholding an anti-inflammatory tone by limiting lipopolysaccharide biosynthesis.

DEDICATION

None of my accomplishments were possible without the support of my family and friends to whom I dedicate this dissertation. My father, Piara, has helped me overcome tremendous adversity; From the passing of my mother, Ravinder, when I was 8 years old, to his long weekend shifts at Wal-Mart, all in the hopes of one day seeing me succeed. His unwavering support and love have not only supported me throughout my life but made me the man I am today. Even though I'm 29 years old, there is still a lot I can learn from him regarding hard work, endurance and appreciating all that life has to offer. My step-mother, Veena, has always been there to listen, love and provide a seemingly never-ending supply of food which I greatly appreciate. Without the support of my aunt, Joyti, and uncle, Jay, who took us in during our darkest hour, despite my rough edges, there is no way I would be anywhere close to where I am today. My wife, Cassandra, is my closest friend and confidant. She has been a constant source of encouragement, love, and has supported me in my every endeavor. For most of my life I have felt like a lost traveler, but with her love and affection along with the support of my father-in-law, Lonnie, my mother-in-law, Nancy, and sister-in-law, Carissa, Fargo has become my home. I want to thank them for making me part of their family.

I am very thankful for all the love, support and guidance from all my family and friends.

"It would be possible to describe everything scientifically, but it would make no sense; it would be without meaning, as if you described a Beethoven symphony as a variation of wave pressure."

- Albert Einstein

TABLE OF CONTENTS

LIST OF TABLES

LIST OF FIGURES

LIST OF ABBREVIATIONS

AA .... Amino Acid

Ab .... Antibody

ADCY .... Adenylyl cyclase type

ADHD .... Attention deficit hyperactivity disorder

ANOVA .... Analysis of variance

APC .... Antigen presenting cell

ATCC .... American Type Cell Culture

ATP .... Adenosine triphosphate

BAL .... Bronchoalveolar lavage

BDNF .... Brain-derived neurotropic factor

BM .... Bone marrow

BSA .... Bovine serum albumin

Ca^{2+} .... Calcium ion

cAMP .... Cyclic adenosine monophosphate

CD .... Cluster of differentiation

chFBS .... Characterized fetal bovine serum

CNG .... Cyclic nucleotide-gated ion channels

CNS .... Central nervous system

COX .... Cyclooxygenase

DEP .... Dielectrophoretic label

DMEM .... Dulbecco's Modified Eagle Medium

DMSO .... Dimethyl sulfoxide

DNA .... Deoxyribose nucleic acid

EAE .... Experimental autoimmune encephalomyelitis

PKC..Protein Kinase C

PRP ....PACAP-related peptide

PRRs ....Pattern recognition receptors

PSA ....Polysaccharide A

qPCR...Quantitative polymerase chain reaction

qRT-PCR...Quantitative reverse transcriptase polymerase chain reaction

RA ....Rheumatoid Arthritis

RNA ....Ribonucleic acid

ROS ....Reactive oxygen species

RPMI ....Roswell Park Memorial Institute Medium

rRNA ....Ribosomal ribonucleic acid

RT-PCR..Reverse transcriptase polymerase chain reaction

SCFA...Short chain fatty acid

SEM ....Standard error of mean

Siglec-F...Sialic acid-binding immunoglobulin-like lectin F

siRNA ....Small interfering RNA

SL..Stem loop

snoRNA...Small nucleolar RNA

T cell ....T lymphocyte cell

T-MyD88KO..T-cell specific MyD88 knockout

Th ....T helper l

TMD ....Transmembrane domain

TNF...Tumor necrosis factor

VIP ....Vasoactive intestinal peptide

LIST OF APPENDIX TABLES

LIST OF APPENDIX FIGURES

1. INTRODUCTION

This first paragraph summarizes the structure and assists in visualizing the makeup of each of the five chapters of my dissertation. The first chapter consists of a literature review, while chapters 2, 3, and 4 concentrate on performed research with the 5th holding the references. Chapter 1 delves into the history of vasoactive intestinal peptide (VIP) and its receptors, discusses G-protein coupled receptor signaling and describes the roles of VIP in bodily systems and disease. The second chapter contains a literature review of recent microbiome research and discusses our 16S rRNA sequencing findings regarding changes in the intestinal microbiota due to the genetic silencing of the VIP ligand in both sexes of mice. The third chapter reviews the role of VIP in the immune system. It discusses my cAMP quantification contributions towards a laboratory publication, research into different receptor profiles of human T-cell lines, and how VIP signals through each receptor on T-cells, as well as eosinophilic differentiation of VPAC2 knockout mice whom exhibit a delayed eosinophilic response during allergic asthma versus wild type. A side-collaboration with Dr. Nawarathna's laboratory in the Department of Electrical and Computer engineering is discussed in chapter 4. My contributions to this project included qRT-PCR expertise which were used to determine the efficacy of the new *iLluminate-miRNA* microRNA detection technique. The last chapter (5) contains references for all of the previous chapters. I hope you enjoy reading this dissertation as much as I enjoyed writing it and learn something new and interesting along the way.

1.1. General introduction and background

1.1.1. Vasoactive intestinal peptide

Vasoactive intestinal peptide (VIP) is a 3.3 kilodalton (kDa) protein consisting of 28-amino acids (AA), and is expressed heterogeneously in mammalian tissues. VIP was first

discovered in porcine intestines by Sami Said and Viktor Mutt in 1970 who hypnotized there

were vasoactive proteins located in the gut (Said and Mutt 1970). Two years later, the same two

scientists confirmed VIP's vasodilatory role using canine femoral arteries (Said and Mutt 1972).

The peptide's discovery in the intestines, and its vasoactive activity resulting in increased artery

diameters, contributed to its designation as vasoactive intestinal peptide or VIP for short.

Located on position 25.2 of the longer arm of the 6th human chromosome (Kitts et al. 2016), VIP

is a member of a family of evolutionarily related proteins called the Secretin family (Ulrich,

Holtmann, and Miller 1998). This peptide family is composed of 15 known peptide hormones

whose ligands share amino acid similarity, and their endogenous receptors possess structural

likeness (Millar, Newton, and Roseweir 2012). Some of these peptides include: glucagon, gastric

inhibitory polypeptide (GIP), secretin, pituitary adenylate cyclase activating polypeptide

(PACAP) (see table 1) (Segre and Goldring 1993). When aligned at the amino acid level, as

displayed in Table 1, the members of this family share AA sequence similarities, with the

primary AA sequences of VIP and PACAP sharing the most at 68% similarity (Ng et al. 2012).

This AA similarity permits cross-reactivity, called receptor shuffling (Hamann, Hartmann, and

van Lier 1996), allowing VIP and PACAP ligands to bind common receptors (Shivers et al.

1991).

Table 1.   Amino acid (AA) sequence comparison between VIP and the other Secretin family members.

Family member (% similarity)	Amino acid residues								
VIP (100%)	**HSDAV**	**FTDNY**	**TRLRK**	**QMAVK**	**KYLNS**	**ILN**			
PACAP (68%)	**HSD**GI	**FTD**S**Y**	S**R**Y**RK**	**QMAVK**	**KY**AAV	V**L**			
PHI-27 (39%)	**H**A**DG**V	**FT**SDF	S**RL**LG	**Q**LSA**K**	KY**L**E**S**	LI			
Secretin (32%)	**HSD**GT	**FT**SEL	S**RLR**E	GARLQ	RL**L**QG	LV			
GHRH (29%)	YA**DA**I	**FT**NS**Y**	RKVLG	**Q**LSAR	**K**LL**Q**I	DIMSE	QQGES	NQERG	ARARL
Glucagon (18%)	**HS**QGT	**FT**SD**Y**	SKYLD	SRRAQ	DFVQW	LMNT			
GIP (10%)	YAEGT	**F**ISD**Y**	SIAMD	KIHQQ	DFVNW	L**L**AQK	GKKND	WKHNI	TQ
Transthyretin (7%)	GPTGT GESKC PLMV**K** VLDAV RGSPA **I**NVAV HVFRK AADDT WEPFA SGKTS ESGEL HGLTT EEEFV EGIYK VEIDT KSYWK ALGIS PFHEH AEVVF TANDS GPRRY TIAAL LSPYS YSTTA VVTNP KE								

1.1.1.1. VIP amino acid sequence

Table 1 utilizes single letter abbreviations for amino acids. The three letter primary amino acid sequence for human VIP is His-Ser-Asp-Ala-Val-Phe-Thr-Asp-Asn-Tyr-Thr-Arg-Leu-Arg-Lys-Gln-Met-Ala-Val-Lys-Lys-Tyr-Leu-Asn-Ser-Ile-Leu-Asn (Mutt and Said 1974). Determined by Edman degradation, this amino acid sequence is completely conserved in other mammals studied, such as cows, mice, rats, horses and dogs. So far, the guinea pig is the only mammal studied whose VIP AA sequence is not 100% identical to humans. Their VIP sequence is 86% homologous at the amino acid level due to four amino acid substitutions (Du et al. 1985). Table 2 compares VIP sequences between a variety of different species. What is made clear by analysis of these AA sequences is that VIP has been evolutionarily conserved for over hundreds of millions of years. Evidence for this was provided by Kumar and Hedges, who analyzed differences between 658 nuclear genes to determine that Cod (*Gadus morhua*), from class

3

Actinopterygii, and humans (*Homo sapiens*) from class Mammalia, are evolutionarily separated by over 450 million years (Kumar and Hedges 1998). Maintenance of AA sequence identity of VIP between Cod and Human (83%, see table 2) (Smalley, Barrow, and Foster 2009), suggests an essential role for the VIP peptide and may explain its stringent evolutionary sequence conservation over this geological time-frame of nearly half a billion years.
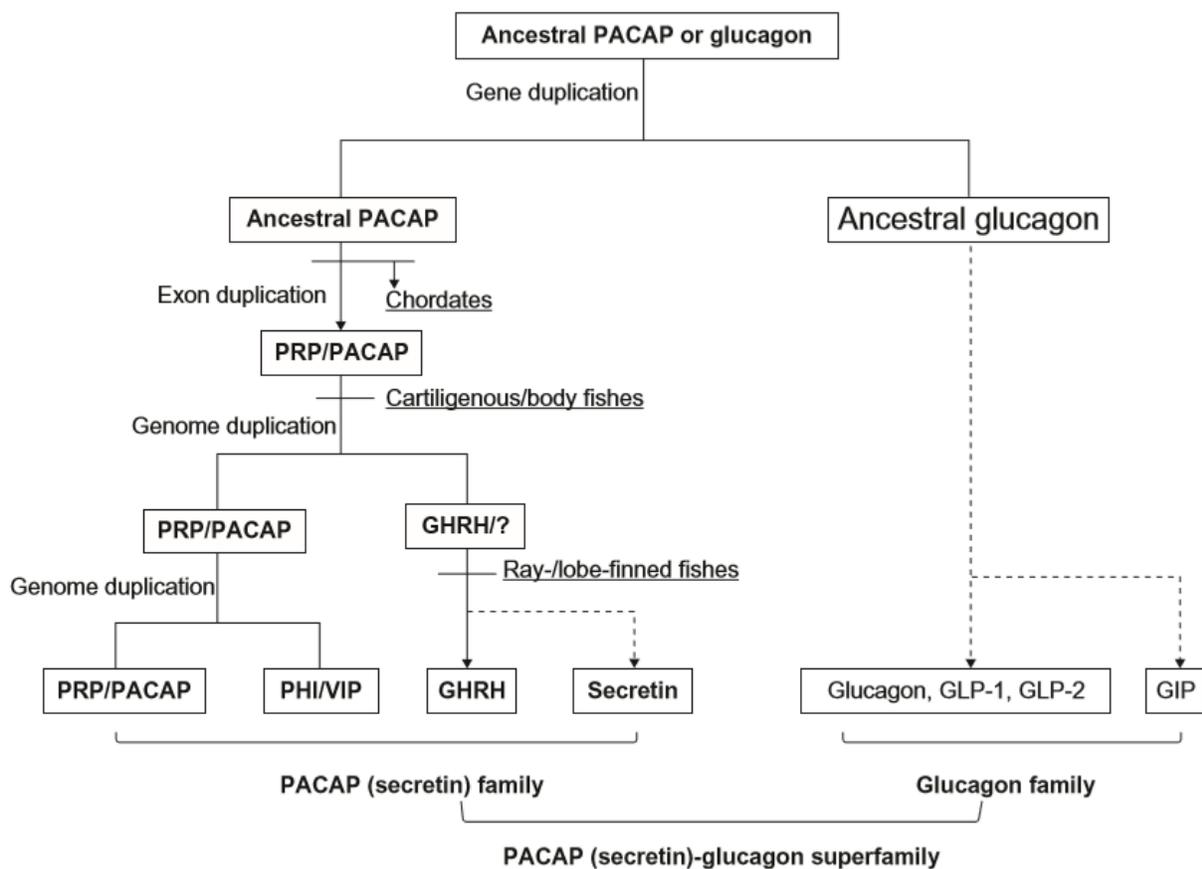
Figure 1.   The evolutionary history of the secretin-glucagon superfamily.
Hundreds of millions of years of evolution have resulted in the formation of different ligands from one ancestral gene (PACAP/glucagon). It is currently theorized that numerous duplications of the gene have resulted in our current repertoire of ligands. (Figure from Handbook of Hormones, 2016, and Yoshio Takei (Takei 2016)).

Table 2.   VIP AA sequence homology among different species

Species	% sequence homology to human VIP	VIP amino acid residues					
Human pig mouse cow rat horse dog cat (Du et al. 1985)	100%	HSDAV	FTDNY	TRLRK	QMAVK	KYLNS	ILN
Guinea pig (Smalley, Barrow, and Foster 2009)	86%	HSDA**L**	FTD**T**Y	TRLRK	QMA**M**K	KYLNS	**V**LN
Chicken (Nilsson 1975)	86%	HSDAV	FTDNY	**S**R**F**RK	QMAVK	KYLNS	**V**L**T**
Alligator (Wang and Conlon 1993)	86%	HSDAV	FTDNY	**S**R**F**RK	QMAVK	KYLNS	**V**L**T**
Frog (Chartrel et al. 1995)	86%	HSDAV	FTDNY	**S**R**F**RK	QMAVK	KYLNS	**V**L**T**
Cod (Thwaites et al. 1989)	83%	HSDAV	FTDNY	**S**R**F**RK	QMA**A**K	KYLNS	**V**L**T**

This table was recreated from data compiled by (Smalley, Barrow, and Foster 2009).

1.1.1.2. Creation of the VIP protein

VIP is initially translated into a 170-amino acid polypeptide, [prepro-VIP], which is post-translationally tailored to generate the full length, 28 AA VIP ligand (Kristensen, Georg, and Fahrenkrug 1997). Biosynthesis of the prepro-VIP forerunner supplies, PHI (peptide histidine isoleucine) in mice, or its human counterpart PHM (peptide histidine methionine), or a C-terminally extended form of PHI/M, called PHV (peptide histidine valine) in all species (Harmar et al. 2012), and VIP in all species, by proteolytic processing (visualized in figure 2) (Noguchi et al. 1989). Post-translational proteolytic processing allows for removal of the signal sequence once the protein has been directed to the lumen of the endoplasmic reticulum (Tsukada et al. 1985). As the prepro-VIP protein migrates to the Golgi apparatus, proteases tailor it to yield VIP and related peptides for secretion, thus generating multiple peptide products (Ballesta et al. 1985).

Tissue-specific variations in the generation and processing of prepro-VIP along with alternative splicing at the mRNA level (Fahrenkrug 1985) are additional mechanisms that can alter expression levels of the prepro-VIP related peptides, resulting in differential expression profiles of VIP and PHM/V in various tissues (Ishihara et al. 1992). Importantly, it should be noted that each of the three bioactive peptides are encoded entirely within a single gene (PHM/PHI/PHV encoded by exon 4 and VIP encoded by exon 5) (You et al. 1995; Kitts et al. 2016), thus allowing mRNA splicing mechanisms to tailor the final mRNA product with both or one of the VIP-related peptides encoded in the processed mRNA template. Examples of expression of VIP have come from measurements of cerebral cortex and suprachiasmatic nucleus extracts revealing that among the peptides synthesized downstream of the prepro-VIP peptide, VIP was found in the highest concentrations (Mikkelsen and Fahrenkrug 1994). Analysis of these peptides in the gastrointestinal tract (focused organ for chapter 2 research), revealed greater expression of VIP-immunoreactive nerves. VIP and PHI concentrations were similar in all regions of the gut except the fundus (cranial portion of the stomach), where VIP presence far exceeded PHI (Bishop et al. 1984). Various biologically active peptide derivatives of VIP include: VIP_{4-28}, VIP_{6-28} and VIP_{10-28}. VIP_{4-28} acts as a potent agonist for VIP's vasoactive intestinal peptide/pituitary adenylate cyclase activating polypeptide receptor 1 (VPAC1) receptor and acts as an antagonist for the VPAC2 receptor (Summers et al. 2003). VIP_{6-28} and VIP_{10-28} both act as antagonists for both VIP receptors (discussed later) (Fishbein et al. 1994; Mohney and Zigmond 1998; Turner, Jones, and Bylund 1986).
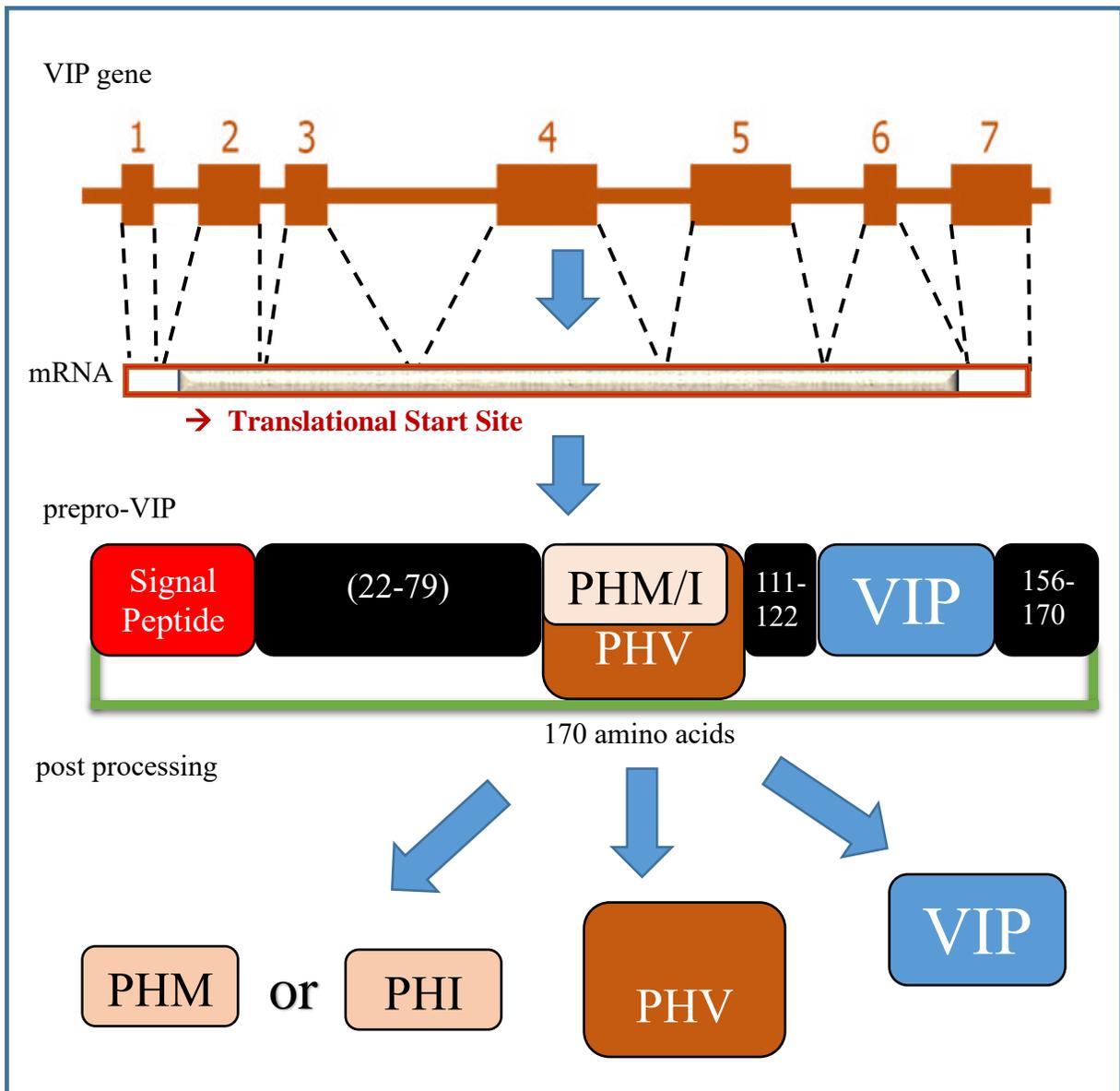
Figure 2. Central dogma scheme for the VIP gene.
The VIP gene consists of 7 exons (rectangles) transcribed into an mRNA molecule as indicated. This is translated into a 170-amino acid polypeptide known as prepro-VIP. The signal peptide, sometimes referred to as the localization sequence, is a short N-terminal peptide that directs the protein towards the secretory pathway (Blobel et al. 1979). Post processing results in the formation of PHM (human) (27 AA), PHI (mouse) (27 AA), PHV (all species) (42 AA), and VIP (all species) (28 AA) (Dejda, Matczak, and Nowak 2004), which are present in various concentrations in most regions of the body (Palle, Ottesen, and Fahrenkrug 1992).

1.1.2. Pituitary adenylate cyclase-activating peptide (PACAP): gene to protein

PACAP, the member of the Secretin family that shares the greatest AA similarity (68%) to VIP and is hypothesized to be the progenitor gene for VIP. As demonstrated in figure 3, PACAP is also organized at the DNA level and synthesized into a bioactive peptide in a similar fashion to VIP. This likeness at the DNA and protein level gives support for a gene duplication mechanism giving rise to VIP, GHRH, and secretin genes (see Figure 1). The name pituitary adenylate cyclase activating polypeptide originates from this protein's ability to activate the adenylyl cyclase enzyme in pituitary cells (Miyata et al. 1989). At least two forms of PACAP are synthesized and denoted by a number that refers to its AA length. For example, PACAP-27, consists of 27 AA, and is very similar in length to VIP sharing 68% AA sequence similarity (Miyata et al. 1990). At the C-terminal end, PACAP-38 is extended C-terminally by an additional 11 amino acids. The initial translated precursor polypeptide, which is later post-translationally modified by proteases to form both forms of PACAP, is called prepro-PACAP (Okazaki et al. 1992). Similar to VIP's prepro precursor, this 176 AA sequence also encodes an additional bioactive peptide called PRP (PACAP-related peptide) and PACAP (Hosoya et al. 1992). Depending on intracellular processing location, the PACAP sequence results in a mutually-exclusive PACAP-27 or PACAP-38 protein from the prepro-PACAP precursor (Tam, Lee, and Chow 2007).
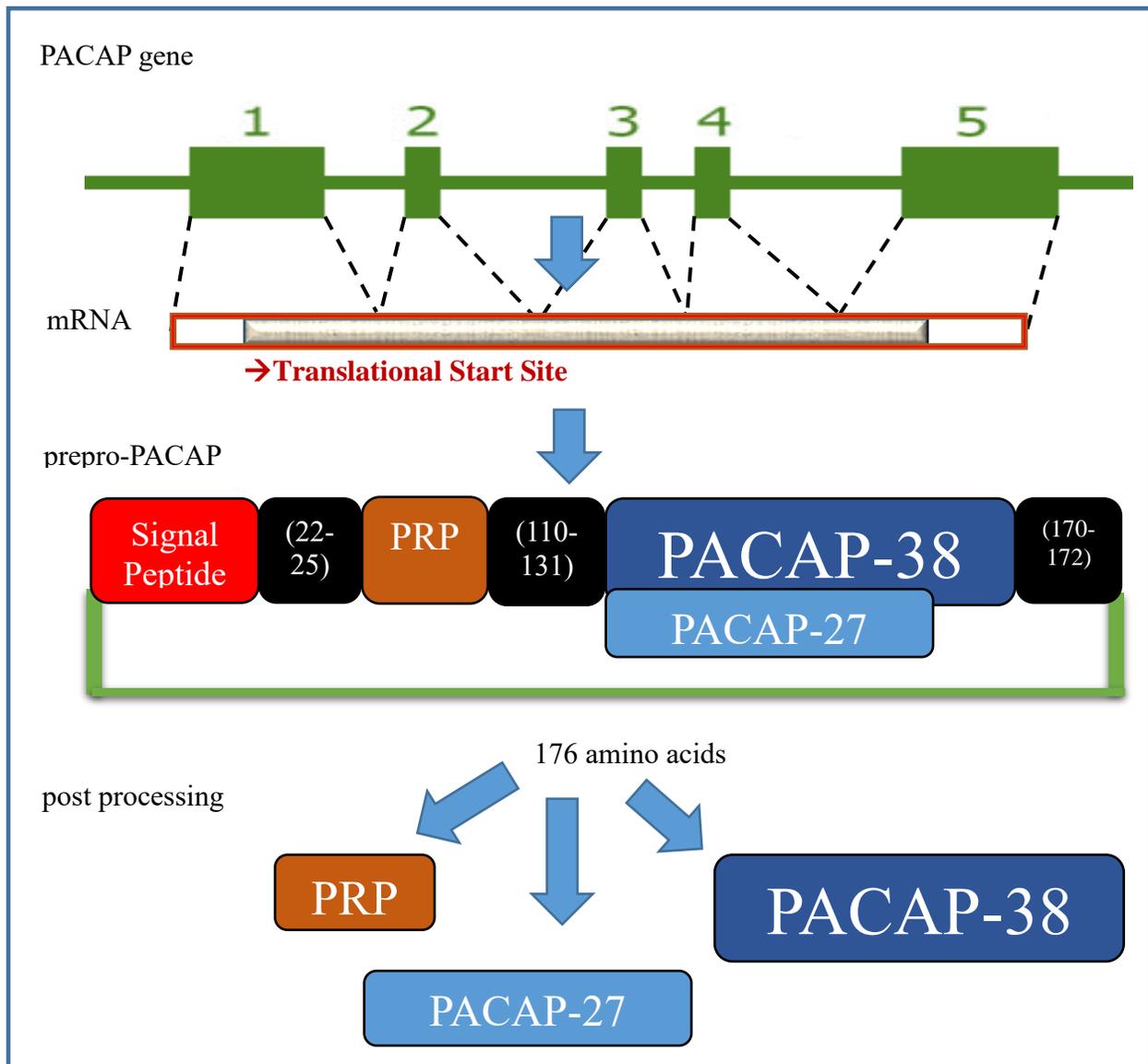
Figure 3.   Information flow for the PACAP gene.
The gene that encodes for PACAP consists of 5 exons that are transcribed and translated into the 176 AA prepro-PACAP protein precursor. Post-translational modification of this polypeptide results in the formation of PRP (29 AA) and PACAP-27 (27 AA) or PACAP-38 (38 AA), all of which are present in all species (Tam, Lee, and Chow 2007; Lee et al. 2009).

1.1.3. G-protein coupled receptors

VIP and PACAP are part of the secretin superfamily of peptide hormones, which signal through G-protein coupled receptors (GPCRs) (Bell 1986). The secretin superfamily is

comprised of evolutionarily related peptides that cross link GPCRs to induce signal transduction (Parker et al. 1984). GPCRs are the largest family of receptors comprising over 800 unique genes encoded in the human body (Bjarnadottir et al. 2006). Crystallographers Robert Lefkowitz and Brian Kobika, both received the Nobel prize in chemistry in 2012 for their discovery of GPCR structure (Kobilka 1995). Found primarily in eukaryotes, GPCR's are vital to cellular function, and they represent about 3% of encoded genes within in the human genome (based on an estimate of 22 thousand genes in the human genome) (Fredriksson et al. 2003). To date, around 45% of all pharmaceutical drugs target GPCR's, and/or associated upstream/downstream signaling molecules (Drews 2000), further supporting these receptors as an important "lynchpin" regulating human health and disease (Overington, Al-Lazikani, and Hopkins 2006). All known cellular effects mediated by VIP and PACAP are manifested through the binding and subsequent signal transduction from at least three endogenously expressed GPCRs that will be the focus of the next section (Leceta et al. 2000).

1.1.3.1. VIP Receptors denoted as VPAC1 and VPAC2

The receptors for VIP and PACAP include <u>v</u>asoactive intestinal peptide/<u>p</u>ituitary <u>a</u>denylate <u>c</u>yclase activating polypeptide receptor 1 (VPAC1) and VPAC2, while PACAP preferentially (1000x greater affinity compared to VIP) binds to pituitary adenylate cyclase-activating polypeptide receptor type I (PAC1) (Nussdorfer and Malendowicz 1998). As the naming implies, VPAC1 and VPAC2 are receptors for both VIP and PACAP, while PAC1 preferentially binds to PACAP. VIP does bind to PAC1, but the binding affinity is a thousand times lower than PACAP. Both VPAC1 and VPAC2 bind VIP and PACAP with equal affinity ($K_d \approx 1$ nM). PAC1 has high affinity for PACAP-27 and PACAP-38 ($K_d \approx 0.5$ nM), and low affinity for VIP ($K_d > 500$ nM) (Shivers et al. 1991) (Robberecht et al. 1991). This was

determined with receptor autoradiography, where excess VIP did not displace either PACAP-27 or 38 (Shivers et al. 1991). For this reason, VPAC1 and VPAC2 do not discriminate between either VIP or PACAP peptide, where PAC1 is more selective towards PACAP. VPAC1 is located at position 22.1 of the short arm of the third human chromosome (position 72.5 of the long arm of the ninth mouse chromosome), VPAC2 is located at position 36.3 on the long arm of the seventh human chromosome (position 62.6 on the long arm of the twelfth mouse chromosome), and PAC1 is found at position 14 on the short arm of the seventh human chromosome (position 7 on the short arm of the seventeenth mouse chromosome) (Kitts et al. 2016).

1.1.3.2. GPCR characteristics

GPCRs are characterized by a few similar features. First, the amino terminus of the GPCR polypeptide exists in the extracellular environment, called the ectodomain and this N-terminus makes up part of the ligand binding site. The peptide chain then "snakes" through the plasma membrane seven times (Palczewski et al. 2000). This membrane spanning alpha-helical hydrophobic region was, and continues to be, problematic with respect to obtaining enzyme crystals, due to its extensive hydrophobic (e.g. greasy) nature, and is why GPCRs have been historically so difficult to obtain X-ray structure information (Gether and Kobilka 1998). The carboxyl terminus, which resides within the cytoplasm, interacts with signaling proteins to transmit information from the plasma membrane to internal locales in the cell (Michino et al. 2009). One important signaling protein target that the C-terminus recognizes upon ligand binding-induced conformational changes are heterotrimeric G proteins (Gilman 1970).

The repeated zigzagging of the protein's primary sequence through the plasma membrane results in the formation of three extracellular and intracellular loops connecting the seven

transmembrane domains of the GPCR protein (see Figure 4) (Trumpp-Kallmeyer et al. 1992).

The transmembrane domains work to lock the protein into the membrane and form the three

intracellular and extracellular loops (ICL$_{1-3}$, ECL$_{1-3}$). The extracellular loops are important for

receptor stability and work with the ectodomain for ligand recognition, binding and specificity

(Cook and Eidne 1997). Together the intracellular loops 2 and 3 form a guanine-nucleotide

exchange factor (GEF) responsible for signal transduction (Natochin, Gasimov, and Artemyev

2001). These structural features are all shared by the 800 different GPCR receptors in the human

body and have been categorized into multiple groups that will now be discussed.
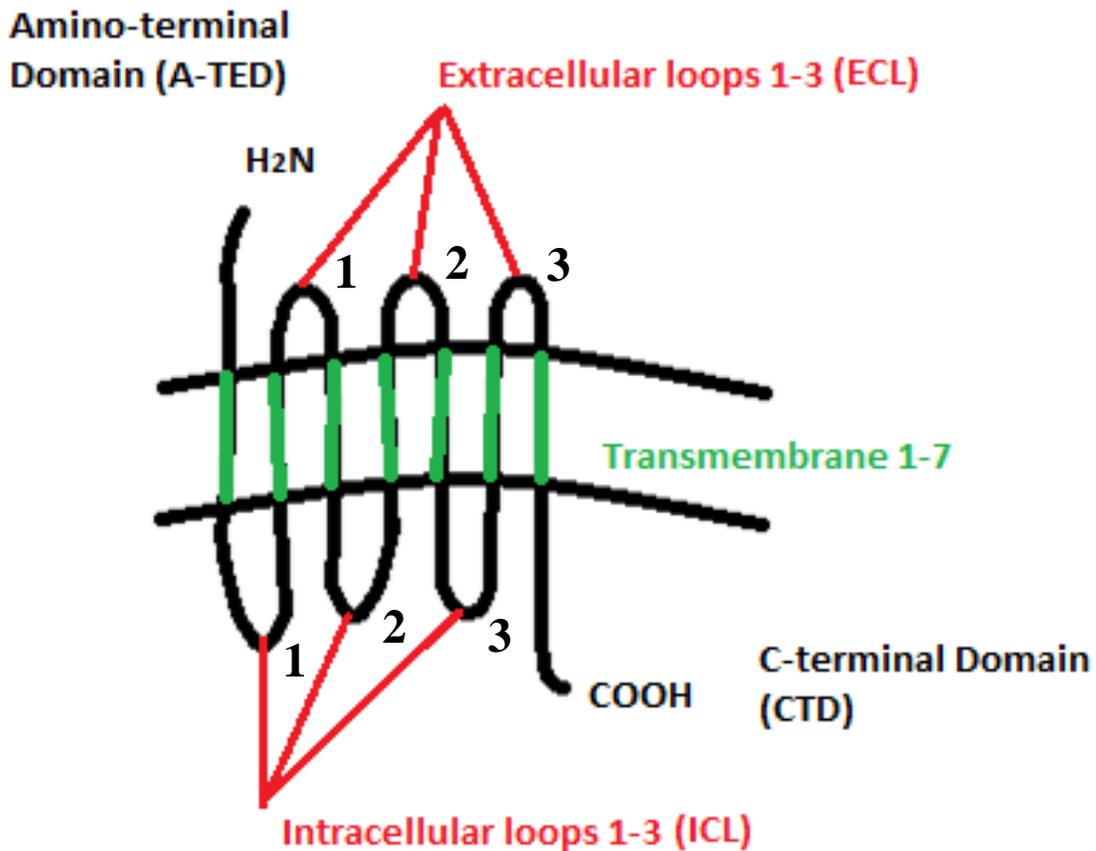
Figure 4.   Defining characteristics of GPCRs.
The two horizontal lines represent the phospholipid bilayer of the plasma membrane of the cell. A GPCR is defined as a receptor which contains 7 transmembrane domains. These are accompanied by 3 intracellular, 3 extracellular loops, an N-terminus ectodomain, and an intracellular C-terminus region.

1.1.3.3. Class 1 GPCRs

GPCRs are categorized into five individual GPCR families (Fredriksson et al. 2003; Graul and Sadée 2001; Bockaert and Pin 1999). The first family, commonly known as class 1 or class A, possesses the largest molecular mass of the GPCR families (Angel, Chance, and Palczewski 2009). Class 1 family GPCRs perform a multitude of critical biological functions, including light detection, hormonal secretion and extracellular signaling (Kakarala and Jamil 2014). Currently, receptors in class 1 have been divided into 19 sub-groups (Joost and Methner 2002). Since rhodopsin was the first discovered member of this family, Class 1 is also frequently referred to as the rhodopsin family. Rhodopsin, the eponym for this family, was the first GPCR classified in this family and is a light-sensitive receptor found in the rods of the retina and is involved in visual transduction. This receptor binds to a light sensitive biological pigment, known as retinal, that absorbs energy in the visible range (~400 – 700 nm) range of the electromagnetic radiation spectrum causing it to change its shape, which in turn causes a conformational change in Rhodopsin initiating signal transduction and the conversion of light into electrical signals (Farrens et al. 1996). Class 1 GPCRs bind their ligands between the outer 1/3 of the transmembrane region of the protein (Trumpp-Kallmeyer et al. 1995) (see figure 5).

1.1.3.4. Class 2 GPCRs

The second receptor family is titled class 2, class B, or the secretin family. This family binds VIP, PHM/I, PHV, PACAP, PRR, glucagon, secretin, peptide HI-27, transthyretin (prealbumin), GIP (gastric inhibitory peptide) and GHRH (growth hormone-releasing hormone), (non-exhaustive list) (Laburthe, Couvineau, and Tan 2007). All members of this family physically recognize peptide ligands, unlike class 1, that can recognize different classes of molecular signals, including photons (Okada et al. 2001), and chemical pheromones (Choi et al.

2003). Class 2 GPCRs have an extended N-terminal domain, called the ectodomain, which

assists in binding their peptide ligands (Pantaloni et al. 1996). To illicit down-stream signaling,

the ligands bind between the amino terminal domain and the transmembrane domains (Hoare

2005).

1.1.3.5. Class 3, 4, and 5 GPCRs

The class 3 GPCRs or class C, is referred to as the glutamate family of GPCRs and

possesses a distinct extracellular domain called the Venus flytrap module (VFTM) (Wu et al.

2014; Bargmann 1997). This domain functions in a similar trapping manner as the carnivorous

plant, *Dionaea muscipula* or Venus flytrap. The ligand binds the extracellular ectodomain and

the receptor closes around it (Pin et al. 2004). The adhesion family, also called class 4 or class D,

has an extremely long amino terminal domain, in comparison to other GPCR families, which

does not bind to peptides but rather to components of the extracellular matrix (Bjarnadóttir et al.

2004). An example of this family is G protein-coupled receptor 56 (GPR56), whose ligand is

type III collagen (Luo et al. 2011). The final family is called Frizzled GPCRs, class 5, or class E.

This unconventional group contains the remainder of GPCRs that do not fall into classes 1-4

(Schulte and Bryja 2007). Frizzleds are activated by the wingless/int1 (WNT) family of

lipoglycoproteins (Koval et al. 2011).
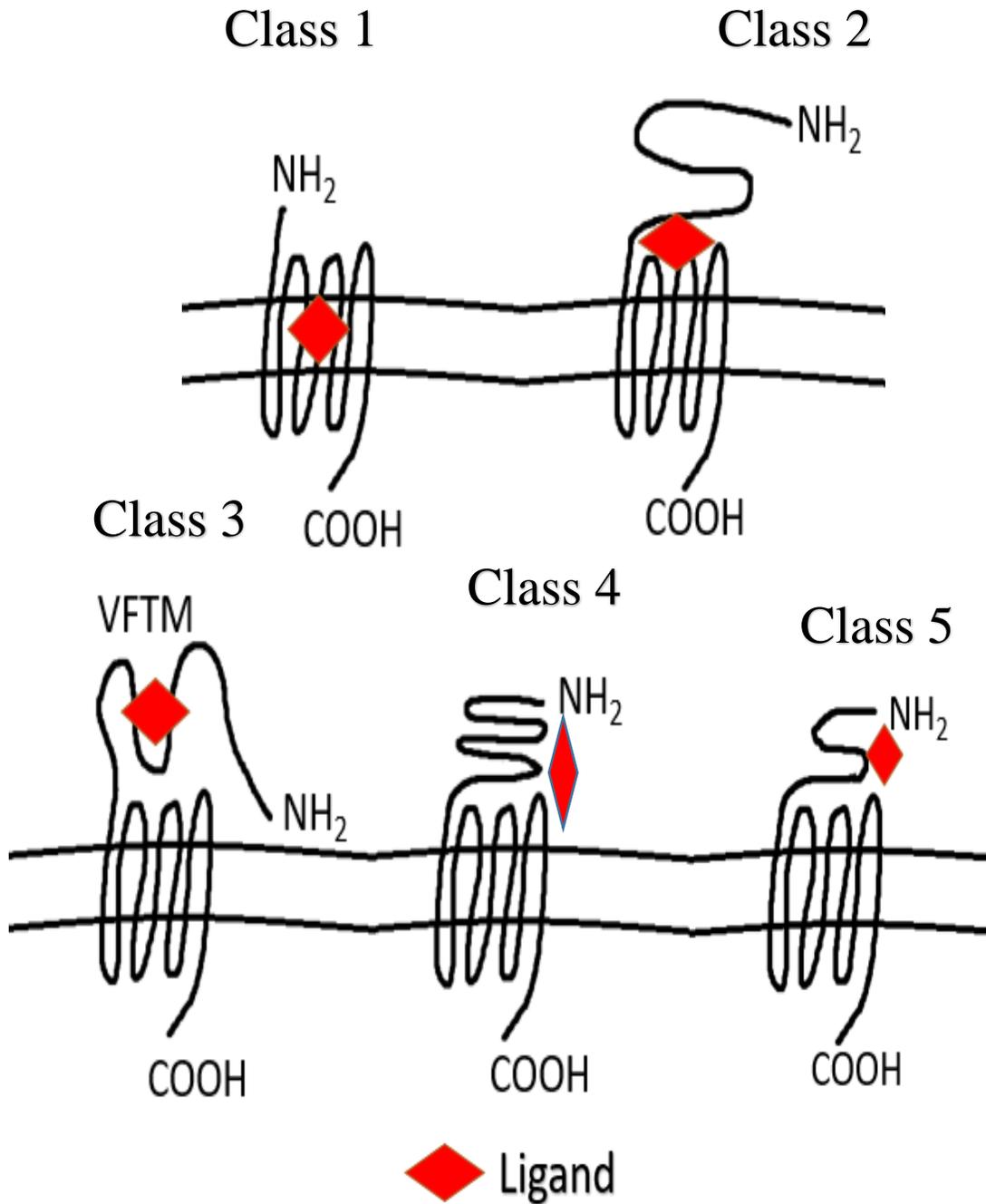
Figure 5.   The 5 classes of GPCRs.
Schmatic representation of all five GPCR classes with ligand binding sites denoted by diamonds. All of these classes share certain defining characteristics. For example, they share a seven-transmembrane region, but the location of ligand binding differs for all five classes as depicted. N-terminus (NH_2) and C-terminus (COOH) are indicated for each GPCR class. Venus Fly Trap mechanism (VFTm) is emphasized for class 3 GPCRs.

1.1.3.6. VIP signaling via Heterotrimeric G-proteins

Once VIP binds to one of its class 2 receptors (VPAC1/2 $K_d \approx 1$ nM) (PAC1 $K_d \approx 1$ μM) (Shivers et al. 1991) (Robberecht et al. 1991), the ligand binding causes conformational changes within the GPCR structure, which illicit downstream signaling by binding and activating heterotrimeric G-proteins (Unger et al. 1997; Baldwin, Schertler, and Unger 1997). Three individual subunits make up heterotrimeric G-proteins, called alpha, beta, and gamma proteins (Noel, Hamm, and Sigler 1993). These are not integral membrane proteins. The alpha subunit is targeted to and becomes associated with the cell membrane through a lipid palmitoyl post-translational modification (PTM), that inserts the alpha subunit into the cell's plasma membrane (Linder et al. 1993). The alpha-protein is activated when bound to GTP (guanosine triphosphate). Upon the hydrolysis of GTP to GDP (guanosine diphosphate), the alpha protein becomes inactivated (Coleman et al. 1994; Markby, Onrust, and Bourne 1993).

The G-alpha subunit exists in several sub-types. For class 2 GPCR's the primary subunits are $G_{\alpha s}$ (adenylate cyclase stimulator) and $G_{\alpha i}$ (adenylate cyclase inhibitor) (Sprang 1997). The $G_{\alpha s}$ subunit increases the production of intracellular cAMP (cyclic adenosine monophosphate) from ATP (adenosine triphosphate) hydrolysis by binding to and stimulating the enzyme adenylyl cyclase (Gilman 1990). The $G_{\alpha i}$ subunit counteracts the $G_{\alpha s}$ subunit and inhibits the conversion of ATP to cAMP (Coleman et al. 1994). The adenylyl cyclase enzyme contains one binding site for $G_{\alpha i}$ and another for $G_{\alpha s}$ (Tang and Gilman 1991; Gilman 1984). A Nobel prize was awarded to Alfred Gilman in 1994 for his work on the regulation of adenylyl cyclase by G proteins (Gilman 1995).

The gamma subunit also utilizes a lipid moiety for insertion into the plasma membrane's phospholipid bilayer (Linder et al. 1991). Under physiological conditions the beta and gamma

subunits are typically found together, and are collectively known as the beta-gamma complex (Pitcher et al. 1992). These three G-proteins are found as a heterotrimeric complex only when the alpha subunit is in the inactive, or off state (GDP bound). Upon ligand/ GPCR binding the α-subunit dissociates from the beta-gamma dimer, inducing the α monomer to exchange GDP for a free GTP; Thus activating the α-subunit. (Oldham and Hamm 2008). $G_{\alpha/GTPactive}$ then moves within the membrane plane from the receptor to bind to adenylyl cyclase and increase its K_{cat} and formation of the secondary signaling messenger, cAMP (visualized in figure 6) (Robishaw, Smigel, and Gilman 1986).
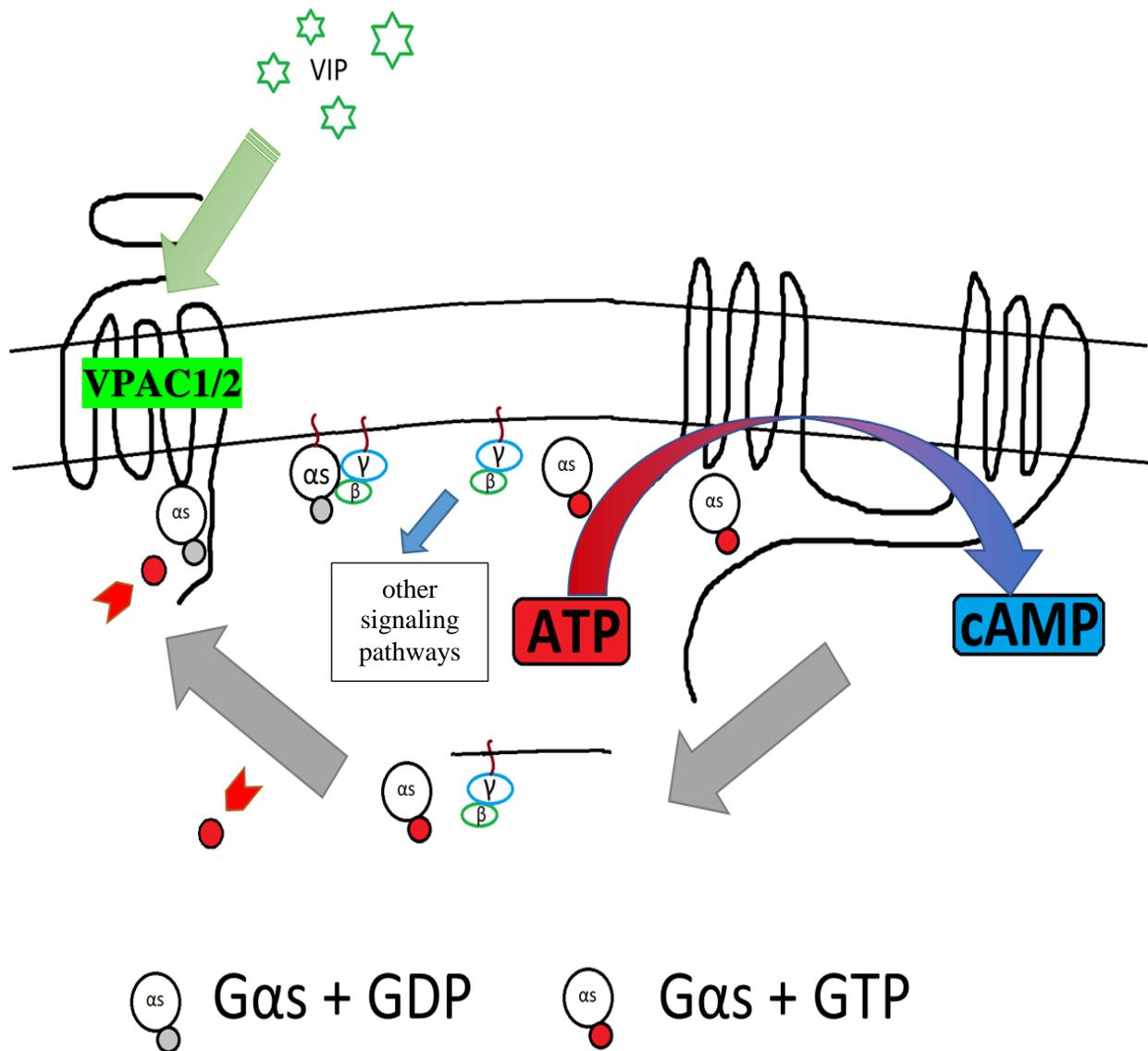
Figure 6.   VIP/VPAC1/2 signaling by eliciting [cAMP] through heterotrimeric G-protein activation of adenylyl cyclase.

The binding of the VIP ligand causes a conformational change in the VPAC1/2 GPCR for G_α binding and its exchange of GTP for GDP to its active form. The G_α GTP active protein dissociates from the $G_{\beta\gamma}$ complex to bind and activate adenylyl cyclase, which coverts ATP to cAMP and organic phosphates. The G_α GTP active becomes inactivated as the GTP is replaced by GDP, which allows for the reformation of the heterotrimeric G-protein and terminates the signal as $G_{\alpha s}$ GDP inactive dissociates from adenylyl cyclase resulting in the reduction of its activity. Figure recreated by author and based on Respiratory Research 2003 (Billington and Penn 2003).

1.1.3.7. G-protein signaling

The cycle of G-protein signaling begins with ligand binding. Once binding has occurred to its cognate receptor, conformational changes in the GPCR allow for the binding of the heterotrimeric G-protein complex by physically engaging the alpha subunit. Once bound to the receptor, the alpha subunit is in the off-state and bound to GDP. It becomes induced to exchange GDP for GTP by binding to the GPCR, thereby converting G_α into an active, or the on-state. The GPCR, therefore, acts as a guanine nucleotide exchange factor (GEF) by stimulating the release of GDP and allowing the binding of GTP (Luttrell, Daaka, and Lefkowitz 1999; Buday and Downward 1993). The activated state of G_α/GTP induces the dissociation of the alpha-subunit from the beta-gamma complex. This dissociation results in an activated alpha subunit bound to the GPCR and the beta-gamma complex moving away to induce other signaling that will not be discussed (van Biesen et al. 1995). Here, the beta-gamma complex functions as a negative regulator of the G_α protein. In the heterotrimeric form, the $G_{\beta\gamma}$ subunit also increases the affinity of the G protein for GDP, keeping it in an inactive state (Brandt and Ross 1985). The alpha subunit preferentially binds to the GPCR if complexed with the beta-gamma complex and therefore the G_α subunit is delivered to the GEF-activating GPCR to induce: 1. Exchange GDP for GTP and 2. G_α GTP:active dissociation for the $G_{\beta\gamma}$ dimer (Naor, Benard, and Seger 2000) (Markby, Onrust, and Bourne 1993).

The active G_α/GTP subunit binds to adenylyl cyclase increasing its enzyme kinetics to promote increasing the conversion of ATP to cAMP; a necessary secondary messenger for protein kinase A (PKA) activation and other down-stream signaling molecules (Dessauer and Gilman 1997). The alpha subunit is categorized as a GTPase, hydrolyzing GTP to GDP + inorganic phosphate (Kleuss et al. 1994). Upon binding to its target, in this case adenylyl

cyclase, the active alpha subunit hydrolyzes GTP to GDP inducing its off-state and dissociation from adenylyl cyclase (Cassel and Selinger 1978). Thus, intrinsic GTPase activity limits its time bound to adenylyl cyclase and acts as a self-limiting "timer" for adenylyl cyclase activation. The kcat for this reaction is very slow and takes about 5 minutes. The free roaming G-alpha subunit (GDP) re-attaches to a beta-gamma complex to form a heterotrimeric G-protein complex (Logothetis et al. 1987). This cycle of activation and inactivation allows for intracellular signaling to occur. These steps occur for VIP's two primary receptors VPAC1 and VPAC2 (Murthy et al. 1993).

1.1.4. Adenylyl cyclase enzyme

In mammals, currently there are ten known isoforms of adenylyl cyclase enzymes, dubbed ADCY1 through ADCY10 (Hanoune and Defer 2001). Of these ten, ADCY1 through ADCY9 are transmembrane enzymes, while ADCY10 is the only soluble form identified to date (Chen et al. 2013). Found primarily in the male spermatozoa, ADCY10 functions independent of G protein dependent signaling, but rather acts as a pH (potential of hydrogen) sensor within the cell. Researchers discovered ADCY10 when trying to understand the cAMP-dependent activation process in mature male sperm (spermatozoa) (Chen et al. 2000). ADCY1 through ADCY9 are made up of a single polypeptide (~154 kDa (Neer 1976)) and have very similar structures (Harayama 2013).

The ADCYe proteins are comprised of two transmembrane domains (TMD) 1 and TMD2. Each transmembrane domain has a cluster of 6 transmembrane segments that "wind" through and anchor the enzyme into the plasma membrane (Tang and Gilman 1995). The small bridge between TMD1 and TMD2 is named the C1 domain, while the peptides near the

carboxylic acid terminus are called the C2 domain. Each of these domains is further separated into 2 sections, called C1a and C1b, and C2a and C2b (Zhang et al. 1997).

When these two domains are distal from each other (figure 7), the adenylyl cyclase enzyme is in its inactive state. The $G_{\alpha s}$/GTP subunit unifies these two domains by joining the C2a domain with the C1a and C1b domains. The dimerization of these two domains then allows for the enzymatic conversion of ATP to cAMP and pyrophosphate (Yan et al. 1996; Whisnant, Gilman, and Dessauer 1996; Yan et al. 1997; Zimmermann, Zhou, and Taussig 1998). The $G_{\alpha i}$ subunit reverses these steps and switches adenylyl cyclase into the off state. The small "bridge" created by $G_{\alpha s}$ acts as the binding site for $G_{\alpha i}$ inactivating the enzyme and stopping cAMP production (Dessauer et al. 1998). Interestingly $G_{\alpha s}$ GTP active binding to adenylyl cyclase is responsible for generating a $G_{\alpha i}$ GTP active binding site, therefore allowing the cell to limit adenylyl cyclase acitivity even more rapidly than the GTPase activity of $G_{\alpha s}$.

The G-beta-gamma complex that dissociates from the $G_{\alpha i/\alpha s}$ proteins can also act upon adenylyl cyclase (Diel et al. 2006). A binding site for the $G_{\beta\gamma}$ complex is present on adenylyl cyclase and can act to temporarily upregulate this enzyme (Chen et al. 1995). In addition to adenylyl cyclase activation from $G_{\alpha s}$, $G_{\beta\gamma}$ can also activate adenylyl cyclase and i[cAMP] elevation (Inglese et al. 1994) (Wittpoth et al. 1999). Adenylyl cyclase can also be activated by directly bypassing the GPCR, through forskolin, a tool to induce cAMP production, which binds to the $G_{\alpha s}$ site on adenylyl cyclase (Shu and J. Scarpace 1994), and can increase its enzymatic activity by 10^3 (Liu et al. 1997). The cAMP produced by adenylyl cyclase continues the downstream signaling of the GPCR and is pictured in figure 7. The amount of cAMP produced along with the pathways activated/inhibited by cAMP are cell specific.
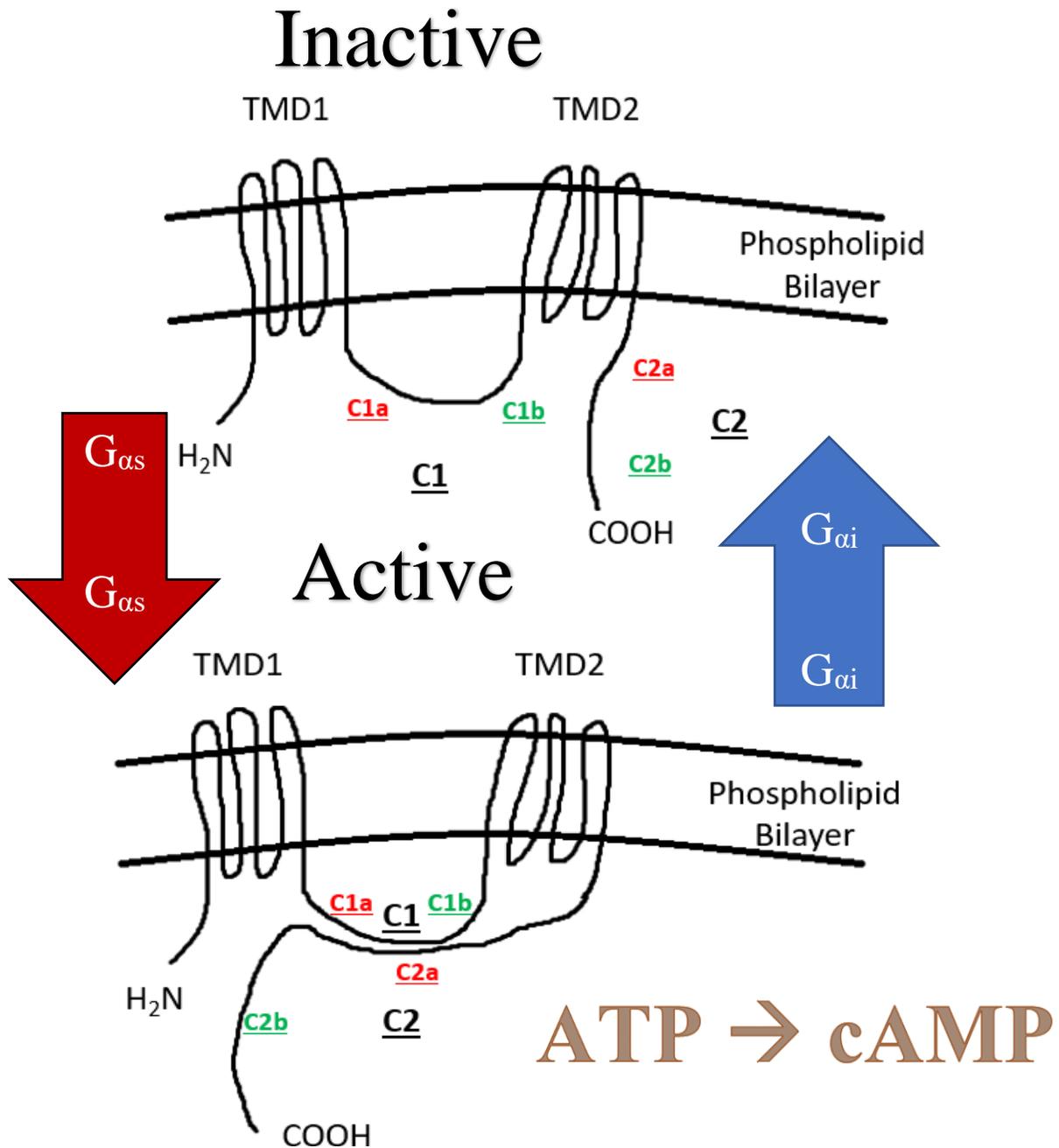
Figure 7.   Schematic representation of the enzymatic regulation of AC by G-protein binding.

The adenylyl cyclase enzyme contains 12 trans-membrane anchors (TMD1 and TMD2), with a C1 and C2 domain, which needs to become "tethered" together to promote a functional active site for conversion of ATP to cAMP + Pi. Activation by $G_{\alpha s}$ "wraps" the C2a domain over the C1 domain and increases the enzymatic activity of AC. This "wrap" creates a binding site for $G_{\alpha i,}$ which reverses the domain overlap and halts enzymatic activity and subsequent cAMP production.

1.1.5. Multiple GPCR pathways

GPCRs like VPAC1/2 through their heterotrimeric G-proteins, can activate several

different pathways. Through adenylyl cyclase, the cAMP pathway can stimulate hormone

receptors (Filardo 2002; Reiter et al. 2001; Ji et al. 2002), activate protein kinase A (PKA)

(Thevelein and de Winde 1999), stimulate cyclic nucleotide-gated (CNG) ion channels (Rakhilin

et al. 2004) and nucleotide exchange factors directly activated by cAMP (EPAC) (Borland,

Smith, and Yarwood 2009), all of which illicit downstream signaling pathways of their own.

These pathways modulate cell adhesion and migration (Kinashi and Katagiri 2005), vascular

inflammation regulation (Schmidt et al. 2007), cytokine signaling regulation (Sands et al. 2006),

cell proliferation modulation (Stork and Schmitt 2002), cellular differentiation (Hoffman et al.

1994), and cellular hypo/hypertrophy (Ulucan et al. 2007). The variety, cellular concentrations,

intracellular targeting GPCRs through heterotrimeric G-proteins and the competition between

$G_{\alpha s}$, $G_{\alpha i}$ and $G_{\beta \gamma}$ binding, can all impact VIP's ability to illicit cellular effects (Hillenbrand et al.

2015). Moreover, newer models of GPCR functional activity have demonstrated the importance

of extra/intracellular proteins on GPCR activation. This overturns the simple "on/off" theory,

adding additional complexity to these receptors (Maudsley et al. 2012).

1.1.6. Biological functions of VIP signaling

1.1.6.1. VIP receptor localization

Over the past half century, VIP research has demonstrated that this peptide plays

important biological roles in the brain, gastrointestinal tract, cardiovascular system and immune

system. Although VIP receptors are disseminated throughout the body, the expression patterns of

VPAC1 and VPAC2 receptors differ. VPAC1 is found in the liver, kidneys, spleen, breast tissue,

prostate, bladder, immune cells, lungs, gastrointestinal mucosa, thyroid, and lymphoid tissues (locations represented in figure 8) (Reubi 2000).

In the central nervous system (CNS), VPAC1 is found the supraoptic nucleus, pyriform cortex, the putamen, and the pineal gland. The VPAC2 receptor is found throughout smooth muscle layers in blood vessels, gastrointestinal tract, lung, reproductive tract. It is also found in the vasculature of the kidney, the colon, the thyroid, pancreas, and immune cells (Harmar et al. 2004). In the CNS, VPAC2 is found in the amygdala, the hypothalamus, the thalamus, periventricular nucleus, cerebral cortex, and the suprachiasmatic nucleus (Vertongen et al. 1998) (Usdin, Bonner, and Mezey 1994).

1.1.6.2. VIP signaling in the nervous system

Through VPAC2, VIP serves as a master regulator of the circadian rhythm, managing the oscillation of our endogenous 24-hour circadian clock in the brain (Pauls et al. 2014) (Vosko et al. 2015). This circadian regulation was discovered by Harmar et. al who generated a VPAC2 knockout mouse strain. They discovered that the disruption of this signaling pathway resulted in disrupted wheel-running activity when compared to the WT strain. Clock genes, which act as circadian pacemakers in the brain, were found to be weakly expressed in the VPAC2 receptor knockout mice with their rhythmicity disrupted upon dark conditions (Harmar et al. 2002). VIP signaling is also upstream of brain-derived neurotropic factor (BDNF), which is critical in day/night synchronization and neural structural plasticity, the ability of the brain to strengthen and create new synaptic connections (Girardet et al. 2013).

To determine the signaling pathway responsible for VIP's neuroprotective effects against neuro-excitotoxicity, it was demonstrated that VIP's protection was lost in VPAC2 knockout mice and/or when VPAC1 agonists were utilized (Rangon et al. 2006). Through the VPAC1

receptor, VIP stimulates neuroprotective proteins, which have been implicated in the treatment of

Alzheimer's disease (Gozes 2001). VIP is also linked in neurotoxicity reduction, through its

recognition of neurotoxins, which are plaque forming substances including β-amyloid (Offen et

al. 2000). VIP's ability to prevent neurodegeneration, suggests the potential therapeutic use of

VIP in neurogenerative disorders like multiple sclerosis and Parkinson's disease (Delgado and

Ganea 2003; Korkmaz et al. 2010; Fernandez-Martin et al. 2006).
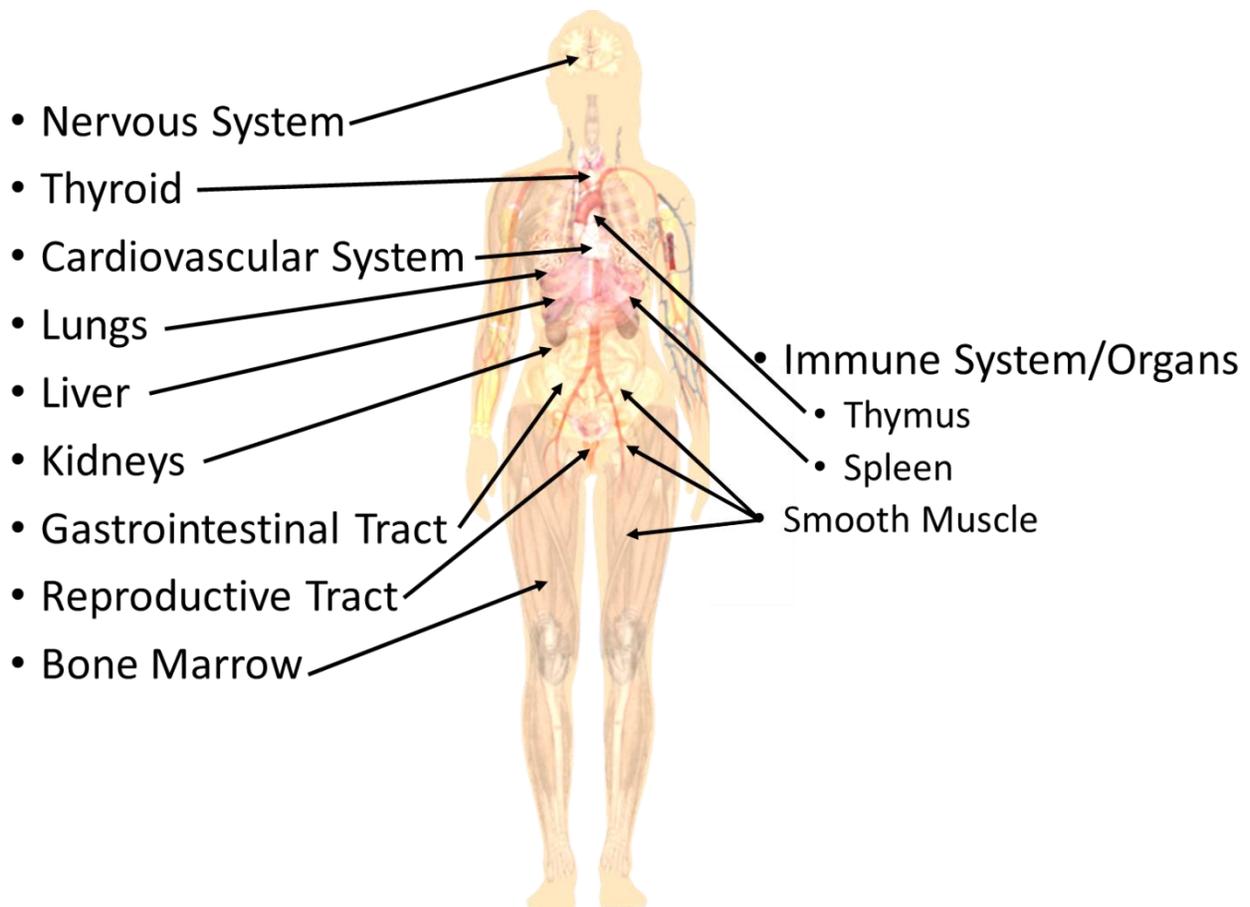
Figure 8.   Locations of VIP receptors.
The distribution of VPAC1/2 receptors throughout the human body suggests the importance
of this peptide signaling in physiology. Human body picture is a public domain image
(Wikimedia commons).

1.1.6.3. The gastrointestinal tract and VIP

In the gastrointestinal tract, VIP functions as a promoter of intestinal barrier homeostasis and a protector against inflammatory bowel diseases (IBD) by downregulating inflammatory cytokine production (Wu, Conlin, et al. 2015). VIP promotes intestinal barrier homeostasis by its ability to restore protein kinase C (PKC) pathways disrupted during infection (Morampudi et al. 2015). Mice deficient in VIP (VIP knockout; VIPKO), have demonstrated distorted colonic crypts, defective epithelial proliferation and increased permeability (Wu, Conlin, et al. 2015). In the mucosa-associated lymphoid tissues (MALT) of the gastrointestinal tract, VIP upregulates cell junctions and decreases intestinal permeability, reducing pathogen uptake (Abad et al. 2003; Jonsson, Norrgard, and Forsgren 2012). VIP's regulation of smooth muscle contraction, is also involved in gastric motility, peristalsis and sphincter function (Love, Go, and Szurszewski 1988; Biancani et al. 1988). Moreover, VIP acts as an important metabolic regulator in both the brain and gut and its removal in mice results in weight loss and fat storage deficits, supporting the notion that VIP signaling is an essential regulator to metabolic homeostasis (Vu et al. 2015).

VIP signaling plays a key role in appetite control, fat mass accumulation, and metabolic hormone regulation. VIPKO mice, when compared to their wild type (WT) littermates, showed significantly lower body weight and lower body fat percentage. Interestingly, while they consumed similar amounts of food as WT littermates, they consumed food throughout the day and night, whereas the WT mice consumed their food during the night (mice are nocturnal animals). In the VIPKO mice, researchers found increased leptin, "the full hormone" and decreased ghrelin, "the hunger hormone" which works in opposition of leptin. These levels remained unchanged after food consumption (Vu et al. 2015). Leptin acts as satiety sensor, notifying your brain you have eaten enough, while ghrelin informs your body you need to eat

(Schussler et al. 2012). Research by Liu et al. analyzing gene pathways predisposing individuals to obesity demonstrated that the VIP signaling pathway was the most important in the development of higher BMI and body fat ass. This study genotyped ~500,000 single-nucleotide polymorphisms in 1,000 US caucasian males analyzing over 960 different pathways to establish VIP's reputation (Liu et al. 2010).

1.1.6.4. Role of VIP in the cardiovascular system

The substantial cardiovascular effects of VIP suggest that this peptide is important in regulation of arterial blood flow, cardiac contraction, and heart rate. Two years after its discovery, VIP was found to relax vascular smooth musculature. As the Hagen-Poiseuille law states, this reduces the pressure upon arterial walls, allowing for greater blood flow (Said and Mutt 1972). Research in feline craniums demonstrated that VIP's involvement in lowering blood pressure was extended to neurogenic dilation, or a severe drop in blood pressure that reduces the amount of blood returning to the heart (Bevan et al. 1986). During disrupted heart rhythm or atrial fibrillation, oxygen scarcity and heart failure, VIP is released by intracardiac neurons around the atrioventricular nodes to reduce blood pressure (Xi et al. 2013). In healthy subjects, VIP infusions caused sustained vasodilation and decreased arterial pressure (Frase et al. 1987). Exogenous released and endogenously injected VIP can significantly increase heart rate and has a more potent effect on heart rate than norepinephrine (Henning and Sawmiller 2001). VIP deficiency has also displayed lower body temperatures, due to weaker heart rates caused by disrupted physiological circadian rhythmicity in the heart (Schroeder et al. 2011). It's ability to reduce blood pressure has resulted in its consideration as a drug for pulmonary hypertension treatment (Petkov et al. 2003).

1.1.6.5. Immunoregulation by VIP

With respect to immunity, VIP acts as a chemoattractant (e.g. acts as a chemical recruiter) of leukocytes and mediates anti-inflammatory effects (El-Shazly et al. 2013). In 1978, it was discovered that VIP can be produced by immune cells (Cutz et al. 1978). A few years later, mast cells were found to produce a truncated form of VIP (10-28), which acts as an antagonist to VIP signaling by competing for VPAC1/2 binding sites (Wershil et al. 1993). Examples of VIP's anti-inflammatory role include its inhibition of proinflammatory cytokines like TNFα, IL-6, and IL-12 to name a few. It also upregulates the production of IL-10, a potent anti-inflammatory cytokine (Feldmann, Brennan, and Maini 1996). VIP supports the survival and generation of T_{H2} cells (Delgado 2003).

During sepsis, VIP is significantly increased in plasma assisting in inflammation reduction (Kuncova et al. 2011). VIP's extensive presence throughout the gastrointestinal tract, its involvement in inflammatory bowel diseases as well as the disruption of the intestinal epithelium in VIP knockout mice, eludes to its importance in the alimentary canal. Changes in receptor expression in resting versus activated lymphocytes, along with delayed eosinophilic response during allergy in VPAC2 knockout mice, advocates for its significance as an immune modulator (Dorsam et al. 2010; Vomhof-DeKrey and Dorsam 2008). To gain a better understanding of VIP's role in the digestive and immune systems, microbiome and eosinophil differentiation experiments were conducted (discussed in chapter 2 and 3).

2. VIP/PHI DEFICIENCY CAUSES MOUSE GUT DYSBIOSIS

2.1. Our microbiota

Altogether, it is estimated that our planet is host to nearly 6 x 10^{30} bacterial cells. This far exceeds the biomass of all other kingdoms (animalia, plantae, fungi and protists) on the phylogenetic tree of life (Whitman, Coleman, and Wiebe 1998). The bustling communities of symbiotic, commensal, and pathogenic microorganisms that call our body home are our microbiota. This term is very general, and includes all microorganisms like, viruses, archaea, fungi and bacteria existing in an environment. The microbiome on the other hand refers to the genetic composition of this microbiota or all the genes of a microbial population. Bacteria, the largest kingdom of prokaryotes inhabit all known environments on our planet. They are found in even the most environments, such as deserts, rainforests, the frozen tundra and plains. They can even survive in harshest known surroundings, like the town of Pripyat, Ukraine, which has been saturated with high-levels of radiation since the level 7 nuclear energy accident (Chernobyl disaster) in 1986 (Zavilgelsky et al. 1998). Research by Igor Shuryak has demonstrated cooperation between these communities, where radiosensitive bacteria are protected from ionizing radiation by neighboring radio-resistant ones (Shuryak et al. 2017). Bacteria have also been found to dominate the harsh environments of deep-sea hydrothermal vents, once thought to be void of life (Xu et al. 2014).

2.1.1. Discovery of E. coli and the coining of the microbiome

The discovery of *Escherichia coli,* by Theodor Escherich in the 1880's, opened the door to the isolation of numerous oral, digestive, and respiratory flora. It led to the realization that we are not "alone", and that our bodies play host to numerous other organisms. Since then, researchers have speculated on the importance of our bacterial communities. To gain a better

understanding of the significance of our microbiota, the use of pathogen-free laboratory animals was suggested in 1962 (Petter-Lane 1962). The utilization of germ-free animals has been critical in illuminating the interplay between our bodies and the microorganisms that "call it home". Although the individual who first coined the term "microbiome" is uncertain, it was first authored in a manuscript by John Whipps in 1988 (Whipps JM 1988).

2.1.1.1. Relative number of bacteria

Although many publications credit Dwayne Savage for determining the intestinal bacterial load in late 1972, it was T. D. Luckey from the University of Missouri, Columbia, whom postulated that the microbial population of our bodies, our microbiota, outnumber our cells 10 to 1 (Savage 1977; Luckey 1972). Luckey estimated there were 37.2×10^{13} bacterial cells with an estimated 3.72×10^{13} human cells (Bianconi et al. 2013). This number (37.2×10^{13}) was estimated based upon the total number of microbes/gram found in the intestinal tract and the total volume capacity of the alimentary tract estimated to be 1 L. Nearly four and a half decades later, T. D. Luckey's hypothesis was challenged and reanalysis by Ron Sender who calculated that the ratio was closer to 1 to 1. This was based upon the revised total volume capacity of the intestinal tract to be around 0.4 mL based on magnetic resonance imaging (MRI) scans. Using this reduced capacity and the microorganism density throughout the alimentary canal, Sender approximated that our microbial populations amounted to nearly 3.7×10^{13} cells, the same estimated number of cells that make up our own body (Sender, Fuchs, and Milo 2016).

In terms of genomics, the 2.91 billion base pair human genome was first published in 2001 (Venter et al. 2001; International Human Genome Sequencing 2001) and later revised/finalized in 2003. Prior to the revealing of its sequence, it was estimated that the human genome was composed of nearly 100,000 protein encoding genes. Surprisingly, the human

genome project demonstrated that there were only a scant 20,500 protein-coding genes (Clamp et al. 2007). In comparison, metagenomic analysis of the human gut microbiota has characterized 3.3 million non-redundant genes; a gene set around 150 times larger than the human genome. Analysis found the human microbiome to contain nearly 8 million unique protein coding genes or 390 times more than the human genome (Qin et al. 2010). What consequence could this immense genetic content and protein producing potential have on the health and disease of the host?

The 6.5-meter length of the human gastrointestinal tract hosts the highest presence of microorganisms and therefore the "lion's share" of this extended bacterial genome. The microbial biomass in the human small intestines reaches cellular densities between 10^4 and 10^5 per milliliter of chime, while the large intestines plays host to considerably higher amounts, estimated between 10^8 and 10^{11} cells per milliliter of fecal matter (Wang et al. 2005; Wang et al. 2003). Visualized in figure 9, the microbial biomass changes throughout the alimentary canal, with the highest concentration present in the large intestine. This is primarily due to the drastic changes in pH that occur throughout the tract and resources availability (Walter and Ley 2011). The desire to determine which microbes are present and how they may impact host physiology has opened up the field of microbiome sequencing. Its history is discussed in the next section.
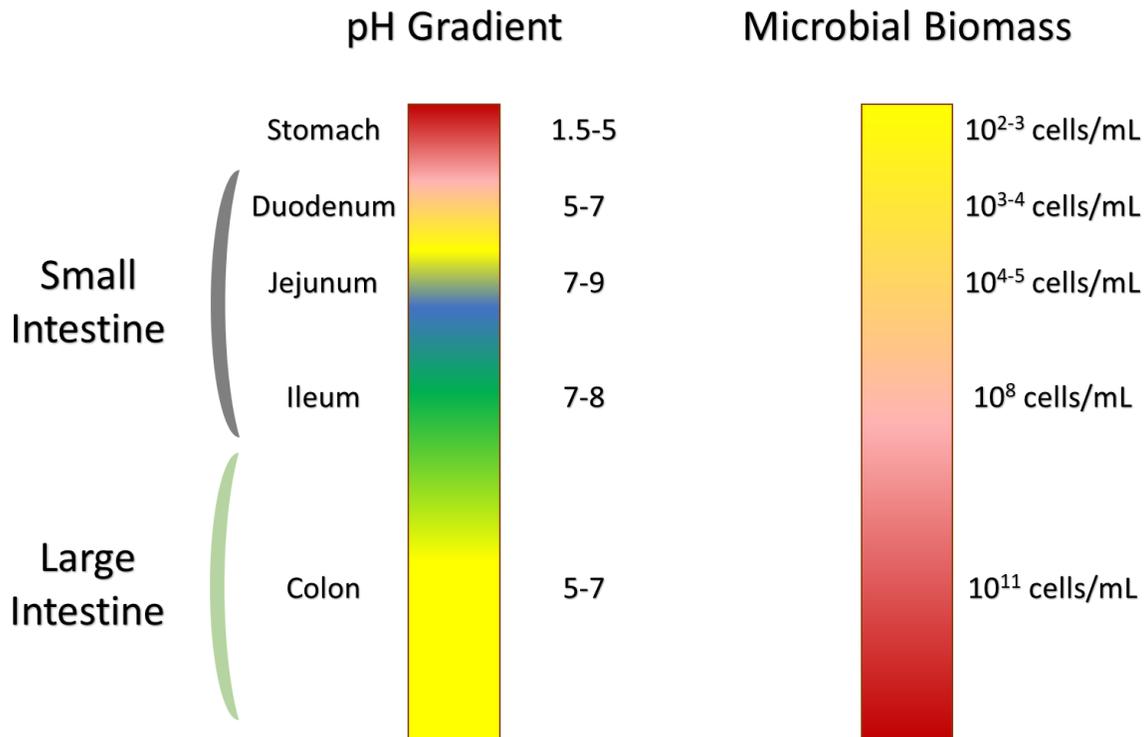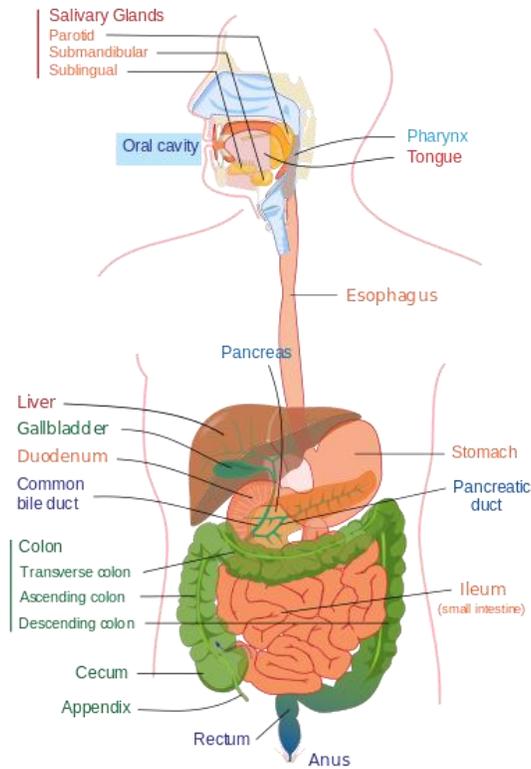
Figure 9.   Diversity of biomass through the human gastrointestinal tract.
Differences in bacterial load between different parts of the alimentary canal as pH changes.
Figure recreated by author (GI tract is a public domain image (Wikimedia commons)) and
based on Jens Walter, Annual Review of Microbiology (Walter and Ley 2011).

2.1.1.2. Sequencing and analysis history of the microbiome

Our ability to determine the nucleotide sequence of a DNA fragment has increased in accuracy and speed exponentially over the past century, since Ray Wu first published a method for DNA sequencing in 1972 (Wu 1972). This string of nucleotides, the DNA molecules, were first identified by Friedrich Miescher in 1871 (Miescher-Rüsch 1871). Nineteen years after the accurate deduction of the DNA double helix by James Watson, Francis Crick and Rosalind Franklin (Watson and Crick 1953), it was Ray Wu at Cornell who developed the first method for DNA sequencing (Wu 1972). Double Nobel laureate and sequencing pioneer, Frederick Sanger added his primer-extension technique to create more rapid DNA sequencing techniques (Sanger, Nicklen, and Coulson 1977). These techniques will be discussed later in this chapter.

Sanger was the first to publish an entire genome of an organism; The bacteriophage phi X174, which contained approximately 5,375 nucleotides (Sanger et al. 1977). Sanger's chain-termination method, better known as Sanger sequencing, was the method of choice for DNA sequencing until the mid-2000s. Advancements to the Sanger sequencing technique, including faster reading techniques, were responsible for the completion of the first complete human genome (Venter et al. 2001; International Human Genome Sequencing 2001). Sequence commercialization and advancements in computing have resulted in the creation of numerous industrial high-throughput methods, such as Illumina sequencing (used in this study), 454-Pyrosequencing, Ion Torrent sequencing and Single-molecule real time sequencing. Detailed description of these methods will be discussed later in this chapter.

2.1.2. Background

2.1.2.1. The microbiota

Our understanding of the microbial communities in the environment has surged over the past few decades with the development of high throughput DNA sequencing technologies, cultivating with next generation sequencing technologies. This is primarily due to the speed and accuracy at which these microbes can now be identified as well as computing advances (bioinformatics) in analysis of results. Most microorganisms are difficult to culture and thus have historically been difficult to identify. Culturing microbes from a variety of environments can also result in favorable environments for some and unfavorable for others, thus biasing the results and changing the total compositional profile. Utilization of gel electrophoresis technologies by Sanger sequencing were slow compared to modern technologies and required immense manpower for sequencing. This was because each nucleotide was determined by each individual lane in the gel, as demonstrated later in this chapter (2.1.5 Sequencing Techniques). Since then, the generation of a more robust Taq polymerase through DNA recombinant technologies, the ability to fluorescently tag nucleotides, improvements in fluorophore detection and the prodigious advancements in computer science have rendered these older techniques obsolete. The identification of microbes using culture-independent DNA sequencing acts as a magnifying glass, allowing us to discover and catalog the world of microbes.
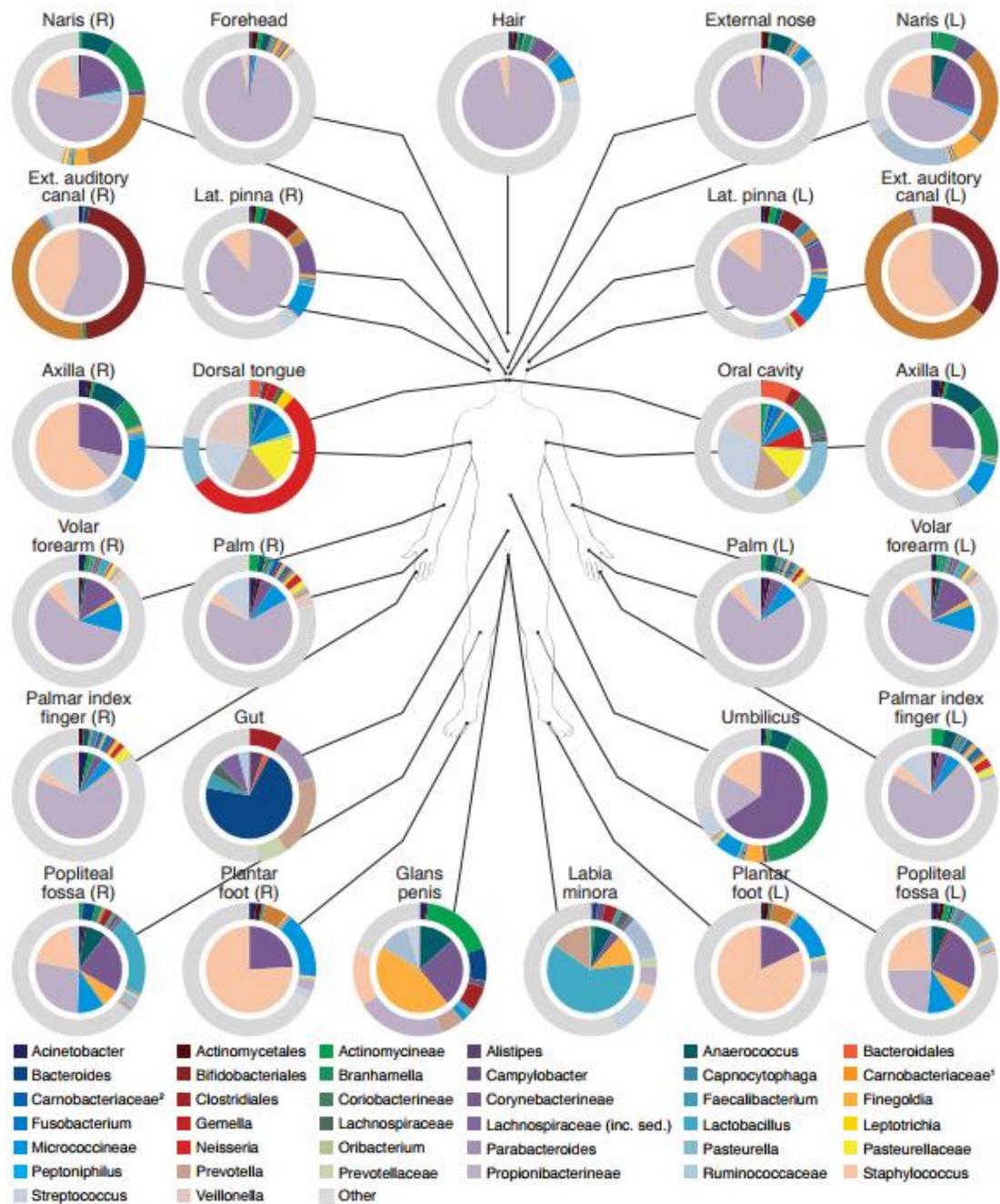
Figure 10. Assortment of microbial populations throughout the human body.
The biodiversity of bacterial communities throughout the human habitat is extreme as shown
by pie graphs for different regions throughout the body. Visualization of the varied
populations, demonstrates that our bodies may be better defined as ecosystems. Figure
obtained from Elizabeth Costello, Science 2009 (Costello et al. 2009).

35

Our microbiota is comprised of a wide group of microorganisms, ranging from bacteria and archaea to fungi and viruses. In total they make up around 3% of our body mass, resulting in nearly two and a half kilograms (5.5 lbs.) in an eighty-kilogram (176.4 lbs.) adult. The variety in bacterial composition as well as their colonization locations are demonstrated in figure 10. Research has shown the importance of the microbial presence with the formation of germ-free mice. It has been reported that the microbiota in our gut is responsible for metabolism of non-digestible carbohydrates to yield short chain fatty acids (SCFA) as a waste product of fermentation, which act as an energy source for intestinal epithelial cells (Layden et al. 2013). Essential amino acids, vitamin K, B vitamins and folic acid are synthesized by the intestinal microbial population and are absorbed by the host (LeBlanc et al. 2013). The regulation of the endocrine network by the microbiota through manipulation of bile acids, gastrointestinal hormones, lipid metabolites and neurotransmitters has also been demonstrated (Ridlon et al. 2014; Kasubuchi et al. 2015).

2.1.2.2. Microbial co-evolution

The co-existence of microorganisms with animals has been found throughout the animal kingdom. Little was understood about our inventory of microbes just a decade ago. The co-evolution of the host and their microbial counterparts is almost impossible to establish, due to lack of coprolites, or fossilized feces. One exception to this was in 2008 when Raúl Tito examined two 1,300-year-old paleofecal samples from cave deposits near Durango, Mexico. Conclusions from their next generation sequencing study showed the prominence of both *Bacteroidetes* and *Firmicutes* phyla (Tito et al. 2008), similar to predominant phyla found in the current human gut (Qin et al. 2010).
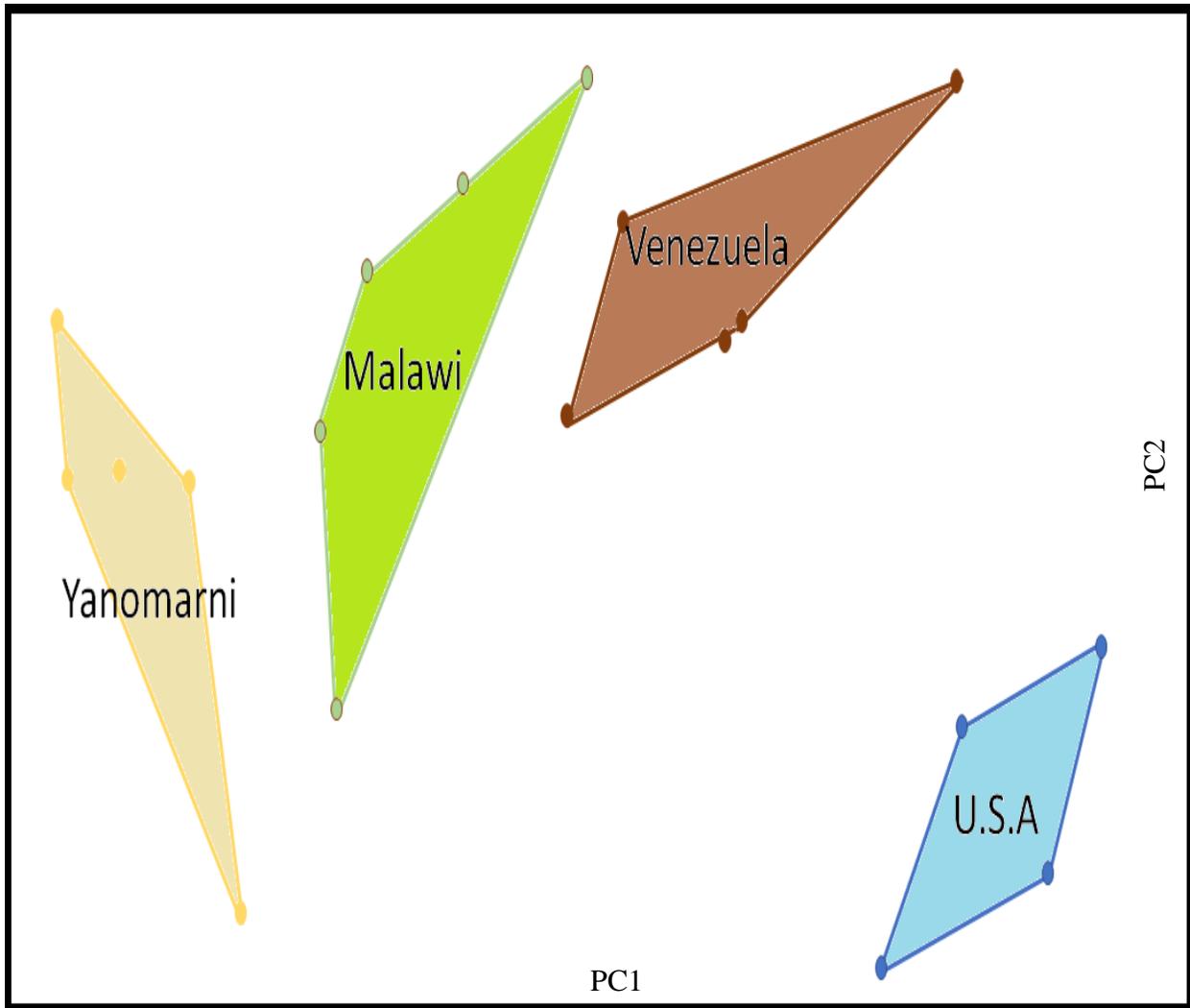
Figure 11. Changes in human gut microbiota diversity based upon location.
This recreated graph demonstrates the impact of food and our environment on our microbial population. Each dot is a raw component score graphed by the researches (recreated here) and compared on a principle coordinates analysis (PCA) plot. Samples from individuals with comparable diet and locations were clustered together demonstrating similarities between them, while differences in diet and location cluster apart. Figure visually adapted from Emily Davenport, BMC Biology (Davenport et al. 2017) .

The Hologenome theory of evolution developed by Eugene Rosenberg and Ilana Zilber-Rosenberg, considers both the animal or plant along with all of its associated microorganisms together as units of selection in evolution (Zilber-Rosenberg and Rosenberg 2008). The

importance of bacterial populations in *Drosophila melanogaster* demonstrated this concept by

showing that manipulations of fruit fly intestinal flora resulted in altered mating patterns and a

change in offspring production. (Sharon et al. 2011). Furthermore, changes in gut bacteria also

modulated body mass of female, but not male fly offspring, suggesting a trans-generational

effect of parental gut-microbiota (Morimoto, Simpson, and Ponton 2017).

2.1.2.3. The Homo sapiens ecosystem

You are your body's "wildlife" manager. Our bodies represent a biosphere that possesses

a wide variety of ecosystems, similar to deserts and rainforests, each colonized by different

animals and planets. These microbes have evolved to replicate and flourish in their particular

microenvironment on our body. Just like these larger ecosystems on the Earth, various human

body parts form microbial communities that coexist with us. These ecosystems require

organisms to be able to obtain resources and survive challenges generated by different variables

within a particular including temperature, pH, water availability, oxygen richness, and resource

accessibility. These stressors impact the presence of the microorganisms that reside there,

altering their composition, genetic materials, metabolites and consequently their impact on our

bodies (Jordan et al. 2015). The selectivity of the human GI tract in comparison to other

ecosystems can be seen in figure 13, where two bacterial phyla, Bacteroidetes and Firmicutes,

primarily dominate the vertebrate gut in comparison to soil samples, where more than 70

different phyla can be present.
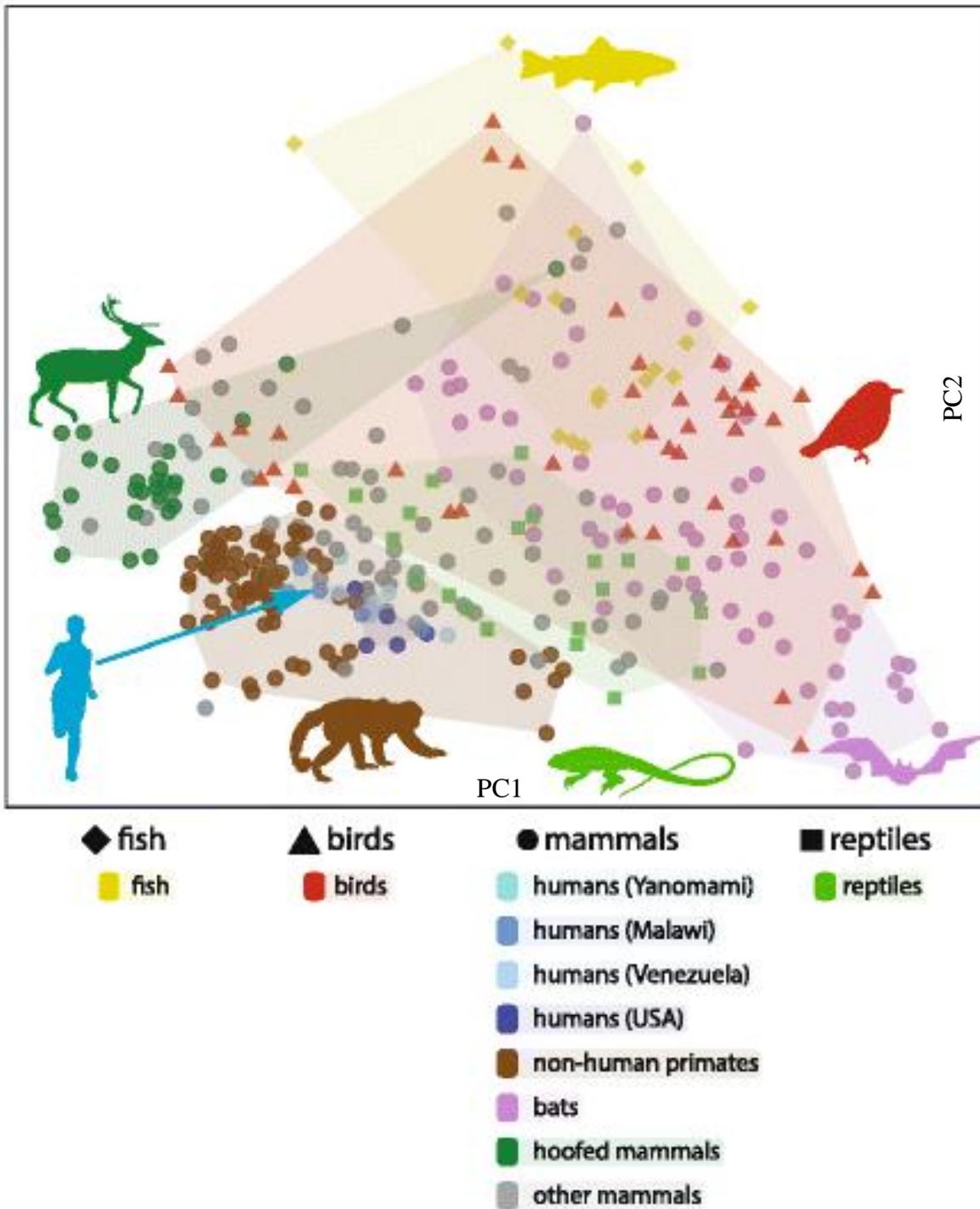
Figure 12. Gut microbiota diversity amongst the biological kingdom Animalia.
This figure demonstrates that when compared to other residents of the animal kingdom, the human intestines are very selective towards microbial populations whereas variations between human populations seems indiscernible. Raw component scores from each population are represented as colored dots on a PCA plot with the legend equating colors to animals. Figure adapted from Emily Davenport, BMC Biology (Davenport et al. 2017).

2.1.2.4. Diversity of the gut microbiome

Within the human gut resides an estimated 160 distinct species of bacteria (Qin et al. 2010). The majority of these belong to the *Bacteroidetes, Firmicutes, Actinobacteria,* and *Proteobacteria* phyla. Amongst human populations, the percentage of these phyla differs based upon location, diet and environment (Moodley et al. 2009). For example, comparisons between the microbial populations of humans residing in industrialized regions, such as the United States, versus non-industrialized areas, such as the amazon, (Figure 11) demonstrates the changes in diversity of these microorganisms. Analysis by 16S rRNA sequencing, has shown that the intestinal microbiota of humans in first world countries, contains lower diversity levels than their third world cousins (Davenport et al. 2017). Diversity meaning the difference in abundance between the different types of microorganisms that reside within the intestinal tract (analyzed through fecal matter) of these populations.

Detailed analysis of diversity changes in gut microbiota moving to other taxonomic levels was accumulated by Davenport et al.. The graphed results (Figure 12) illustrate the changes in microbiota during evolution. As the microbial compositions of more evolved organisms are analyzed, they cluster closer together, for example in birds (lower on the evolutionary tree) the 16S reads are dispersed when compared to hoofed mammals (higher on the evolutionary tree) whose reads are clustered closer together. This suggests that as more complex species evolve, selective pressure is placed on the microbial community that reside on them and their bacterial diversity is reduced. Although figure 11 seems to show big differences between human populations, analysis against mammals, fish, birds and reptiles, minimizes these distances when compared against others in the animal kingdom (Figure 12) (Davenport et al. 2017).
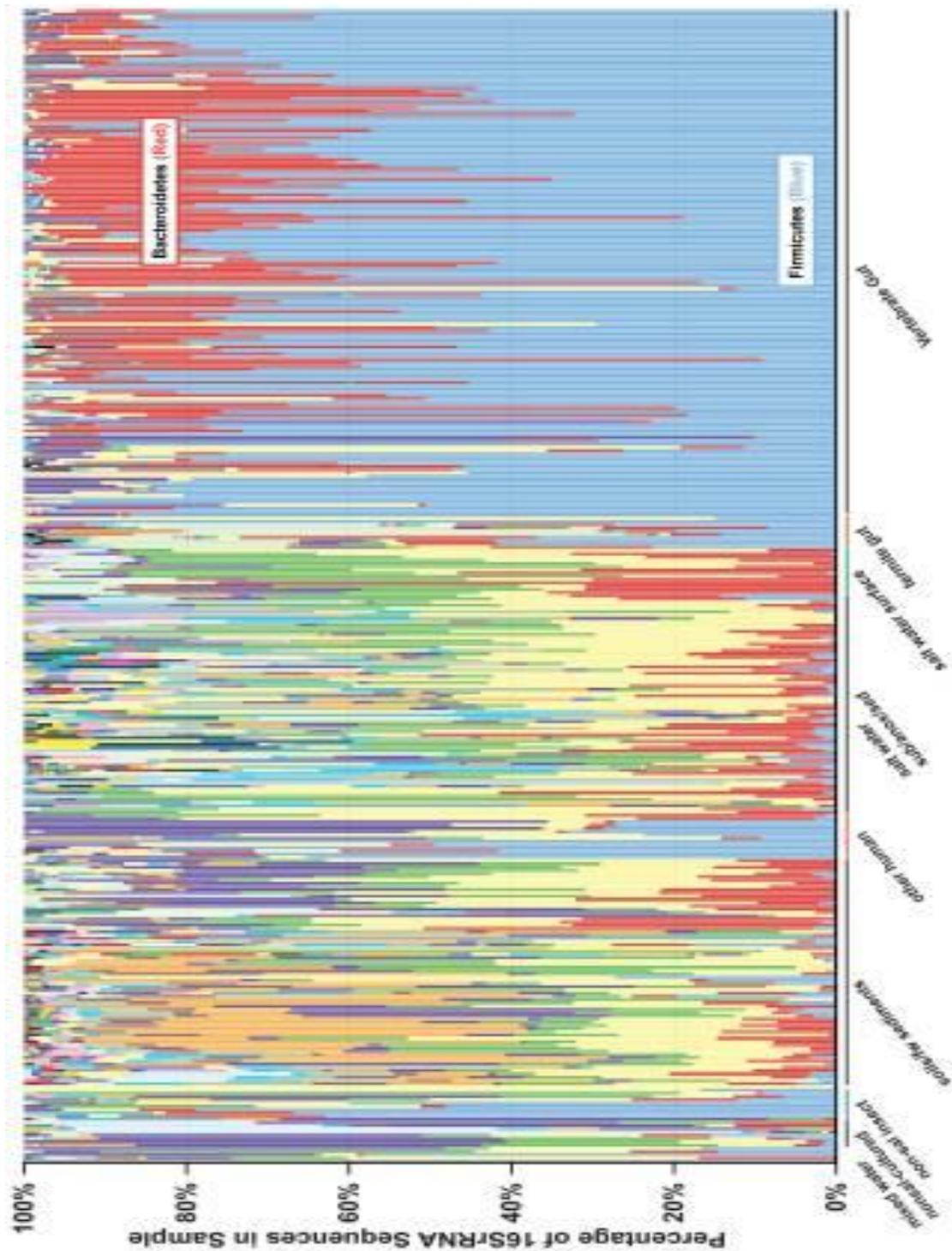
Figure 13. Selectivity of the human gut in comparison to other ecosystems.
Each color in this bar graph represents the percent of a particular phylum present within a
sample which is indicated on the x-axis. This demonstrates the selectivity of the vertebrate
gut and its two primary phyla, Bacteroidetes (red) and Firmicutes (blue), when compared to
other environments such as soil and salt water. Figure from ('Structure, function and diversity
of the healthy human microbiome' 2012).

41

When analyzed, the microbiomes of humans consuming a western diet (60 kcal% fat) vs a non-western diet (10 kcal% fat), were considerably different. The western diet microbiomes were composed of higher percentages of Bacteroides in comparison to non-western microbiomes, that consisted of higher percentages of Firmicutes and Proteobacteria (Rampelli et al. 2015; Schnorr et al. 2014; Clemente et al. 2015). The western populations also consisted of 15 to 30% fewer microbial species than non-western populations. This has led to the hypothesis that industrialization and westernization are responsible for the reduction of intestinal diversity (or the gradual disappearance in species from the human gut over time). It is theorized this is due to the focus on sanitation and drastic changes in our diet, such as increased consumption of animal products (Segata 2015). The western diets are also rich in sugars and fats, and poor in fiber; which is the opposite of non-western diets. This along with the bigger focus on hygiene and greater use of antibiotics in western populations may be responsible for decreased diversity (Blaser and Falkow 2009).

2.1.2.5. Causes of gut microbiota change

Methods of fetal delivery, such as cesarean section vs natural delivery can inoculate a newborn with different bacteria. The natural delivery method results in introduction from the mother's fecal and vaginal microbes, whereas a cesarean birth (C-section) results in the introduction of skin microbes (Gueimonde et al. 2006). In addition to the mother's skin, C-section infants are exposed bacteria present in the operating room (Shin et al. 2015). Babies are born with a small placental microbiome present and an intestinal tract that becomes colonized with different microbial populations over time (Wassenaar and Panigrahi 2014). These bacterial populations constitute the newborns GI tract immediately after birth. For the first three months of life, C-section infants, in contrast to natural born babies, possess a lower diversity of

Actinobacteria, *Bacteroidetes* and *Bifidobacterium* with a concomitant increase in variety of

Firmicutes in their feces (Rutayisire et al. 2016). Chu et al. have demonstrated that the microbial

community structure is only impacted by birthing method during the first 6 weeks of life, after

which it is primarily driven by differences in food intake (Chu et al. 2017). Other studies have

suggested the change can last 6 to 12 months (Rutayisire et al. 2016) or even up to 2 years

(Jakobsson et al. 2014). This lack of consistency can be linked to difficulties in controlling infant

environment and diet.

The differences in the type of milk fed to the infant can also impact their gut microbiota.

The specific compounds present in human milk are thought to be involved in the establishment

and development of the early gut bacteria. Commensal bacterial populations seem to benefit

from the intake of breast milk in comparison to formula (Holscher et al. 2012). The addition of

prebiotic oligosaccharides to formula has shown to bring the gastrointestinal microbiota closer to

that of breast fed infants. These prebiotics also decrease fecal pH and increase short chain fatty

acids (SCFA) while reducing diarrhea and bringing fecal consistency to a similar level to breast

fed infants (Vandenplas, Zakharova, and Dmitrieva 2015). By eleven months, the microbiota of

the infant becomes distinct from their mother (Vaishampayan et al. 2010). After the first year,

the gastrointestinal microbiota starts to resemble that of an adult human (Palmer et al. 2007).

From this age (> 1 year), the types of food eaten and the environment in which the child resides,

play the largest roles in shaping the microbiota composition. As visualized in figure 14, the

human microbial composition changes with age and influences human health. A study in Japan

analyzed the microbiomes of subjects ranging from newborns to centenarians and demonstrated

that the gut microbiota changes throughout our lifespan (Odamaki et al. 2016). Below is a list of

the modifying factors that alter gut microbiota composition throughout life. List generated based on data from Abubucker et al. (Abubucker et al. 2012).

- Infant (up to 2–3 years)

  - Vaginal vs caesarian delivery

  - Gestational age

  - Infant hospitalization

  - Breast vs formula fed

  - Age at solid food introduction

  - Malnutrition

  - Antibiotic treatments

- Adult

  - Diet

  - Hormonal cycles

  - Travel

  - Therapies

  - Illness

- Elderly (> 70 years)

  - Lifestyle changes

  - Nutritional changes

  - Increased susceptibility to infections and inflammatory diseases

  - Use of more medications
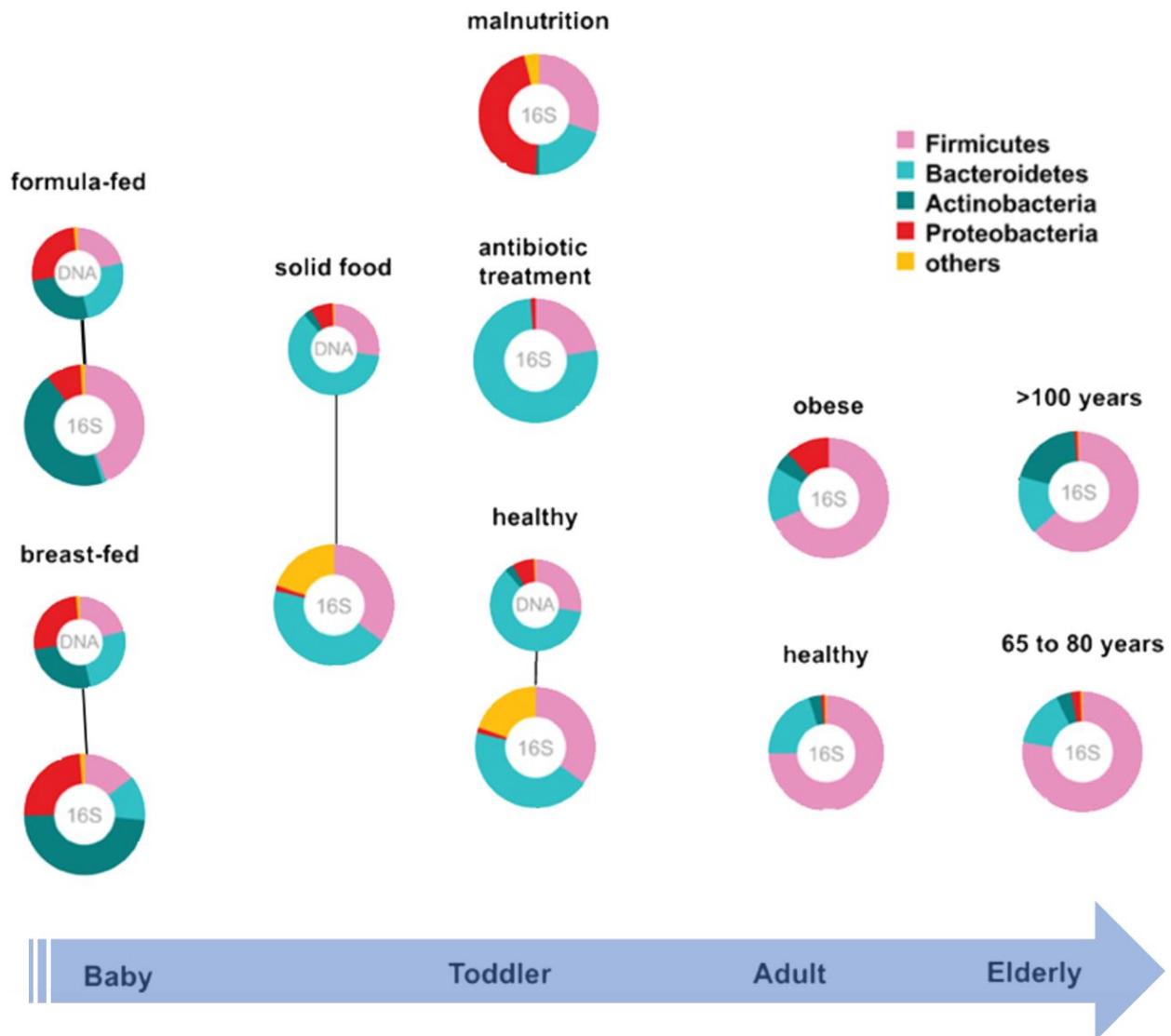
Figure 14. The change in our intestinal microbiota composition through different stages of life.
This figure complies changes in the main bacterial phyla from different studies and visually demonstrates the key established factors that determine how they could change over a lifetime. The blue arrow demonstrates human age with above pie charts representing bacterial phyla. Figure recreated with data and pie charts from (Ottman, Smidt, and Belzer 2012).

2.1.3. Implications in disease

The composition of microorganisms that inhabit the human body can vary. Their vast

metagenomic capability have resulted in the classification of the microbiota as an invisible

endocrine organ. Comparisons between the microbiota and other endocrine organs are discussed later in this chapter. An imbalance in this organ/community, through high-fat, high-sugar western diets or the excessive use of antibiotics can lead to changes in its composition, as well as changes to host endocrine secretions. For example, Aquilera et al. demonstrated that the use of antibiotics and stress (water avoidance) resulted in increased bacteria with the ability to adhere to the intestinal mucosa (Aguilera, Vergara, and Martinez 2013).

Barouei et al. showed that a high fat diet altered liver hormones, reduced short chain fatty acids (SCFA) in the intestines and urine metabolites along with the intestinal microbiota (Barouei et al. 2017). The impact of microbial secretions and their impact on numerous body systems has led to the association of the microbiota with a number of diseases, such as metabolic syndromes (obesity), diabetes, rheumatoid arthritis, Crohn's disease, ulcerative colitis, cardiovascular disease, autoimmune diseases and neurological disorders such as autism (Tremaroli and Backhed 2012; Tilg and Moschen 2014; Singh, Qin, and Reid 2015; Petra et al. 2015).

2.1.3.1. Obesity

Obesity is an energy disorder, where net excess intake of calories compared to energy expenditure causes increased fat deposition and body weight. Studies of the microbiome of obese and normal mice have demonstrated differences in the composition and function. Obese mice particularly exhibited a reduction in the total percentage of Bacteroidetes and an increase in the Firmicutes phyla (Ley et al. 2005). The change of this ratio has also been demonstrated in human populations. Studies of obese patients revealed the same increase in Firmicutes and decrease in Bacteroidetes (Murphy, Velazquez, and Herbert 2015). Interestingly, once these obese patients

were placed on a calorie restrictive diet, this F:B relationship reverted to ones found in leaner individuals (Ley et al. 2006).

Using C57BL/6J (B6) WT and Rag1$^{-/-}$ mice, Fredrik Bäckhed, demonstrated that the obesity phenotype was transmissible through the microbiota and not dependent on lymphocytes (Rag1$^{-/-}$). In their first experiment (figure 15a), both wild type and germ-free mice were fed a high-fat/high-sugar western diet, but the obesity phenotype was only observed in the wild type mice. The microbiota of the wild type mouse was altered (↑ F/B ratio) along with weight gain. This result suggests that the lack of a microbial community in the germ-free mice protects the mouse from died induced obesity. In their second experiment (figure 15b), three groups of germ-free and three groups of wild type mice were utilized. The wild type mice were split into normal, obese and underweight categories. Microbiota from each of these three wild type categories were transplanted into each of the three germ-free groups. Remarkably, the previously-germ-free recipients group adopted the phenotypes of their donors, resulting in a normal, obese and underweight phenotype (Bäckhed et al. 2004). Similar findings have been discovered with fecal microbiota transfers from obese human donors to germ-free mouse. The mice in these studies have also resulted in donor phenotype adoption. This observation has been contested by other researchers who failed to find phyla level differences based upon obesity (Bell 2015; Rabot et al. 2016). Recent advancements on this ratio have focused on the ratio of gram negative to gram positive bacteria rather than the ratio of these two phyla (Kasselman et al. 2018).
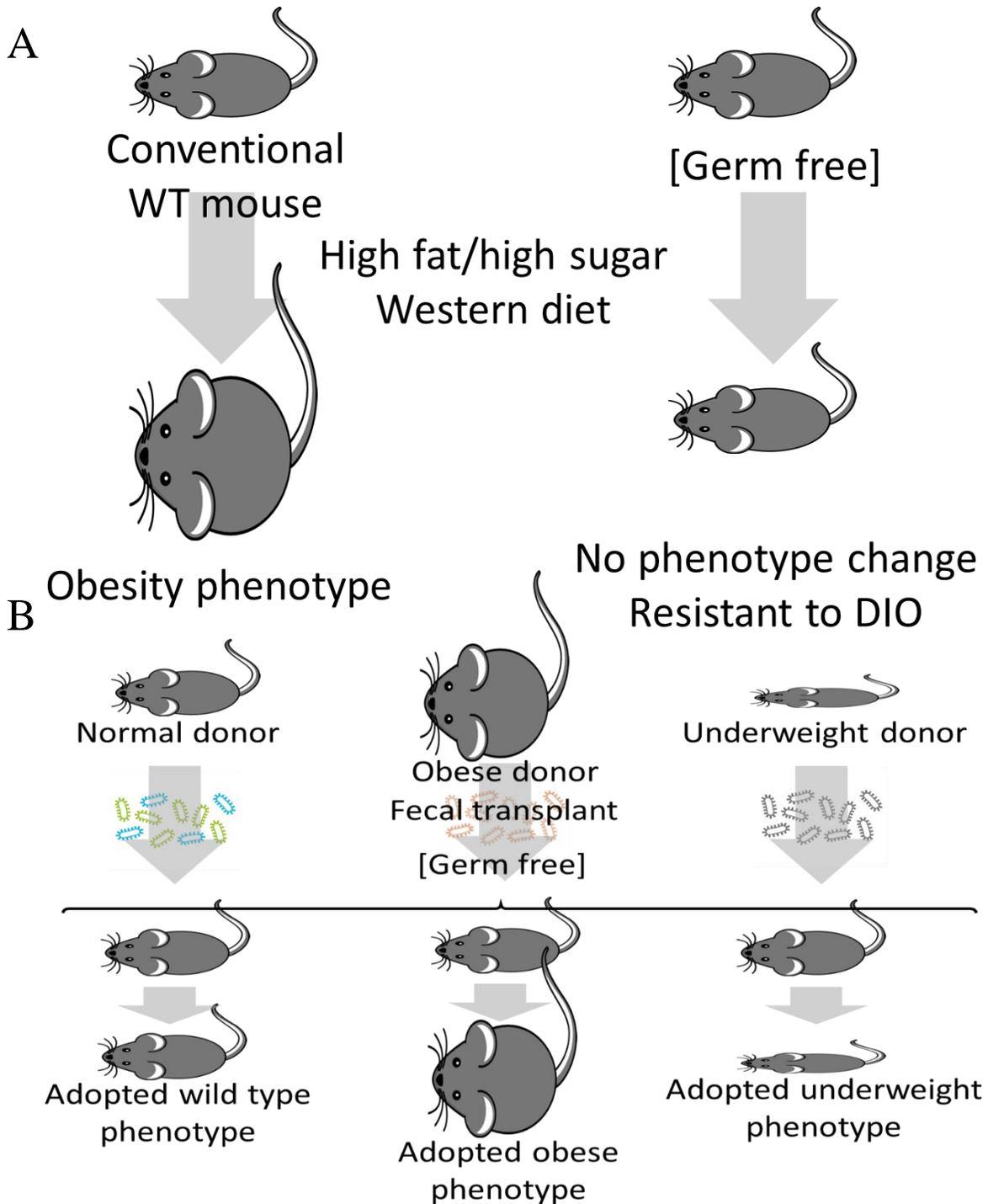
Figure 15. Importance of microbiota function in weight control.
A. The utilization of a high fat/high sugar diet in conventional versus germ free mice results in the adoption of an obese phenotype in the conventional wild type mice whereas the germ-free mice remain resistant to diet induced obesity (DIO). B. Transplantation of the intestinal microbiota from wild type, obese, and underweight donors into germ-free mice results in the adoption of the donor phenotype in the fecal recipient. Figure recreated and based on data from (Clarke et al. 2014).

Numerous individual bacteria have been implicated in obesity. One study in Shanghai, China, sequenced the microbiome of a morbidly obese volunteer, and found 35% of his gut bacteria to be *Enterobacter*. This opportunistic pathogen dropped to undetectable levels after the individual lost 51.4 kg (113.3 lbs.) of his total 174.8 kg (385.37 lbs.) weight, by dieting for 23 weeks. Upon isolation and introduction of this endotoxin producing pathogen into germ-free mice on a high-fat diet, researchers found the mice to become obese and insulin resistant when compared to mice not inoculated with the *Enterobacter*. This same phenotype was not observed with normal chow, suggesting a dramatic increase in *Enterobacter* through high fat diet consumption and may contribute to the obesity phenotype in humans (Fei and Zhao 2013). This relationship between obesity and the microbiota may hold potential therapeutic implications.

2.1.3.2. Inflammatory bowel diseases

Research into inflammatory bowel diseases (IBD) has suggested a link between microbial composition and the severity of these conditions (Becker, Neurath, and Wirtz 2015; Sheehan, Moran, and Shanahan 2015). An estimated 3 million adults in the United States are diagnosed with IBD annually (Dahlhamer et al. 2016). IBD is an umbrella term used to describe chronic, idiopathic, inflammatory gastrointestinal (GI) disorders. Ulcerative colitis and Crohn's disease, are collectively defined as inflammatory bowel diseases. These two disorders have distinct pathogenic and inflammatory profiles (figure 16). Ulcerative colitis is characterized by continuous rectal bleeding, diarrhea, abdominal pain, and mucosal inflammation in the rectum that spreads proximally up the large intestine. Crohn's disease may affect any part of the gastrointestinal tract and patients suffer from weight loss, diarrhea and pain with increased risk of cancer.
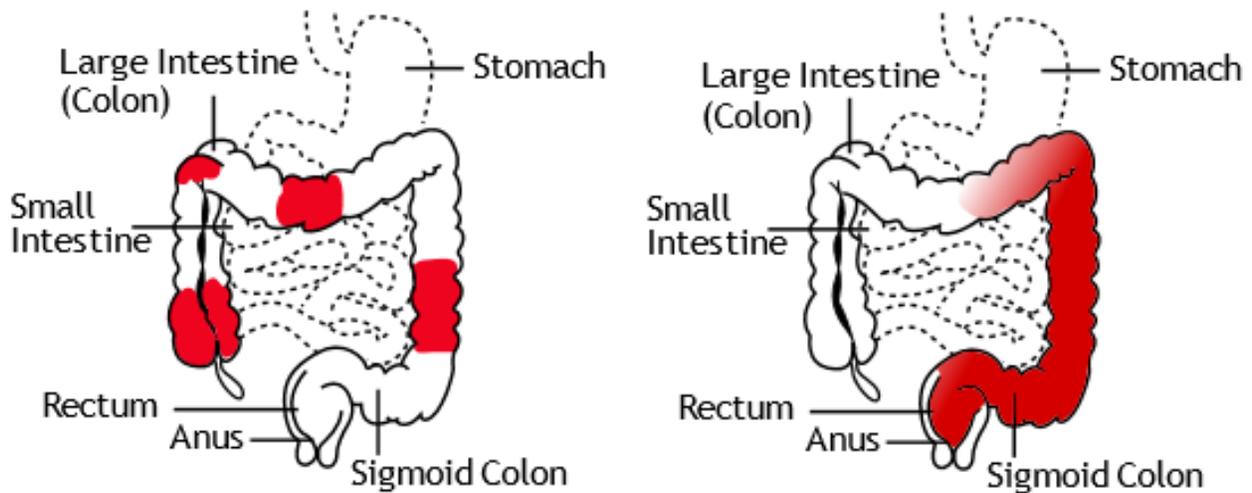
| Crohn's Disease | Ulcerative Colitis |

Figure 16. Disease state differences between Crohn's disease and ulcerative colitis. This figure demonstrates inflammation patterns (red color) between Ulcerative colitis and Crohn's disease. Ulcerative colitis only affects the large intestine and moves proximally up the colon while Crohn's disease can affect the entire gastrointestinal tract, with a discontinuous pattern of inflammation that can develop anywhere throughout the alimentary canal, from the mouth all the way to the anus. Image adapted from Wikimedia commons, under the creative commons license.

The gastrointestinal tract and the microbiota contained within are responsible for food digestion, nutrient extraction, absorption and waste expulsion. Disruption of these essential processes can be extremely harmful to the body. Researchers have confirmed that IBD patients suffer from numerous vitamin deficiencies and have lower levels of minerals, such as zinc, iron, and magnesium proposed to be caused by a reduction in intestinal absorption (Valberg et al. 1986; Dotevall and G Kock 1968; Lomer et al. 2004). A characteristic of IBD is damage to the intestinal mucosal epithelium. A study conducted by Sarkis K. Mazmanian showed the protective capacity of the human microbiota against IBD inflammatory parameters and epithelial mucosal tight junctions. Mazmanian reported that *Bacteroides fragilis* protected mice from colitis induced

by an opportunistic pathogen, *Helicobacter hepaticus*, through the production of polysaccharide A (PSA). This was done by comparing a mutant strain of *Bacteroides fragilis* that did not possess the ability to produce PSA against the wild type strain. Previous studies that analyzed the immune response during IBD have demonstrated that IL-17 is a key mediator of colitis (Elson et al. 2007). When Mazmanian et al. analyzed the two groups, they observed that mice without PSA expressed significantly higher amounts of IL-17 in comparison to their PSA counterparts. They concluded that PSA administration was required to suppress IL-17 inflammatory response in intestinal immune cells. In contrast, mice housing *B. fragilis*, but not expressing PSA, experienced H. hepaticus mediated IBD. PSA was also found to increase IL-10 production, a potent anti-inflammatory cytokine (Mazmanian, Round, and Kasper 2008). PSA mediates immune anti-inflammatory response through IL-10 secretion induced by plasmacytoid dendritic cell which when exposed to PSA stimulate IL-10 secretion by CD4+ T-cells (Dasgupta et al. 2014). This along with other studies speak to the importance of a healthy microbiota and to the connection between microbial dysbiosis and IBD.

2.1.3.3. Integumentary system ailments

The skin, hair and nails all make up the integumentary system, which is also colonized by a heterogeneous population of bacteria. Visualized in figure 17, the variety of microbes that inhabit the various regions of the integumentary system demonstrates the various ecosystems present on the human body. Colonization of these ecosystems is driven by the ecology of the specific environment, which depends primarily on exogenous environmental factors, like temperature, sun exposure, humidity, food availability, pH and region of the host (Grice and Segre 2011). Skin diseases like psoriasis, acne and eczema all seem to be directly related to changes in microbial composition (Kong 2011). The relapsing pruritic inflammatory skin

disorder known as eczema has been on the rize over the past 30 years. Ninety percent of eczema patients show an increase in the presence of *Staphylococcus aureus* on their skin, a bacteria not seen on control patients. This bloom in *S. aureus*, decreases microbial diversity on the skin possibly driving the pathobiology of eczema (Kong et al. 2012). *S. aureus* blooms were limited by the presense of *Staphylococcus epidermidis*, which inhibits *S. aureus* growth (Iwase et al. 2010). These findings demonstrate a possible novel approach where microbes could be used to combat worrisome pathogens instead of current antibiotic therapeutic treatments.
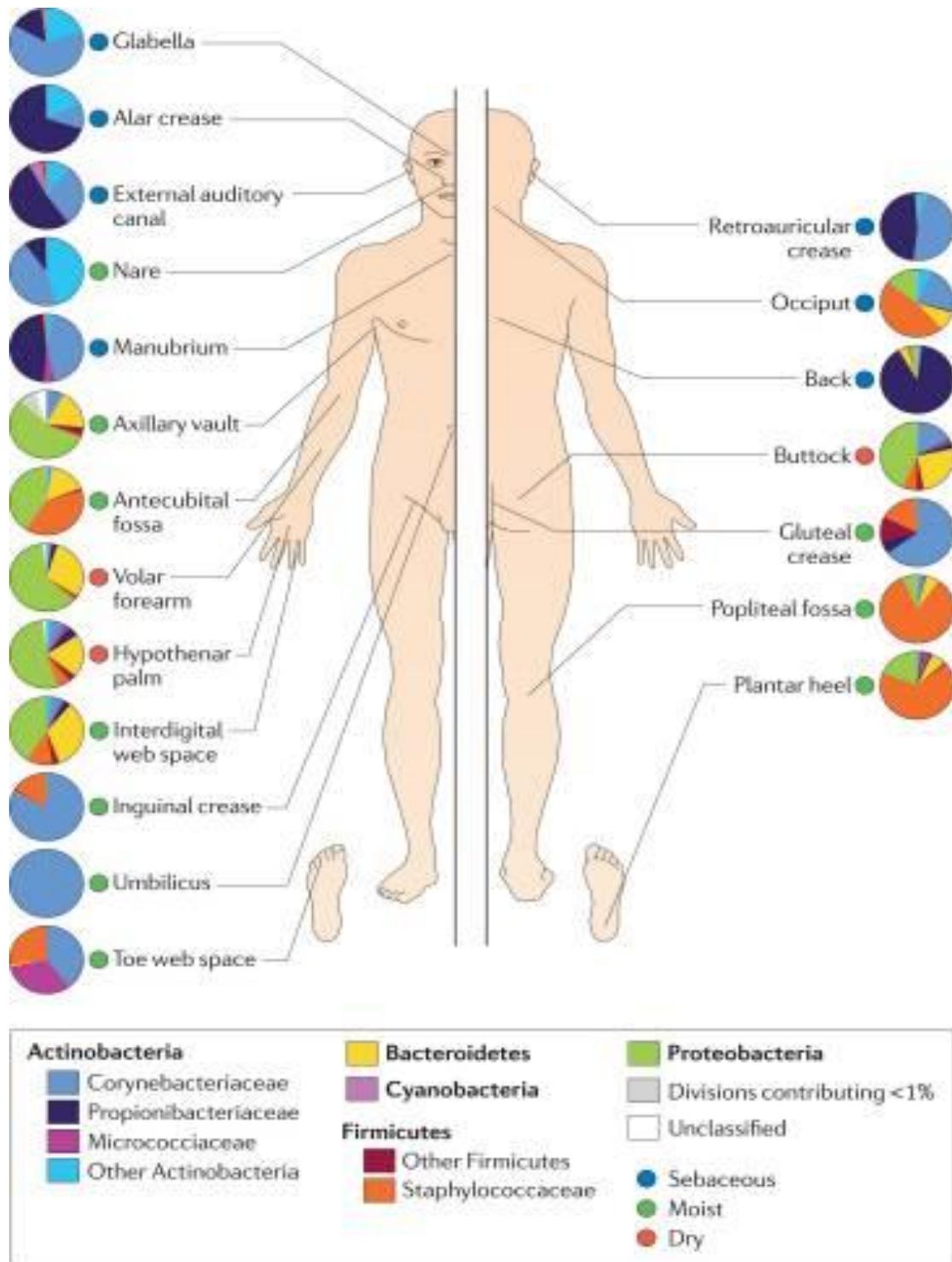
Figure 17. Distribution of bacterial populations on the skin.
This figure demonstrates the drastic changes in bacterial populations throughout the integumentary system. Colors on the pie chart are representative of families of bacteria and correspond with skin sites all over the body. The sites seem to group in correspondence with the presence of oils and moisture. Figure from Elizabeth Grice, Nature (Grice and Segre 2011)

2.1.3.4. Immune system disorders

According to the National Institutes of Health, the immune system is a network of cells, tissues, and organs that work together to protect the body from infecticious diseases and self diseases like cancers (Candeias and Gaipl 2016). Research into autoimmune diseases, has demonstrated a connection between host microbiota and immune response/activation (Thaiss et al. 2016). For example, polysccharide A protects against IBD (discussed in 2.1.3.2. Inflammatory Bowel Diseases) and is secreted by *B. fragilis*. Proteolytically processed peptides from PSA are presented to CD4 T-cells on MHC class II complexes by dendritic cells resulting in cytokine production which stimulates T regulatory (Treg) cell development and increases non-inflammatory cytokines like IL-10. Utilization of a PSA mutant was unable to restore normal immunological function. Germ free mice (not possessing any microbiota) have reported defects in splenic size, cell number, and development. The addition of wild type *B. fragilis* seems to restore the mouse spleens to normality, while germ-free mice colonized with *B. fragilis* with mutated PSA, were unable to commence splenic organogensis, demonstrating the direct link between PSA from bacteria influencing immune cell numbers (Mazmanian et al. 2005).

This relationship is seen in a number of autoimmune disorders such as diabetes mellitus type 1. This debilitating disease is caused by the autoimmune destruction of insulin producing β cells in the pancreas (Xie, Chang, and Zhou 2014). The rise of this devastating autoimmune disorder in the developed world has caused many scientists to purpose a connection to environment, diet and the host microbiota (Patterson et al. 2001). Non-obese diabetic (NOD) mice can be utilized to better understand type 1 diabetes, due to their spontaneous development of the disease. The rates of these incidents can be affected by alterations to their microbiota (Sadelain et al. 1990). Amazingly, NOD mice deficient in myeloid differentiation primary

54

response 88 (MyD88) protein are resistant to type 1 diabetes while NOD MyD88WT are not, suggesting an innate immune mechanism as MyD88 is essential for toll like receptor signaling during PAMP recognition (Wen et al. 2008).

The pathway for the MyD88 intracellular signaling molecule is initiated from multiple toll like receptors (except TLR4 and TLR3) to activate nuclear factor-κB (NF-κB). A study conducted by Kubinak et al. demonstrated that signaling through the T-cell MyD88 pathway was essential for the development of IgA secreting B-cells in lymphoid germinal centers. This was tested by comparing wild type to T-cell specific MyD88 knockout (T-MyD88KO) mice. The T-MyD88KO mice had reduced numbers of IgA secreting B-cells, suggesting the importance of T-cell specific MyD88 signaling for germinal center activation of these B-cells. Analysis into the impacts on the microbial populations by the research team also showed community dissimilarities and changes in the mucosal bacterial populations (Kubinak et al. 2015). Other studies have also demonstarted the importance of MYD88 signaling in immune homeostates, protection from infection (Brandl et al. 2007) and intestinal epithelial repair (Pull et al. 2005).

Another major immune disorder linked with the microbiota is Rheumatoid Arthritis (RA). This disease is characterized by chronic pain and inflammation in the joints. Like type 1 diabetes, RA levels in the developed world are also increasing. Human microbiota dysbiosis linked to the widespread use of antibiotics has been considered a culprit in these actions (Patterson et al. 2001). Patients suffering from RA present increased Treg cell numbers in circulation and increased IL-17 levels in the joints (Hot and Miossec 2011). The cause of this increase is currently unkown. Jose Scher has hypothesized that gut disbyosis caused by environmental or genetic factors could allow for the domination of harmful microorganisms. Expansion of a proinflammatory response along with the activation of other immune components

(T cells, B cells and macrophages) could migrate to synovial tissue within the joints and lead to arthritis (Scher and Abramson 2011).

2.1.3.5. Nervous system disorders

Variations in the intestinal microbiota have been linked to several nervous system disorders like autism, multiple sclerosis (MS) and anxiety. These are hypothesized due to molecular interactions between the central nervous system and the intestines, dubbed the microbiota-gut-brain axis. This multifaceted axis of communication refers to the cross-talk of metabolites between the microbiota and the brain (Burokas et al. 2015).Thus, the microbiota-gut-brain axis is much more influential than was previously realized.

According to the National Autism Association, "Autism is a bio-neurological developmental disability, which impacts the normal development of the brain in the areas of social interaction, communication skills, and cognitive function." The rise in incidence of this disorder has caused scientists to purpose numerous environmental factors that could play a role such as antibiotics, drugs, infections and the gut microbiota (Dietert, Dietert, and Dewitt 2011). Common symptoms connected with autism include diarrhea, vomiting, constipation and acid reflux. Comparative taxonomic analysis of the intestinal microbiota by 16S rRNA sequencing between control children and ones suffering from autism, showed the genus Sutterella represented 1 to 7% of the autistic children's microbiomes, and was not detected in the control children (Benach, Li, and McGovern 2012). Other studies comparing the two microbiome groups have demonstrated greater amounts of Clostridium species in autistic children in comparison to controls (Finegold et al. 2002). The use of probiotics (ingested microorganisms) along with targeted short term antibiotics has showed temporary improvements in autism intestinal symptoms, which are remarkably similar to those seen in IBD patients (Critchfield et al. 2011).

Multiple sclerosis (MS) is characterized by damage to myelin sheaths of neurons, demyelination, in the brain and spinal cord (Makris, Piperopoulos, and Karmaniolou 2014). This degenerative disease occurs over time and results in a gradual lack of muscle control (Bhargava and Mowry 2014). Currently, the best animal model for MS is the induction of myelin proteins emulsified in an adjuvant to induce an immune reaction. This induced animal model is called experimental autoimmune encephalomyelitis (EAE). The connection between MS and environmental factors such as gut commensal bacteria has been established. Research by Ochoa-Repáraz, demonstrated the reduction of gut bacteria impaired EAE development. They used antibiotic treatment to modify the microbial populations and protect against the onset of MS (Ochoa-Reparaz et al. 2009).

A study conducted by Miyake et al. compared patients suffering from MS to those who were not diagnosed with the disease. While conducting 16S sequences Miyake found changes in MS patients with a depletion in the Clostridia and Bacteroidetes lineages (Miyake et al. 2015). Studies analyzing early onset pediatric MS by Tremlett et al. demonstrated changes in their microbiota composition. Metagenomic analysis by Phylogenetic Investigation of Communities by Reconstruction of Unobserved States (PICRUSt) (discussed later in this chapter), predicted an increase in neurodegenerative pathways (Tremlett et al. 2016). The purposed use of targeted antibiotics or microbiota transfers may provide novel therapies for patients struggling with these neurological diseases (Ren et al. 2017).

2.1.4. Neuropeptides and the microbiota

2.1.4.1. The microbiota-gut-brain axis

The coevolved mutualistic relationship between the host and the gut microbiota has brought about multiple communicational pathways between the microbiota, gastrointestinal

track, and the brain. The multiple signaling pathways between the gut microbiota and the brain have resulted in their denotation as the microbiota-gut-brain axis (Sampson and Mazmanian 2015). Imbalances in this bidirectional communicational conduit have been implicated in numerous diseases such as IBD, MS, or immune system disorders. An example of this includes influence over gastrointestinal hormone production based on the presence of certain probiotics (Dockray 2014). These changes in hormones like ghrelin, the hunger hormone, can allow the intestinal microbiota to regulate appetite (Darzi, Frost, and Robertson 2011).

2.1.4.2. Endocrine classification of the microbiome

The biochemical capacity of the microbiota is colossal. The microorganisms of the human gut perform several essential functions though out our body. Due to microbiota's broad influence and its methods of communication with host tissues, researchers have begun to classify our microbiota as an additional endocrine organ (Clarke et al. 2014). Messages from this "organ" can be carried through the vagus nerve, afferent neurons, cytokines and/or microbial factors secreted into the blood stream (Collins, Surette, and Bercik 2012). The composition of the microbiome can even impact mammalian emotion. Research by Neufeld et al. has demonstrated that germ free mice when compared to specific pathogen-free mice expresses different behaviors. These were tested using mazes and locomotor activity (anxiety measurement). In the maze tests, germ free mice seemed to be more active over time in contrast to specific germ free mice. It was also determined using motor activity tests that the germ free mice acted in a less anxious manner (Neufeld et al. 2011). This suggests that the microbial population may assist in our emotional and mental development.
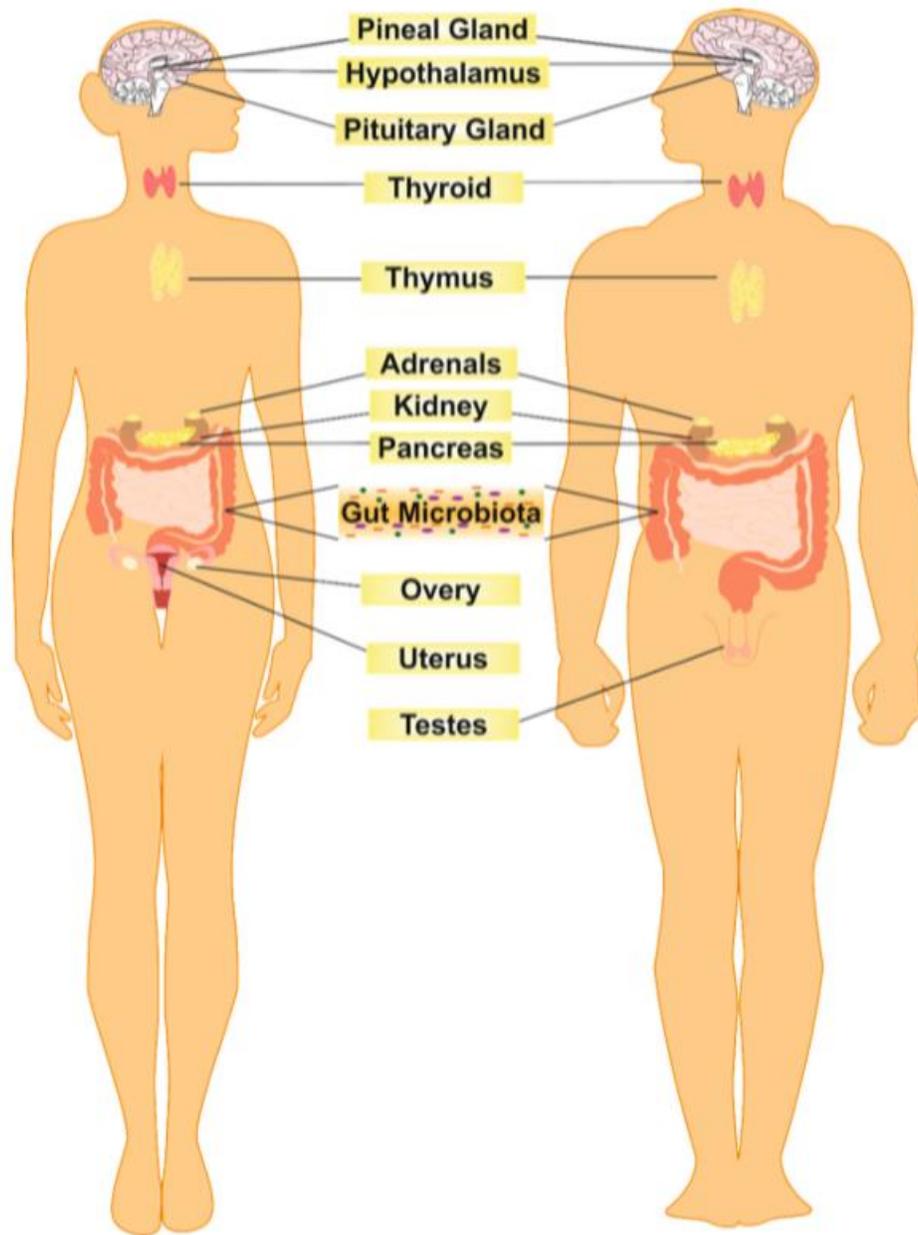
Figure 18. The endocrine organs of the human body.
Endocrine glands across the body produce regulatory metabolic humoral agents. The biochemical capacity of the gut microbiota surpasses all of these organs, justifying its consideration as an endocrine organ. Figure from (Clarke et al. 2014).

2.1.4.3. Neurotransmitters and the microbiome

Neuropeptides, such as VIP, are important mediators in the microbiota-gut-brain axis. Several neuropeptides function as gut hormones as well as neuronal signal transducers. Our microbiota has the capacity to secrete a number of neurotransmitters, as displayed in table 3. Microbiota derived neuronal factors like dopamine have been suggested to play a role in the rate of nutrient absorption in the intestinal lumen (Asano et al. 2012). Research from Aarts et. al. demonstrates that the microbial composition of adults diagnosed with attention deficit hyperactivity disorder (ADHD) included an increase in the Bifidobacterium genus. Although the shift in bacterial structure was not drastic, predictive 16S metagenomic analysis using the bioinformatics software, Phylogenetic Investigation of Communities by Reconstruction of Unobserved States (PICRUSt), demonstrated that the bacterial gene responsible for the creation of arogenate dehydratase, was significantly enhanced in ADHD cases. Arogenate dehydratase is a precursor for dopamine and may decrease the neural response to reward expectation. This decrease in reward expectation is considered a hallmark of ADHD (Aarts et al. 2017).

The activation of the histamine receptor 2 (H2R) is also associated with the microbiota. Like VIP's receptors, the activation of H2R (a GPCR), stimulates adenylate cyclase via $G_{\alpha s}$ and results in anti-inflammatory effects (Seifert et al. 2013). A number of bacterium, including *L. saerimneri* strain 30a and *L. rhamnosus* have been demonstrated to have the capacity to activate the H2R receptor. When the THP-1 human white blood cell line was cultured with *L saerimneri,* the response to LPS was significantly reduced when compared to LPS alone (with *L saerimneri* no present) (Ferstl et al. 2014). A study conducted by Frei et al. demonstrated that the anti-inflammatory effects of these microorganisms were nullified in H2R deficient mice (Frei et al. 2013).

Table 3.   Neurotransmitter secretions by microorganisms.

Neurotransmitters	Bacterial Strain
Serotonin	Lactococcus lactis subsp. cremoris (MG 1363)
	L. lactis subsp. lactis (IL1403)
	Lactobacillus plantarum (FI8595)
	Streptococcus thermophilus (NCFB2392)
	Escherichia coli K-12
	Morganella morganii (NCIMB, 10466)
	Klebsiella pneumoniae (NCIMB, 673)
	Hafnia alvei (NCIMB, 11999)
Dopamine	Bacillus cereus
	B. mycoides
	B. subtilis
	Proteus vulgaris
	Serratia marcescens
	S. aureus
	E.coli
	E. coli K-12
	M. morganii (NCIMB, 10466)
	K. pneumoniae (NCIMB, 673)
	H. alvei (NCIMB, 11999)
Noradrenaline	B. mycoides
	B. subtilis
	P. vulgaris
	S. marcescens

Table 3.   Neurotransmitter secretions by microorganisms (continued).

Neurotransmitters	Bacterial Strain
	E. coli K-12
GABA	L. brevis DPC6108
	B. adolescentis DPC6044
	B. dentium DPC6333
	B. dentium NFBC2243
	B. infantis UCC35624
	L. rhamnosus YS9
Acetylcholine	L. plantarum
Histamine	L. lactis subsp. cremoris (MG 1363)
	L. lactis subsp. lactis (IL1403)
	L. plantarum (FI8595)
	S. thermophiles (NCFB2392)
	M. morganii (NCIMB, 10466)
	K. pneumoniae (NCIMB, 673)
	H. alvei (NCIMB, 11999)

Examples of bacterial strains present in the human microbiota and the neurotransmitters they can produce. Table adapted from (Clarke et al. 2014)

Serotonin is another neurotransmitter secreted by the intestinal microbiota which also binds GPCRs. This tryptophan derived chemical regulates intestinal movement (Barboza, Okun, and Moshiree 2015), immune response and inflammation (Shajib and Khan 2015), regulates metabolism (El-Merahbi et al. 2015) and impacts mood and cognition (Jenkins et al. 2016). In germ-free mice the plasma concentrations of tryptophan and serotonin are greatly increased, perhaps due to compensatory mechanisms by the host and were restored to normal levels once

the mice were recolonized with normal gut flora (Clarke et al. 2012). The absence of a gut

microbiota, like that of germ-free mice, can profoundly disturb central nervous system pathways.

This imbalance was found to be extremely difficult to restore if the normal gut flora is not

restored in childhood.

2.1.4.4. VIP and the microbiome

VIP signaling pathways are prominent in the gastrointestinal tract (its original place of

discovery) and is involved in similar pathways to the neurotransmitters previously discussed.

Inside the intestines, vasoactive intestinal peptide functions to prevent epithelial barrier

disruption during infection through reduction of intestinal inflammatory response (Morampudi et

al. 2015). In inflammatory bowel diseases, such as Crohn's and ulcerative colitis, VIP signaling

cascades are disrupted (Wu, Conlin, et al. 2015). Mice deficient in VIP (same strain studied in

this dissertation) were more susceptible to induced colitis models (Colwell et al. 2003). These

mice also displayed disruption in intestinal epithelial morphology (Vu et al. 2014). After

analyzing nearly 963 pathways Liu et al. confirmed that the VIP signaling axis is the most

important in the development of obese phenotypes (Liu et al. 2010).

First published in the American Journal of Physiology, Conlin et al. demonstrated that

VIP was essential for the regulation of intestinal epithelial permeability. To test this, researchers

administered *Citrobacter rodentium*, a murine pathogen known to infect colonic epithelium,

cause increased permeability and induce ulcerative colitis in mice. The introduction of this

pathogen resulted in a significant increase in epithelial VIP secretion and an overall reduction in

body weight. Intraperitoneal injections of additional VIP prevented this weight loss. Mannitol

was added to mouse diet and its measurements were taken in the intestinal lumen and serous

membrane. While diseased mice showed a significant increase in unidirectional mannitol flow,

amazingly, mice given additional VIP returned to nearly control levels for intestinal permeability. Histological evaluations of the intestines also displayed an ablation of ulcerative colitis in mice given VIP (Conlin et al. 2009). Research published later from the same group demonstrated that the protective capacity of VIP was through the protein kinase C (PKC) pathway, which is activated by the VIP-cAMP signaling axis (Morampudi et al. 2015).

VIP and the microbiome have also both been implicated in circadian synchronization. This hormonal internal clock is controlled by rhythms in gene expression and light detection. VIP has been shown to mediate the expression of clock genes mediated through its VPAC2 receptor which is highly expressed in the suprachiasmatic nucleus in the brain (Miller et al. 2014; Shen et al. 2000). This region of the hypothalamus acts as the circadian pacemaker for the host and the lack of VIP (like in VIP knockout mice) shifts behavior (Lucassen et al. 2012), alters sleep patterns (Hu et al. 2011) and through altered clock gene expression can even affect cardiovascular function (Schroeder et al. 2011). The microbiome of mice whose circadian rhythm is dysregulated are altered when compared to control mice. Research by Voigt et al. demonstrated that mice with disrupted circadian cycling by mutated Clock(Δ19) gene had altered microbial composition as well as decreased diversity in comparison to their wild type counterparts (Voigt et al. 2016). This was confirmed by Liang et al. who analyzed the impact of Bmal1, another circadian regulation gene, causing microbiota compositional changes. Their study demonstrated that the lack of circadian synchronization affects feeding times, fecal composition and changes based on gender of the mouse (Liang, Bushman, and FitzGerald 2015). The importance of this rhythm is also essential for immune homeostasis. A publication by Lange et al. demonstrated the increased presence of immune cells in blood during sleep. These cells

seem to work in contrast to epinephrine and noradrenaline which interestingly can be secreted by the microbiota (Lange, Dimitrov, and Born 2010).

Disruptions in vasoactive intestinal peptide signaling and the intestinal microbiota are associated with similar diseases including inflammatory bowel disease, circadian dysregulation, obesity and immune regulation. Despite this overlap, the potential relationship between VIP signaling and the intestinal microbiota is currently unknown; therefore, in this study, VIP signaling disruption with the application of knockout mouse models was used to determine the impact on the intestinal microbiome. Below we demonstrate that the genetic removal of VIP results in compositional microbial changes in the intestines. Moreover, the overall diversity of the microbiota is reduced in VIP deficient mice. These changes also results in altered metabolomic predicts which suggest an increase in the glyoxylate cycle, gluconeogenesis, and the pentose phosphate pathway, perhaps caused by an increased presence of fats in the intestinal lumen.

2.1.5. Nucleotide sequencing techniques

2.1.5.1. Sanger Sequencing (Chain termination method)

Although it has mostly been replaced by high-throughput sequencing methods, Sanger sequencing or chain termination sequencing was the gold standard for DNA sequencing for nearly 30 years (Sanger et al. 1977). It utilizes two forms of deoxynucleotide substrates. The first is the naturally occurring deoxyculeotides (dNTPs) and the second is the chain terminating dideoxynucleoties (ddNTPs). Four reactions are utilized containing all four deoxynucleotides (dATP, dTTP, dCTP and dGTP) at 100x and a different modified chain-terminating dideoxynucleotides (ddATP, ddTTP, ddCTP and ddGTP) per reaction at 1x, along with template DNA, a primer and DNA polymerase. The modified ddNTPs are chain-elongating terminators

with no 3'-hydroxy group, but rather an electrophile, incapable of forming a phosphodiester bond, thereby terminating the elongation of the DNA strand (Sanger, Nicklen, and Coulson 1977). These DNA strands are then heat denatured to remove template DNA and separated by size using polyacrylamide gel electrophoresis (Sanger and Coulson 1978). The visualization of these reactions from the gel allows for sequencing as demonstrated in figure 19. An advancement to this technique was employing fluorescently labeled ddNTPs, each with a different fluorophore, allowing for a single reaction coupled with a more rapid gel reading by a laser, which drastically increased the sequencing time (Quesada et al. 1991).
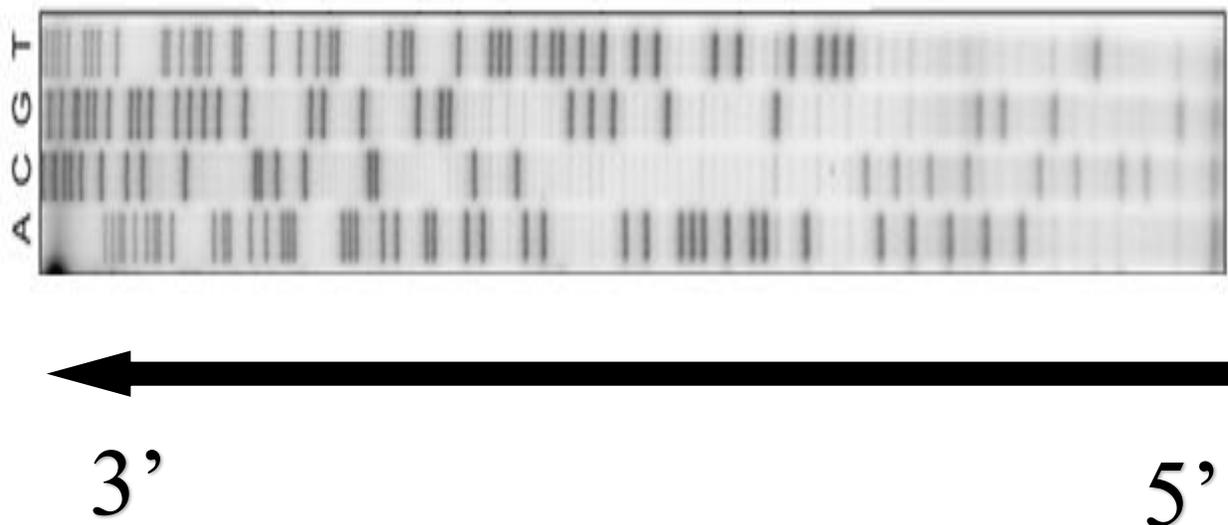
Figure 19. Gel electrophoresis result from an example Sanger sequencing run.
This figure contains an example Sanger DNA sequencing run gel. The arrow indicates the direction for reading DNA sequences in a 5' to 3' manner. Figure modified and adapted from (Lorenzo-Díaz et al. 2012)

2.1.5.2. 454-Pyrosequencing

The 454-pyrosequencing DNA order determination technique utilizes fragmented base DNA sequences. After fragmentation, the ends of the DNA sequences are ligated with adapters of known DNA sequences and then denatured to produce single stranded DNA molecules. Aided

66

by the adapters, the sequences are then captured through hybridization onto beads, with a unique DNA fragment binding per bead. These beads are spread across a slide, where each bead is placed into an individual well. A single dNTP is then flooded onto the plate and if added to the complementary sequence by the DNA polymerase, an enzymatic reaction produces light that a highly sensitive camera detects the emission wavelength of each well. The wells are washed and the process repeated until the DNA fragments, acting as templates for the synthesis of complementary strand are completely sequenced. These individual pieces of fragmented DNA are then assembled into one large sequence. This technology is also no longer in use due to its replacement by newer sequencing platforms.

2.1.5.3. Ion Torrent sequencing

The Ion Torrent sequencing platform from Thermo Fisher Scientific (Waltham, Massachusetts) utilizes a digital semiconductor chip to determine nucleotide order. Similar to 454-pyrosequencing, fragmented DNA strands are hybridized onto individual beads. The DNA strands on these beads are copied until the entire bead is covered with the same DNA strand. These beads are then placed into individual wells on a digital semiconductor. Wells are immersed with one of the four nucleotides, with the addition of each nucleotide releasing a hydrogen ion, which changes the pH of the solution in each individual well to identify DNA sequence of the growing complementary strand. Beneath the semiconductor is a pH sensitive layer, which can measure the change in pH caused by the binding of the added nucleotide. Each dNTP produces the same change in pH, but since only one dNTP is added to the wells at a time and then removed, it can be determined which dNTP was added to which well. In the event of a repeated sequence with more than one of the same nucleotide in a row, the pH change is greater and is recorded. The wells are repeatedly washed and the next nucleotide is added. The

sequences of each individual well are then overlapped and assembled into a large sequence

(Rothberg et al. 2011).

2.1.5.4. Single-molecule real time sequencing (SMRT sequencing)

The SMRT DNA sequencing technique was created by Pacific Biosciences (Menlo Park,

CA) and contains a chip with tens of thousands of wells, each containing a single DNA

polymerase. The unique feature of this technique is its ability to sequence long strands of DNA,

where all other techniques require the fragmentation of DNA into short strands. These DNA

strands are added to this chip resulting in an estimated one strand per well (containing the DNA

polymerase). The presence of one polymerase per well eliminates the possibility of sequencing

multiple strands at the same time. The four nucleotides are simultaneously added across this

chip, each labeled with a different fluorophore molecule. The utilization of these nucleotides by

the DNA polymerase enzyme, results in their release and the emission of a specific wavelength

of light. This light is detected by a photo-multiplying plate and turned into electrical conductivity

that corresponds to a specific nucleotide. These sequences are overlapped and converted into one

large DNA sequence. SMRT sequencing and the Illumina sequencing platforms are the two

primary strategies for DNA sequencing used today. The Illumina platform is well ahead in

utilization and is currently considered the gold standard for DNA sequencing. It will be covered

in the materials and methods section of this chapter.

2.1.5.5. Illumina sequencing

The most widely used sequencing technology is called Illumina and is a product of

Illumina Inc. (San Diego, CA). This technology in able to read the nucleotide arrangement using

cluster generation followed by DNA sequencing. Although there are various methods for sample

preparation, typically DNA samples are first hydrolyzed into smaller sequences between 200 and

600 base pairs. To these fragment adapters, or short known DNA sequences, are added on both the 5' and 3' ends. These adapters also contain sequences complementary to oligos bound to the flow cell. The flow cell is a glass slide where amplification and DNA sequence reads occur. Once the adapters are added the samples are washed across the flow cell. Here, the adapter sequences bind to the DNA previously attached to the flow cell and form a lawn of small clusters of similar sequences.

Once bound, a polymerase enzyme catalyzes a complementary DNA strand of the DNA fragment hybridized to the surface. The original sample of DNA is now washed away and the complementary strand folds over, and the adapter on the other side binds a nearby previously attached DNA stand on the surface. This process, called bridge amplification, repeats these steps over and over again, resulting in expansion of all of the fragments and creating numerous clonal DNA clusters. Reverse DNA strands are now washed away and the sequencing of the DNA begins. Fluorescently labeled nucleotides are added to the flow cell similar to current DNA sequencing catalyzed by DNA polymerase. As each complementary nucleotide binds and is added to the 3' end of the growing complementary strand, a particular wavelength of light is emitted and recorded by the instrument. Each wavelength produced by each cluster is analyzed by a photodetector to determine sequence. This process is known as bridge-amplification and sequencing by synthesis.

2.2. Materials and methods

2.2.1. Mouse husbandry

The C57 Black 6 mice (C57BL/6) were purchased from Jackson Laboratories (Bar Harbor, ME). Mice deficient in VIP were obtained from James Waschek at the University of California, Los Angeles (Colwell et al. 2003). Mice missing the VPAC1 gene (VPAC1KO) were

given to our laboratory by Mary Sue O'Dorisio, Univeristy of Iowa, Iowa City (Fabricius et al. 2011). VPAC2 knockout (VPAC2KO) mice originally created by John Harmar were a kind gift from Jane Schuh at North Dakota State University (Harmar et al. 2002). All of these mouse strains were bred and housed in the Dorsam lab mouse vivarium at the Animal Nutrition and Physiology Center (ANPC) at North Dakota State University and met compliance rules approved by the IACUC committee at NDSU and satisfied all state and federal regulations. Mice were fed Laboratory Rodent Diet 5001 from LabDiet (St. Louis, MO), which was purchased through the Animal Supply Company (Irving, TX). Animals were fed food and water ad libitum and maintained on a 12-hour day/night cycle.

Animals were housed in material vented cages (13.5" L x 11.5" W x 6.1" H; 75 square inches) from Animal Care Systems (Centennial, CO). The Optimice caging system from Animal Care System includes a 100-cage carrying capacity each equipped with air filters and utilized Alpha-Dri paper bedding (Shepherd Specialty Papers, Milford NJ). Most breeding of these knockout strains used a harem breeding method of two females (+/-) and one male (+/-); at times a single female was used based on supply. In order to increase the frequency of WT or KO VPAC1 or VPAC2, some breeding cages used WT or KO males, but the females were always heterozygous as gut microbiota are vertically transferred down to offspring. Only brother-sister breeding was employed in order to reduce genetic drift. (Schei et al. 2017). All pups were cohoused until maturity (4 weeks), at which time they were weaned into new cages based upon gender. During the weaning process, mice were identified with ear punches and tail biopsies collected to determine genotype by PCR. Mice were limited to 4 males or 5 females per cage irrespective of genotype. All studies were conducted with protocols approved by the NDSU Institutional Animal Care and Use Committee (IACUC) and met all state and federal regulations.

2.2.2. Genomic DNA extraction from tail biopsies

From each weaned pup, a 2 to 4 mm tail biopsy was collected using alcohol sterilized forceps and scissors and placed into a 1.5 mL centrifuge tube on ice. These tail clips were either exacted immediately or stored in a -20°C freezer until assayed. To extract DNA, extraction solution (Sigma Aldrich, Catalog # E7526-24ML) and tissue preparation (Sigma Aldrich, Catalog # T3073-30ML) were mixed in a 4 (40 µL) to 1 (10 µL) ratio, respectively, and 50 µL total was added to tail tissue. After a brief ten second microcentrifuge, to ensure tail submersion, the tubes were incubated at room temperature for 20-120 minutes to ensure cell lysis. Samples were then placed in a 95°C sand bath for 4 minutes. Neutralization buffer (40 µL) (Sigma Aldrich, Catalog # N3910-24ML) was added, and samples were vortexed for 30 seconds. Tail samples were diluted 1/20 in nuclease free water or TE buffer, and then added to the PCR reaction. Polymerase chain reaction (PCR) was conducted to determine the genotype of each tail.

2.2.3. Genotyping

PCR was performed to interrogate the presence of wild type and/or mutant alleles after DNA extraction. The green GoTaq® G2 master mix system (Promega, Catalog # M7823) was used to perform the PCR reaction. A mixture of four total primers (each pair of primers specific for the WT or KO allele) was used for the VPAC1KO and three primers for VIP and VPAC2KO mouse strains. Here, the VIP + VPAC2KO reactions, utilized unique 5' primers specific for the WT or KO allele sequence and a common 3' primer. Primer sets are listed in table 4 below with figures 20, 21, and 22 demonstrating the strategy behind the creation of the knockout mice and the primer hybridization location on the allele.

Table 4.   PCR primers used to interrogate WT and KO alleles for VIP, VPAC1, and VPAC2.

Strain	Primer Name	Primer Sequence
VIP		
Both	**V1**	5' - TTTCAAGGTGTGGGGCTAGAGACATACA - 3'
WT allele	**V2**	5' - TTACCTGATTCGTTTGCCAATGAGTGAC - 3'
KO allele	**N1**	5' - GCCCGGAGATGAGGAAGAGGAGAACAG- 3'
VPAC1		
WT allele	**VPAC1WT 5'**	5' - GGTTGCCATGGCTATCTTGA - 3'
WT allele	**VPAC1WT 3'**	5' - AGTGGTCTGTCTCCCCGTTGTT - 3'
KO allele	**VPAC1KO 5'**	5' - TTCAACTGTTTTCCCCCATTCAC - 3'
KO allele	**VPAC1KO 3'**	5' - CCAGCTCATTCCTCCCACTCA - 3'
VPAC2		
WT allele	**P2**	5' - TAGGGGTGTTCCCAACTCCA - 3'
KO allele	**P4**	5' - GGAAGCATTCTGCTCTGGAT - 3'
Both	**596**	5' – ACTTCAACCCCACTTCTGGC – 3'

A list of the primers used to interrogate WT and KO alleles in the mouse genome.
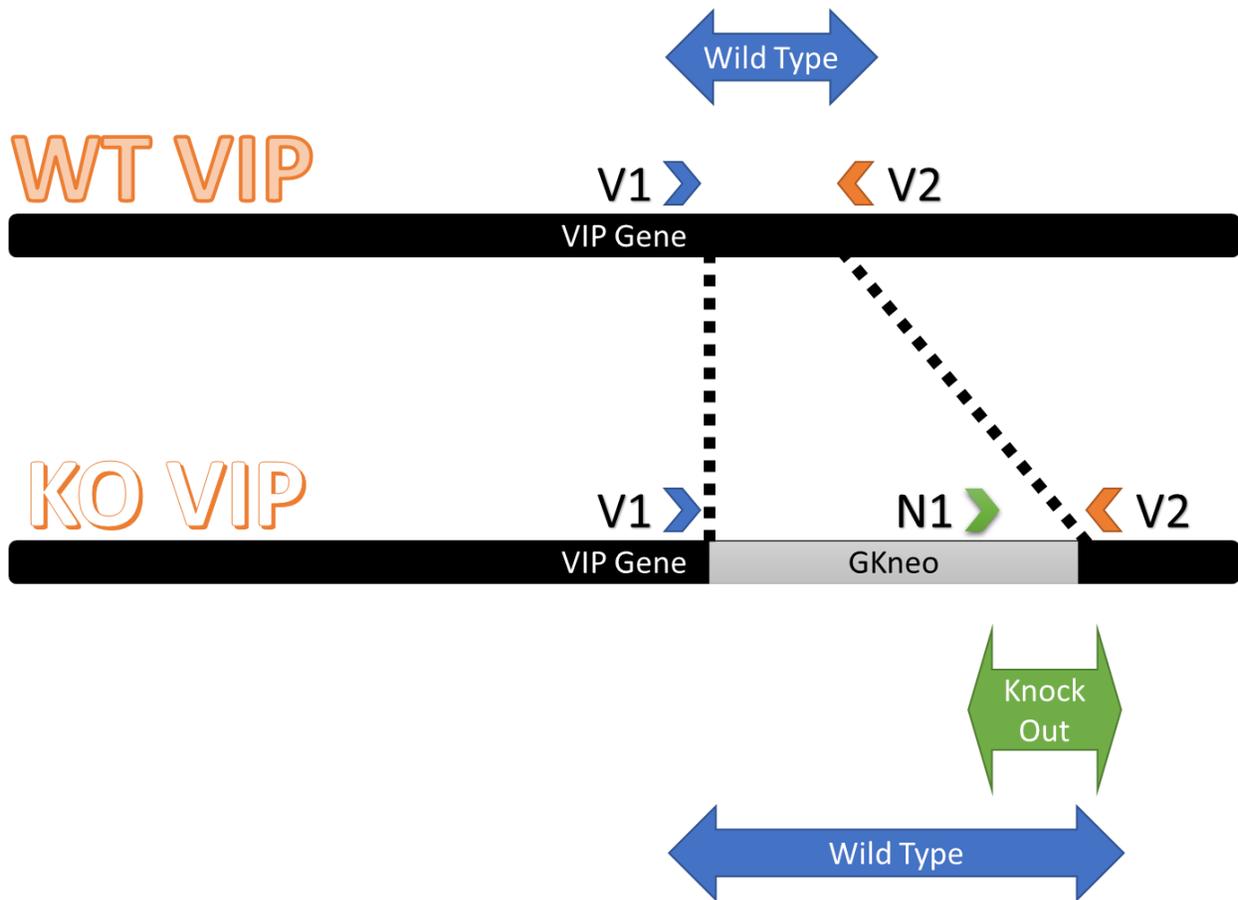
Figure 20. VIPKO generation and primer target location.
Above is the schematic used by Colwell et al. in the creation of the VIPKO strain. The
complementary binding sites for the VIP primers used in our genotyping protocol are
displayed with the V2 primer binding for both WT and KO, while the V1 and N1 only
binding for WT and KO respectively. Figure recreated and adapted from (Colwell et al.
2003)
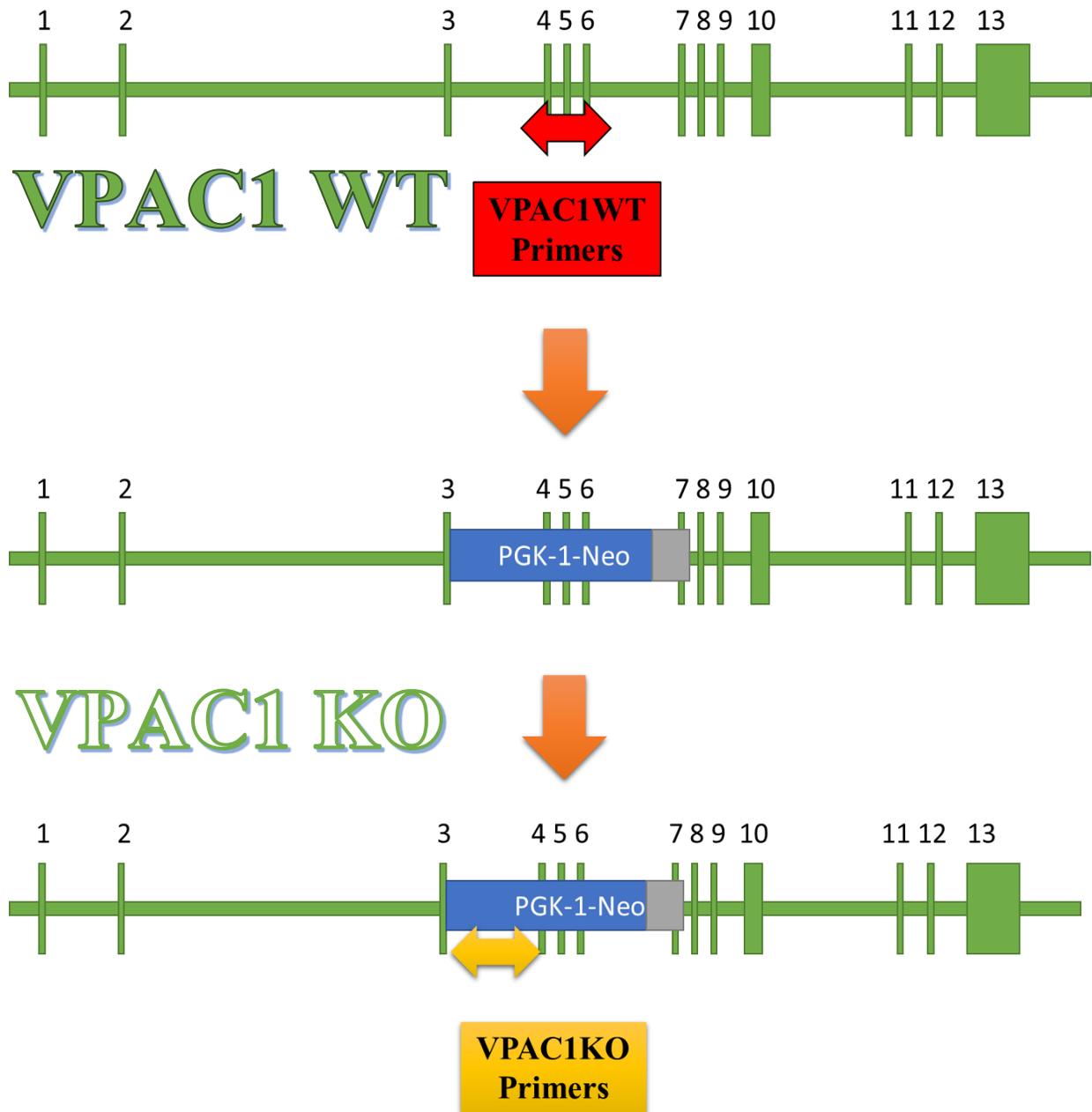
Figure 21. Replacement of VPAC1 exons 4 to 6 with PGK-1-Neomycin cassette. To determine mouse genotype the PCR primers used examine the exon 4 to 6 region. The WT primers will engage a region present between exons 4 and 6, while the KO primers will engage a region on the cassette itself. Figure recreated and adapted from (Fabricius et al. 2011)
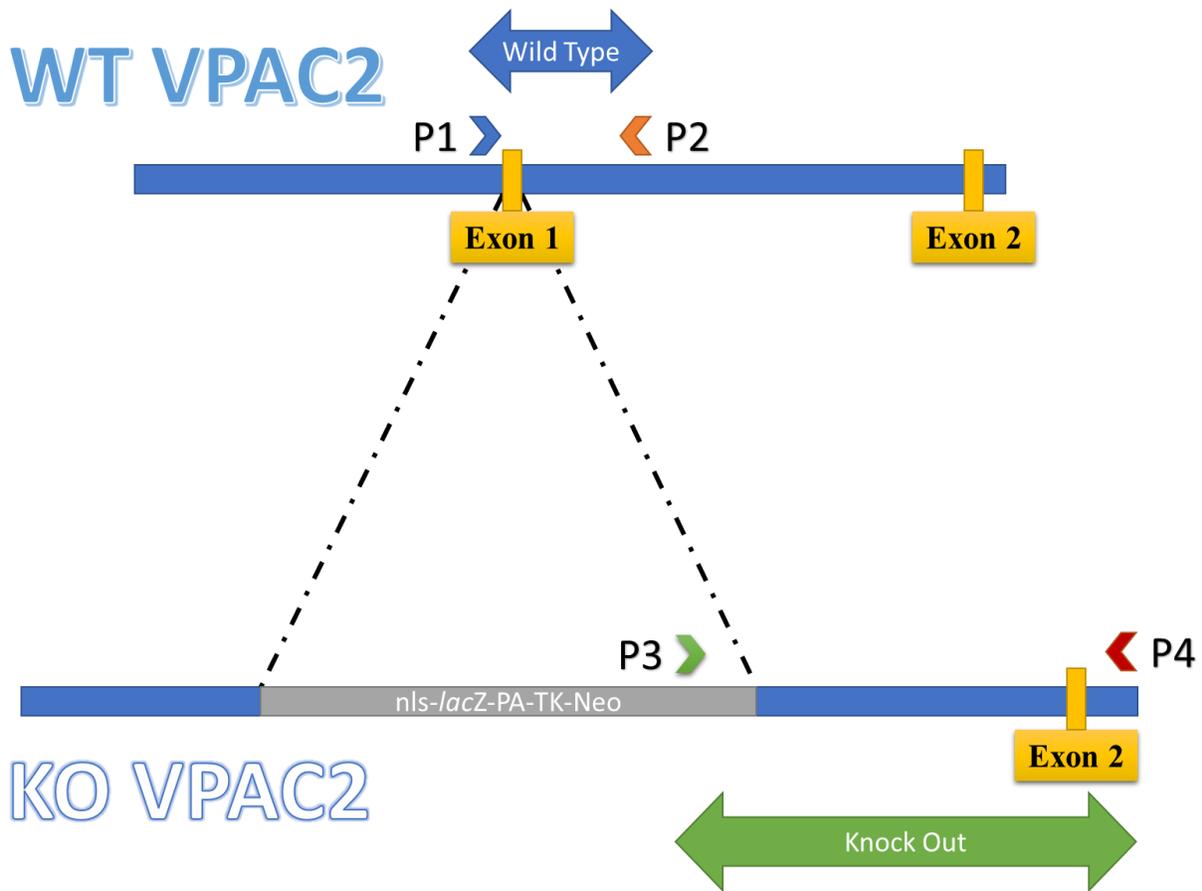
Figure 22. Generation of VPAC2 knockout mice.
A neomycin-resistance gene was inserted into the VPAC2 gene. P1 and P2 primers were used to interrogate the WT gene and the P3 and P4 primers to interrogate the ends of the neomycin gene. Figure recreated and adapted from (Harmar et al. 2002)

Table 5.   Master mix recipe.

Reagents	µl/rxn	# of reactions	Volume (µl)
H$_2$O	7.75	10	77.5
Primer sets at 25 uM each	0.25	10	2.5
2X G2 GoTaq	10	10	100

PCR reaction master mix composition and reaction example.

PCR reactions were performed under the following parameters: 94°C for 3'→ 94°C for 15''→ 62°C for 45''→ 72°C for 1'←→ Repeat a total 40 cycles → 72°C for 1'' → 4°C

indefinitely. EZ-Vision dye (Amresco, Catalog # N391-15MLDRP) was added 3 µL (diluted 1/6 with H_2O) to the PCR samples to visualize DNA amplicons by UV light exposure (302 nm trans illumination) and the mixture (~16 µL) was added to wells in 1.5% agarose gels. After separation of amplicons by gel electrophoreses (~100 V/hr), gels were imaged by the Syngene Chemi Genius 2 platform (Syngene Frederick, MD) or similar UV detection systems. Genotypes for all mice were confirmed by two individuals, performing separate PCR reactions from the same extracted DNA samples.

2.2.4. Fecal sample collection

At 8 weeks of age (53 – 59 days old), fecal samples were collected between 10 and 11 am on Thursday or Friday of each calendar week. Mice were placed inside a sterile autoclaved filtered cage and two fecal pellets were collected from each mouse using sterile toothpicks and placed into sterilized 2 mL microcentrifuge tubes. These tubes were instantly placed on ice and transferred to the a -80°C freezer. The samples were then shipped drozen to the University of Missouri Metagenomics Center (MUMC) by overnight shipping.

Eight fecal samples were collected from both male and female wild type (WT), heterozygous (HET) and homozygous mutant (KO) littermates from VIP, VPAC1 and VPAC2 strains. All three strains are on C57BL/6 genetic background and therefore to increase thoroughness and rigor an additional eight fecal samples for male and females were also collected from wild type C57BL/6 mice from Jackson Labs (Bar Harbor, ME). Table 6 below summaries the fecal samples collected for this study. Figure 23 is a visual representation of how the mice were housed and a timeline of when fecal samples were obtained.

Table 6. Fecal sample collection summary for this study.

	Male			Female			Total
	♂			♀			
C57BL/6 Wild Type	8			8			**16**
	WT	**HET**	**KO**	**WT**	**HET**	**KO**	
VIP	8	8	8	8	8	8	**48**
VPAC1	8	8	8	8	8	8	**48**
VPAC2	8	8	8	8	8	8	**48**
Subtotal [Entire Study]	32	24	24	32	24	24	**160**
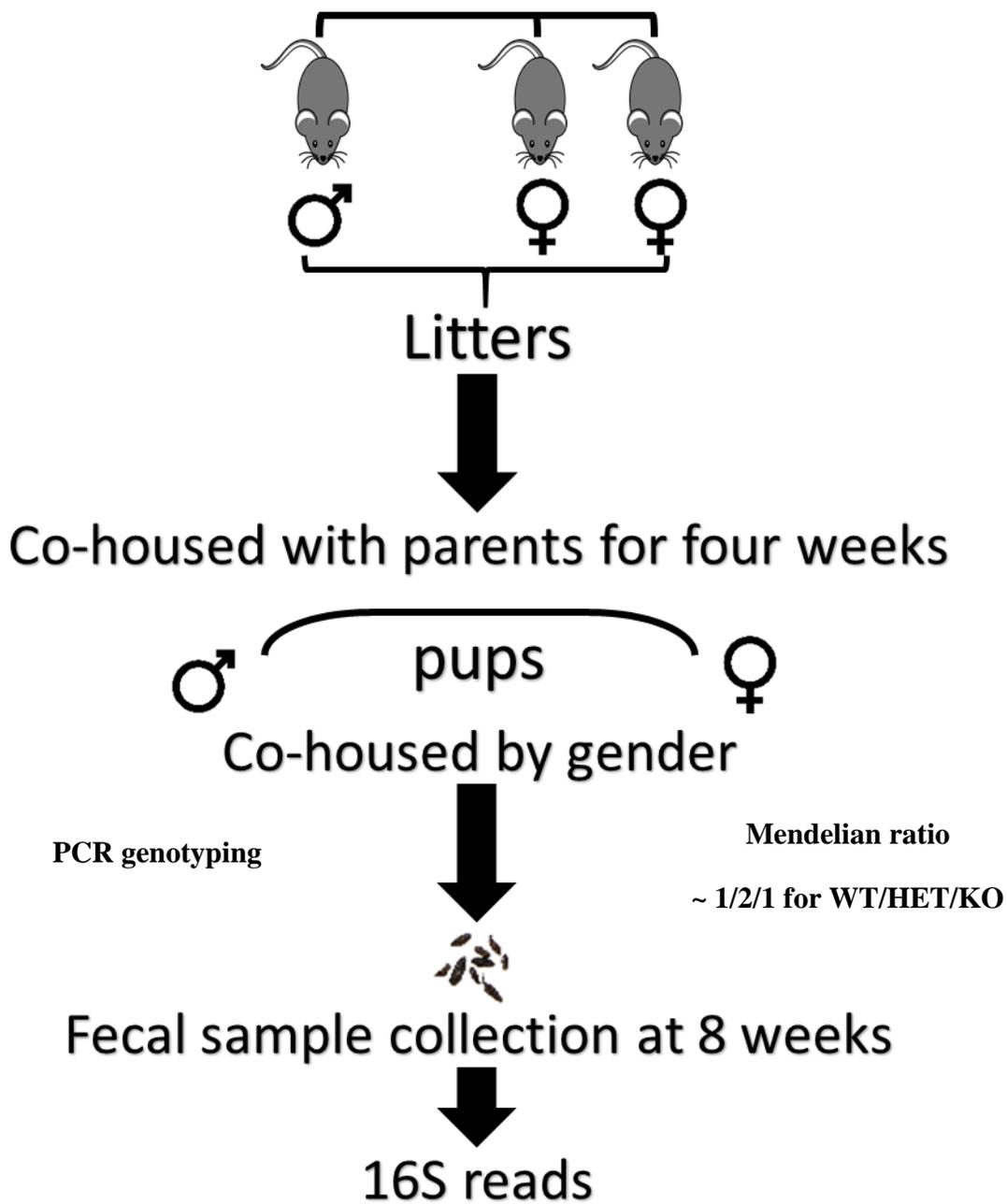
Figure 23. Fecal sample collection strategy.
Collected in accordance with table 5, this breeding and collection strategy was applied for all strains. After 4 weeks of co-housing with breeding pairs, pups were weaned, separated by gender, ear clipped, and genotyped by PCR. At 8 weeks of age, fecal samples were collected and sequenced.

2.2.5. DNA extraction (performed at MUMC)

DNA from fecal samples were extracted using the Qiagen DNeasy Blood and Tissue kit extraction method. In a recent comparative study, this method was found to be the best at DNA extraction (Hart et al. 2015). Eight hundred µL of lysis buffer (500 mM NaCl, 50 mM Tris-HCl pH 8.0, 50 mM EDTA, and 4% sodium dodecyl sulfate) and a stainless-steel bead were added the fecal samples. The Qiagen TissueLyser II was used for mechanical disruption of the samples at 30 Hz for 3 minutes. The samples were centrifuged after a 70°C incubation for twenty minutes. The supernatants were transferred to a new tube containing 200 µL of 10 mM ammonium acetate. After a 5-minute centrifuge at 5,000 x g, the supernatant was transferred to a tube on ice containing chilled isopropanol for 30 minutes. Samples were then centrifuged at 4°C for 15 minutes at 16,000 x g. The supernatant was discarded and DNA pellets were washed several times with 70% ethanol. Pellets were then resuspended in 150 µL of Tris-EDTA, 15 µL of proteinase K and 200 µL of AL buffer (provided by Qiagen). After a 10-minute incubation at 70°C, 200 µL of 100% ethanol was added. Samples were applied to the DNeasy spin column and eluted into EB buffer (Qiagen, DNeasy Blood and Tissue Kit Catalog # 69506)

2.2.6. Next generation rRNA sequencing (performed at MUMC)

The Illumina MiSeq platform was used for 16S rRNA sequencing at the University of Missouri Core facility. The V4 hypervariable region of the 16S gene was targeted by universal primers created William Walters et al. U515F (5′-GTGCCAGCMGCCGCGGTAA-3′) and R806 (5′-GGACTACHVGGGTWTCTAAT-3′) (Walters et al. 2011). The PCR parameters were: 98ºC for 3' → 98ºC for 15'' → 50ºC for 30'' → 72ºC for 30'' ← → Repeat a total 25 cycles] → 72ºC for 7' → 4ºC indefinitely. The product was washed with 80% ethanol and resuspended in Qiagen EB buffer. The amplicons were then pooled for sequencing using the Illumina MiSeq platform.

The MiSeq platform utilizes adaptors which are added to the ends of the amplified DNA fragments. Here, regions complementary to the adaptors are bound to the bottom of the Illumina MiSeq flow cell. The fragments of each sample are then added to a lane on the Illumina flow cell and bind to their complementary oligos. The double stranded strands are denatured with one strand binding to the complementary oligo and the other being washed away. Bound to the flow cell, the fragment folds over and binds to the other oligo on the cell. DNA polymerases are then used to form the complementary strands and create double stranded bridges all over the cell. Denaturing of this bridge results in two copies of the strand. These steps are repeated continuously for clonal amplification of the DNA strand. The reverse strands are then cleaved and washed off. As with other sequencing techniques, fluorescently labeled nucleotides are then added and upon binding emit a fluorescent signal. This signal is then picked up by a detector and all of the signals are read simultaneously. The millions of reads are then overlapped and contiguous sequences are formed.

2.2.7. Bioinformatics analysis

2.2.7.1. Paired-end FASTQ processing

The Qiime 1.9.1 software, created by the Knight Laboratory at the University of California San Diego, was utilized for analysis of the 16S DNA reads (Kuczynski et al. 2012). To ensure quality reads, a Phred quality score of 20 were utilized. This ensured the probability of an incorrect base call at 1 in 100 or 99% accurate. The *join_paired_ends.py* script took forward and reverse reads and joined them together, with a minimum overlap length of 10 base-pairs and a maximum percent difference within overlap set at 25%. The maximum bad run length, or number of consecutive low-quality reads before truncation was set to 3. The *make_mapping_files.py* and *validate_mapping_files.py* commands were used to remove barcode

sequences (mapping file displayed in table 7 below). The *split_libraries_fastq.py* script was used

for quality trimming and placement into a sequence file.

Table 7.   Qiime mapping file.

SampleID	BarcodeSequence	ForwardFastqFile	ReverseFastqFile	TreatmentGroup	Description
1MWT	CTTGAGCTTTGA	MB001-B2_S14_L001_R1_001.fastq	MB001-B2_S14_L001_R2_001.fastq	1_MWT	MWT1
2MWT	CACCGATTGGTA	MB002-B3_S15_L001_R1_001.fastq	MB002-B3_S15_L001_R2_001.fastq	1_MWT	MWT2
3MWT	TGGTTCGAGTAC	MB003-B4_S16_L001_R1_001.fastq	MB003-B4_S16_L001_R2_001.fastq	1_MWT	MWT3
4MWT	CAATCGCCGGAA	MB004-B5_S17_L001_R1_001.fastq	MB004-B5_S17_L001_R2_001.fastq	1_MWT	MWT4
5MWT	TCTCCGCATGTC	MB005-B6_S18_L001_R1_001.fastq	MB005-B6_S18_L001_R2_001.fastq	1_MWT	MWT5
6MWT	TGTATGGGTGCG	MB006-B7_S19_L001_R1_001.fastq	MB006-B7_S19_L001_R2_001.fastq	1_MWT	MWT6
7MWT	ACGCTTCAATGT	MB007-B8_S20_L001_R1_001.fastq	MB007-B8_S20_L001_R2_001.fastq	1_MWT	MWT7
8MWT	CTAAATGTCGTC	MB008-B9_S21_L001_R1_001.fastq	MB008-B9_S21_L001_R2_001.fastq	1_MWT	MWT8
9MHET	CCGAGTAGTTGG	MB009-B10_S22_L001_R1_001.fastq	MB009-B10_S22_L001_R2_001.fastq	2_MHET	MHET1
10MHET	CGCTGATAACGG	MB010-B11_S23_L001_R1_001.fastq	MB010-B11_S23_L001_R2_001.fastq	2_MHET	MHET2
11MHET	GGTTTGGCCATA	MB011-B12_S24_L001_R1_001.fastq	MB011-B12_S24_L001_R2_001.fastq	2_MHET	MHET3
12MHET	CTCTCCCGTGAT	MB012-C1_S25_L001_R1_001.fastq	MB012-C1_S25_L001_R2_001.fastq	2_MHET	MHET4
13MHET	TCCTAGCAGTGA	MB013-C2_S26_L001_R1_001.fastq	MB013-C2_S26_L001_R2_001.fastq	2_MHET	MHET5
14MHET	CACTCTGATTAG	MB014-C3_S27_L001_R1_001.fastq	MB014-C3_S27_L001_R2_001.fastq	2_MHET	MHET6
15MHET	TGCCAATGCCAA	MB015-C4_S28_L001_R1_001.fastq	MB015-C4_S28_L001_R2_001.fastq	2_MHET	MHET7
16MHET	CCTCGGATTATA	MB016-C5_S29_L001_R1_001.fastq	MB016-C5_S29_L001_R2_001.fastq	2_MHET	MHET8
17MKO	ACGCTATCTGGA	MB017-C6_S30_L001_R1_001.fastq	MB017-C6_S30_L001_R2_001.fastq	3_MKO	MKO1
18MKO	GGTGACCGGATT	MB018-C7_S31_L001_R1_001.fastq	MB018-C7_S31_L001_R2_001.fastq	3_MKO	MKO2
19MKO	TACCAAGCACTT	MB019-C8_S32_L001_R1_001.fastq	MB019-C8_S32_L001_R2_001.fastq	3_MKO	MKO3
20MKO	CGACCCTTTACC	MB020-C9_S33_L001_R1_001.fastq	MB020-C9_S33_L001_R2_001.fastq	3_MKO	MKO4
21MKO	GATTGAGAAAGC	MB021-C10_S34_L001_R1_001.fastq	MB021-C10_S34_L001_R2_001.fastq	3_MKO	MKO5
22MKO	AGGACGCACTGT	MB022-C11_S35_L001_R1_001.fastq	MB022-C11_S35_L001_R2_001.fastq	3_MKO	MKO6
23MKO	GGTACATCGGTT	MB024-D1_S37_L001_R1_001.fastq	MB024-D1_S37_L001_R2_001.fastq	3_MKO	MKO8
24FWT	ACGGCCAATCGA	MB025-D2_S38_L001_R1_001.fastq	MB025-D2_S38_L001_R2_001.fastq	4_FWT	FWT1
25FWT	GTCCAGTAATGC	MB026-D3_S39_L001_R1_001.fastq	MB026-D3_S39_L001_R2_001.fastq	4_FWT	FWT2
26FWT	TATGTGGCCCAA	MB027-D4_S40_L001_R1_001.fastq	MB027-D4_S40_L001_R2_001.fastq	4_FWT	FWT3
27FWT	TGACTTTGTGTG	MB028-D5_S41_L001_R1_001.fastq	MB028-D5_S41_L001_R2_001.fastq	4_FWT	FWT4
28FWT	CCTATCCTTGGC	MB029-D6_S42_L001_R1_001.fastq	MB029-D6_S42_L001_R2_001.fastq	4_FWT	FWT5
29FWT	ATACACGTGGCG	MB030-D7_S43_L001_R1_001.fastq	MB030-D7_S43_L001_R2_001.fastq	4_FWT	FWT6
30FWT	ACAATCGGTTGC	MB031-D8_S44_L001_R1_001.fastq	MB031-D8_S44_L001_R2_001.fastq	4_FWT	FWT7
31FWT	CCTAAGCACATG	MB032-D9_S45_L001_R1_001.fastq	MB032-D9_S45_L001_R2_001.fastq	4_FWT	FWT8
32FHET1	TAATGGAGGAAC	MB033-D10_S46_L001_R1_001.fastq	MB033-D10_S46_L001_R2_001.fastq	5_FHET	FHET1
33FHET2	GAAAGGACAGGT	MB034-D11_S47_L001_R1_001.fastq	MB034-D11_S47_L001_R2_001.fastq	5_FHET	FHET2
34FHET3	TTGGGCGTGAAC	MB035-D12_S48_L001_R1_001.fastq	MB035-D12_S48_L001_R2_001.fastq	5_FHET	FHET3
35FHET4	CGTTGCCTCGTT	MB036-E1_S49_L001_R1_001.fastq	MB036-E1_S49_L001_R2_001.fastq	5_FHET	FHET4
36FHET5	GTCGCTGTCTTC	MB037-E2_S50_L001_R1_001.fastq	MB037-E2_S50_L001_R2_001.fastq	5_FHET	FHET5
37FHET6	GATCGCAGGTGT	MB038-E3_S51_L001_R1_001.fastq	MB038-E3_S51_L001_R2_001.fastq	5_FHET	FHET6
38FHET7	GAATGCAACGCC	MB039-E4_S52_L001_R1_001.fastq	MB039-E4_S52_L001_R2_001.fastq	5_FHET	FHET7
39FHET8	CTGAACGCTAGT	MB040-E5_S53_L001_R1_001.fastq	MB040-E5_S53_L001_R2_001.fastq	5_FHET	FHET8
40FKO1	ACTTTGTCGCAA	MB041-E6_S54_L001_R1_001.fastq	MB041-E6_S54_L001_R2_001.fastq	6_FKO	FKO1
41FKO2	CATATACTCGCA	MB042-E7_S55_L001_R1_001.fastq	MB042-E7_S55_L001_R2_001.fastq	6_FKO	FKO2
42FKO3	TTCGTTGTGGTA	MB043-E8_S56_L001_R1_001.fastq	MB043-E8_S56_L001_R2_001.fastq	6_FKO	FKO3
43FKO4	AACCGTTCCAGA	MB044-E9_S57_L001_R1_001.fastq	MB044-E9_S57_L001_R2_001.fastq	6_FKO	FKO4
44FKO5	CCGAGGTAGTAC	MB045-E10_S58_L001_R1_001.fastq	MB045-E10_S58_L001_R2_001.fastq	6_FKO	FKO5
45FKO6	GGTTAACAGGAA	MB046-E11_S59_L001_R1_001.fastq	MB046-E11_S59_L001_R2_001.fastq	6_FKO	FKO6
46FKO7	CCACTTGGATAG	MB047-E12_S60_L001_R1_001.fastq	MB047-E12_S60_L001_R2_001.fastq	6_FKO	FKO7
47FKO8	ATCCGTCATAAC	MB048-F1_S61_L001_R1_001.fastq	MB048-F1_S61_L001_R2_001.fastq	6_FKO	FKO8

Table including all sample IDs, barcode sequences, groups and forward and reverse files for the VIP group of samples.

2.2.7.2. OTU assignment

The output file from the *split_libraries_fastq.py* script was used to pick closed reference operational taxonomic units (OTUs) using *pick_closed_reference_otus.py* command. This OTU picking process clusters the reads against a reference sequence database. Any sequences not found in this collection are excluded and removed from any downstream analysis. For our analysis the SILVA database, release 128, was used for sequence comparison (Quast et al. 2013). The threshold for sequence clustering similarity within individual OTUs was set to 99%. For PICURSt analysis, the Greengenes database was used for sequence assessment (DeSantis et al. 2006). A phylogenetic tree was constructed using the *make_phylogeny.py* command and an otu_table.biom file was made through *make_otu_table.py*. The resulting otu_table.biom file was utilized for core diversity analysis.

2.2.7.3. Alpha and beta diversity

Qiime was utilized to calculate alpha and beta diversity from our dataset. The terms alpha, beta and gamma diversity were introduced by Robert Wittaker (Whittaker 1972, 1960). Alpha diversity refers to changes within each group and beta diversity represents differences amongst various groups. Gamma diversity is the measurement of variety within an entire landscape, such as a rainforest and not relevant to this analysis. For alpha diversity analysis observed species (Mittelbach Gary et al. 2001), PD whole tree (Faith 1992), chao1 (Chao 1984) and Shannon indexes (Shannon 1948) were utilized for comparison. The number of different species present in a community is a measure of richness, which is the only variable in the observed species analysis. Chao1 and the Shannon indexes measure both richness and evenness. Evenness is the measurement of the relative abundance of all of the species present in a sample. The PD whole tree analysis includes richness, evenness and it measures the length of branches

on the phylogenetic tree. The core_diversity_analysis.py command utilized the OTU dataset to calculate these different diversities.

Beta diversity measurements, represented as weighted or unweighted unique fraction, were for sample to sample comparisons. The weighted analysis compares the abundance of individual microorganisms while the unweighted analysis compares just the presence and absence of these individuals introspective of their abundance. These results were visualized using a Principal Coordinates Analysis (PCoA) matrix. This three-dimensional plot visually displays the phylogenetic distances between samples in three axes, PC1, PC2 and PC3, with the distance between the plots representing the variation in the dataset. Beta diversity was also measured using the *jackknifed_beta_diversity.py* and *make_boostrapped_tree.py* commands. This allowed for the formation of newick trees which visualized the similarities between samples.

2.2.7.4. PICRUSt

The bioinformatics software PICRUSt (Phylogenetic Investigation of Communities by Reconstruction of Unobserved States) was used to predict metagenomic function. As discussed in the OTU assignment section, to utilize this software the Greengenes database was utilized. The reason for database change was because the PICRUSt predictive tool currently only supports the Greengenes database at 99% similarity (Langille et al. 2013). A closed reference OTU table was picked against the database and the resulting .biom file was utilized for PICRUSt analysis. The *normalize_by_copy_number.py* script was used to normalize the OTU table against a known abundance number. This was followed by the *predict_metagenomics.py* command which compares results against the Kyoto encyclopedia of genes and genomes (KEGG) database (Kanehisa et al. 2017; Kanehisa et al. 2016; Kanehisa and Goto 2000; Kanehisa et al. 2012). The

output file was then mapped and analyzed using the Lda Effective Size (LEfSe) module

visualized in figure 25.

2.2.7.5. Statistics

Statistical analysis and graph creation was done using GraphPad Prism Software v.7.00

(GraphPad La Jolla, CA), Microsoft Excel 2016 (Microsoft Seattle, WA) and Qiime v1.9.1.

Two-Way ANOVA analysis was performed on the taxonomic data with the mean of each

organism within each treatment group at every taxonomic rank compared against the means of

that organism in every other treatment group (figure 24). The Bonferroni multiple comparisons

test was utilized with a 95% confidence interval (0.05 represented by *, 0.005 **, 0.0005 ***

and 0.00005 ****).
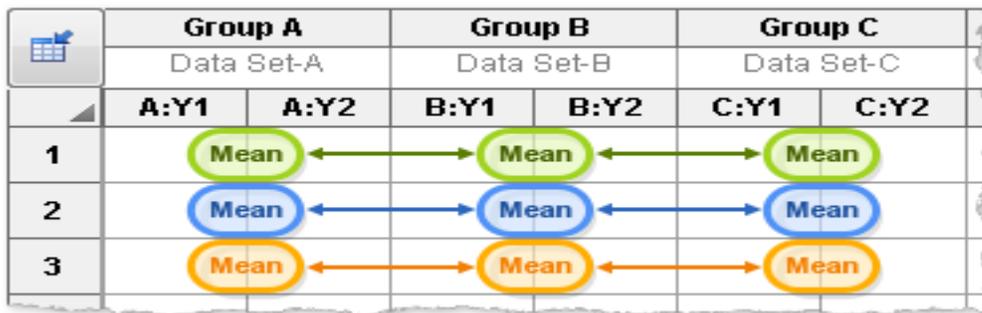
Figure 24. Group mean multiple comparison.
A snapshot of the analysis performed comparing the mean of each bacterium of each strain to every other strain at every taxonomic level. Picture taken from GraphPad Prism Software (La Jolla, CA).
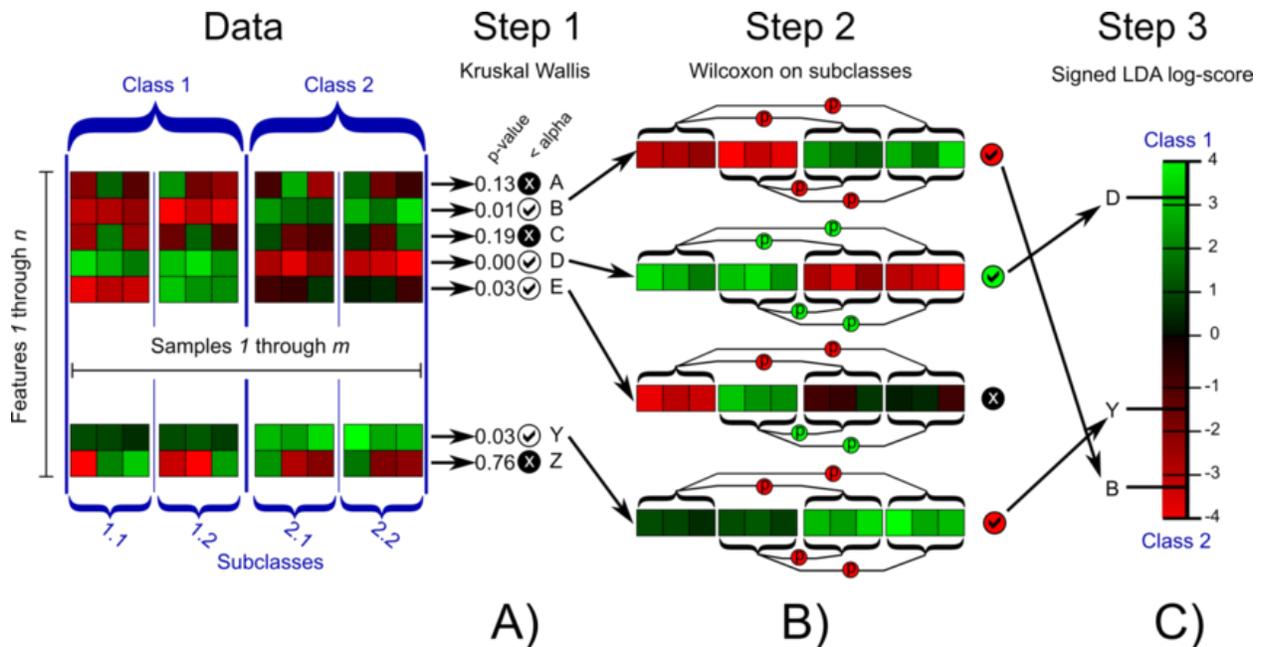
Figure 25. PICRUSt metagenomic analysis using the LEfSe tool.
After the PICRUSt analysis is completed using the predict_metagenomics.py command, the data is input into the LEfSe tool for biomarker discovery. In step one this took uses the Kruskall-Wallis text to determine whether the values are statistically different. Any values over 0.05 p-value do not move on. In step two, a Wilcoxon test checks pairwise comparisons between groups and any that significantly differ from one another are scored and ranked. This method was first devised by Segata et. all in 2011 and has been extensively validated on several microbiomes. Figure from (Segata et al. 2011).

2.3. Results

2.3.1. Genotyping

In order to properly classify mouse genotypes, PCR reactions of tail genomic DNA extracts were performed to interrogate the presence of the WT and/or mutant alleles by use of specific primers. At four weeks, pups were weaned, and tail biopsies collected for genotyping. Males and females were separately cohoused irrespective of genotype until eight weeks of age at which time fecal samples were collected (see figure 23). In theory, the utilization of male HET and female HET breeding pairs should result in a 1:2:1 Mendelian inheritance as demonstrated in figure 26. Genotyping data of over 355 mice over 10 experiments were compiled to determine an

estimated ratio obtained by our laboratory. Although it did not perfectly match predicted values, this ratio was closely maintained for all stains expect VPAC1 which resulted in greater HET +/- and WT +/+ and far fewer KO -/- pups, as demonstrated in figure 26. All PCR reactions were performed with positive and negative controls and repeated by another individual. The positive controls were a previously extracted, stored genomic DNA extract, with confirmed genotype. For example, genotype analysis of VIP mice was conducted with three known WT, HET and KO samples as positive controls. The negative control was nuclease free water, which ensured no primer, water and/or Taq contamination. Figure 27 is a representative agarose gel of these PCR reactions and demonstrates the bands created by each genotype. The analyzed results of this gel are depicted in table 8.

Male Genotype:

⬛	+/-

Female Genotype:

🟥	+/-

Female

		+	-
Male	**+**	+/+	+/-
	-	-/+	-/-

Predicted outcome per offspring:

+/+	1:4	25%
+/-	1:2	50%
-/-	1:4	25%

VIP offspring genotypes:

+/+	3:10	30%
+/-	~1:2	46%
-/-	~1:4	24%

VPAC1 offspring genotypes:

+/+	~1:3	34%
+/-	3:5	60%
-/-	~1:4	6%

VPAC2 offspring genotypes:

+/+	~1:4	23%
+/-	~1:2	54%
-/-	~1:4	23%
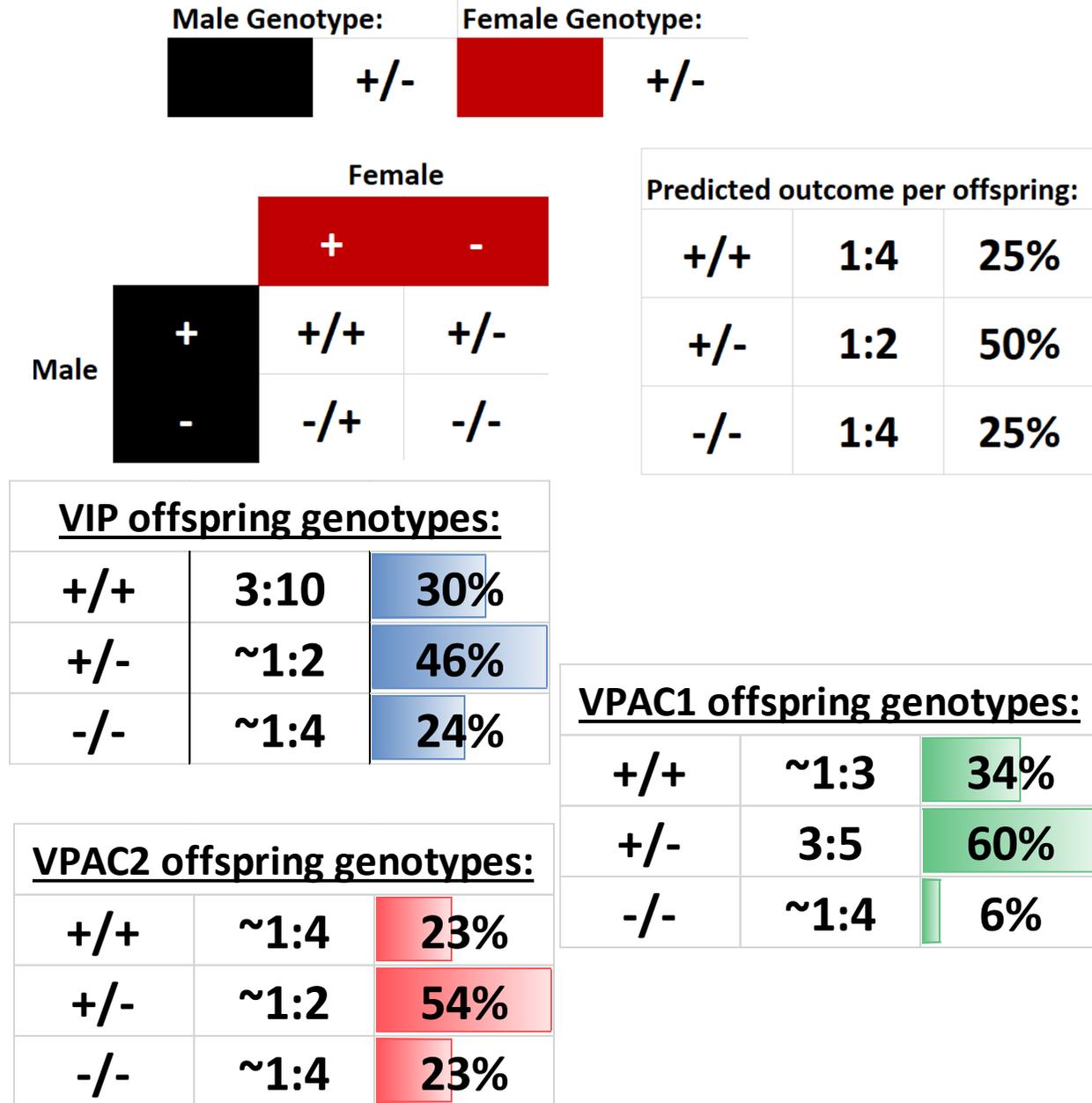
Figure 26. Punnett square demonstrating mouse breeding strategy, predicted and actual outcomes.

Pups created by the harem breeding approach for VIP and VPAC2 strains resulted in a nearly 1:2:1, WT, HET and KO, ratio. This allowed for utilization of littermate pups 16S studies, eliminating concerns regarding environment on microbiota. VPAC1 breeders resulted in lower KO pup production, confirming previously documented work by O'Dorisio lab (Fabricius et al. 2011)
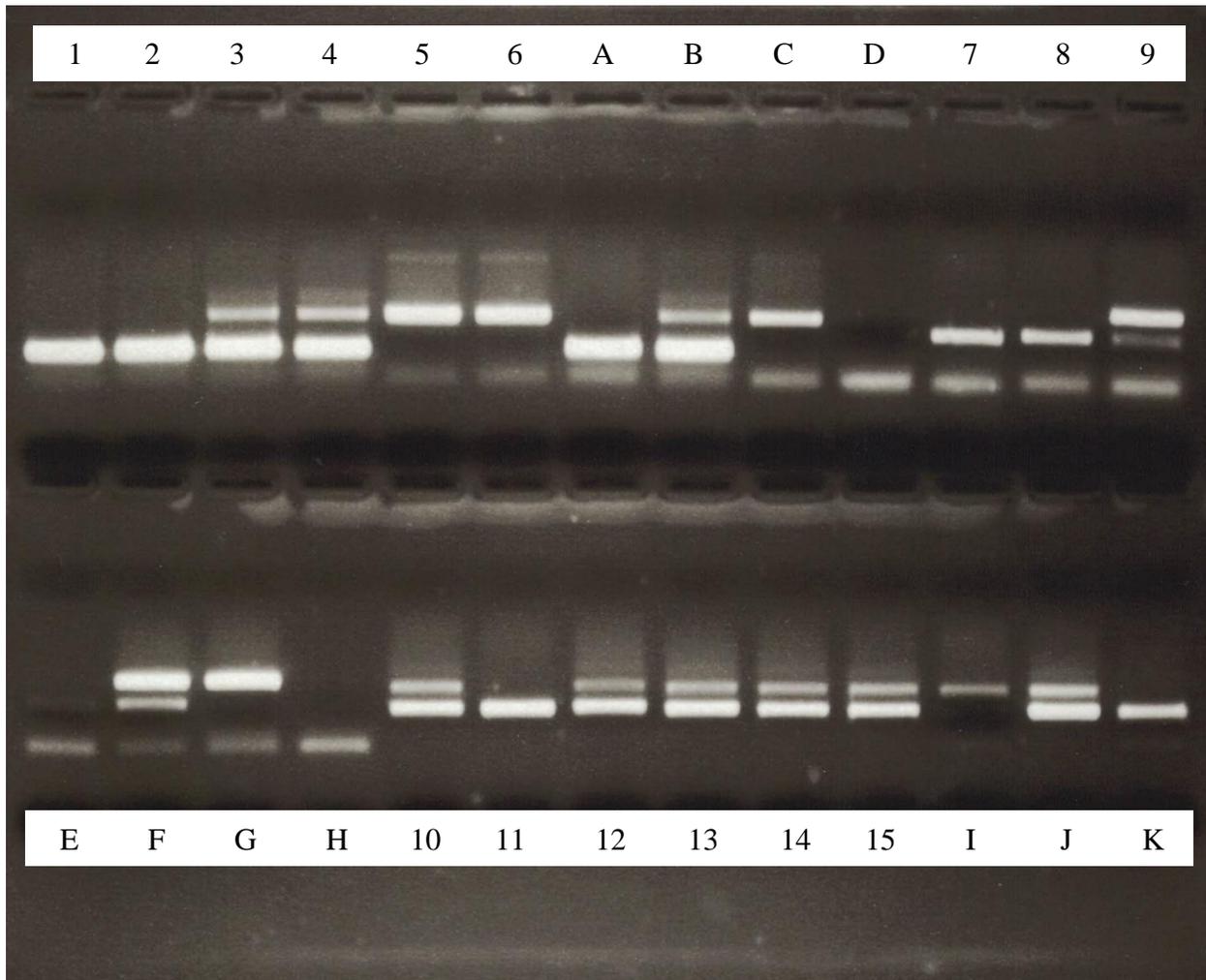
Figure 27. Characteristic example results from the genotyping PCR reaction. Representative gel electrophoresis data of genotyping conducted on VIP, VPAC1 and VPAC2 strains. This gel includes unknown samples as well as controls for each strain with the analysis characterized in table 8.

Table 8.   Legend for figure 27 genotyping

Lane number	Tail number	Strain	Result
1	Unknown 1	VIP	WT
2	Unknown 2	VIP	WT
3	Unknown 3	VIP	HET
4	Unknown 4	VIP	HET
5	Unknown 5	VIP	KO
6	Unknown 6	VIP	KO
A	VIP WT Control	VIP	WT
B	VIP HET Control	VIP	HET
C	VIP KO Control	VIP	KO
D	VIP H_2O Control	VIP	N/D
7	Unknown 7	VPAC1	WT
8	Unknown 8	VPAC1	WT
9	Unknown 9	VPAC1	HET
E	VPAC1 WT Control	VPAC1	WT
F	VPAC1 HET Control	VPAC1	HET
G	VPAC1 KO Control	VPAC1	KO
H	VPAC1 H_2O Control	VPAC1	N/D
10	Unknown 10	VPAC2	HET
11	Unknown 11	VPAC2	KO
12	Unknown 12	VPAC2	HET
13	Unknown 13	VPAC2	HET
14	Unknown 14	VPAC2	HET
15	Unknown 15	VPAC2	HET
I	VPAC2 WT Control	VPAC2	WT
J	VPAC2 HET Control	VPAC2	HET
K	VPAC2 KO Control	VPAC2	KO
I (not shown)	VPAC2 H_2O Control	VPAC2	N/D

2.3.2. Genotype affects taxonomic structure

The vasoactive intestinal peptide and intestinal microbiota signaling pathways have both been implicated in similar settings such as obesity, immune dysregulation and inflammatory bowel diseases. Although their roles in the body intersect, a critical gap in knowledge remains as no research has yet analyzed their potential relationship. We hypothesize that disruption of the VIP signaling pathway will alter the taxonomic make up, as well as the endocrine functionality of the microbiome. The microbial communities from fecal samples of mice lacking the VIP peptide were sequenced to test this hypothesis.

Figure 28 depicts a stacked bar graph representing the 16S sequencing results at the phylum level. Separated into male and female with all three genotypes, we can see a reduction in Firmicutes in both male and female KO mice when compared to WT. This reduction is compensated by an increase in Bacteroidetes and Proteobacteria. The smaller Deferribacteres population is similar in abundance from WT to HET and drops in the KO strain. The removal of VIP regardless of sex reduces Deferribacteres and Firmicutes populations, while increasing the levels of Bacteroidetes. The changes between WT, HET and KO are similar between male and female mouse groups. The main differences are seen in the male and female WT groups. The male WT mice seem to act as an intermediary between the HET and KO mice, and differ from the female WT mice. This is interesting as the male HET and KO strains are similar in microbial abundance when compared to females. This suggests that gender and sex hormones may play a role in bacterial abundance through VIP.

The ratio of the Firmicutes to the Bacteroidetes phyla has been linked to obesity phenotypes in mice and in humans. Discussed to greater detail in 2.1.3.1, increases in Firmicutes and decreases in Bacteroidetes have been linked to obesity in patients. First the average of these

two groups were individually plotted in figure 30. Here we can see that as the gene is extinguished (KO), the levels of Bacteroidetes greatly increase and the levels of Firmicutes decrease. The HET mice for both genders seem to host similar levels of these two phyla. Interestingly, the WT mice have a greater amount of Bacteroidetes, with the male WT levels residing between HET and KO. Our data suggests that the partial removal of VIP results in a shift towards the obese phenotype and an increase in Firmicutes, whereas the complete removal of VIP shifts towards a lean phenotype observed in both sexes.

To determine changes in this relationship, the ratio data was plotted in a box and whisker plot in figure 31. This graph shows a range of ratios for both WT and HET for both sexes with a small F to B ratio in the KO strains. This was important to demonstrate the clear spread between these ratios as well as provide an insight into the differences between genotypes. The WT and HET mouse group data is scattered with ratios ranging from nearly zero all the way to 3.5. The KO mice on the other hand present just the opposite, with a compact ratio between 0 and 1. The data indicates that the lack of VIP reduces the F to B ratio. We conclude that based on the F to B ratio, the KO mice must be leaner in comparison to HET and WT.

The genus level stacked bar graph in figure 29, demonstrates that changes in bacterial abundance can be found all the way to the genus taxonomic level. Both knockout strains show a decrease in uncultured S24-7 Bacteroidales (black) and an increase in Bacteroides (dark green) and Helicobacter (purple). The number of genera present makes for difficult interpretation of the stacked bar data and will be separated out into individual genus later in this section. Although similar compositional changes are seen at every level of the taxonomic tree, for simplicity, only phylum and genus level changes are shown below. The remaining taxonomic graphs and breakdowns can be found in appendix A.

Figure 28. Phylum level taxonomic differences between VIP male and female +/+, +/-
and -/-.
Sequenced fecal sample data is represented as a stacked bar graph. This graph represents
changes at the phyla taxonomic level, with the males on the left and the females on the right.
The key below the graph represents the different phyla indicated by color.

Genus Level Taxonomy
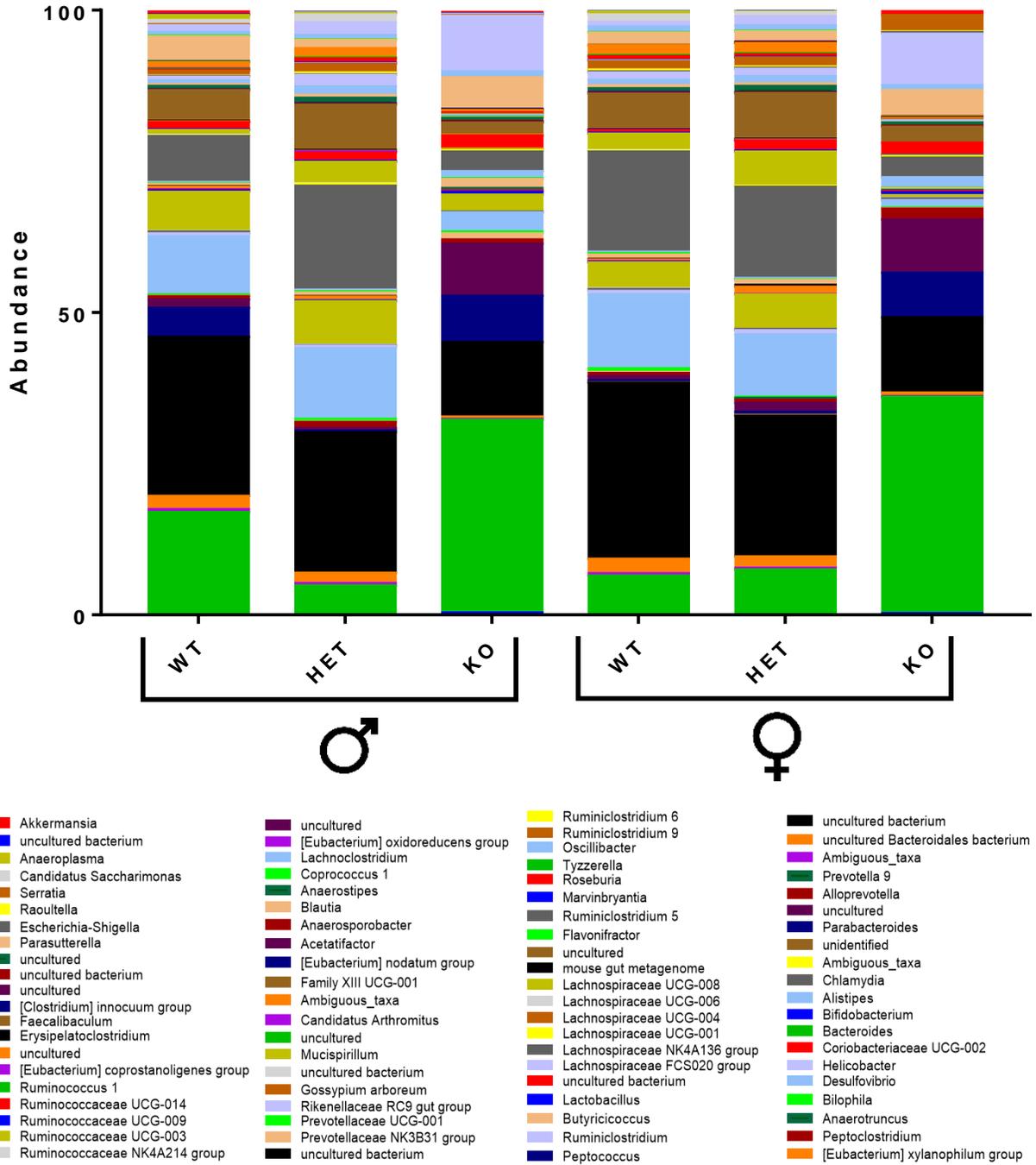
Figure 29. Microbial community changes at the genus level for VIP mouse strains.
This stacked bar graph represents the percent abundance of various bacterial genera for each genotype for both sexes. The figure legend depicts an n=8 (7 for male KO) for all strains. The figure legend below the depicts the various color-coded genera. Percent values are available in appendix A.
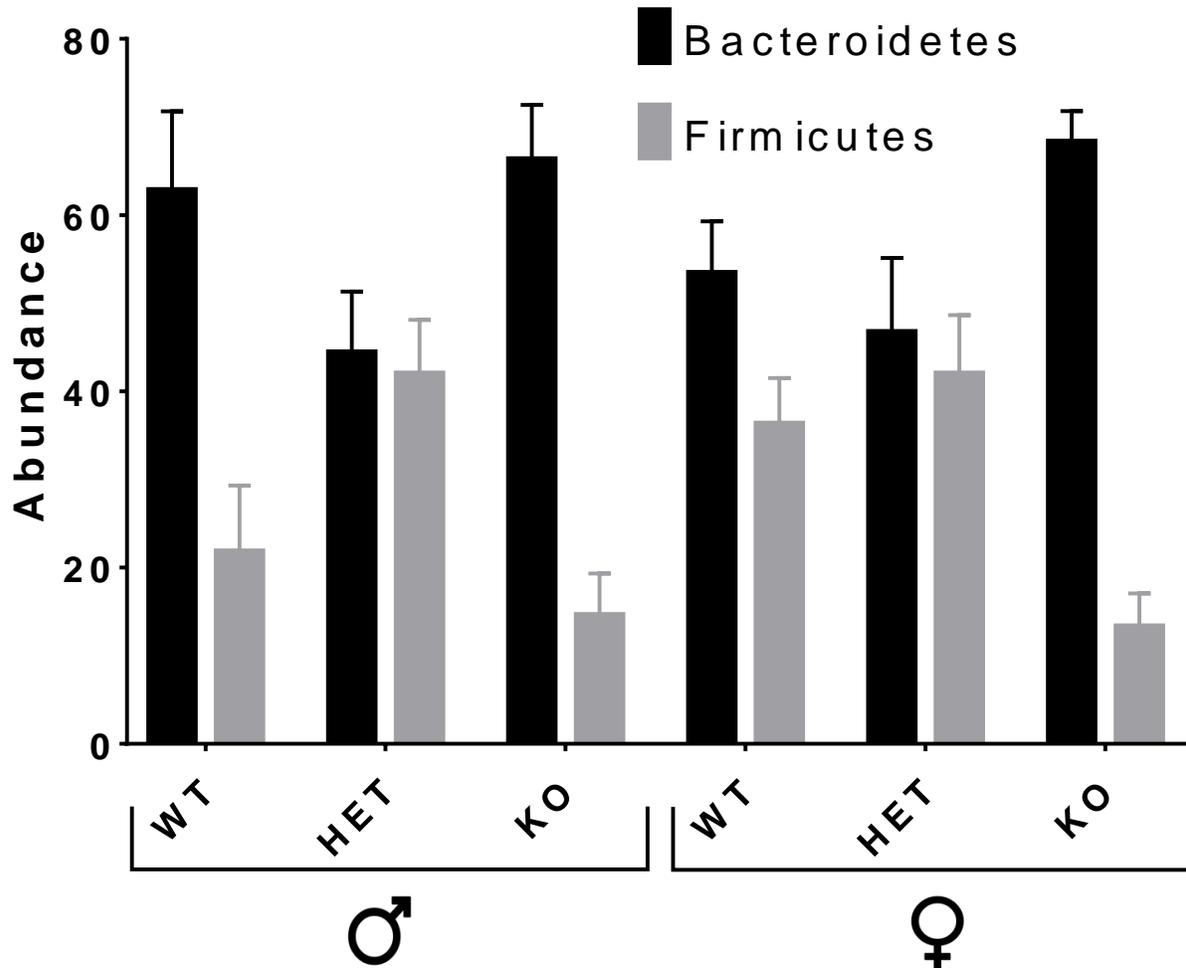
Figure 30. Levels of Bacteroidetes and Firmicutes among the mice strains.
A comparative bar graph of the percent abundance of the Bacteroidetes (black) and Firmicutes (gray) phyla found in each mouse strain. The male mice are on the left and the females on the right. The percent abundance of these phyla was averaged across an n = 8 (7 for male VIP KO), across all strains and the error bars indicate SEM values.
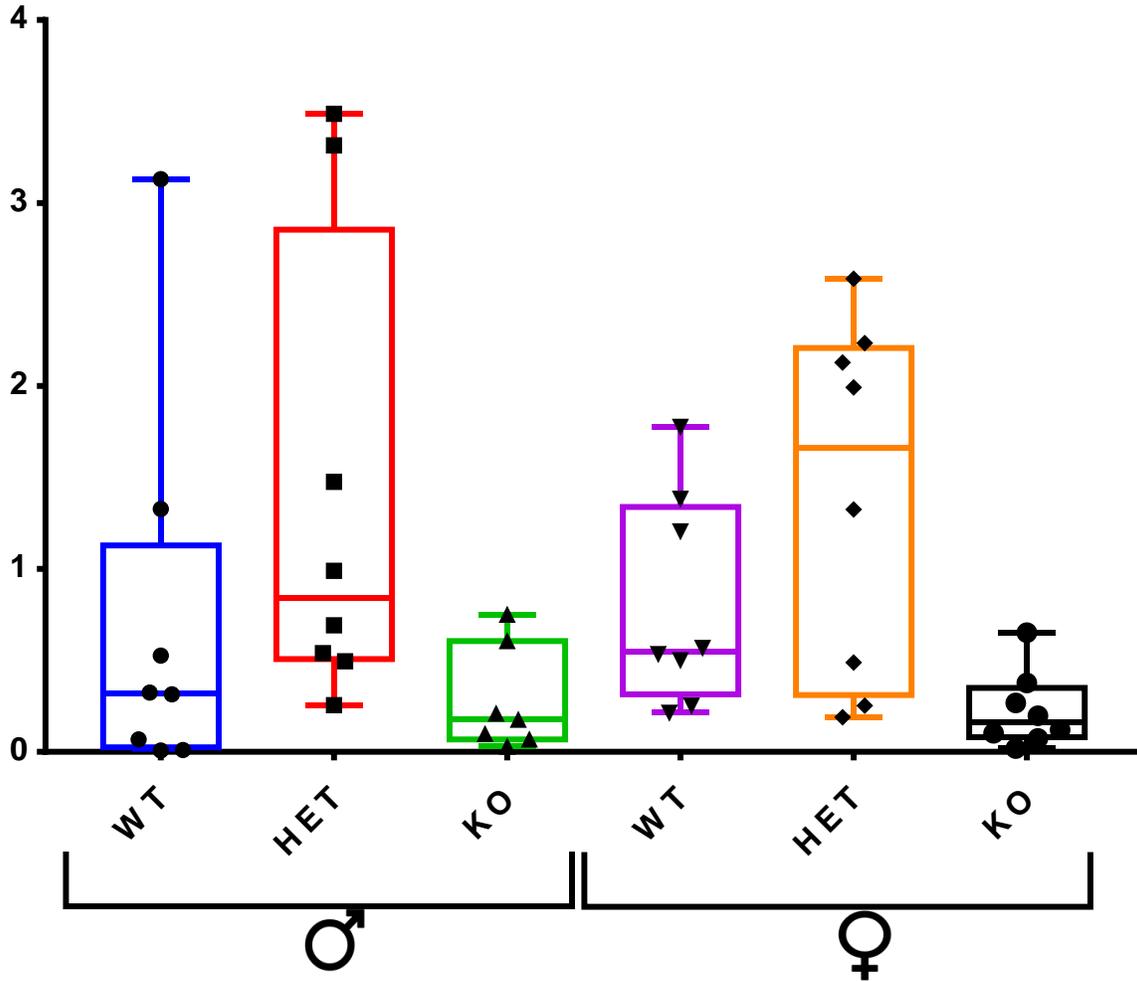
Figure 31. Ratio of Firmicutes to Bacteroidetes between tested mouse strains.
The ratio of Firmicutes to Bacteroidetes in each individual mouse tested in represented above each strain category. The male mice are on the left and the females are on the right. The ratios are then plotted in a box-and-whisker plot representing the maximum, 3rd quartile, median, 1st quartile and minimum values from the top down respectively.

The intersection of VIP and the microbiota signaling pathways suggests a possible relationship between them. Although the stacked bar graphs allow for visualization of fluctuations within the entire microbial community, the analysis of changes in individual phyla is better demonstrated by individual bar graphs. This allows for the addition of standard error of mean (SEM) which is not presentable in the stacked bar graph. Figure 32 shows phyla that exhibited significant changes between VIP strains, using the Bonferroni multiple comparisons test (2.2.7.5). In the Bacteroidetes phyla, the KO strain was statistically higher than both the WT and HET strains. This was not seen in the male mice though, where the KOs were statistically higher than the HET but not the WT. Interestingly, the WT and HET strains seem to have a lower Bacteroidetes percent than the KOs, suggesting that the absence of VIP may be hindering this phylum. The Firmicutes phylum seems to the opposite of the Bacteroidetes phylum, decreasing and increasing in response to the Bacteroidetes change. Similar to the Bacteroidetes, no statistical change is observed between the male WT and KO strains, but is seen in the female mice. In both sexes we observe an increase from WT to HET and a decrease from HET to KO. Proteobacteria, was only present around 3 to 7 percent in the WT and HET strains for both sexes. Although not statistically different in the males, the KO strains both observed a drastic overall increase of nearly 10 percent. Seen in the KOs this increase may suggest that the lack of VIP results in a drastic increase in Proteobacteria. The Actinobacteria phylum was very unique and only observed in the KO mice. The large error bars are the result as not every KO mouse tested contained the phylum. In conclusion, the removal of the VIP signaling pathway greatly changes the percent abundance of the phyla present within the feces. The partial presence of the VIP gene (HET) does not impact the microbiota as much as its complete ablation. The male WT mice also seem to differ from their female counterparts and seem to reside between HET and KO strains.
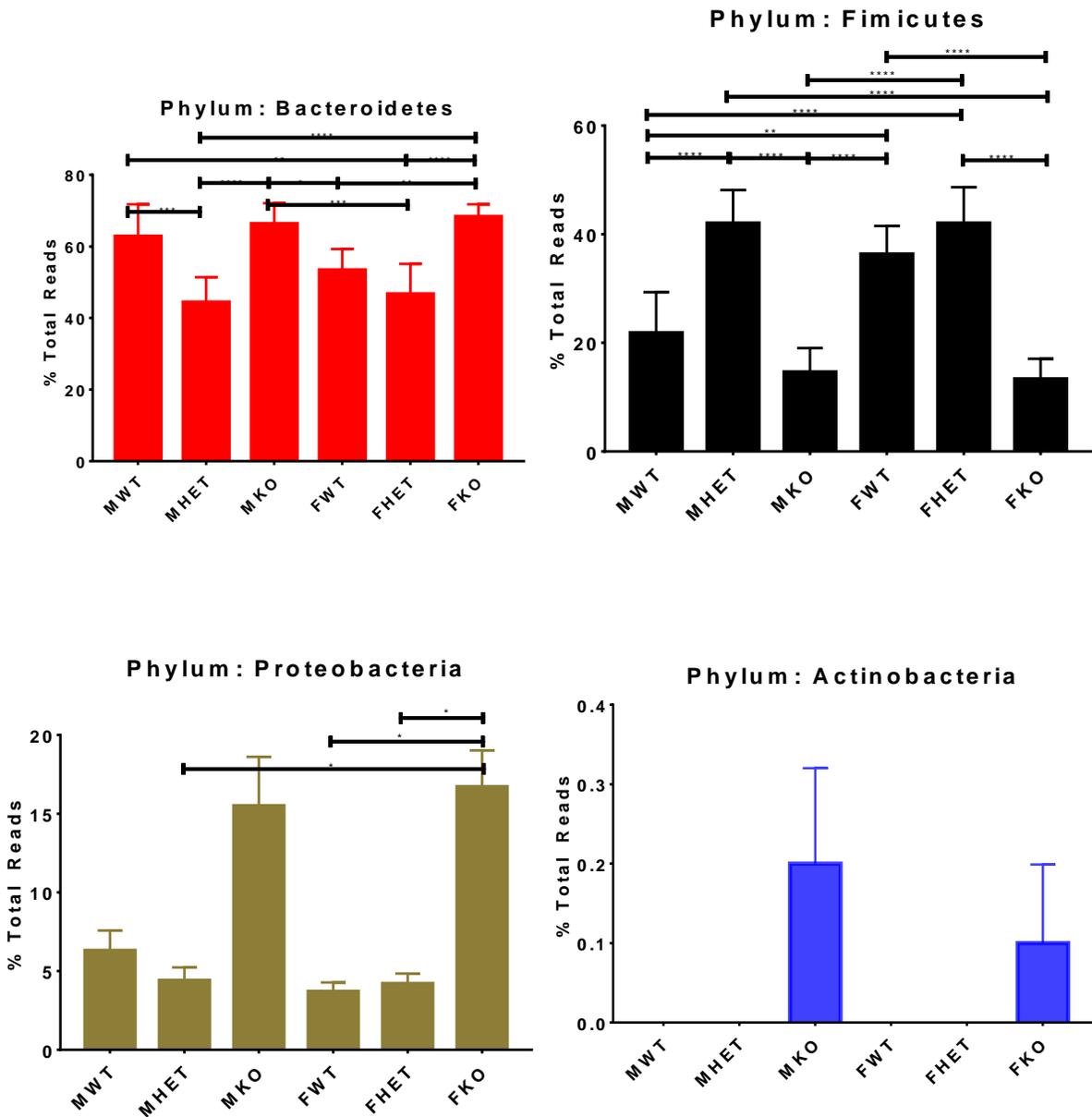
Figure 32. Phylum level statistical differences between VIP strains and sexes.
Each bar graph represents an individual phylum and its changes between the mouse strains.
The male mice are on the left and the female mice are on the right. The error bars depict
calculated SEM values with horizontal lines depicting statistical significance. Stats were run
using the Bonferroni test discussed further in 2.2.7.5.

Although phylum level analysis can reveal changes between the tested strains, it is only the second taxonomic level and just skims the surface of bacterial changes. To better understand the impact of VIP deficiency on the microbiota, genus level changes were analyzed. The 16S genera taxonomic data was split into three groups, based on trends of change between the mouse genotypes. Figure 33 for instance, demonstrates the first group containing the Bacteroides, uncultured Porphyromonadaceae and Helicobacter genera. These three bacterium all increased in number when VIP was absent. Interestingly, the partial removal of VIP, determined by analysis of HET mice, did not statistically change their percentage compared to wild type. These observations were true in both male and female mice. Both uncultured Porphyromonadaceae and Helicobacter increased in the KO strains by nearly 10 percent. A discrepancy was observed with the male WT mice, whom showed an increase in the Bacteroides genus, when compared to HET, but were still statistically lower than the KO.

The second group, visualized in figure 34, is composed of Mucispirillum, Alistipes and uncultured Bacteroidales S24-7. These genera acted opposite to the first group and demonstrated lower levels in the KO strains and higher/similar levels in the WT and HET strains. These 3 genera all demonstrated significant differences between the WT and KO strains, suggesting that the removal of VIP really impacts their abundance. The HET strain did not differ much from the WT group. For these three genera it seems that the partial removal of VIP does not significantly impact their presence. Group 3 (figure 35) is composed of uncultured Peptococcaceae and Lachnospiraceae NK4A136. In males, these two genera showed an increase from WT to HET and a decrease from HET to KO. Male WT in both were much lower than the female WT and similar to the KOs. In females, we see a decrease from WT to HET to KO, with a greater change from HET to KO. We conclude that VIP deficiency impacts the total abundance of these genera.
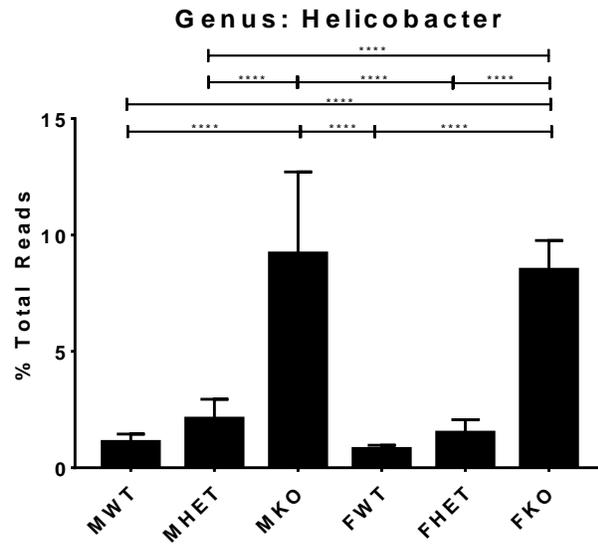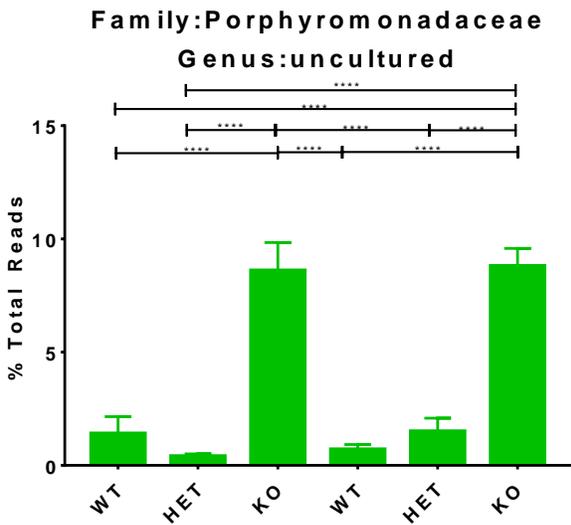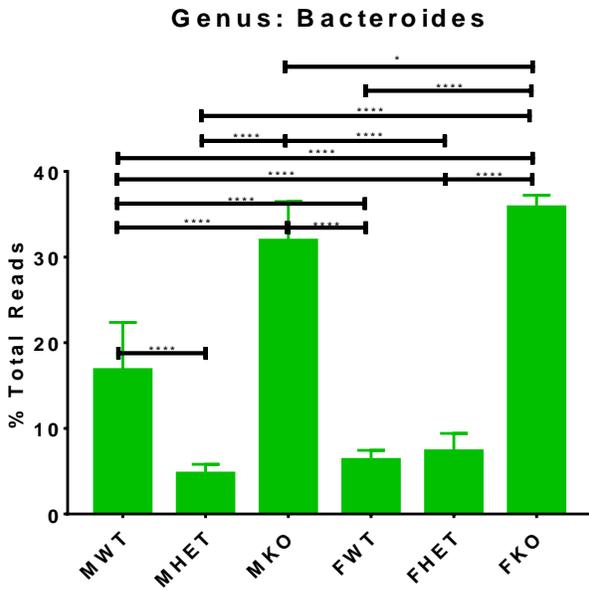
Figure 33. Changes in group 1, Bacteroides, uncultured Porphyromonadaceae and Helicobacter.
These three bar graphs depict the levels of Bacteroides, uncultured Porphyromonadaceae and Helicobacter genera. These were grouped together due to the similarity of their change between genotypes. Both the male and female groups demonstrate a high abundance in the KO and a low abundance in the WT and HET strains. Error bars depict SEM values.
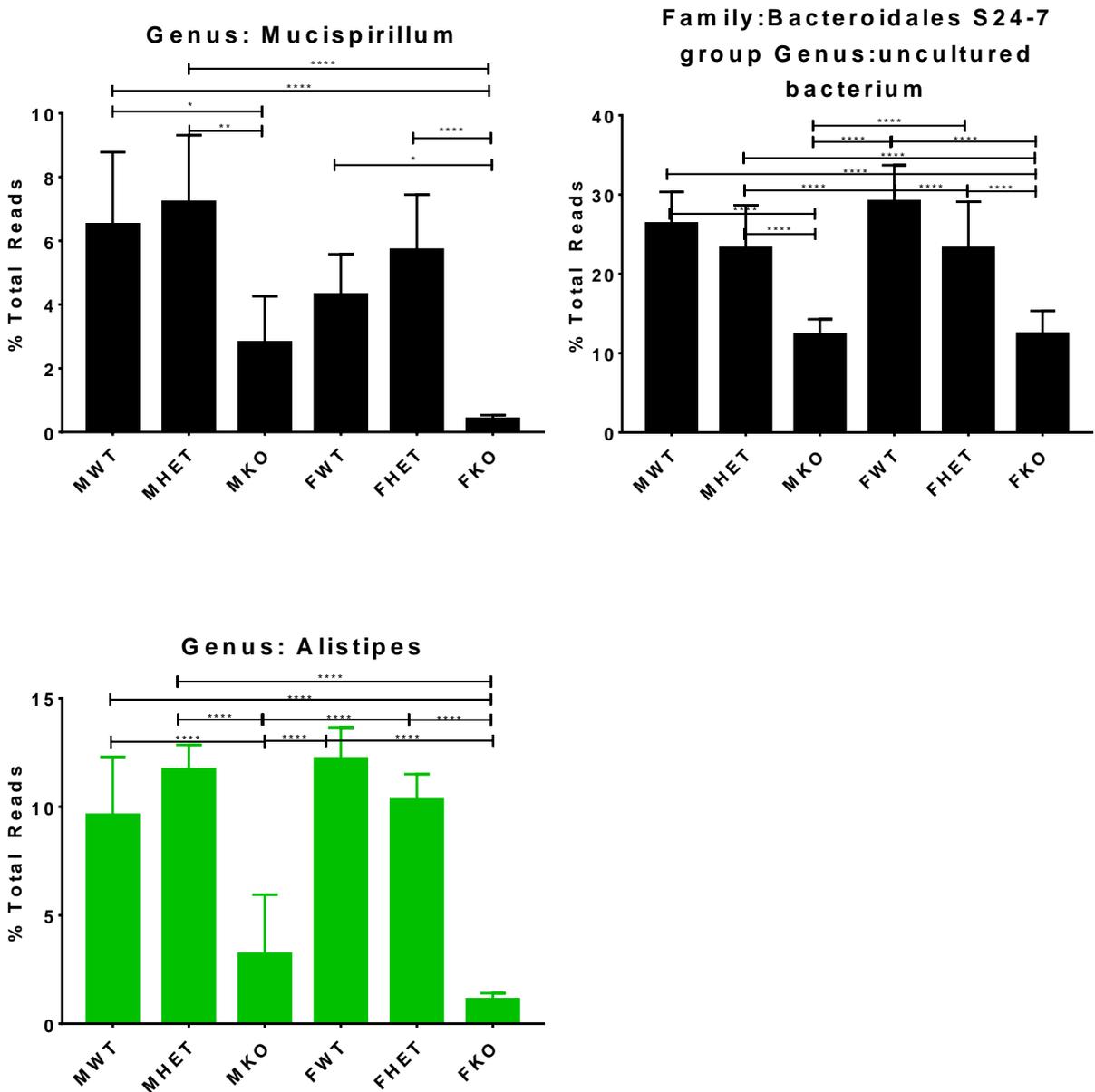
Figure 34. Genus level analysis of group 2, Mucispirillum, Alistipes and uncultured Bacteroidales S24-7.

The average abundance is plotted on individual bar graphs with error bars indicating SEM values. These genera are categorized as group 2 due to similarities in overall change. Male mice are presented on the left and the females are presented on the right.
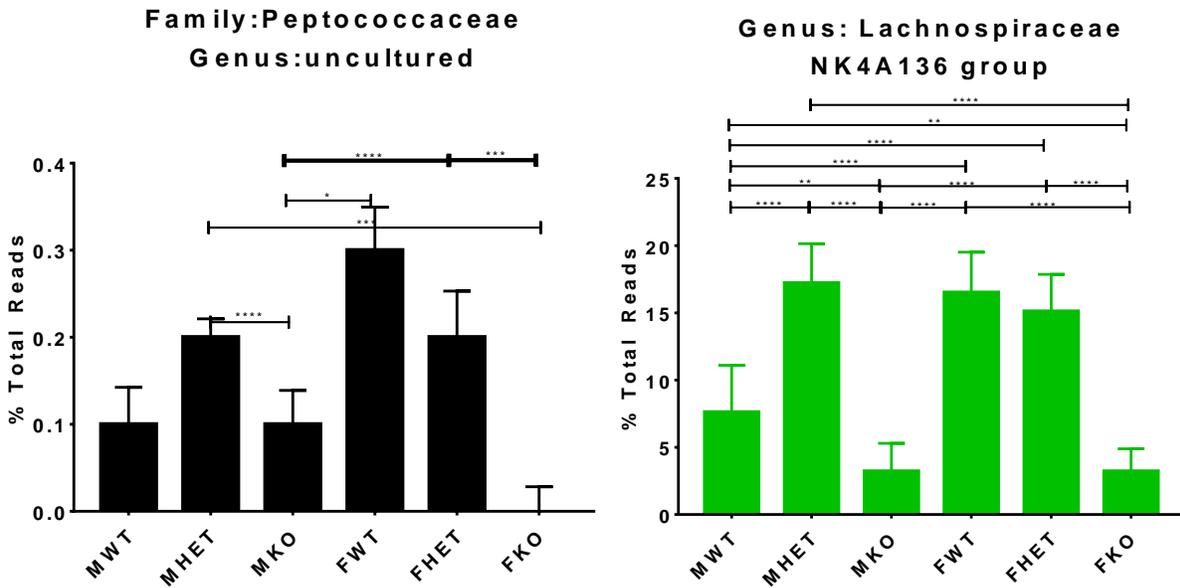
Figure 35. Changes in the Peptococcaceae family and the Lachnospiraceae NK4A136 group (group 3).
These individual bar graphs are at the genus level and demonstrate the changes between mouse strains for the uncultured Peptococcaceae and Lachnospiraceae NK4A136 group. Error bars depict SEM values.

2.3.3. Alpha diversity, within each group, comparisons

To determine changes in species diversity between the different mouse habitats (each mouse genotype), alpha diversity analysis was performed on generated 16S taxonomic data. The alpha diversity analysis of species richness was assessed using the chao1 (Chao 1984), Shannon (Shannon 1948), observed species and PD whole tree (Faith 1992) indexes. Due to the similarity in alpha diversity results between these databases, only the PD whole tree analysis is shown in figure 36. As discussed in the materials and methods section of this chapter, the PD whole tree analysis includes richness, evenness and measures phylogenetic tree branch length. Comparisons between WT and KO shows that in males and females the median species richness is much higher in the WT mice (depicted as a red line). While the minimum measurement in the male

101

WT is similar to the minimum value in male KOs, the 3rd quartile (around 560) and median (around 525) suggests that overall the male WT measurements are higher than their male KO counterparts.

Comparisons between genders do not show significant differences between male and female HET strains. In the WT groups, we see a lower median and a much greater spread in the males than in the females. The female WT samples are compact with a small box and whisker plot while the males are diffused out. The size of the knockout group plot suggests similar variations in richness for both genders. The median for the females suggests higher overall richness than the males, but in comparison to WT and HET we see a drop in richness for both KO genders. In conclusion, both male and female mice see a trend of higher richness in WT and HET mice and a lower richness for the KOs.
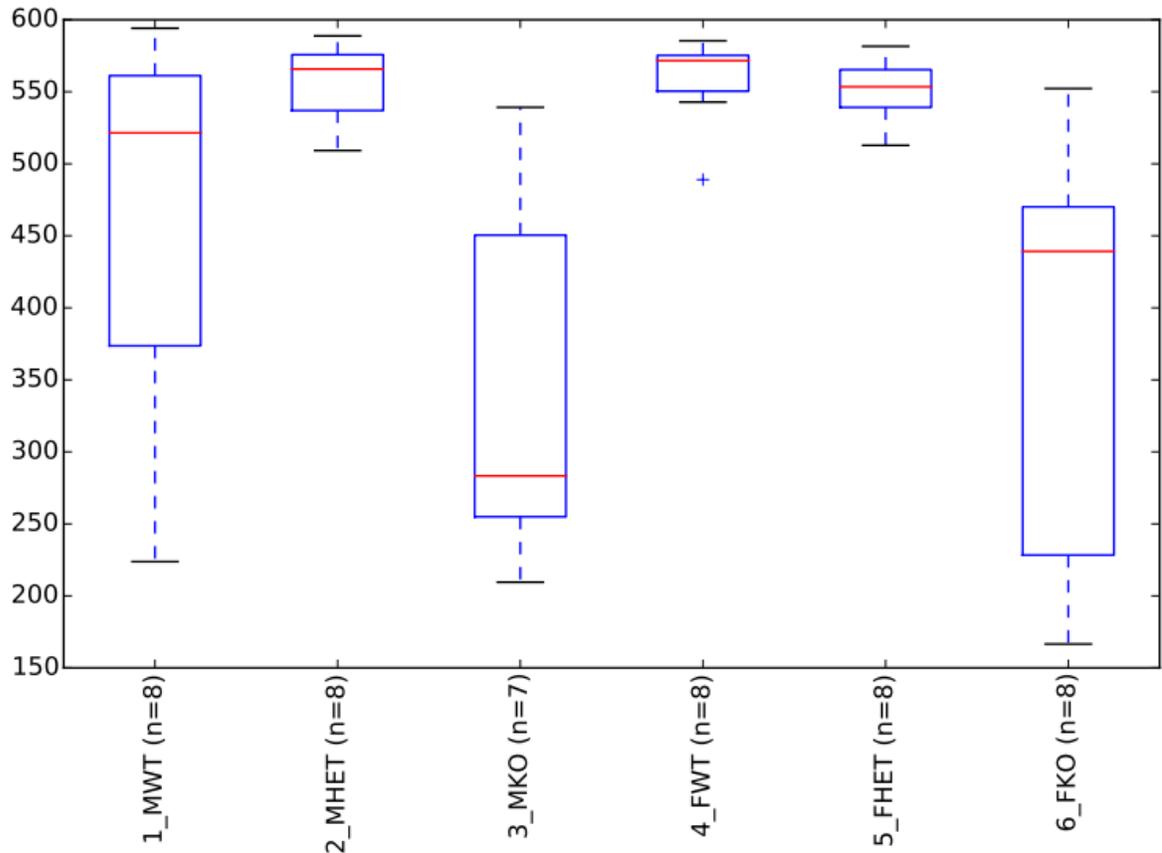
Figure 36. PD whole tree analysis of alpha diversity.
Examination of species richness by PD whole tree looks at branch length as well as differences in species. This box and whisker plot visualizes the drop-in richness in both of the knockout strains, when compared to both WT and HET mice. A drop in microbial diversity is associated with a number of disease phenotype models.

2.3.4. Beta diversity, between the groups, comparison

Beta diversity measurements assist in understanding the differences in species composition between different environments, while alpha diversity analyzes variety at each individual environment. Figure 37 depicts a three-dimensional principle coordinates analysis plot (PCoA) which displays the relative distance relating the different mouse intestinal biological communities. The weighted PCoA plot was chosen because weighted samples take relative abundance of taxa into account while unweighted only considers presence. Each collected

sample is represented as a dot upon the graph with its color representing its genotype and gender. The z-axis (PC3) images are not shown due to lack of separation between the samples in that plane. Two major ovals were added to the PCoA plot to depict clustered samples.

As the blue oval demonstrates, the WT and HET samples from both sexes clustered together. This implies the most similarity between WT and HET groups. As previously seen with taxonomic analysis and with alpha diversity analysis, we see a similarity between WT and HET mice regardless of sex. This infers that the partial removal of the VIP gene does not significantly impact the microbial community. Remarkably, the knockout samples from both sexes grouped together (depicted by the yellow oval) apart from the WT and HET group, with a clear divide between the two ovals. The clustering of KO suggests similarity between the KO samples and a separation from the KO mice to the WT and HET. This data suggests a change in diversity is caused by the environments present between WT and HET, and KO strains. We do see a group of three male WT samples off on their own (once again the odd-ball) which may be leading to alpha diversity and taxonomic differences observed previously. This demonstrates the importance of including both sexes in studies, as we demonstrate that gender may impact the microbiome.
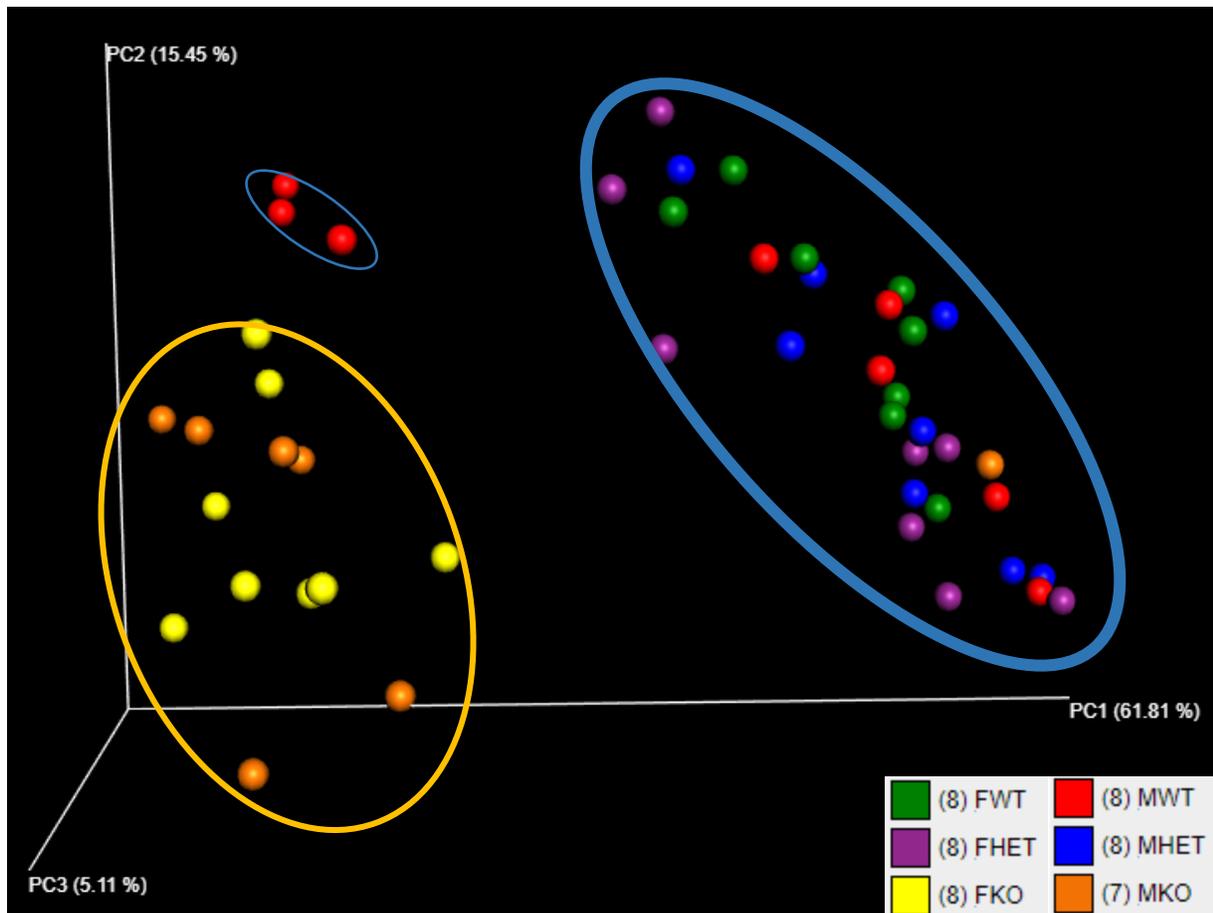
Figure 37. Weighted unifrac beta diversity PCoA analysis.
This three-dimensional principle coordinates analysis plot displays the relative distance comparing the mouse intestinal biological communities from each genotype and gender. Post-analysis ovals are added to demonstrate clustering of similar microbial communities. Each dot on the graph is representative of an individual sample with the legend identifying its genotype and gender. This PCoA plot is 3-dimensional but a focus is placed on the X and Y axis changes as no significant changes were observed in the Z (PC3) plane.

2.3.5. Predictive metagenome functional content with PICRUSt and the KEGG database

The communicational pathways between the microbiota and the host are changed between the knockout, heterozygous and wild type mouse strains. Changes in the microbial community composition can impact the endocrine functions of the microbiome. To determine changes in the metagenome upon removal of VIP, analysis of metabolic pathways was conducted

105

using the PICRUSt bioinformatics software against the KEGG database. This analysis was

performed for all genotypes and genders. The changes in taxonomy between these strains results

in changes in predictive metagenomics between them. Figure 38 visualizes our findings, where

an increase in a number of nucleotide and ATP biosynthesis pathways was found. These were

found to be increased in the KO mouse strains for both genders. The knockout mice also

demonstrated an increase in glyoxylate cycle function, suggesting the utilization of fats for

energy. This may be feeding into the gluconeogenesis cycle as we see an increase in that as well.

This could suggest the presence of excess energy and that the breakdown of glucose is not

necessary for energy generation. An increase in the pentose phosphate pathway indicates the

creation of NADPH which may be used in nucleotide and cholesterol biosynthesis and anabolic

pathways.
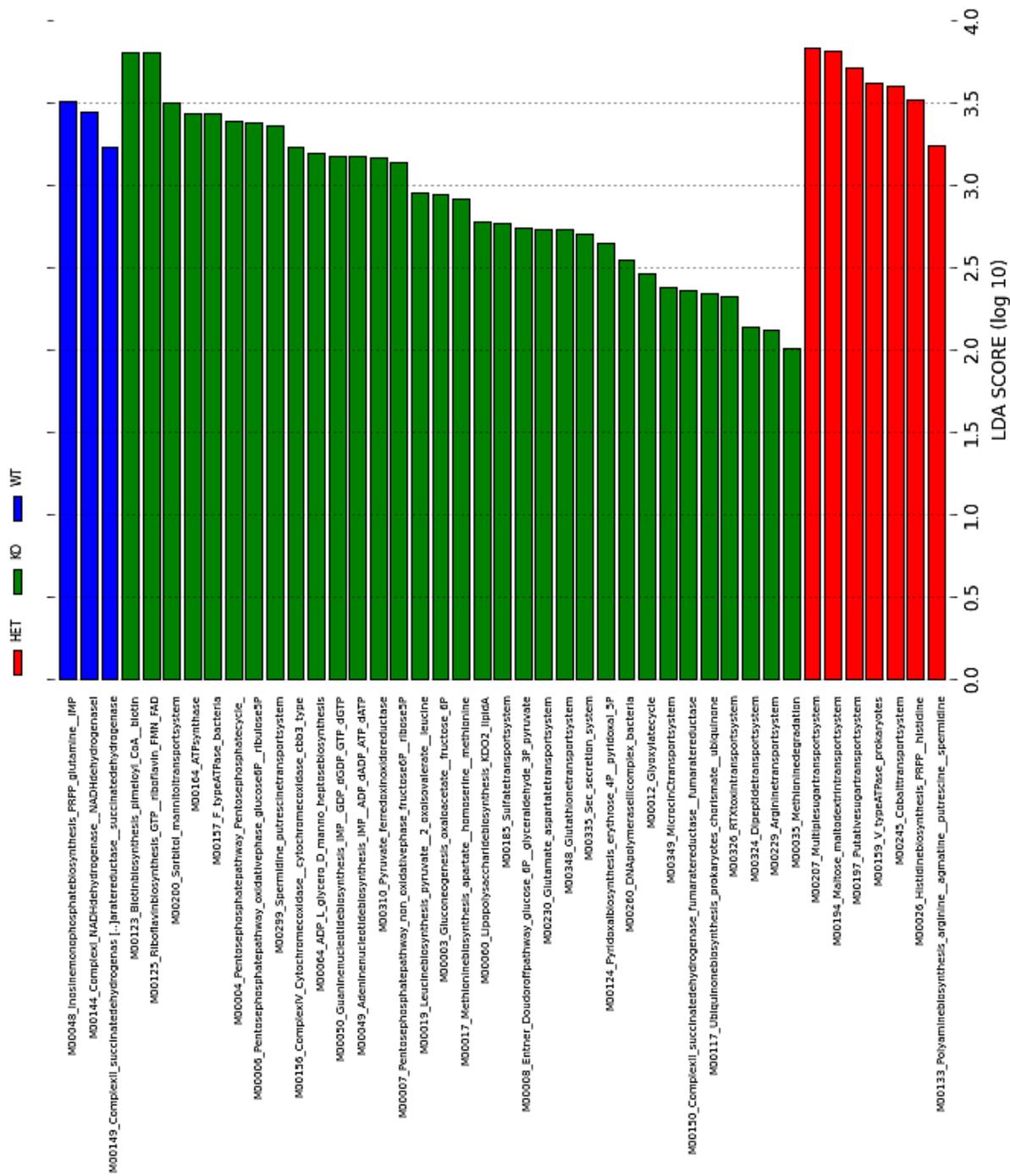
Figure 38. Predicted functional metagenomics using PICRUSt.
This horizontal bar graph depicts changes in metagenomic pathways as analyzed by the
PICRUSt predictive software. PICRUSt investigates changes in bacterial communities and
predictions functional change in pathways based on previously established databases.

2.4. Discussion

This study provided novel and interesting findings regarding the connections between neuropeptides and the gut microbiota. We conclude that the partial or complete genetic removal of VIP results in changes in the taxonomic structure of intestinal bacteria. For example, in the Bacteroidetes phyla, we see an increase of nearly 20% in knockout female mice vs HET and WT. The depletion of VIP also reduces the alpha-diversity within the intestines and is much lower in the VIP -/- strains than the VIP +/+ and +/- littermates. Additionally, we discovered changes in the predicted metagenomic functionality among the strains. In the KO mice for instance, we see an increase in the pentose phosphate and sugar transport pathways. The lack of VIP altered a number of biosynthetic pathways within the microbiota. This research also makes us question whether previous changes observed in VIP KO mice were caused by the altered microbiota or by the lack of VIP alone?

Understanding the importance of VIP in the gastrointestinal tract, we hypothesized that VIP signaling through VPAC1/VPAC2 would change the makeup of the intestinal microbiota. After utilizing PCR to genotype mouse subjects, fecal samples were used to determine microbial composition. The resulting taxonomy graphed in figures 28 through 29 shows these overall changes. These observations demonstrate that the disruption of VIP signaling, whether partial (HET) or complete (KO), results in changes at the taxonomic level. The utilization of HET mice here is important. We hypothesized that these partial knockouts would result in changes intermediary to WT and KO. Even at the top of the taxonomic rankings this hypothesis was disproved.

Our WT compared to C57BL/6 mice from other colonies are similar to some colonies and different from others (Fransen et al. ; Johnson et al. 2016). As discussed previously, the

microbiota can be impacted by a number of things. Differences can be caused by different sources of food and water used in each mouse colony. Things like humidity (Davenport et al. 2014), bedding (Bai et al. 2016), feeding patterns (Zarrinpar et al. 2014), temperature (Chevalier et al. 2015) and type of housing (Ericsson et al. 2015) can also impact the microbiota. A difference in mother's genotypes could also change what bacteria are present. In our studies all of these variables were kept consistent for all test mice used. Only heterozygous mothers were used to produce progeny in order to eliminate impact of breast milk on microbial growth.

Between the wild type and heterozygous mice, we observed a reduction in Bacteroidetes levels and an increase in the Firmicutes phylum. This trend was more apparent in the male gender but still present in the females. The change between WT and HET to KO was consistent between the two sexes. For both males and females, we observed an increase in Bacteroidetes and a greater decrease in Firmicutes. This decrease was compensated by an increase in Proteobacteria in the KO strains. The ratios of Bacteroidetes and Firmicutes have been linked to obesity in a number of publications. It has been published that mice with an obese phenotype will exhibit a reduction in the total percentage of Bacteroidetes and an increase in the Firmicutes phyla.

The ratio of these two phyla is visualized in figures 30 and 31. Figure 30 displays the level of both phylum while 31 displays the ratio between the two. Analysis of this ratio also demonstrates the importance of using both genders in mouse research. In figure 30 the change of Bacteroidetes and Firmicutes in male mice from WT to KO is not statistically different, but in female mice it is. But when the ratio of the two is calculated ($Firmicutes/Bacteroidetes$) with standard error of the mean (SEM), we see the changes becomes more apparent. The trend of

weight for our knockout mice is similar to previous findings, where our knockout mice weight

less than WT and HET.

The KO strains were also the only strain to contain the Actinobacteria phylum. Although

this phylum was present in very low amounts (0.20% MKO and 0.10% FKO), no other strains

contained any Actinobacteria. This interesting phylum is found more often distributed in

terrestrial and aquatic ecosystems (Barka et al. 2016). Downstream at the genus taxonomic rank,

following their phylum, Bifidobacterium are the only Actinobacteria subset with presentation

only in the knockout strains. This interesting genus is very sensitive to O2, suggesting that

perhaps the KO strains have lower oxygen levels in their intestines (Kawasaki et al. 2006).

Recent research has also demonstrated that the utilization of Bifidobacterium as probiotics,

reduces the impacts of Crohn's disease and other inflammatory bowel diseases (Ghouri et al.

2014). A recent study comparing the changes in microbiota between high-fat, low-fat and high

and low fat with exercise, demonstrated that the Bifidobacteriaceae family (the family of

Bifidobacterium) was present only in low fat diet mice and undetected in their high-fat diet

counterparts. Curiously, the low-fat diet mice that exercised lowered their total percent of

Bifidobacteriaceae in comparison to the sedentary group (Evans et al. 2014). This could suggest

that fat is being rapidly used in VIP deficient mice (perhaps by the microbiota), when compared

to HET or WT, leaving a low-fat environment in the external gastro-intestinal tract allowing for

their survival.

As we continue the analysis down to the genus level, the number of differences increases.

The genus Bacteroides, under the Bacteroidetes phylum, seem to change similarly to their

phylum. Bacteroides levels were statistically higher in the knockout strains when compared to

their WT and HET counterparts. This member of the gut microbiota has been shown to

exacerbate Escherichia coli (EHEC) infections in mice. Increasing this microbe during infection resulted in increased gut permeability and an increase in mortality when compared to mice free of this genus (Curtis et al. 2014). Bacteroides also produce metallo-β-lactamase which can shield other microorganisms in the gut from antibiotic attack and even defend pathogens like EHEC (Stiefel, Tima, and Nerandzic 2015). A rise in this genus in the knockout mice, may lead to a decrease in antibiotic functionality. The increased gut permeability caused by the lack of VIP (Wu, Conlin, et al. 2015) may also not be a direct result of the missing VIP, but rather due to the rise in the Bacteroides genus. The utilization of germ-free VIP -/- mice would be important to answer this question.

The Bacteroidales S24-7 family is an example of how far we still have to go to completely understand host microbiota relationships. Out of the total taxonomies identified over all the strains, this family makes up 22.8% of those reads (figure 29). None of these have been identified down to the genus level. On top of that only 47 publications are found when searching "S24-7" on PubMed.gov. Although it has been as widely researched as other microorganisms, the Bacteroidales S24-7 family plays an important role in the intestines. Research by Evans et al. and Tomas et al. demonstrates that mice fed a high-fat diet significantly lowered their S24-7 percentage, but the addition of exercise increased it equally between low fat and high fat diet mice (low-fat diet was still statistically higher than high-fat) (Evans et al. 2014; Tomas et al. 2016). The levels of this family have also been linked to hepatic metabolism and function. Post partial hepatectomy (removal of 2/3rds of the liver), a rapid increase of S24-7 from 11.1% to 47.7% was observed. Analyzing predicted metabolic pathways from PICRUSt, these researchers found the S24-7 family in these mice was responsible for an increase in bile acid production pathways (Liu et al. 2016). In comparison to the WT and HET strains, the KO strains for both

males and females had a reduction in the S24-7 bacterium. From the WT to HET to KO the S24-7 family gradually reduced in percentage (figure 31). This reduction which is opposite of the change in the Bacteroides may suggest a change in the fat content of the chime. Mass spectrometry could be utilized in future studies to determine the composition of intestinal chime in these mouse strains to test this hypothesis.

The change in percentage of the Porphyromonadaceae family and the Helicobacter genus are similar to the Bacteroides genus. The knockout strains for both sexes increase significantly when compared to the HET and the WT strains (figure 32). In 2013, decreases in this family of bacteria was seen in tumor-bearing mice by Zackular et. al. Using antibiotics to manipulate the microbiota resulted in a decrease in the number and size of tumors in these mice. This suggests a link between this family and tumorigenesis (Zackular et al. 2013). The increase of this family in both knockout strains may suggest the elimination of VIP results in resistance to the development of colon cancers and tumor growth.

The discovery of the Helicobacter genus revolutionized microbiota research, by changing previously held beliefs that the stomach was a sterile organ (Marshall and Warren 1984). Since its discovery it has been implicated in a number of gastric cancers, vitamin B12 deficiency, anemia and ulcer formation (Sheh and Fox 2013). In human patients colonization by Helicobacter has been characterized mainly with severe bacteremia (De Witte et al. 2016). The lack of this genera has also recently been associated with disease, with evidence suggesting balance in its levels may be the key to disease prevention (Otero, Ruiz, and Perez Perez 2014). In the six strains tested, the Helicobacter genus made up nearly 9% more of the total taxonomic reads in the male and female knockout strains than in the wild type. Heterozygous mice from both sexes were only slightly higher than the WT and significantly lower than the knockouts

112

(figure 32). This increase in the KO strains may indicate increased susceptibility towards cancers and ulcer formation. Previous research suggests VIP KO mice are more vulnerable to colitis models (Jonsson, Norrgard, and Forsgren 2012), and the presence of this pathogenic strain may be the reason why.

The Mucispirillum and Alistipes genera both share extremely similar trends in change between wild type, heterozygous and knockout between males and females. These two strains impress the importance of utilizing both genders for studies. In the females we see a greater overall reduction in total percentage in comparison to males by nearly 3% (figure 32). The Mucispirillum genus was first discovered in murine intestines. Scientists investigating the mucus layer of the gastrointestinal tract discovered a distinct subgroup that had not previously been characterized (Robertson et al. 2005). Since its discovery, increase in Mucispirillum levels have been pinned as an indicator for oncoming colitis as Mucispirillum acts as a mucin degrader and can provide other microorganisms easier access to the intestinal epithelia (Berry et al. 2012). A reduction in Mucispirillum levels in knockout mice may suggest higher mucus levels in these mice as opposed to their wild type littermates. Reduction of the Alistipes genus was found to be correlated with depression, while an increase has been associated with stress in mice (Naseribafrouei et al. 2014). In humans, a study conducted by David et al. analyzed the influence of animal vs plant-based diets. They found that the change to an animal-based diet increases the abundance of Alistipes and suggested this genus may increase due to its protein fermentative capacity (David et al. 2014).

The Lachnospiraceae NK4A136 group is a prominent member of the intestinal microbiota. When compared to the WT and HET strains, the KO strains had statistically lower amounts of this group. In female knockouts, Lachnospiraceae was reduced by nearly 13%. In

males, the change from HET to KO was just as large as the females. From WT to KO though was only about a 5% decrease. In the gastrointestinal tract, higher levels of this genus have been shown in children with a reduction in adults (Hollister et al. 2015). Reeves et al. inoculated germfree mice with Lachnospiraceae and found that the presence of this genus prevented the colonization of Clostridium difficile. In the United States Clostridium difficile infections affect nearly half a million people annually (Reeves et al. 2012). This number may be reduced by the introduction of Lachnospiraceae as a probiotic. In our mouse strains this could suggest that the knockout mice are more susceptible to disease and infection as compared to the wild type and heterozygous mice.

The overall changes in taxonomy in the VIP knockout mice are similar between the genders. The trends of change from WT to HET to KO seem mostly consistent regardless of sex. There are a few fluctuations at the genus level which indicate differences in total percentage between males and females. Conclusions drawn from the taxonomic data go along with previously published VIP research. Our data suggests that the VIP KO mice contain more bacteria connected with inflammatory bowel disease susceptibility. Previous research has demonstrated that the induction of colitis in the KO strain, results in a more severe response than the WT. These research studies did not consider the role played by the intestinal bacterial communities in inflammation. Therefore, it is entirely plausible that the increased vulnerability to IBD in the KO mice was an indirect effect of the loss of VIP rather than a direct one. In future studies, the utilization of germ-free VIP knockout mice could provide an answer to this question, by eliminating the bacterial component of the equation.

As discussed previously in the introduction section of this chapter, the microbial community plays an essential role in obesity. Previous studies have demonstrated that in both

obese mice and humans, there is a reduction in the total percentage of Bacteroidetes and an increase in the Firmicutes phylum (Ley et al. 2005; Ley et al. 2006; Murphy, Velazquez, and Herbert 2015). These changes were also observed in the strains of mice used for this study. In males, Bacteroidetes levels decreased from WT to HET and increases slightly from WT to KO. The Firmicutes in the male mice increased from WT to HET and decreased from WT to KO. In female mice the trend was similar between HET and KO but different in the WT. The WT in the female mice showed higher Firmicutes than the HET and KO and higher Bacteroidetes than the KO (figure 34). Analysis of the ratio between Bacteroidetes and Firmicutes demonstrated a huge increase in both KO strains (figure 35). This data is similar to published VIPKO data where weights of the knockouts are lower than their wild type littermates.

The influences of the microbiota on host metabolism and its involvement in the gut-brain axis are based on the diversity of bacteria are make it up. Previous research has linked a reduction in bacterial diversity to increased disease susceptibility. In the strains tested, we found that the diversity levels in the knockout strains were significantly lower than their HET and WT counterparts. This was true when alpha-diversity analysis was completed against the Shannon, chao1, observed species and the PD whole tree indices. The PD whole tree analysis used measures not only the species diversity, but also the degree to which they are related. This local measure of species richness demonstrates that there are a lower number of species within the knockout strains compared to both wildtype and heterozygous. Interestingly the diversity in the male wild type strains was widely spread (figure 36). Although the average is still higher than the KO, the high range of male wild types suggests variety between the wild samples collected, confirmed in the beta-diversity analysis. The levels of reduced diversity in the knockout strains is surprising and suggests that VIP plays a major role in modulating taxonomic diversity.

115

The weighted beta diversity in figure 37 demonstrates the differences between all of the samples analyzed. Three ovals have been placed in the figure to demonstrate a grouping phenomenon inside the plot. A quick look shows three male wild type samples grouped separately from the other wild type and heterozygous strains. We suspect these samples are responsible for the spread within the alpha diversity (figure 36) analysis of their category. This may be due to males being more susceptible to microbiota changes or an error in previous steps, like genotyping. A genotyping error may have classified these mice into the wild type category while they may in fact be knockouts. This could cause a ripple effect and alter all taxonomic, diversity and metagenome data, but is important to correct if true. These samples will be re-genotyped to ensure proper categorization. The grouping of the knockout strains together demonstrates that these populations are very similar to each other and far apart from the wild type and heterozygous groups. We believe that this similarity suggests a change in the gastrointestinal environment and a change in the linage of the microorganisms present in the knockout strains versus the WT and HET, due to the lack of VIP. Interestingly, the close proximity of the HET and WT mice, indicates that the partial reduction of VIP does not significantly change the microbial population in comparison to their WT littermates.

The consideration of the intestinal microbiota as an endocrine organ means that changes in its composition may alter the metabolites that are secreted from it. Changes in taxonomy, as found amongst our six strains, results in the change of secretions and metabolites. Comparison of known populations against the KEGG database, predicts a drastic change in the metabolic pathways. The biggest change is observed in the knockout strains, where we find the greatest increase in the biotin and riboflavin biosynthesis pathways. Previous studies have demonstrated that the consumption of a high-fat diet causes a biotin deficiency in mice (Yuasa et al. 2013).

116

Infants fed with formula also result in biotin deficiency (Fujimoto et al. 2005). As previously

hypothesized, we predict this increase in biotin biosynthesis may be due to faster fat uptake by

the host, resulting in a low-fat environment in the intestines, resulting in an increase in biotin

synthesis in the knockout strains. Many riboflavin pathways are location in the nervous system.

An increase in this vitamin has resulted in migraine-headaches in mouse subjects (Butun et al.

2015). The depletion of riboflavin also leads to reduction in ATP levels in cells and an increase

in reactive oxygen species (ROS) (Riboflavin depletion of intestinal cells in vitro leads to

impaired energy generation and enhanced oxidative stress). We hypothesize that the increase in
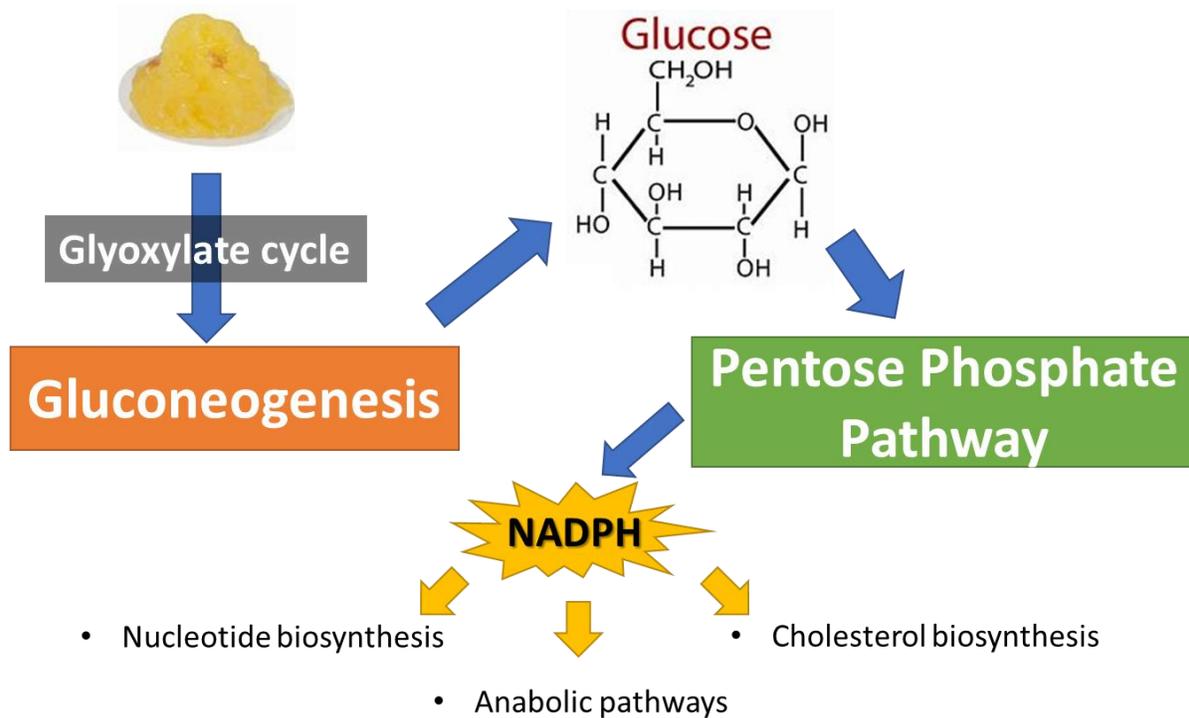
Figure 39. PICRUSt results interpretation.
Data interpretation suggests an increase in the glyoxylate pathway perhaps due to higher fat content in the intestines resulting in conversion of fats to pyruvate, which may be funneled into gluconeogenesis. An increase in gluconeogenesis results in increased glucose production shunted into the pentose phosphate pathway for NADPH formation. This anabolic pathway could be used by the microbiota for fatty acid, nucleotide, and other cellular component synthesis.

riboflavin production in the knockout mice alongside the increase in ATP and GTP synthesis may lead to an abundance of energy for intestinal epithelial cells.

An important observation made is that genotype does directly affect the microbial community. This research is novel in the testing of a neuropeptide deficiency and its link to the microbiota. It provides a clearer understanding of just how influential the gut-brain axis pathway is not just on the host, but also on the microorganisms that reside there. We hypothesize that the change in taxonomic structure, diversity, and predicted metagenome may be caused by an increase in fat absorption rates within the knockout strain. This hypothesis would be difficult to prove as mouse weight data demonstrates that knockout mice are smaller in size, but an increase in uptake does not directly imply an increase in storage. An important question brought forward by this research is the impact of the microbiota on VIP research. A number of papers using VIP knockout mice have published increases in intestinal inflammation and changes in neuronal patterns. These differences may not be directly related to the loss of VIP but may be due to the change in the microbial environment itself. This would call into question whether these changes are a direct or an indirect effect from VIP. We recommend the utilization of germ-free knockout mice as a method for future research to eliminate this question.

3. VIP SIGNALING IN T-LYMPHOCYTES AND EOSINOPHILS

3.1. Introduction

3.1.1. Immune system overview

The mammalian immune system consists of biological proteins, cells, tissues and organs focused on host defense from foreign pathogenic invaders and "rogue" self-cells. This biological security mechanism called the immune system, is found throughout the animal kingdom from fruit flies to humans and immune-like systems even exist in plants and single-celled bacteria. Like an arms race between warring nations, the immune system and the pathogenic microorganisms it fights are perpetually evolving, always trying to gain a selective advantage over one another. The immune system works by first recognizing molecular patterns called antigens, presented on or secreted by pathogens, like parasites, bacteria and viruses, while ensuring the body's own cells remain unscathed, disease and cancer free. Its importance is truly recognized in immunodeficient individuals, whom possess a reduced potential for clearing unwanted foreign/self-cells from the host. This condition, where the hosts body is unable to defend itself against infection for example, can be caused by genetic disorders, cancers and/or pathogens like the human immunodeficiency virus (HIV). These immunocompromised persons are susceptible to opportunistic infections, unnoticed in everyday people. Hormones, circadian rhythm, nutrition and the nervous system are all involved in the regulation of these guardians.

The immune system is categorized into two parts, the innate and adaptive immune systems. This layered defense is divided by specificity. The innate immune system is the first responder and is activated upon the identified of microbes by pattern recognition receptors (PRRs). The cells of the innate immune system respond to stress cytokines and chemotax in response to infected areas. The innate immune system responds in a generic manner and its

defenses are non-specific in comparison to adaptive immunity. The adaptive immune system is activated by the innate immune system, creating a lag time between pathogen exposure and adaptive response. This antibody based, or humoral immune response is specific to the antigens presented to the adaptive immune cells. Adaptive immunity is also crucial for immunological memory, an essential component of vaccine function.

The extensive distribution of VIP is indicative of its various effects throughout the body. It has been demonstrated that in the cardiovascular system VIP effects vasodilation and cardiac output. In the nervous system, VIP influences learning, behavior, and works as a master circadian regulator in the body. Through the gastrointestinal tract VIP works on motility and modulates the pancreatic release of insulin and glucagon. In the immune system VIP acts in an anti-inflammatory aspect, reducing inflammatory marker expression. These effects were made possible through VIP binding to its two receptors VPAC1 and VPAC2. VIP were first found to elicit cAMP production in immune cells by O'Dorisio et al. in 1981 (O'Dorisio et al. 1981). Since then, its receptors have also been found on numerous immune cells like macrophages, dendritic cells, mast cells, CD4 and CD8 T cells. It's actions in the immune system have resulted in its categorization as an anti-inflammatory molecule, downregulating inflammatory cytokines and reducing Th1 immune responses, discussed later in this chapter.

3.1.2. The innate immune system

Innate immunity provides a polyclonal, immediate, non-specific response to pathogens, while the adaptive immune system recognizes and responds to a specific antigen. The innate immune system recognizes pathogen associated molecular patterns (PAMPs) with PRRs in a specific manner. The integumentary system, considered by many to be a part of the innate immune system, acts as a physical and chemical barrier between our body and the external

world. Its epithelial cells line the insides of our respiratory and gastrointestinal tracts and act as the first line of defense against foreign invaders. Goblet cells interspersed within the lining of the epithelial membrane, secrete proteins that make up the mucus layer which traps and removes harmful substances and opportunistic pathogens. This debris littered mucus is then pushed out by hair-like extensions, called cilia, on epithelial cells.

The cells of the innate immune system recognize a group of molecular patterns that are evolutionarily conserved and essential for pathogen survival. These molecular patterns or pathogen-associated molecular patterns (PAMPs), are recognized by the innate immune system's family of receptors called pattern recognition receptors (PRRs). Examples of PAMPs include the whip-like flagella, which allows for the propulsion of bacteria and the lipopolysaccharide (LPS) endotoxin, found in the membrane of gram negative bacteria. These receptors work alongside a group of soluble proteins that stimulate phagocytosis and assist in immune response, called complement proteins. Leukocytes from patients suffering from autoimmune diseases such as Sjögren's syndrome, have a reduced ability to phagocytose pathogens (Hauk et al. 2014). Although it remains to be discovered, it's possible that VIP may play a role in complement activation. A subset of the innate immune system, the complement system is made up of more than 30 soluble proteins produced by hepatocytes in the liver. Circulating in the plasma, these proteins amplify antibody response and act directly with PRRs, aiding in the lysis and phagocytosis of pathogens.

Macrophages are a type of resident innate immune cell that infiltrate tissues during inflammation and remain as immune sentinels protecting against invaders. This cell quickly phagocytes invading microorganisms detected by the PAMP's, which have be coated with complement proteins. A second innate immune cell involved in phagocytosis is the neutrophil.

These cells reside in the blood, but are recruited to sites of infection or inflammation by cytokine and chemoattractant chemicals. Cytokines are small proteins important to cell signaling and can affect cellular behavior. Inflammation is depicted by redness, pain, swelling and heat and is promoted by cytokines like interleukin (IL) -1, IL-12, IL-18 and interferon (IFN)-gamma. Cytokines that work in an anti-inflammatory manner include: IL-4, IL-6, IL-10 and IL-13. Both macrophages and neutrophils express PRRs in order to detect, engulf pathogens and work alongside the complement system. They can also detect the Fc region of antibodies produced by the adaptive immune system, assisting the adaptive immune system in pathogen removal (discussed in greater detail later in this chapter).

Defense against large multicellular parasites, that cannot be phagocytosed is the responsibility of neutrophils and eosinophils. These white blood cells aggregate, surrounding large invaders, where the eosinophils degranulate and rapidly release reactive oxygen (ROS) species in what's called the oxidative burst. ROS can degrade cell membranes, damage DNA and RNA killing invaders. This release of reactive oxygen species from eosinophils can be harmful to both the pathogens and host tissues. While eosinophils make up nearly three percent of white blood cells, they are associated with a number of diseases, like asthma. During asthma the degranulating eosinophils cause unintended damage to the respiratory tract while attempting to eliminate inhaled pathogens like fungi. Eosinophils, along with other lymphocytes also circulate in a circadian manner. Their plasma numbers increase during the night and reduce during the daytime. This circadian synchronization is partially controlled by neurohormones, like VIP.

3.1.3. The adaptive immune system

This second layer of immune defense evolved during the Cambrian explosion over 500 million years ago. This is around the time vertebrate life was dominated by fish and tetrapods

122

(fish out of water) were climbing out of the sea. (Cooper and Herrin 2010). While the innate immune system is essential for basic defense, the adaptive immune system is more precise and specifically target pathogens or antigens. The adaptive system is mediated by antibodies, targeted proteins secreted by B lymphocytes, which assist in cell mediated responses. Adaptive immunity also has a slower response time and can take days before a full response is mounted. This is because the adaptive immune system must be presented an antigen by circulating dendritic cells it recognizes as foreign, which takes time. An adaptive immune response also sometimes leads to the formation of immunological memory, which is what immunologists take advantage of when administering vaccines.

The cellular basis of the adaptive immune response are lymphocytes. These immune cells are concentrated in lymphatic tissues around the body, like lymph nodes, tonsils and the spleen. These are activated in part by antigen-presenting cells (APCs) like dendritic cells, which circulate the body and present microbial antigens to inactivated T-lymphocytes. T-lymphocytes or T-cells derive their name from the thymus, where they develop and mature. Once activated, these T-cells can help activate B-cells to make antibodies against the invader. B-lymphocytes or B-cells are differentiated from hematopoietic stem cells in the bone marrow. All of these cells respond to threats by clonal selection/expansion. Mature B lymphocytes (B-cells), called plasma cells also introduce antibodies into mucosal secretions. Nearly five grams of one of these antibodies, Immunoglobulin A (IgA), in secreted into the intestinal tract daily. This antibody assists in pathogen clearance by blocking bacterial access to epithelial receptors, capturing these microorganisms in mucosal secretions. Present in breast milk, IgA acts as a prebiotic for specific commensal bacteria and reduces the virulence of others (PMC3774538).

In clonal selection, a diverse set of lymphocytes are created, each possessing a unique receptor. Through negative selection, any cell that binds with to host MHC peptides undergoes apoptosis, called clonal deletion. Progenitor T-cells then migrate to the thymus where they mature and depart as naïve T-cells. This process prevents the formation of T-cells that could induce autoimmune diseases. For the activation of the surviving mature lymphocytes, dendritic cells must present complementary antigen on MHC class II molecules. A secondary signal through the binding of CD28 by CD80 must also be present to initialize activation. Upon binding to the receptor, the lymphocyte starts to clonally expand. This results in numerous clones, all of which express matching antigen receptors. This focused approach targets the specific antigen presented to the T-cell by the dendritic cell. After the antigen has been cleared, these clones undergo apoptosis, leaving a few effector cells behind. These effector cells stay alive for years, ready for expansion in case the antigen is seen again. Although the process behind this memory cell formation is not well understood, recent research by Youngblood et al. has demonstrated that memory cells display particular DNA methylation profiles, not seen in cells that undergo apoptosis (Youngblood et al. 2017).

Both innate and adaptive systems work together to protect the host from pathogens. The innate responses are activated directly by the PAMPs, while the stimulation of the adaptive immune arm is done by dendritic cells. Occasionally these safety mechanisms protecting the host can turn against their master, resulting in sometimes fatal autoimmune diseases. This includes diseases such as type 1 diabetes, where the immune system destroys insulin producing pancreatic cells, or rheumatoid arthritis, where antibodies attack the linings of joints. Current treatments for these conditions generally focus on immune system reducing, similar to how asthma and other inflammatory diseases are treated. The protein of focus in our laboratory, VIP, has been

implicated in a number of these immune disease. For instance, research by Martinez et al. has

shown that lower levels of VIP may be an early indicator of arthritis (Martinez et al. 2014).

3.1.4. VIP in the immune system

A look into the expression profiles of VIP receptors in the immune system can give us

insight into the functions of VIP as an immune modulator. In the immune system, the VIP

protein plays a number of roles in both the innate and the adaptive immune systems. VIP is

delivered to immune organs by VIPergic nerves, secreted by epithelial cells and by lymphocytes

themselves. The production of cAMP through the addition of VIP to immune cells in 1981, by

Guerrero et al. and O'Dorisio et al., was the first indication of the existence of VIP receptors on

lymphocytes (O'Dorisio et al. 1981; Guerrero et al. 1981). qRT-PCR and ELISA analysis by

Gomariz et al. demonstrates that human VIP mRNA and protein is produced and present in CD4

and CD8 T-cells and B-cells (Gomariz et al. 1992; Gomariz et al. 1990).

Throughout the immune system, VIP functions as a potent anti-inflammatory molecule,

switching from a proinflammatory Th1 response to an anti-inflammatory Th2 response (Voice et

al. 2003). Inflammation results in the secretion of chemokines and cytokines that induce the

chemotaxis of several immune cells to the inflammatory site. VIP works to block these

pathways, causing a reduction in inflammation. Activated macrophages secrete proinflammatory

cytokines like IL-6 and IL-12, which are inhibited by the activation of the VPAC1 receptor.

Research by Delgado et al. shows the reduction in cyclooxygenase (COX)-2 expression with the

addition of VIP (Delgado et al. 2004). Daily intraperitoneal injections of VIP in mouse colitis

models showed a reduction in TLR expression on macrophages and dendritic cells. The drop in

these expression levels reduces the ability of these innate immune cells to respond to pathogens,

reducing inflammation (Gomariz et al. 2005). VIP has also been coined a macrophage

deactivating factor, where primarily through VPAC1 and cAMP it inhibited proinflammatory cytokine production and reduce macrophage response in disease (Delgado, Munoz-Elias, et al. 1999).

The primary connection between the innate and adaptive immune systems are dendritic cells. The presentation of processed extracellular antigen by dendritic cells, activates CD4 T-cells. This activation requires two signals: the binding of the major histocompatibility complex (MHC) class II to the T-cell receptor (TCR) and co-stimulation by the APC. This co-stimulation is done by the binding of CD28 to CD80/86. Together the CD80 and CD86 proteins make up the B7 protein on the APC. Studies conducted by Delgado et al. have demonstrated that VIP reduces the expression levels of CD80 and CD86, lessening the dendritic cells capacity to activate CD4 T-cells and acting in an anti-inflammatory manner (Delgado, Sun, et al. 1999).

Naïve T-cells or Th_0 cells, transform into either Th_1, Th_2, Th_{17} or T_{reg}, depending on the cytokines they are exposed to by the dendritic cell. This is to ensure a proper response to the diverse type of pathogens our bodies encounter. Th_1 cells function to clear intracellular pathogens or cellular immunity. This pro-inflammatory response assists macrophages and cytotoxic (CD8+) T-cells, to eliminate host cells infected with intracellular pathogens like viruses and/or malignant cells (Yoshimoto et al. 1998). Th_2 cells work to clear extracellular pathogens like parasites and work with humoral immunity. Th_2 response is an anti-inflammatory response, the imbalance of which can cause tissue thickening and is linked with allergic diseases. The Th_2 response activates mast cells and eosinophils and increases mucus production. Both Th_1 and Th_2 responses, are self-promoting and their cytokines act in a positive feedback loop, promoting more of that response while continuing to inhibit the other. Th_{17} cells assist in autoimmunity and help in the clearance of certain extracellular pathogens. This pro-

126

inflammatory subset inhibits the differentiation of T regulatory (Treg) cells (Bettelli et al. 2006). Treg cells suppress the immune response, preventing damage to the host, and build tolerance to communal microorganisms (Korn et al. 2009). This allows for a symbiotic relationship with the microbes that call reside on the human body.

The Th2 skewing ability of VIP is well documented. Ganea et al. demonstrated both in vitro and in vivo that VIP acted to shift cells towards the Th_2 lineage (Ganea, Rodriguez, and Delgado 2003). To determine the receptor responsible for this shift receptor knockout mice were used. Goetzel el al. demonstrated that in mice deficient in the VPAC2 receptor, the Th_1 response was prominent (Goetzl et al. 2001). In contrast, in CD4 T-cell VPAC2 transgenic mice (overexpressing the VPAC2 receptor) by Voice et al., the Th_1 response was reduced and the immune system of these mice skewed towards the Th_2 response. These research studies demonstrate the importance of the role of the VPAC2 receptor and its abundance in T-cell differentiation.

The chemotaxis of these Th_1 and Th_2 T-cells is also affected by VIP. This is not just due to the Th2 skewing ability of VIP, but by its effects on dendritic cells. Jiang et al. studied the immunoregulatory effects of VIP on chemokines and survivability markers, CXCL10 and CCL22. Both of these proteins are secreted by dendritic cells and interact with Th_1 (CXCL10 interacts with CXCR3) and Th_2 (CCL22 acts on CCR4) cells. Dendritic cells isolated from the spleens of male BALB/c mice were cultured with the VIP protein. Another group of the same mice received intraperitoneal injections of VIP, 16 hours after which CXCL10 and CXCR3 levels were measured by ELISA. VIP was found to down regulate the secretion of CXCL10 and increase the secretion of CCL22 both in vivo and ex vivo (Jiang, Jing, and Ganea 2002). The Th_2 skewing effect of VIP, can impact numerous other bodily functions. For instance, Wolf et al.

demonstrated that Th$_2$ cells acted as protectors of central nervous system tissue from secondary injury (Wolf et al. 2002).

Th$_{17}$ cells are a T-cell subset which secretes proinflammatory cytokines. These cells are activated by extracellular pathogens. Th$_{17}$ cells have been implicated in a number of autoimmune diseases such as multiple sclerosis, rheumatoid arthritis and type 1 diabetes. In a type 1 diabetes mouse model using non-obese diabetic mice (NOD), the intraperitoneal injection of VIP reduced the expression profile of Th$_{17}$ cells and delayed the onset of type 1 diabetes (Jimeno et al. 2010). For the autoimmune disorder, rheumatoid arthritis, VIP acts in a therapeutic manner, reducing inflammation and decreasing abnormal immune response. Recent research by Jimeno et al. suggests this may be due the downregulation of cytokines that enhance the pathogenic phenotypes of Th$_{17}$ cells (Jimeno et al. 2015).

Understanding the roles that each of the two VIP receptors (VPAC1 and VPAC2) play in T cell biology is important for gaining a better understanding of how VIP acts. The role VIP plays in T cell morphology is well documented as described in the previous section. Previous studies conducted by Dorsam et al. have demonstrated the differential regulation of nearly 350 gene targets in both resting and activated murine CD4 T-cells by VIP (Dorsam et al. 2010). Further analysis of these gene pathways by Steve Wanjara using qRT-PCR demonstrated increases in EGFR, APP, ADAM15, Grb7, PAK1 and Snail1 over 24 hours after VIP introduction (unpublished data).

This revelation opens the door to determining which of the two receptors is responsible for these changes. To fill this gap in knowledge, this author worked on a research project with Travis Van Der Steen (V. D. Steen et al. 2016). Contributions included cAMP analysis of human T-cells lines to determine cAMP response from agonists for each receptor. The T-cell lines used

included Hut-78 and Molt-4 cells. An epithelial cell line, MCF-7, was also used as a positive control. The Hut-78 cell line exclusively expresses VPAC1 mRNA, while Molt-4 cells primarily express VPAC2 mRNA as confirmed by qPCR (Xia et al. 1996).

3.1.5. VIP in asthma

Asthma is pulmonary disease that affects an estimated 39.5 million Americans, including 10.5 million children. The innate and the adaptive immune systems work together to protect us against a number of respiratory diseases. Some of these diseases, like allergic asthma, are the result immune triggers to non-pathogenic antigens like pollen or pet dander. VIP protein is plentiful in the respiratory system and is secreted by nerve fibers that innervate both the lungs and the arteries around them (Dey, Shannon, and Said 1981). In the respiratory tract, VIP acts as a potent airway and pulmonary artery dilator, emerging as a potential treatment for cardiopulmonary disorders.

Szema et al. used VIP knockout mice to gain a better understanding of the role of VIP in asthma. They discovered that mice lacking VIP were more susceptible to asthma in comparison to their wild type counterparts (Szema et al. 2011). The addition of VIP into tracheobronchial smooth muscle resulted in its relaxation and bronchial dilation (Lundberg et al. 1984). It was shown to counteract the effects of histamines and assist in allergy relief (Groneberg, Springer, and Fischer 2001). VIP knockout mice were shown to have easily triggered bronchospasms with high inflammatory cytokine levels in the bronchoalveolar lavage (BAL). Interestingly, the intraperitoneal reintroduction of VIP eliminated these phenotypes over a two-week period (Szema et al. 2006).

To better understand the VIP pathway responsible for its effects on the respiratory tract receptor knockout mice have been used. Research by Samarasinghe et al. has demonstrated that

three days post-allergen challenge, mice lacking the VPAC2 gene have significantly reduced eosinophilic response in the BAL. Interestingly, the eosinophils in the tissues, as well as other immune cells, were not nearly as effected by the lack of VPAC2 signaling (Samarasinghe, Hoselton, and Schuh 2010a). Another research article by Samarasinghe et al. demonstrated the importance of VIP in asthmatic response. Here Amali Samarasinghe demonstrated in wild type mice via immunohistochemistry (IHC), that within three days following antigen challenge, the amount of VIP present in the lungs decreases radically. During this time the eosinophils invade the lung and attempt to clear out the antigen (Samarasinghe, Hoselton, and Schuh 2010b). This suggests that the presence of VIP acts as a shield, preventing the infiltration of eosinophils into the BAL, while its ablation allows for eosinophilic invasion. Figure 39 shows the reduction in VIP protein after allergen challenge and an increase in eosinophil numbers in the BAL during that time.
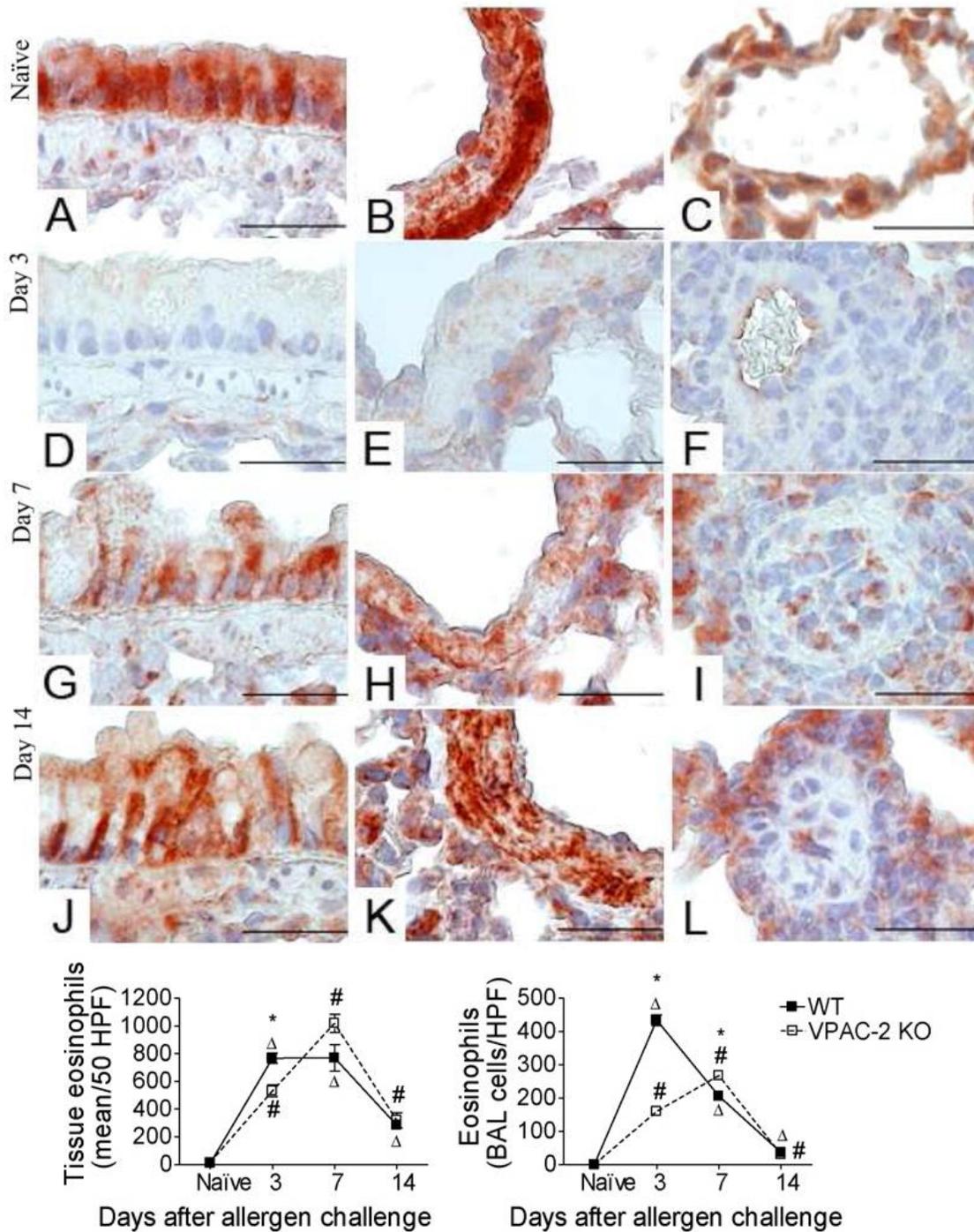
Figure 40. The localization of VIP throughout the alveolar epithelium during allergen challenge.

This IHC VIP stain (brown) demonstrates the change in VIP levels after allergic response. The three columns represent epithelial tissue, smooth muscle and blood vessels. Reduction in VIP levels is seen in all tissue samples on day 3 and returns by day 14. Line graphs of eosinophil numbers in BAL follow the opposite pattern with an increase in number at day 3 and reduction by day 14. Figure from (Samarasinghe, Hoselton, and Schuh 2010b)

The reduction in eosinophil numbers in VPAC2 KO mice opens a gap in knowledge. Why are there fewer eosinophils present in the BAL of the VPAC2 deficient mice when compared to wild type? A hypothesis put forward from this observation suggested this reduction may be due to the hinderance of eosinophil production within the bone marrow of VPAC2 KO mice. To test this, bone marrow cells from VPAC2 KO and WT mice were obtained and differentiated into eosinophils. First published in 2009, Dyer et al. demonstrated different rates of eosinophil differentiation in toll like receptor (TLR) 3 knockout mice (Dyer, Percopo, and Rosenberg 2009). These experiments were used as guidelines to determine the impact of lack of VPAC2 on eosinophil generation.

3.1.6. Eosinophils and T-cells in IBD and immune cell trafficking

Eosinophils are distinguishable by large granules held within their cytoplasm and their bilobed nucleus (figure 49). These innate immune cells mature in the bone marrow where they are differentiated from hematopoietic stem cells (HSCs). HSCs, which give rise to all blood cells, differentiate into eosinophils when exposed to certain cytokines, such as IL-5, a system which our research group manipulated to create in vitro eosinophils from mouse bone marrow cells (3.2.3) (Lampinen et al. 2004). Recent research has pointed to a connection between inflammatory bowel diseases (IBD) and eosinophil migration to the gastrointestinal tract. The inflammatory process of these diseases involves a number of inflammatory immune cells such as eosinophils and T-cells. Patients suffering from IBD present more active eosinophils than controls. During IBD remission, these numbers remain high, but the eosinophils present a resting phenotype (Lampinen et al. 2005).

In the bone marrow, eosinophils are derived from CD34$^+$ pluripotent HSCs. Eosinophils develop in response to IL-5 and IL-3, after which they are released into the blood stream

(Sitkauskiene et al. 2004). A number of chemo attractants induce chemotaxis in eosinophils, such as the eotaxin group. Serum analysis of patients suffering from IBD have demonstrated elevated levels of eotaxin (Chen et al. 2001; Mir et al. 2002). The expression of these chemo attractants and the secretion of IL-5 (some by T-cells and mast cells), which increases during inflammation, in the GI tract result in the recruitment of eosinophils to the alimentary canal (Mishra et al. 1999). Biopsies taken from patients with active IBD found larger numbers of eosinophils present, with a larger number degranulated when compared to controls (Garcia-Zepeda et al. 1996). The explosive degranulation of eosinophils expels cytotoxic granule cationic proteins (for example: eosinophil cationic protein, eosinophil peroxidase, and eosinophil-derived neurotoxin) which can damage local tissues (Gleich and Adolphson 1986). Attempts at reducing eosinophilic response in IBD by using antibodies to IL-5 showed a reduction in intestinal inflammation and suggest a possible therapy to counter IBD (Lampinen et al. 2001).

T-cells which assist in eosinophil recruiting are also actively involved in IBD (Carvalho et al. 2003). Recent research has pointed to an increase in the number of CD4+ T-lymphocytes in the intestinal walls of patients suffering from IBD. T-cell generation starts with the migration of HSCs from the bone marrow to the thymus. Here, T-cells develop specific T-cell markers, such as CD3, CD4, or CD8. Through positive selection, which occurs in the thymus cortex, CD4 and CD8 cells are allowed to survive. In the medulla of the thymus, negative selection allows for the removal of self-reactive T-cells which bind with high affinity to self-antigens (Sprent et al. 1988). Recent studies have demonstrated the importance of these cells in IBD pathology (Zenewicz, Antov, and Flavell 2009).

The influx of T-cells to inflamed GI tissues suggests a key role in IBD pathogenesis. Research by Smids et. al, focused on profiling intestinal T-cells in IBD patients and found higher

133

percentage of CD4+ and Tregs when compared to healthy controls (Smids et al. 2018). These T-regs for example were also shown to have altered properties in IBD patients (Muzes, Molnar, and Sipos 2012). Utilization of animal disease models for IBD, shows an increase in mortality when T-cell populations were removed (Kuhl et al. 2002). Similarly, IBD patients who are also infected with HIV, and in turn reduce numbers of CD4+ T-cells, demonstrate a reduce inflammatory profile compared to controls (Viazis et al. 2010). These reports have resulted in the utilization of drugs to target CD4+ T-cell trafficking and reduce cell numbers to manage IBD (Mosli, Rivera-Nieves, and Feagan 2014). The intestinal microbiota differs greatly between individuals and its composition is greatly dependent on genetics, diet, and the environment. Dysregulation of the relationship between the microbiota and the immune system (discussed in the previous chapter), plays an important role in determining the immune response during IBD (Larmonier et al. 2015).

3.2. Materials and methods

3.2.1. Animal cell culture

Three tissue culture cell lines were used for these experiments all of which were purchased from the American Type Culture Collection (ATCC, Manassas, VA). They included, Molt-4, Hut-78 and MCF-7 cells. Molt-4 cells are a human T-lymphocyte cell line derived from a 19-year-old male patient, and primarily express the VPAC2 receptor mRNA. Hut-78 cells are another *Homo sapien* T lymphocyte cell line, which were derived from a 53-year-old male, and solely express the VPAC1 receptor mRNA. The MCF-7 cell line is an epithelial cell like taken from the mammary glands of a 69-year-old female. MCF-7 cells express both VPAC1 and VPAC2 receptors.

These cells were cultured according to ATCC guidelines. Both the Hut-78 and Molt-4 cells were cultured in 89% Roswell Park Memorial Institute medium (RPMI-1640, GE Life Sciences, Pittsburgh, PA), with 10% characterized fetal bovine serum (chFBS) and 1% 100µg/mL penicillin/streptomycin (penn/strep). During culturing, these non-adherent cells were washed off their individual flasks with phosphate buffer solution (PBS) and centrifuged for 5 minutes at 300 x g. They were then stained with the living cell exclusion dye, trypan blue, counted using a hemocytometer and reseeded to continue the culture. Both cell lines were cultured twice a week at a concentration of 300,000 cells/mL (M and W), and at 200,000 cells/mL on Fridays.

The MCF-7 cells were cultured in ATCC-formulated Eagle's Minimum Essential Medium (EMEM, GE Life Sciences, Pittsburgh, PA), also containing 10% chFBS and 1% 100µg/mL penn/strep. This adherent cell line was cultured three times a week (M, W, and F). The cell layer was rinsed with PBS to remove any residual media, and trypsin-EDTA solution is added to the flask. After a 5 to 10-minute incubation, the cells were observed to ensure dispersion from the flask and centrifuged. These cells were centrifuged at 300 x g for 5 minutes, resuspended in fresh EMEM media and reseeded.

ATCC guidelines were followed for culture conditions and cryopreservation. All three cell lines were cultured in an incubator maintained at 37°C with a 95% air and 5% carbon dioxide (CO_2) atmosphere ratio. Cryopreservation freeze media was composed of 95% complete growth media (medium, chFBS and penn/strep) and 5% dimethyl sulfoxide (DMSO), followed by storage in liquid nitrogen.

3.2.2. cAMP assay

3.2.2.1. Preparation

For this experiment, Hut-78, Molt-4 and MCF-7 cells were used. In preparation for the cAMP assay, all three cell lines were centrifuged, counted and resuspended into 2 mL of Hank's balanced salt solution (HBSS) buffer (HBSS + 0.5% bovine serum albumin (BSA)) at a concentration of 0.5 x 10^6 cells/mL. To each sample 750 µM of isobutylmethylxanthine (IBMX), a phosphodiesterase inhibitor, was added to prevent cAMP degradation. The cells were then incubated at 37°C for 45 minutes. Seven different sample groups were used for each cell type in triplicate. These sample groups included:

1. HBSS (negative control)

2. VIP 10^-6 or VIP 10^-10 (test)

3. VIP 10-28 10^-6 (VIP antagonist)

4. [Ala2,8,9,11,19,22,24,25,27,28]-VIP (VPAC1 agonist test)

5. Bay 55-9837 (VPAC2 agonist test)

6. DMSO (VIP vehicle negative control)

7. Forskolin (50 uM final concentration) (positive control)

These samples were incubated at 37°C for 30 minutes in a 24 well plate, before 1 mL of 0.2 M hydrochloric acid (HCl) was added to each well. The 24 well plate was then placed on a shaker for 30 minutes at room temperature. After the thirty minutes, the cells were frozen at -20°C or kept cool at 4°C before performing the cAMP ELISA.

3.2.2.2. ELISA

The Cayman chemical (Ann Arbor, MI) cyclic AMP enzyme-linked immunosorbent assay (ELISA) kit was utilized to determine cAMP concentrations within the cultured cells. The 24 well plate was thawed and the mixture was triturated. The plate was then centrifuged at 1000

x g for 10 minutes and the supernatant was used to determine cAMP levels. Eight 1:3 serial

diluted sample standards were used starting with 750 pmol/mL and ending with 0.3 pmol/mL.

These standards were used to uncover cAMP levels in each of the test groups.

3.2.3. Bone-marrow derived eosinophils

3.2.3.1. Day 0

The legs from sacrificed mice were isolated with a focus on sterility. The cut was made

above the head of the femur and at the distal articular surface of the tibia. Once isolated, the tibia

and the femur were separated, and any tissue remaining and was scraped off. The top and bottom

of the femur and the tibia where cut, allowing access to the bone marrow inside the tubular

middle section of the bones. Held by forceps, the bone marrow was flushed out by a needle and

isolation buffer (PBS with 2% cfFBS and 1 mM EDTA added). Once the redness in the bones

was no longer visible, the isolation buffer and the cells inside it was passed through a 70 µm

filter. The media was then centrifuged at 300 x g for 5 minutes.

Red blood cell removal and cell counts were performed before the bone marrow cells

were cultured. This was done by removing the media after centrifugation and resuspending the

pellet in 3 mL of 1x red blood cell (RBC) lysis buffer (eBiosciences ThermoFisher, Waltham,

MA). This was vortexed and incubated at room temperature with regular hand inversions for 3

minutes. Forty-seven mL of PBS (1x) was added for a total volume of 50 mL. These 50 mL were

passed through another 70 µm filter and centrifuged. The pellet was then resuspended in bone

marrow media (80% RPMI, 20% chFBS, 1% penn/strep, 1% glutamine, 1mM sodium pyruvate

and 50 µM beta-mercaptoethanol (β-ME). After trituration, the cells were counted and seeded

into bone marrow media along with 100 ng/mL (1x) stem cell factor (SCF) and 100 ng/mL (1x)

fms-like tyrosine kinase 3 (FLT-3). This was placed into a 37°C incubator with an atmosphere

setting of 5% CO_2 and 95% external air. These steps are visualized in figure 40 as shown by

Madaan et al..
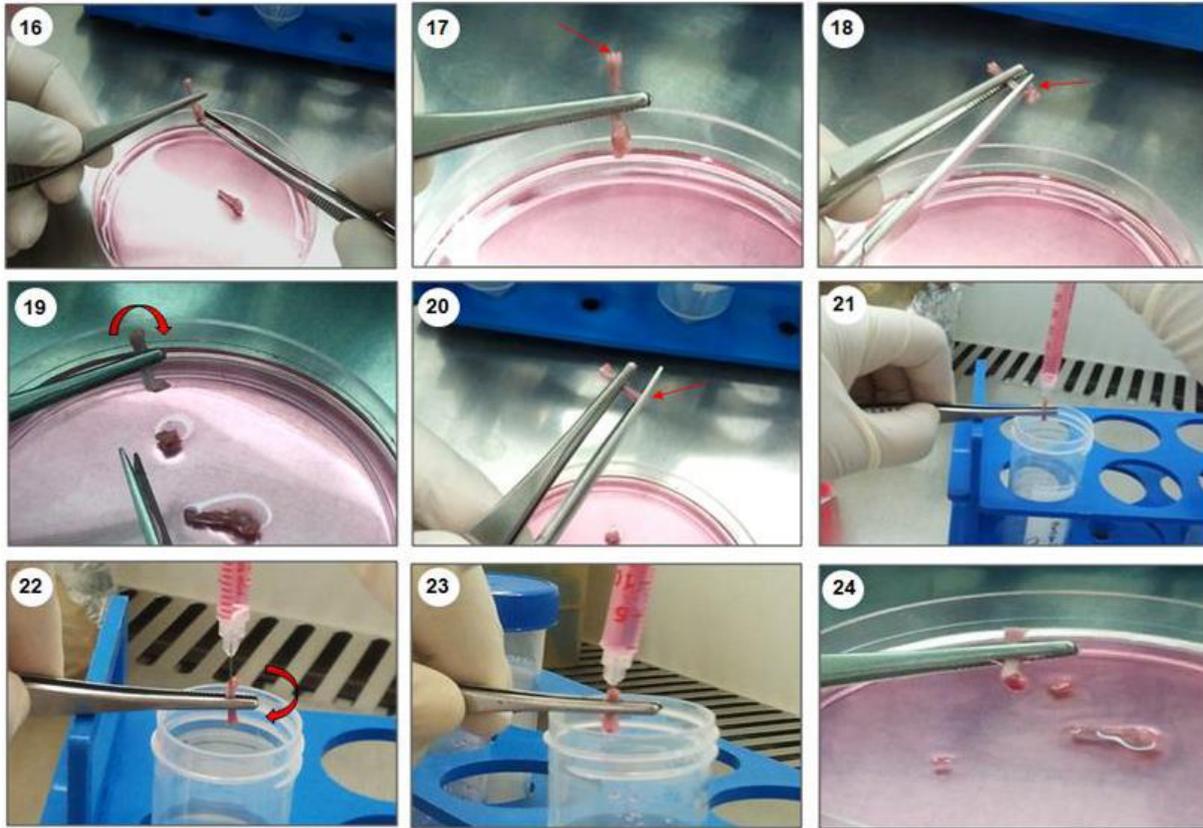
Figure 41. Visualized bone marrow isolation protocol.
Bone marrow isolation steps demonstrated by (Madaan et al. 2014). Each step demonstrates
the processes of flushing bone to obtain cells for culture.

3.2.3.2. Day 4, 8, 10, 12 and 14

Four days after the initial seeding of the bone marrow cells, the cells were centrifuged

and counted. The cells were removed from the flask and centrifuged at 300 x g for 10 minutes.

Half of the conditioned media was repurposed for resuspension and reused in the same flask.

Only on day 8 are the cells moved to a new flask. After counting the cells, they were

resuspended in half of the total volume of fresh bone marrow media with 2x interleukin-5 (IL-5)

spiked in. The cells and the new media were added to the conditioned media and incubated for 4

138

or 2 days. On day 14, the cells were analyzed by flow cytometry and cytospins to ensure

eosinophil differentiation. The complete protocol is visualized in figures 41 and 42.

Day 0

- Seed cells at 1E6 cells/mL or 5E6 cells/mL
- Add FLT-3 & SCF (100 ng/mL each)

Day 4

- Add fresh media with IL-5 (10 ng/mL)

Day 8

- Retain ½ conditioned media for cells
- Add fresh IL-5 (10 ng/mL)
- Change Flask

Day 10

- Retain ½ conditioned media for cells
- Add fresh IL-5 (10 ng/mL)
- Retain Flask

Day 12

- Retain ½ conditioned media for cells
- Add fresh IL-5 (10 ng/mL)
- Retain Flask

Day 14

- Analyze Cells
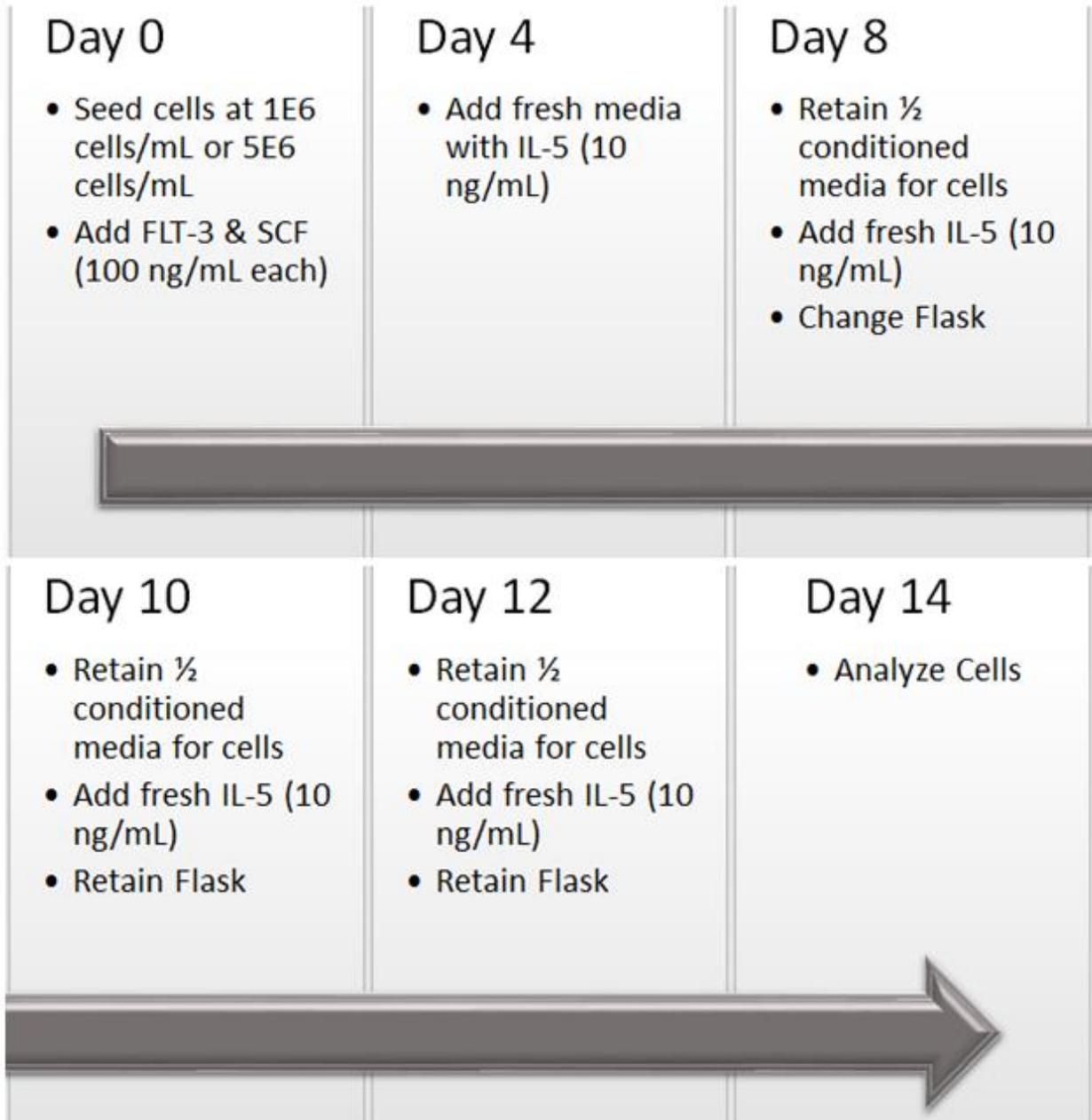
Figure 42. Bone marrow derived eosinophil generation protocol.
Steps performed over a 14-day period to obtain eosinophils from bone marrow.

3.2.4. Flow cytometry

To confirm eosinophil differentiation from bone marrow cells, an anti-sialic acid-binding immunoglobulin-like lectin F (Siglec-F) (CD170) -phycoerythrin (PE) and isotype control antibodies was used for cellular staining. A total of 30,000 events were counted, with 1 million cells resuspended in flow binding buffer (1% BSA and PBS). These cells were incubated with their respective antibody, with one cells alone negative control without any antibody, for 30 minutes at 4°C in the dark to prevent photobleaching. After antibody staining, the cells were washed with 3 mL of PBS twice and centrifuged at 300 x g. These cells were resuspended into 200 µL of binding buffer and analyzed using the BD Accuri C6 Plus (San Jose, CA) flow cytometer.

3.3. Results

3.3.1. cAMP

Microarray analysis by the Dorsam laboratory has demonstrated changes in transcriptome of activated and resting mouse CD4 T-cells. This revealed that over 530 transcripts were modulated by VIP binding (Dorsam et al. 2010). What this study didn't show, was which receptor was responsible for these changes. The two VIP receptors have previously been implicated in the chemotaxis of human T cells (Schratzberger et al. 1998). Contrary to this finding, the chemotaxis of the Hut-78 cell line, which exclusively express VPAC1 mRNA, are repelled by VIP (Xia et al. 1996). This change in cellular motility could be caused by a cAMP response due to VIP receptor signaling.

To discover this, inactivated T-lymphocyte cell lines were used to determine the differences in cAMP response between the two VIP receptors. To accomplish this, three cell lines, including 2 T-cells and 1 epithelial cell line, were tested. Each cell line was exposed to a

concentration of VIP known to elicit the highest cAMP response, along with a VPAC1 agonist (V1 in graphs), VPAC2 agonist (V2 in graphs), and positive (Forskolin) and negative controls (H$_2$O and DMSO). DMSO is used as a vehicle control for the VIP protein. Forskolin is a tool to increase cAMP levels by the direct activation of the adenylyl cyclase enzyme. The standard curve generated from one of the ELISA's is displayed in figure 42 with a linear trend line equation of $y = -0.637 \ln x + 1.5592$ and an r^2 values of 0.9961. This r^2 value is consistent between cAMP assay runs.

Figures 44, 45 and 46 demonstrate the cAMP changes in each of the three cell lines tested with error bars representing SEM values. In the Hut-78 cells, no distinguishable change between the different test groups was seen. The Molt-4 cells did demonstrate higher amounts of cAMP from the VPAC2 agonist in comparison to the controls but was not statistically significant. To remove any concerns over peptide/agonist viability/functionality, the cAMP assay did show an increase in cAMP production in MCF-7 cells from VIP, VPAC1 agonist, VPAC2 agonist and forskolin. In conclusion the effects of VIP on inactivated T-cells are not statistically significant but a slight increase in Molt-4 cells by the VPAC2 agonist is detected. The MCF-7 epithelial cell line seems more susceptible to VIP/receptor agonist induced production of cAMP than the T-cell lines.

Standard Curve

$y = -0.637\ln(x) + 1.5592$
$R^2 = 0.9961$
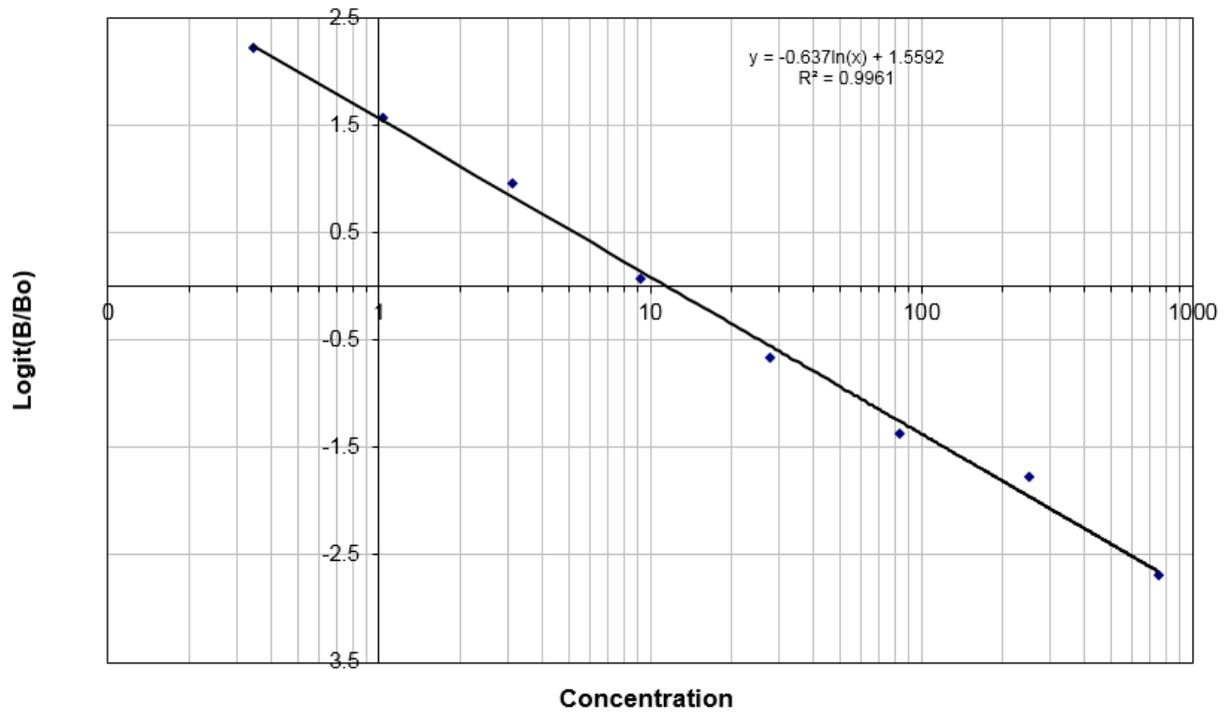
Figure 43. cAMP ELISA standard curve.
A line graph of known cAMP concentration serial dilutions to determine unknown
concentrations. Each dot is a plotted point with a plotted trendline with an R^2 value of 0.9961.

cAMP concentration in Hut-78 cells
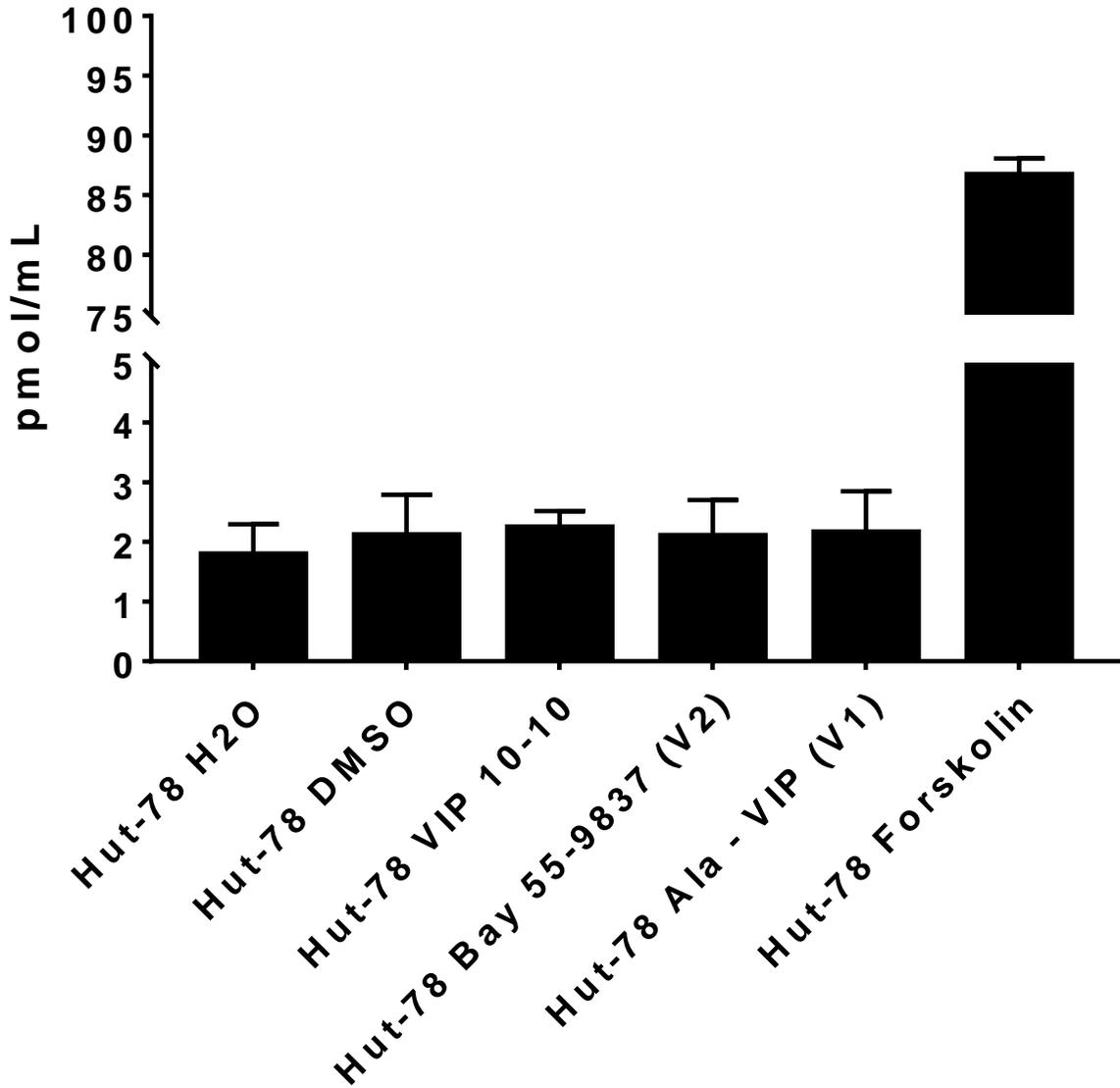
Figure 44. Changes in cAMP concentration in Hut-78 cells by VIP.
This bar graph depicts pmol/mL of cAMP levels in the Hut-78 T-cell line which only contains VPAC1 receptors. H2O and DMSO are negative controls with forskolin acting as the positive control. SEM values are plotted above each bar.

cAMP concentration in Molt-4 cells
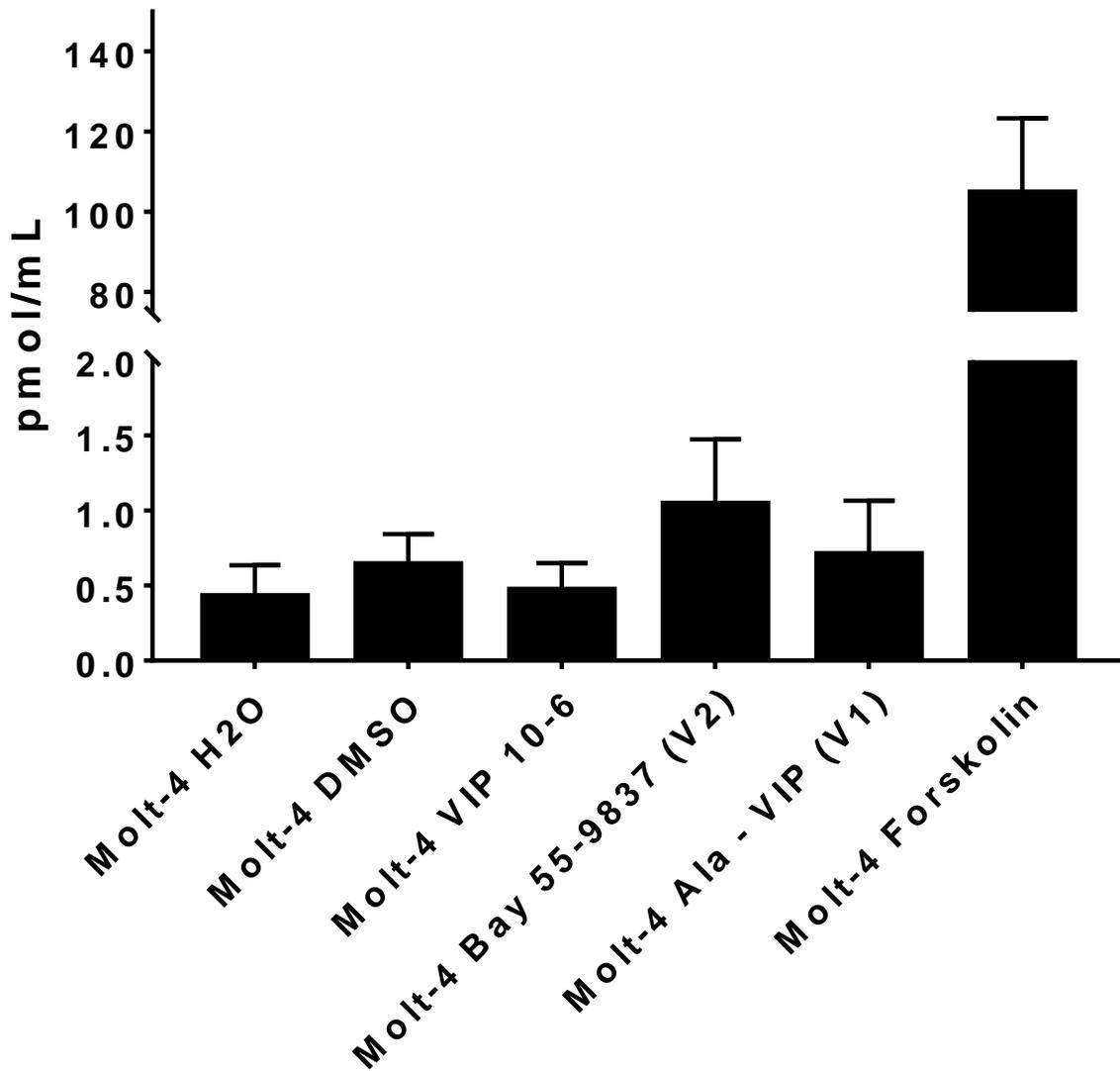
Figure 45. Effects of VIP signaling on cAMP in Molt-4 cells.
Bar graphs are representative of cAMP concentration within Molt-4 cells. The small Y-axis demonstrates low endogenous cAMP levels. VIP, VPAC2 agonist (V2), and VPAC1 agonist (V1) show no significant change over control. Error bars indicate SEM values.

cAMP concentration in MCF-7 cells
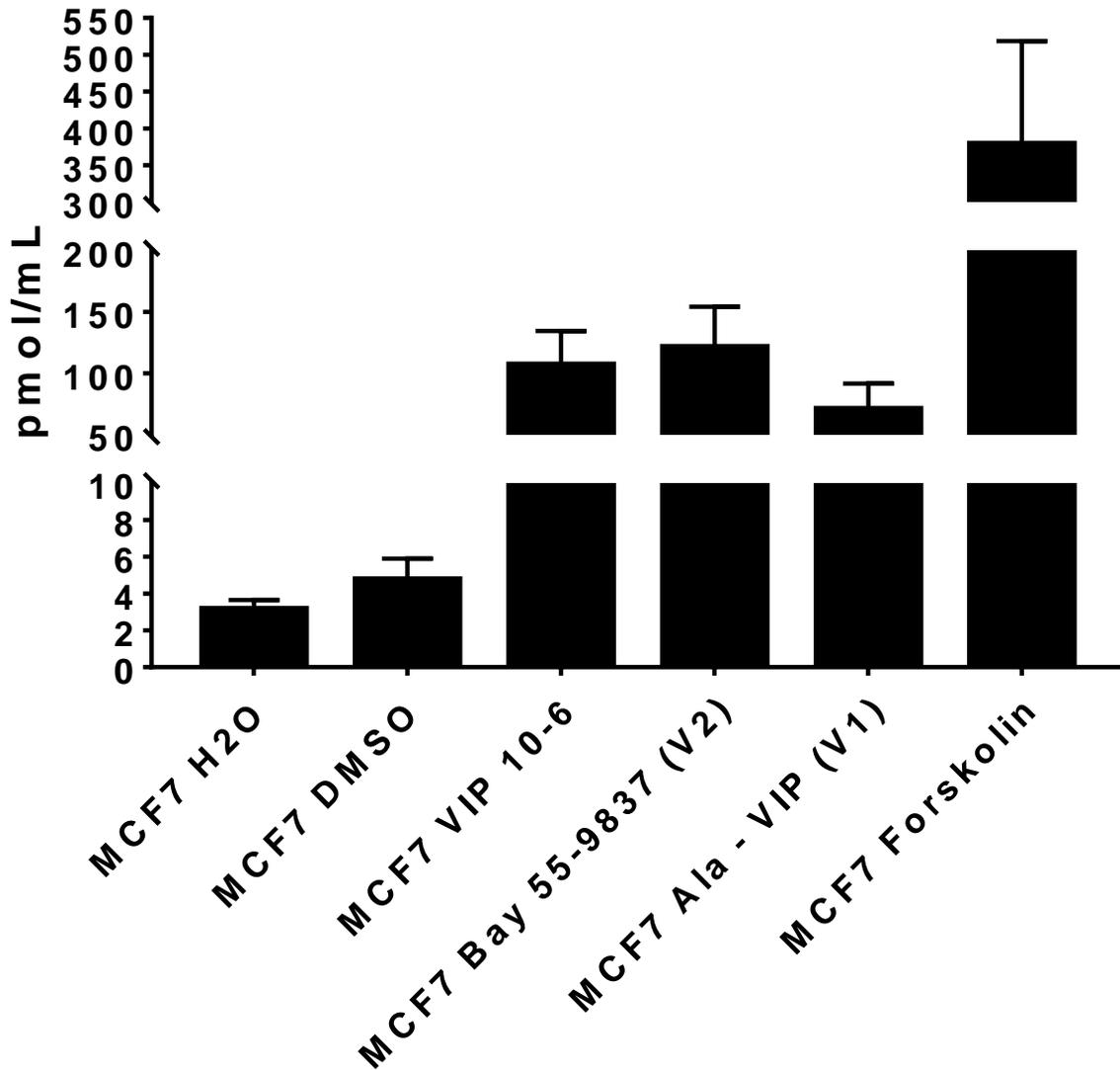
Figure 46. Impact of VIP signaling pathway on MCF-7 epithelial cell line cAMP
levels.
MCF7 H2O and DMSO bar graphs demonstrate endogenous cAMP levels and control for
forskolin respectively. Increases in cAMP are caused by VIP and both receptor agonists with
forskolin confirming assay functionality.

3.3.2. Bone marrow eosinophil differentiation

To determine the impact of the lack of the VPAC2 receptor on eosinophil differentiation, differences in rate of bone marrow eosinophil differentiation were tested using bone marrow cells from VPAC2 KO and WT mice. As discussed previously, bone marrow cells were obtained from both strains of mice and incubated with cytokines over 14 days. These cells were counted during these 14 days to determine changes in differentiation rates. The cells were also visualized on a microscope whose pictures are displayed in figure 47. Two different seeding concentrations, 5×10^6 and 1×10^6 cells/mL were used for the initial seeding of bone marrow cells. Both seeding concentrations followed the same culturing protocol.

The cell count results for 5×10^6 cells/mL from sixteen wild type and twelve knock out replicates are displayed in figure 48 with SEM values. Figure 49 shows cell count results from nine wild type and three knock out replicates at 1×10^6 cells/mL with SEM values. The p-values between the two strains were not statistically different for either initial seeding concentration, for any of the five days where the cells were counted. The 5×10^6 cells/mL flasks reduced in total cell number over the 14 days and both strains seemed to change numbers in a similar manner. The 1×10^6 cells/mL initial seed flasks, seemed to increase in total cell number in the middle of the 14-day study and reduced to about half of the initial seeding concentration by day 14. Analysis of this data suggests that the rate of in vitro differentiation of eosinophils from bone marrow precursor cells is not different between the two strains.
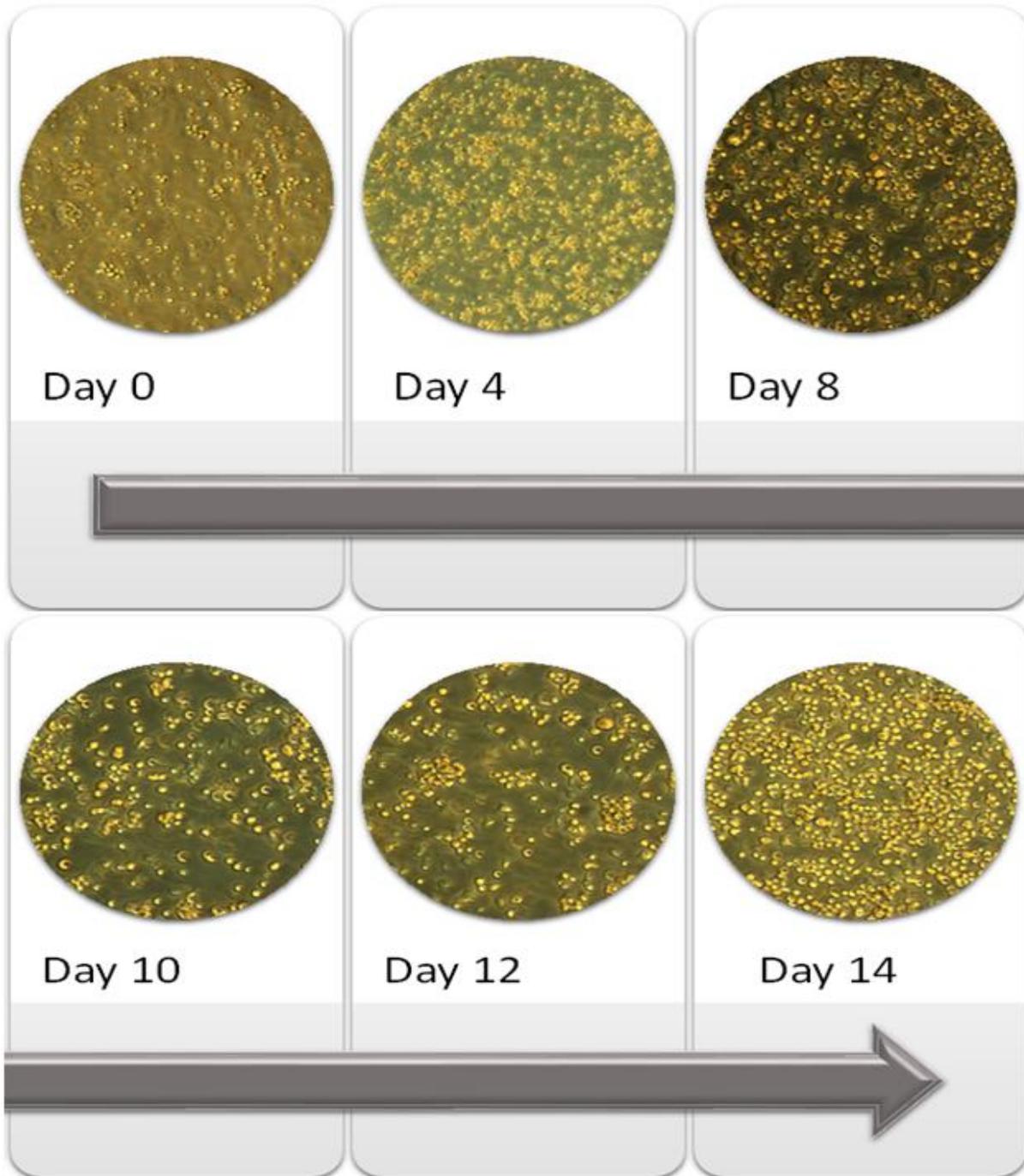
Figure 47. Changes in cell density during the 14-day differentiation protocol. Microscopy images of bone marrow cells over the completion of the eosinophil generation protocol. Changing flasks, as discussed in figure 41 removes a large number of adherent cells. Pictures were taken after completion of steps per day.

Eosinophil differentiation with 5E6 cells/mL
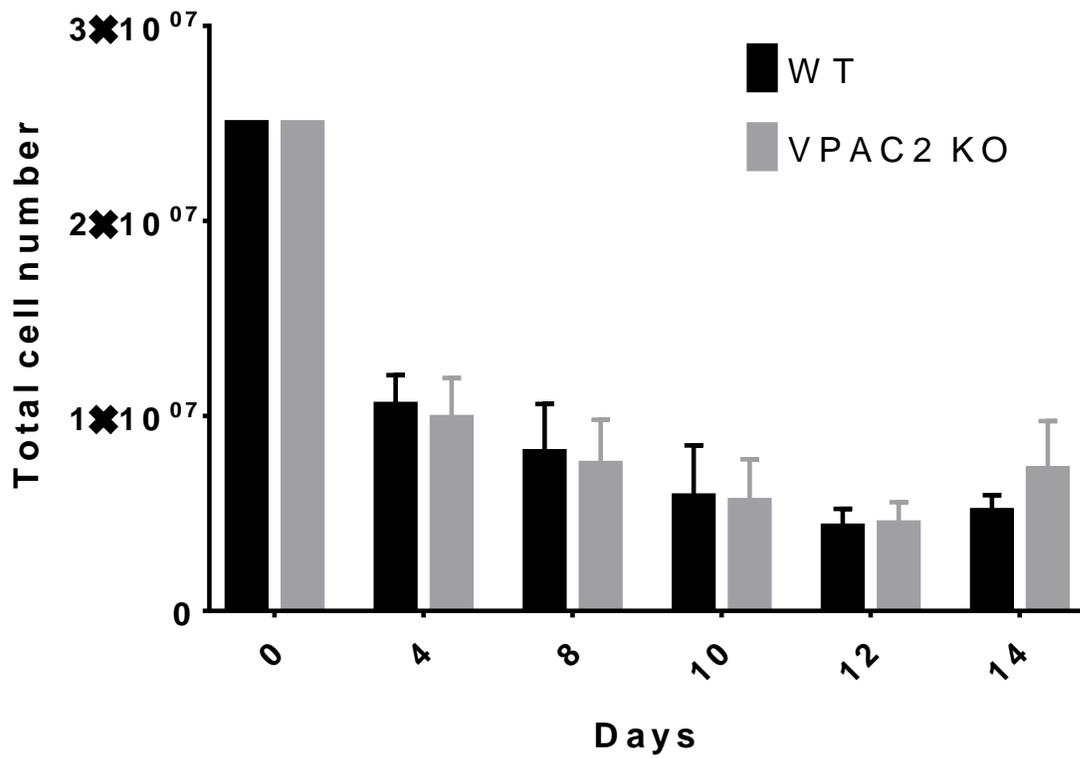
Figure 48. Eosinophil generation from bone marrow with 25 million seeded cells in 5 mL.
This bar graph depicts cell counts over the 14-day protocol. Black bars are WT samples and gray bars are VPAC2 KO samples. Error bars depict SEM values.

Eosinophil differentiation with 1E6 cells/mL
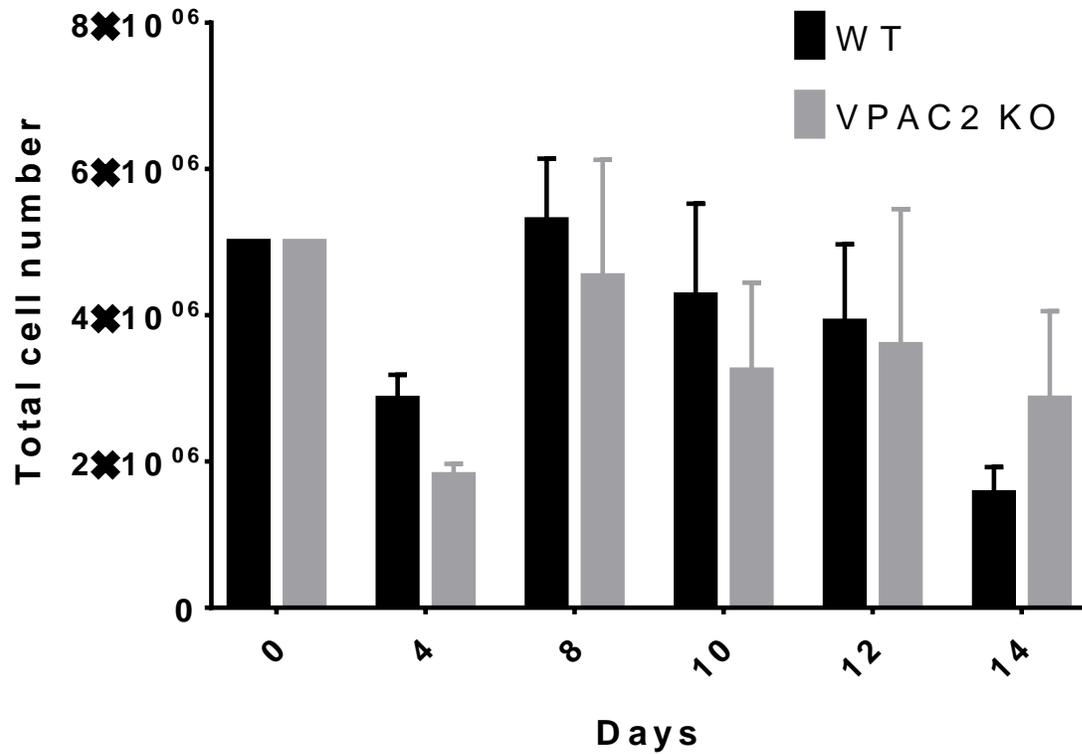
Figure 49. Changes in eosinophil numbers over 14 days when seeded at 1 x10^6 cells/mL.
Cell number differences between WT (black) and VPAC2 (gray) differentiation are depicted as bar graphs.

3.3.3. Eosinophil differentiation verification

Cytospins and flow cytometry were used to verify that the seeded bone marrow cells indeed differentiated into eosinophils. These tests were run on day 14 cells of the experiment. The cytospun slides were stained with hematoxylin and eosin (H&E) and viewed on a microscope. Figure 50 demonstrates an example of the cytospin results obtained on day 14. Flow cytometry experiments were conducted using the BD Accuri C6 with an anti-SIGLEC-F mouse antibody used to determine eosinophilic differentiation. Figure 51 is demonstrating the shift in SIGLEC-F expression when compared to isotype control for each sample. In this figure a shift of 96.3% was seen, suggesting a highly enriched eosinophil population. For most of the eosinophil differentiation runs, a greater than 90% shift was seen when compared to isotype control. These results suggest that although a difference in eosinophil number is not seen, the cells seeded initially do become eosinophils by day 14.
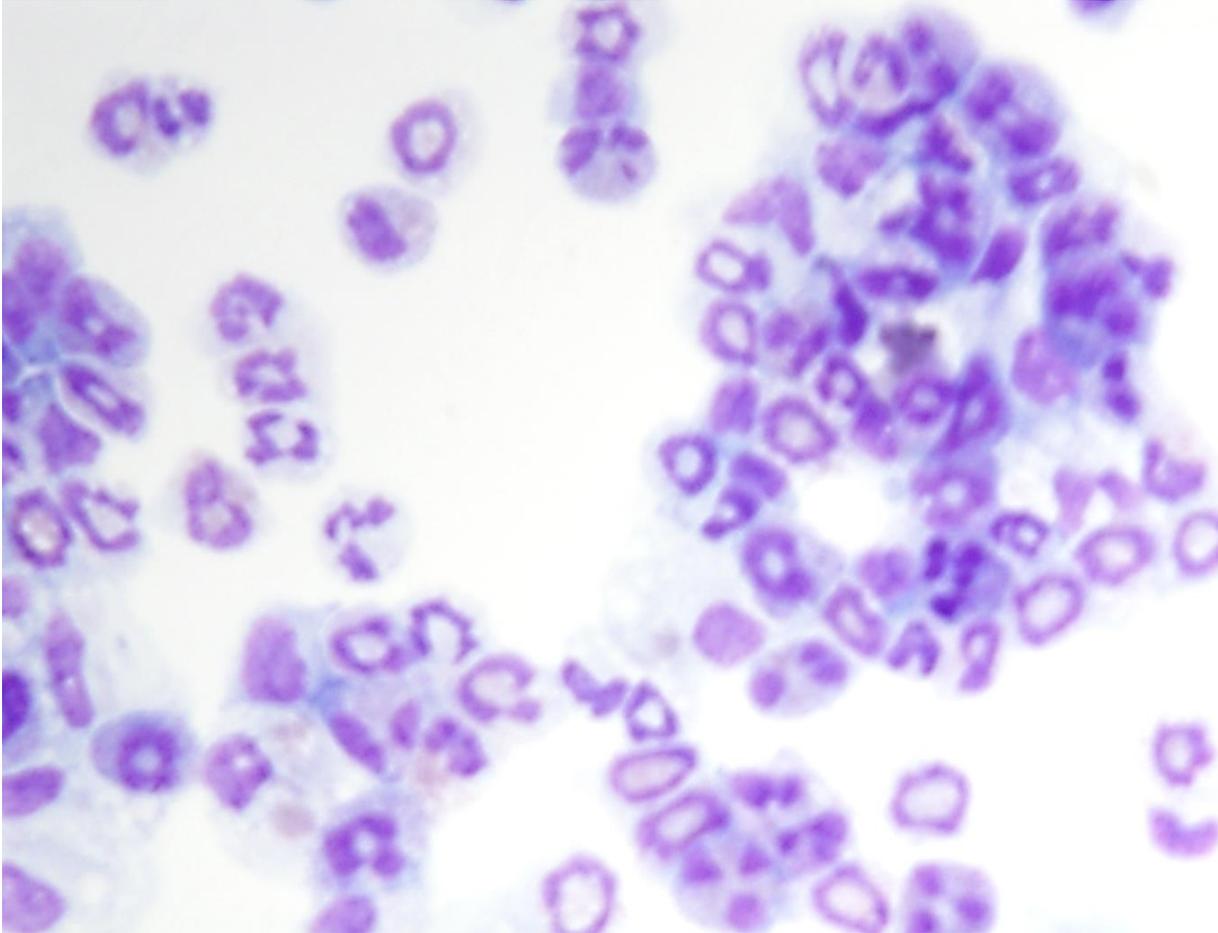
Figure 50. Cytospin verification of bone marrow derived eosinophils.
Changes in bone marrow cell morphology after 14 days. This picture is a cytospin of the cells remaining on day 14 stained with H&E stain. The purple bilobed nuclei are characteristic of eosinophils.
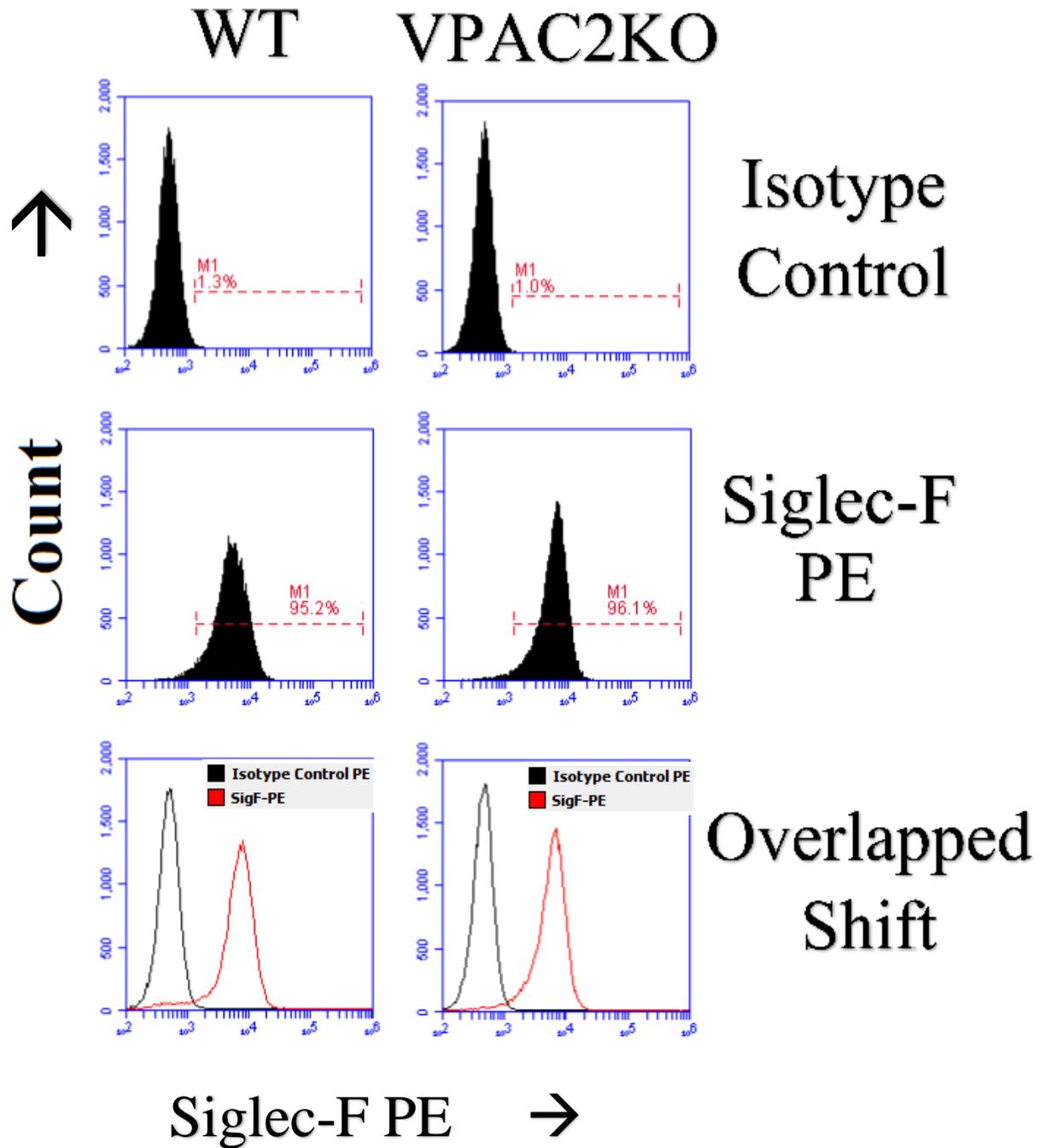
Figure 51. Flow cytometry analysis of Siglec-F PE expression levels on day 14. Utilization of the mouse anti-Siglec-F antibody conjugated to PE in comparison to isotype control for both WT and VPAC2 KO samples. A shift of nearly 95% is seen over isotype for both mouse genotypes. This is a representative of flow analysis completed on all eosinophil differentiation samples.

3.4. Discussion

3.4.1. cAMP assay

One of the major finding of this cAMP study was the diminutive cAMP produced by VIP signaling for the two human T-cell lines, Hut-78 and Molt-4. The change in cAMP was indiscernible in the Hut-78 cell line. Neither VIP or the two receptor agonists created significant change in cAMP levels over H_2O and DMSO. Previous research by Xia et al. has demonstrated that the Hut-78 cell line expresses low levels of VPAC1, which may be the reason that no significant cAMP changes were detected (Xia et al. 1996). A similar trend was seen in the Molt-4 cells, where cAMP levels did not significantly change between the experimental vs control groups. As previously reported by Summers et al., the Molt-4 cells only express the VPAC2 receptor (Summers et al. 2003). A slight upwards trend was detected with the addition of the Bay-55-9837 VPAC2 agonist, which seems logical as only the VPAC2 receptor is expressed on Molt-4 cells.

This was confirmed by microarray analysis conducted on these two cell lines by Travis Van Der Steen, which showed no changes in gene expression after exposure to VIP (V. D. Steen et al. 2016). QRT-PCR analysis by Steve Wanjara with assistance from myself, has demonstrated that in mouse CD4 T-cells, the addition of VIP upregulates mRNA levels of an EGFR-pathway (currently unpublished data). This pathway was not upregulated when the same analysis was done using donor human blood isolated CD4 T-cells. While this makes it difficult to understand which receptor is responsible for the chemotactic effects of VIP on these cells, it does tell us that VIP performs different functions between human and mouse CD4 T-cells.

Interestingly, the MCF-7 epithelial cell line demonstrated nearly a 20-fold increase in cAMP concentration when exposed to VIP. These cells also responded to both receptor agonists

which was not seen in either of the T-cell lines. Previous research with these cells has shown that the addition of VIP, inhibits the growth of this breast cancer line (Moody et al. 2002). The drastic increase in cAMP in this cell line when compared to the T-cell lines may suggest a greater role of VIP in the epithelia than in the immune system. Future studies can include the utilization of other T-cell lines. A previous publication by Dorsam et al. contains a comprehensive list of VIP receptor expression in human and mouse T-cell lines (Dorsam et al. 2011). This allows for the utilization of other lines such as H9, which exclusively expresses the VPAC1 receptor (Xia et al. 1996), and Sup T1s, which solely express VPAC2 (Goursaud et al. 2005). Also, the utilization of CD4 T-cells from VPAC1 and VPAC2 knockout mice, could answer the question as to which receptor is responsible for changes in the mouse CD4 T-cells. Obtaining cells from knockout mice would allow for the use of just VIP and remove the agonists from future experiments. qRT-PCR analysis of knockout CD4 T-cells would also answer the question posed by Steve Wanjara's research as to which receptor is altering the EGFR pathway.

3.4.2. Eosinophil differentiation

The results of the 14-day differentiation study from donor bone marrow cells tell us that between mice lacking VPAC2 and their WT counterparts, there are no significant changes in the rate of eosinophil differentiation. This lack of change was observed in both 1×10^6 cells/mL and 5×10^6 cells/mL concentrations. Interestingly, the slope of the numbers of cells over the 14 days differed between these two concentrations. In the 5×10^6 cells/mL experiment a large number of cells died off within the first four days, with a slight U-shaped decline over the remaining ten days. There was a trend towards an increase in day 14 in VPAC2KO, suggesting that perhaps if the experiment was expanded into more days a difference could be visualized.

In the 1 x 10^6 cells/mL cellular concentration, there was cell death between days 0 and 4 as well, but not as great a change in total number as in the 5 x 10^6 cells/mL. Over the remaining ten days of the experiment an initial increase in total cell number for both strains was observed, with a decrease towards the end. As previously mentioned for 5 x 10^6 cells/mL, on day 14 of the 1 x 10^6 cells/mL experiment, a large margin of error for the VPAC2KO mice with a trend towards an increase in that population over WT, was observed. An expansion of the experimental days may result in a significant change over time.

Analysis of cytospins confirmed that the cells observed on day 14 of the experiments were indeed eosinophils. The cytospin pictures were very similar to those published by Dyer et al. (Dyer et al. 2008) confirming the change from bone marrow progenitors to eosinophils. The sickle shaped nucleus of the cells is a hallmark of eosinophils, with pink spots depicting the small granules within the eosinophil's cytoplasm which was observed in bone marrow derived eosinophils from both strains. Flow cytometry analysis confirmed the cytospin analysis by using Siglec-F antibody against the derived cells. An average shift of 95% for the Siglec-F receptor was seen in both WT and VPAC2KO strains throughout the numerous runs. Although Dyer et al. did not publish the numerical percent shifts over isotype control, the visual change in Siglec-F decades observed for both strains is extremely similar to ours (Dyer et al. 2008).

This lack in significance of eosinophil differentiation was similar between both strains, suggesting that perhaps there is no difference in the ability of stem cell progenitors of either strain to differentiate into eosinophils. The total number of these stem cells between VPAC2KO and WT may also be similar. A possible explanation for the difference in eosinophilic response to fungus induced allergic asthma in the VPAC2 knockout as reported by Samarasinghe et al may be differences in IL-5 levels in either mouse strain (Samarasinghe, Hoselton, and Schuh

2010a). Preliminary data gathered by myself using a proteome profiler (R&D Systems, Minneapolis, MN) has uncovered a fold increase of 2.54 in serum IL-5 levels, which is a major regulator of eosinophilic endurance and function. IL-5 ELISA work needs to be conducted to confirm the validity of this preliminary data and hypothesis. Changes in the rate of differentiation have been published in other knockout mouse models such as miR-223 deficient mice reported by Lu et al. (Lu et al. 2013) and CCR3 deficient mice published by Sturm et al. (Sturm et al. 2013). Changes in rate of eosinophil growth in the BALB/c mouse strain has been demonstrated to be much faster when compared to the C57 BL/6 linage used in our laboratory (Dyer et al. 2008).

Future aims to explain the delayed arrival of eosinophils in the BAL of VPAC2KO mice include, the chemotactic capabilities of VIP on eosinophils and the blunted infiltrabilities of eosinophils in VPAC2KO mice. This could involve analysis of the degranulability of eosinophils for both strains. The addition of VPAC1, VIP and CRTH2 knockout mice to these experiments could shed light the functions of VIP and its other receptor. Although eosinophils contain neither VPAC1 or VPAC2 receptors, research by El-Shazly et al. has uncovered the association of VIP and the CRTH2 receptor (El-Shazly et al. 2013). It seems this prostaglandin-D2 (PGD2) receptor (CRTH2) binds VIP (also secreted in an autocrine fashion by eosinophils) and induces eosinophilic chemotaxis (eosinophilotactis) at levels just below eotaxin, the benchmark for eosinophil chemotaxis (Rothenberg et al. 1996). Taking these knockouts through the allergic asthma model could help better understand how these proteins affect eosinophil function.

4. *ILLUMINATE-MIRNA:* PARADIGM FOR HIGH-THROUGHPUT, LOW-COST, AND SENSITIVE MIRNA DETECTION IN SERUM SAMPLES AT POINT-OF-CARE SETTINGS

4.1. Introduction

First discovered in the 1990's, microRNAs (miRNA) are a class of small, non-coding RNA molecules that are involved in translational gene regulation. These non-coding RNAs are found in most eukaryotes and account for nearly 5 % of the human genome. Since their discovery, researchers have uncovered a great deal about the life cycle of miRNAs, of which this chapter provides a brief overview. Mature miRNA molecules bind messenger RNA (mRNA) and prevent the translation of mRNA into protein. MiRNAs have also been implicated in various stages of cancer progression. The changes in profile expression can be used as cancer biomarkers for various tumor types.

There are many different classifications for small, non-coding RNA molecules, such as small interfering RNA (siRNA), small nucleolar RNA (snoRNA), ribosomal RNA (rRNA) and micro RNA (miRNA). Each classification describes the function of that individual group of small RNA molecules. Between these small RNA molecules are arbitrary distinctions but no unified agreement upon classification or differentiation (Li and Liu 2011). This results in some small RNA molecules being classified into multiple categories based upon the researcher's discretion. Ribosomal RNA (rRNA) for instance, is a component of the ribosome, which is approximately 60% RNA by weight and is crucial for protein synthesis as it acts as the enzymatic catalyst for peptide bond formation inside the cell. Small nucleolar RNAs act as guides for other RNA molecules (Kiss 2001). For example, the snR30 snoRNA was found by Lemay et al. to be essential for the 18S ribosome formation in yeast cells (Lemay et al. 2011).

SiRNA are similar to miRNA in size and operate within similar pathways. Discovered by Andrew Fire and Craig Mello, whom received the Nobel Prize for this discovery (Fire and Mello 2006), siRNA interfere with specific gene function and expression by mRNA degradation (Yoshizawa et al. 2015).

MiRNAs, the focus of this research, function in inhibiting mRNA directed protein translation. Although similar to other small non-coding RNA molecules, miRNAs form hairpin loops upon biosynthesis by folding upon themselves due to intramolecular complementary sequences. The first miRNA to be discovered was lin-4, by Lee et al. in 1993. Lin-4 is essential in the postembryonic development of the transparent nematode (roundworm) known as *C. elegans* (Lee, Feinbaum, and Ambros 1993). So far, we know that a majority of miRNAs are transcribed by RNA polymerase II and a few by RNA polymerase III (Lee et al. 2004). The miRNAs transcribed by RNA polymerase III are critical for the regulation of the mammalian cell cycle, and the cell's growth and maintenance (Goodfellow and White 2007). Although the bulk of miRNAs function within the cytoplasm, some extracellular miRNAs are found in carriers, such as exosomes. Known as circulating microRNA, these molecules are found in whole blood and plasma or serum. These are found in exosomes, which are used to deliver miRNAs to nearby tissues and cells (Yeh et al. 2015).

4.1.1. MicroRNA (miRNA) biosynthesis

RNA polymerase II or III transcribe most eukaryotic microRNA genes, generating a primary transcript or pri-microRNA sequence (Borchert, Lanier, and Davidson 2006). After transcription, the pri-microRNA sequence folds into a stem loop structure with numerous unpaired nucleotide sequences throughout the double strand (visualized in figure 51) (Cramer 2004). This pri-microRNA is then processed by Drosha (called the microprocessor) and DGCR8

(Denli et al. 2004). These two proteins form a complex known as the microprocessor complex, which cleaves the 5' and 3' ends of the pri-microRNA, releasing a 60 to 70 nucleotide sequence known as pre-microRNA (Hutvagner et al. 2001). The pre-microRNA is then recognized by a nuclear export factor known as Exportin-5 (Exp5) (Bohnsack, Czaplinski, and Gorlich 2004). This Exp5 protein mediates the export of the pre-microRNA molecules from the nucleus and into the cytoplasm (Yi et al. 2003). These steps are presented in figure 51.

In the cytoplasm, the pre-microRNA molecules encounter Dicer, an endonuclease that is present in all eukaryotes (Zhang et al. 2002). The product of this Dicer enzyme is known as the miR:miR*duplex. This duplex carries two strands, one called the guide strand and the other called the passenger strand (Lau et al. 2001; Schwarz et al. 2003). The miR:miR*duplex carries two nucleotide 3' overhangs which are complementary (Rand et al. 2005). The Argonaut enzyme grabs the duplex and removes the miR*passenger strand leaving the guide strand with its nucleotides exposed. Once the miR*passenger strand is removed, the Argonaut protein and its guide strand are known as the miRISC complex (Matranga et al. 2005). This complex then searches for complementary RNA or DNA sequence for gene silencing. Once a sequence has been found, transcription/translation is repressed and the mRNA sequence is destabilized (Zeng, Yi, and Cullen 2003). While recent research has determined how miRNAs are generated, their regulation and expression still remains largely unknown (Ha and Kim 2014; He and Hannon 2004; Hayes, Peruzzi, and Lawler 2014).
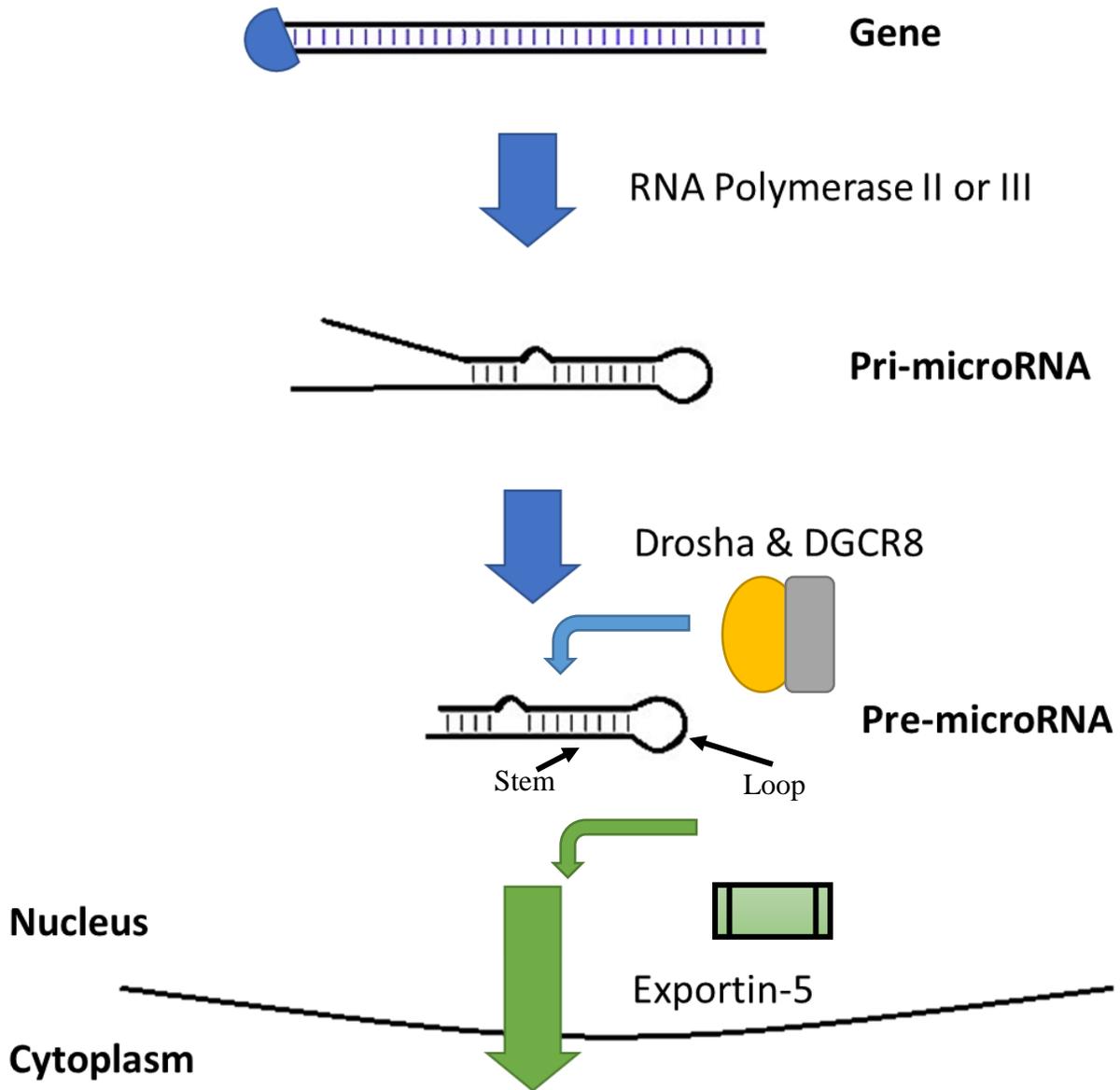
Figure 52. Nuclear miRNA biosynthesis steps.
MicroRNA genes are transcribed by RNA polymerase II or III (cut blue oval) into (70-80 bp) Pri-microRNA, where intro-complementary regions cause the molecule to take on a stem-loop structure. The Drosha and DGCR8 enzymes cleave its 5' and 3' ends generating Pre-microRNA. The Exportion-5 protein present in the nuclear membrane transports the Pre-microRNA into the cytoplasm.
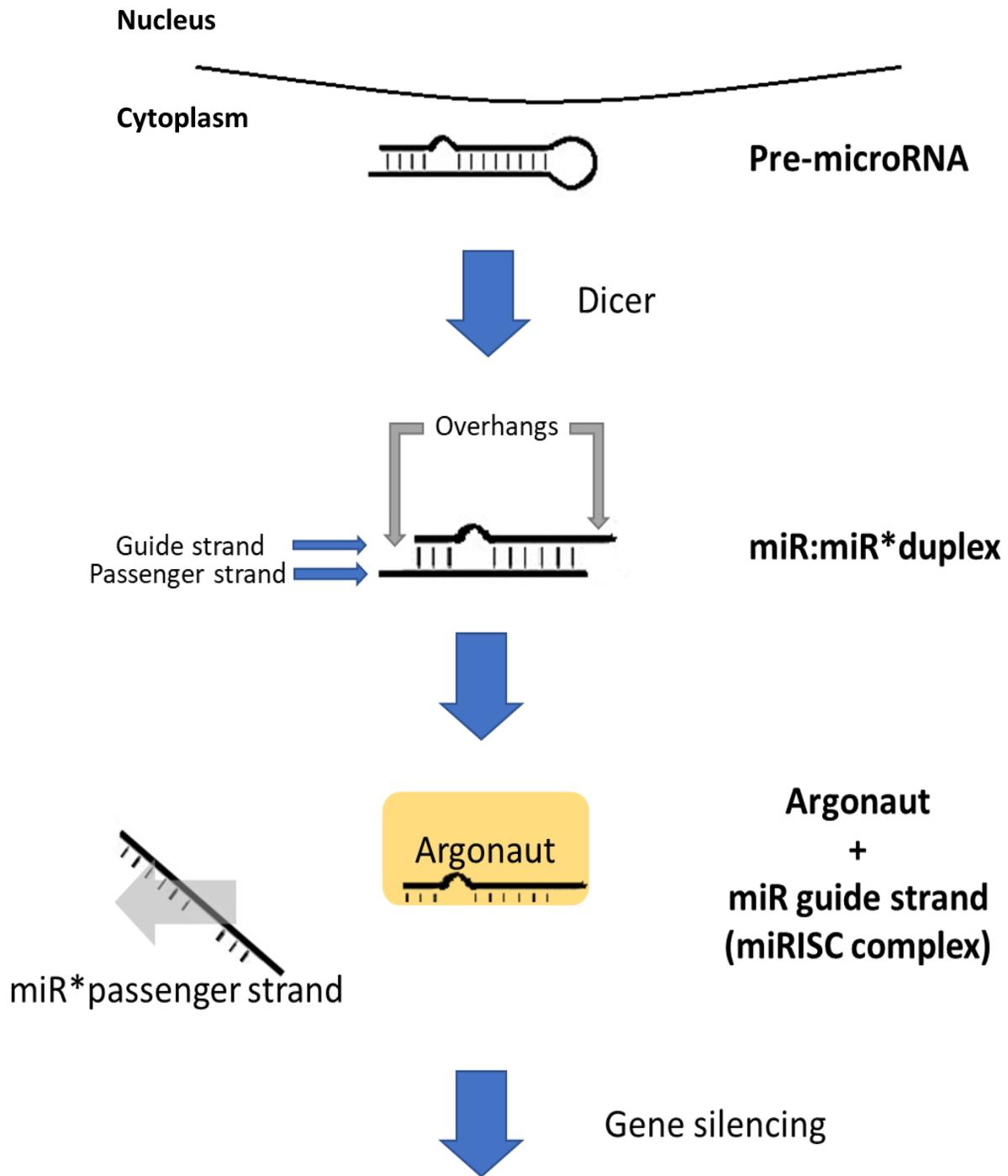
Figure 53. Cytoplasmic modifications and protein translation silencing by miRNA. In the cytoplasm, the ends of the pre-microRNA are cleaved by the Dicer enzyme, which leaves the miR:miR*duplex with overhangs. This duplex is loaded into the Argonaut protein which removes the miR*passenger strand, leaving the Argonaut protein with the miR guide strand. This is known as the miRISC complex, which binds complementary DNA or RNA sequences silencing translation.

4.1.2. MicroRNAs as disease biomarkers

Over the past decade, researchers have found a link between miRNA expression profiles and disease states in the body (Ebert and Sharp 2012). The link between microRNA dysregulation and cancer was first established by Calin et. al who demonstrated that more than half of leukemia patients suffered from the deletion of a microRNA gene region (Calin et al. 2002). Since then, the role of microRNA's in the regulation of oncogenes and tumor suppressors has been better established (Stahlhut and Slack 2013). A database linking known microRNAs to their cancer targets, known as the Tarbase was established by Sethupathy et al (Sethupathy, Corda, and Hatzigeorgiou 2006). MicroRNA-34A for instance, was shown to inhibit the metastasis of human gastric cancer, where its expression was down-regulated (Peng et al. 2014)..

The let-7 microRNA family has also been implicated in cancers and neurological diseases. Research into this thirteen-member family has demonstrated a decline in let-7 expression in lung cancer (Takamizawa et al. 2004), lymphoma and sarcoma (O'Hara et al. 2009) and ovarian cancer (Dahiya et al. 2008). A more comprehensive list of cancers affected, and the Let-7 family members involved are listed in table 9 below and on the next page.

Table 9.   Let-7 expression levels in different human cancers.

Family member	Cancer type	
	Downregulated ⇊	Up-regulated ⇈
7a	Breast	
	Lung	
	Melanoma	
	Pancreatic	
	Primary pigmented nodular adrenocortical disease (PPNAD)	
		Lung
		Lymphoma
		Ovarian

Table 9.   Let-7 expression levels in different human cancers (continued).

Family member	Cancer type	
	Downregulated ⇓⇓	Up-regulated ⇑⇑
7b	Childhood acute lymphoblastic leukemia (ALL)	
	Melanoma	
	Ovarian	
	PPNAD	
	Prostate	
	Retinoblastoma	
		Gastrointestinal stromal tumor (GIST)
		Lymphoma
7c	Burkitt lymphoma	
	Lung	
	PPNAD	
	Prostate	
7d	Head and neck squamous cell carcinoma (HNSCC)	
	Ovarian	
	Prostate	
7e	Ovarian	
	Prostate	
7f	Lung	
	Ovarian	
	Prostate	
	Sarcoma	
		Breast
7g	Lung	
	PPNAD	
	Prostate	
7i	Ovarian	
	Prostate	
		HNSCC
		Lymphoma

Modified table compiled by and obtained from (Boyerinas et al. 2010)

As reported by Wu et al., the precise expression levels of let-7 are important for tumor detection and suppression. These microRNAs are also correlated with numerous oncogenic pathways. The overexpression of let-7 microRNAs can result in liver damage, an increased susceptibility to hepatic cancers and obstruction of liver regeneration (Wu, Nguyen, et al. 2015). This family has also been implicated in the myelination of nerves. Research by Gökbuget et al. demonstrated that the suppression of notch1 by let-7 was essential for proper myelination of Schwann cells. In mice with reduced levels of let-7 resulted in a demyelination phenotype(Gokbuget et al. 2015).

The importance of these microRNA's in disease regulation also lends to their importance as biomarkers. Over the past few years, researchers have been pursuing numerous different methods to quantify microRNA levels in serum as a non-invasive strategy for early diagnosis. An approach by Liu et al. utilized magnetic microparticles with complimentary sequences to bind target microRNA's. The researchers claimed that the device was able to detect as low as 1 fmol of target microRNA in binding buffer (Liu, Zhou, and Xing 2014). Other techniques, such as one from the RIKEN biological laboratory have also been published. These engineers utilized complementary DNA strands bound to glass slides to capture desired microRNA's. Secondary antibodies with fluorophores were then added to allow for microRNA detection. These researchers were able to detect a minimum of 0.5 pM of microRNA sample (Arata, Hosokawa, and Maeda 2014).

In addition to the utilization of hybridization detection methods that are non-enzymatic in nature, the gold standard for detection is still the enzymatic based quantitative reverse transcription polymerase chain reaction (qRT-PCR) (Costa, Leitao, and Enguita 2014). Due to the short length of microRNA samples, additional strategies have been necessary to successfully

use qRT-PCR. One of these includes the utilization of stem-loop (SL) primers. The SL primer allows for superior binding specificity to short nucleotide sequences and easier access/amplification by the taq polymerase (Tong et al. 2015). Another is the improved isolation of microRNAs from exosomes. Research by Gallo et al. has demonstrated that in serum a majority of detectable microRNAs are tightly associated with exosomes. To demonstrate this, serum samples were separated into two fractions, exosome-depleted serum fraction and serum containing exosomes fraction. qRT-PCR reactions conducted on both groups showed that the exosome intact group contained significantly greater amounts of miRNA than the exosome-depleted samples (Gallo et al. 2012).

A fast and accurate detection platform of microRNAs is important for early detection in an effort to save lives. However, qRT-PCR reactions are costly and require time (hours/days) to detect specific microRNA's in human serum. In order to provide accurate results in point-of-care settings such as hospitals, more rapid and cost-effective methods are required. To fill this void, Keerthi Nawarathna Ph.D., an assistant professor at NDSU in the Department of Electrical Engineering, alongside his graduate student Logeeshan Velmanickam, developed a novel high-throughput, low-cost microRNA detection platform called iLluminate-miRNA. A collaborative effort between the Nawarathna and the Dorsam labs was initiated for our lab's expertise in qRT-PCR technology. My contributions included conducting miRNA isolation, running parallel qRT-PCR experiments, teaching Logeeshan molecular biology techniques, weekly lab meetings, and assistance with writing the manuscript currently under review.

4.2. Materials and methods

4.2.1. Micro RNA isolation

For isolation of miRNAs from serum and water, the Sigma-Aldrich mirPremier microRNA Isolation Column Chromatography kit (St. Louis, MO) was used. Let-7b miRNA (5' -UGAGGUAGUAGGUUGUGUGGUU - 3') was purchased from the Midland Certified Reagent Company (Midland, TX). Let-7b miRNA was spiked into water starting at 1 nM and 10 subsequent ¼ serial dilutions were performed ending with 11.44 fM. Let-7b was also spiked into human serum obtained from Innovate Research (Novi, MI) at concentrations ranging from 12 nM to 120 fM. Both serum and water samples were also spiked with Let-7c miRNA (5' - UGAGGUAGUAGGUUGUAUGGUU - 3'), which differs from Let-7b by a single nucleotide change, and a random scrambled miRNA sequence (5' – UGAGGUAGUAGGUUGUAUGGUU – 3'), both purchased from Midland Certified Reagent Company (Midland, TX), to assess specificity of the new iLluminate-miRNA detection platform.

The provided Sigma-Aldrich protocol (2017) was followed for isolation. Each sample concentration was placed in a 2 mL microcentrifuge tube with 700 µL of lysis buffer. Samples were incubated for 5 minutes with gentle rocking followed by centrifugation at 16,000 x g for 5 minutes. The supernatant was collected into a fresh tube, diluted with equal volume of 100% ethanol, mixed by pipetting and applied to a binding column. Samples were centrifuged at 16,000 x g for 5 minutes and after decanting the flow-through, a second 100% ethanol solution was applied to the column and centrifuged as above. A third centrifugation step was performed to dry the column, followed by the addition of 50 µL of elution buffer and centrifugation repeated, to eluate purified miRNA. This was stored at -20°C until the first strand cDNA synthesis step was performed.

4.2.2. First strand cDNA synthesis

The Agilent Technologies (Santa Clara, CA) miRNA 1st-strand cDNA Synthesis Kit was used. First, a polyadenylation reaction was catalyzed by *E. coli* poly A polymerase and performed to add poly(A) tail to isolated miRNA. Complementary DNA was then synthesized from the miRNA template molecules using a poly-T primer, for reverse transcription of newly generated poly-A tail-miRNA molecules. Samples were placed into a thermocycler for the following incubation steps.

Polyadenylation

1. 37°C for 30 minutes

2. 95°C for 5 minutes

3. Immediate transfer to -20°C for storage or cDNA synthesis

cDNA synthesis

1. 55°C for 5 minutes

2. 25°C for 15 minutes

3. 42°C for 30 minutes

4. 95°C for 5 minutes

5. Stored at -20°C

4.2.3. qRT-PCR

Analysis of miRNA was performed by reverse transcription PCR (qRT-PCR) analysis utilizing the Aglient miRNA QPCR Master Mix Kit and using cDNA generated from purified miRNA samples treated with poly-A polymerase. This kit uses the EvaGreen® dye to analyze double-stranded DNA amplification. The miRNA qRT-PCR master mix, a universal reverse primer and a Let-7b specific primer were added together to form a master mix, which was added to each individual well of a 96-well plate. Complementary DNA samples (4 µL) were added to

appropriate wells and the Bio-rad CFX96 Real-Time PCR instrument was used to analyze the

samples. The incubation steps of the machine were as follows:

1. 95°C for 10 min

2. 40 cycles of 95°C for 10 seconds

3. 60°C for 15 seconds.

4. Go to 2, 40 x

5. Melt Curve

    a. 65°C to 95°C, in increments of 0.5°C

4.2.4. Percent recovery calculations

Ct values for each diluted sample were subtracted from the lowest Ct value detected in

water or serum (ΔCt). Fold-differences for each diluted sample were calculated by using: $2^{(-\Delta Ct)}$,

and % recoveries were calculated in an identical manner as the iLluminate-miRNA (Table 10).

Briefly, fold-differences for each diluted sample (numerator) were divided by its maximum at 12

nM in water (denominator) and normalized by multiplying by the dilution factor.

4.2.5. *iLluminate-miRNA* miRNA detection

The *iLluminate-miRNA* platform uses miRNA duplexes in 0.01x TE buffer, containing

isolated miRNA samples hybridized to their complementary DNA. The fluorescently labeled

(Fluoresce) probes are added at 10x excess. This mixture is heated up to 95°C for 5 minutes and

then allowed to cool slowly at room temperature for an hour to allow for complete hybridization.

These samples are then plated onto a T-shaped interdigitated array of microelectrodes (TIAM)

electrode array. Evaporation of the buffer increases the concentration of the miRNA/probe

duplexes within the TIAM electrode array. This focusses the miRNA/probe duplexes into semi-

circle shaped nano-gaps, or "hotspots" within the array where the electric field is enhanced

(Figure 54). The application of a 1000 kHz non-uniform electric field, or dielectrophoresis,

simultaneously pushes single stranded DNA molecules away while attracting double stranded complexes towards the nano-gaps on the TIAM array (Velmanickam, Laudenbach, and Nawarathna 2016). The size of the nano-gaps also allows for fluorescence enhancement. The nano-gaps are smaller than the emission wavelength of Fluorescein (512 nm in water), causing the continuous excitement of the fluorophore up to a billion-fold (Velmanickam et al. 2017). After hybridization this process took ten minutes for completion. After 10 minutes, images were obtained using fluorescent microscopy and enhancement intensity was calculated using the MATLAB software (Natick, MA) conducted by professor Nawarathna's laboratory.

Figure 54. Experimental strategy for miRNA detection method testing.
This outline describes the scheme used to compare qRT-PCR to iLluminate-miRNA (DEP) technologies where Let-7b was spiked into water or human serum and subsequent serial dilutions. Eluted miRNA samples were split between the two methods for validation. Time required for the completion of iLluminate-miRNA was significantly lower than qRT-PCR as indicated.
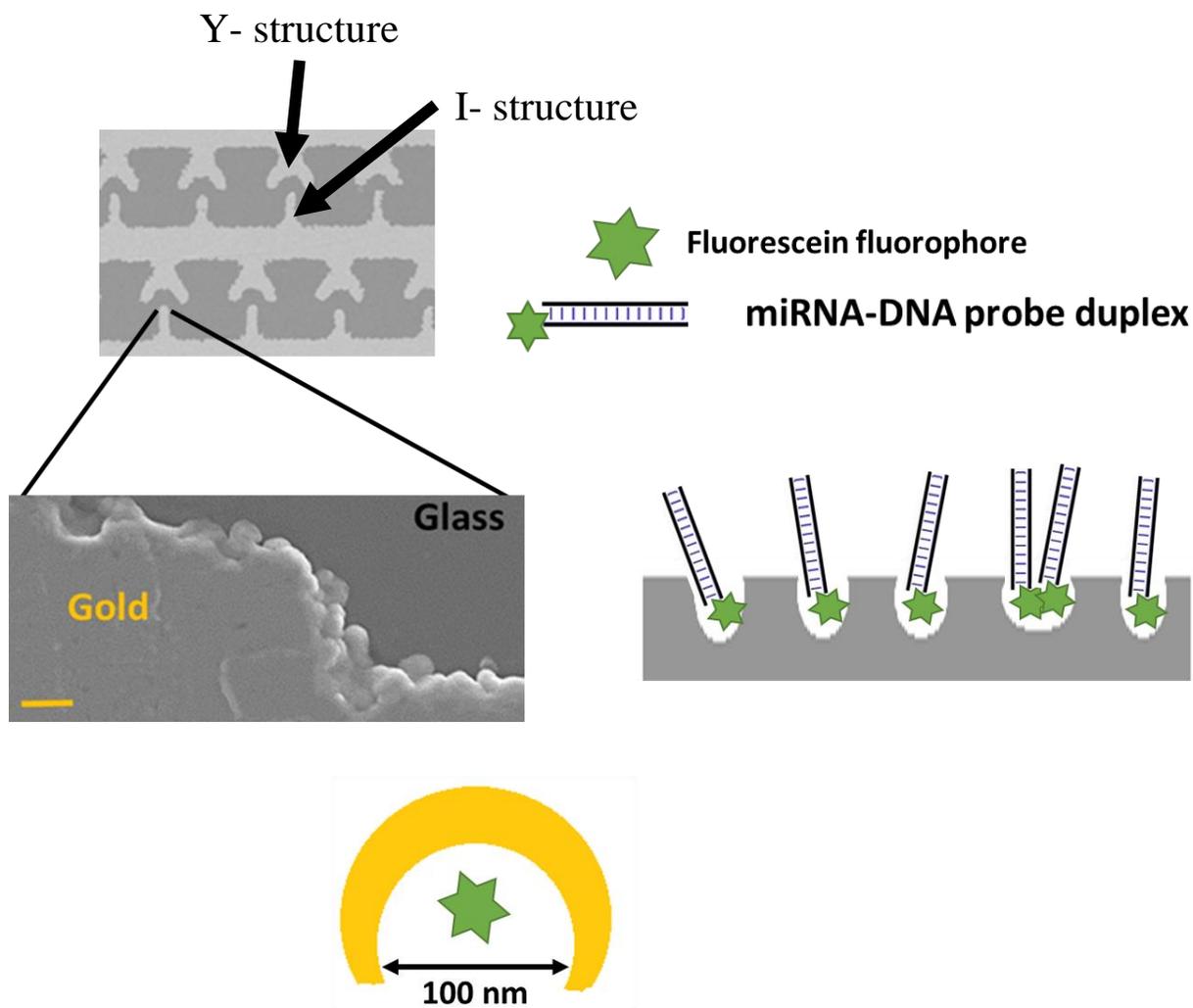
Figure 55. Nanogap structure and fluorescent enhancement due to nanogap size.
A scanning electron microscopy picture of the TIAM electrode array discussed in section
4.2.5 shows the Y and I shaped structures. The light gray color represents the electrode and
the dark gray color represents the glass slide background. Magnification of the array displays
the small nanogaps or "hotspots" present within the gold array. An artistic rendition of how
miRNA-DNA probe duplexes with attached fluorescein are positioned within the nanogaps is
depicted. The size of the nanogaps in comparison to the excitation wavelength allows for the
enhancement of the fluorescent signal.

4.3. Results

4.3.1. MicroRNA detection

We present proof-of-concept data showing that the iLluminate-miRNA method was able to detect Let-7b miRNA in a quantitative and specific manner. To this end, we used water and human serum solutions, which were spiked with known concentrations of Let-7b miRNA. Samples were divided equally after column chromatography, measured by the iLluminate-miRNA and compared to qRT-PCR measurements. It is worth noting the rapid measurement time and cost-effective nature of the iLluminate-miRNA method relative to qRT-PCR (Figure 53). This study confirmed that both the iLluminate-miRNA method and qRT-PCR were effective at measuring purified Let-7b miRNA (range: 0.0114 pM–12 nM) spiked into water (Figure 55 and Table 10) or human serum (Figure 56 and Table 10).

However, comparison of the percent recoveries of spiked-in Let-7b miRNA to a 100% predicted recovery (represented as a green line in figures 55 and 56), clearly showed that the iLluminate-miRNA method was more accurate and precise at all spiked-in Let-7b miRNA concentrations using both water and human serum as solvents. Compared to qRT-PCR, the iLluminate-miRNA method resulted in smaller standard errors of the mean (SEM) for Let-7b miRNA concentrations (Table 10), especially in water. To ensure specificity, figure 57 illustrates the detection of 12 nM of Let-7b miRNA, but not a randomly generated miRNA (22mer called scrambled – scr.), for the iLluminate-miRNA technique when spiked into water (set arbitrarily to 100%) or human serum (52%), respectively.

The reduction in percent recovery in serum versus water for the same Let-7b miRNA (12 nM) might not be directly due to the iLluminate-miRNA detection method per se, but rather because of a reduction in Let-7b miRNA yield during column chromatography. Lastly, the

iLluminate-miRNA method was nearly 10- and 660-fold more sensitive at detecting 12 nM spiked-in Let-7b miRNA compared to qRT-PCR in water or serum (Figure 58). Table 11 summarizes the overall means, +/- SEM and p values for the two methods. These results support our conclusion that our miRNA detection technique can successfully quantitate Let-7b miRNA molecules after purification from water or biological fluids in an inexpensive, rapid, accurate, and precise manner that outperforms the current gold-standard approach of qRT-PCR.
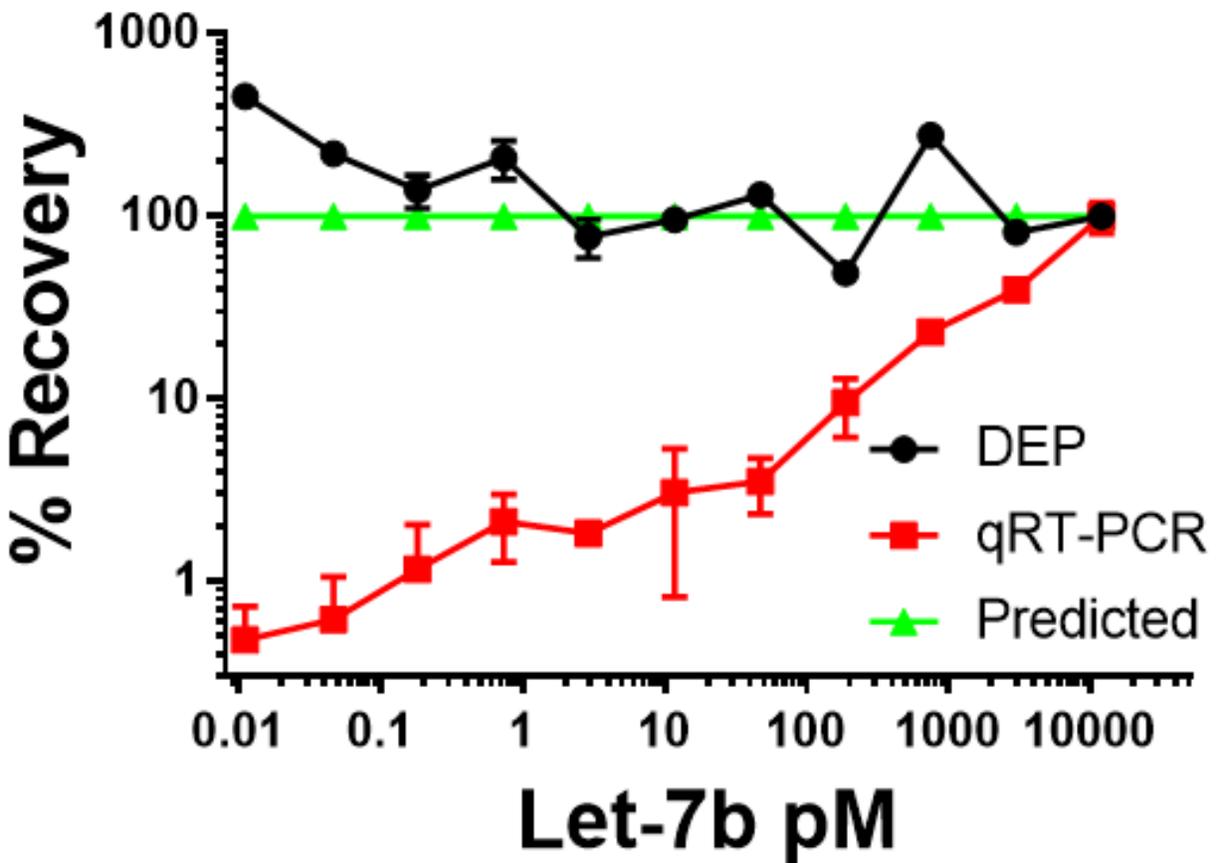
Figure 56. Let-7b recovery in water sample.
This line graph depicts the percent recovery of spiked in Let-7b for both iLluminate-miRNA (DEP) (black line) and qRT-PCR (red line) in comparison to the predicted value. The predicted values were based upon a 100% recovery rate at the 12nM concentration.
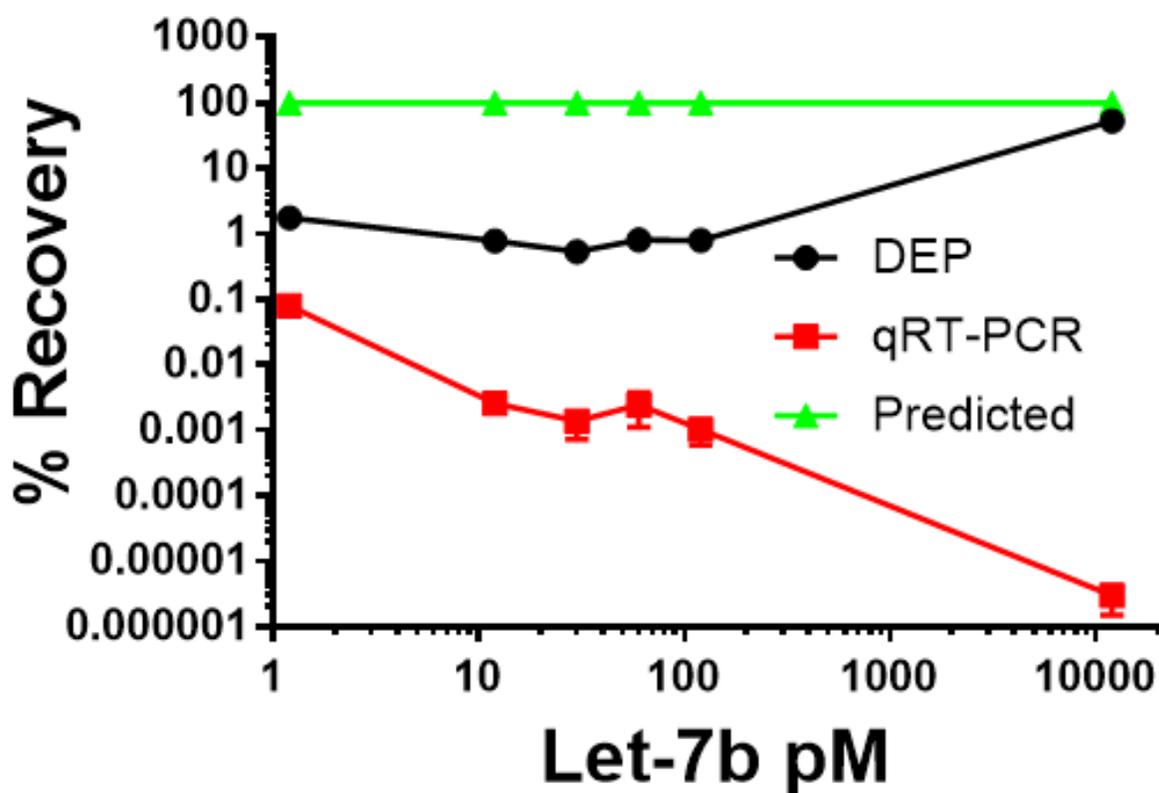
Figure 57. Percent recovery of Let-7b spiked into human serum samples.
Human serum samples spiked in with various concentrations of Let-7b miRNA was detected
by both iLluminate-miRNA (DEP) (black line) and qRT-PCR (red line). The line graph
shows the percent recovery values of Let-7b for both techniques compared to 100% predicted
(green line), based on 100% recovery at 12nM concentration. All subsequent calculations
were based on this maximum % recovery value.
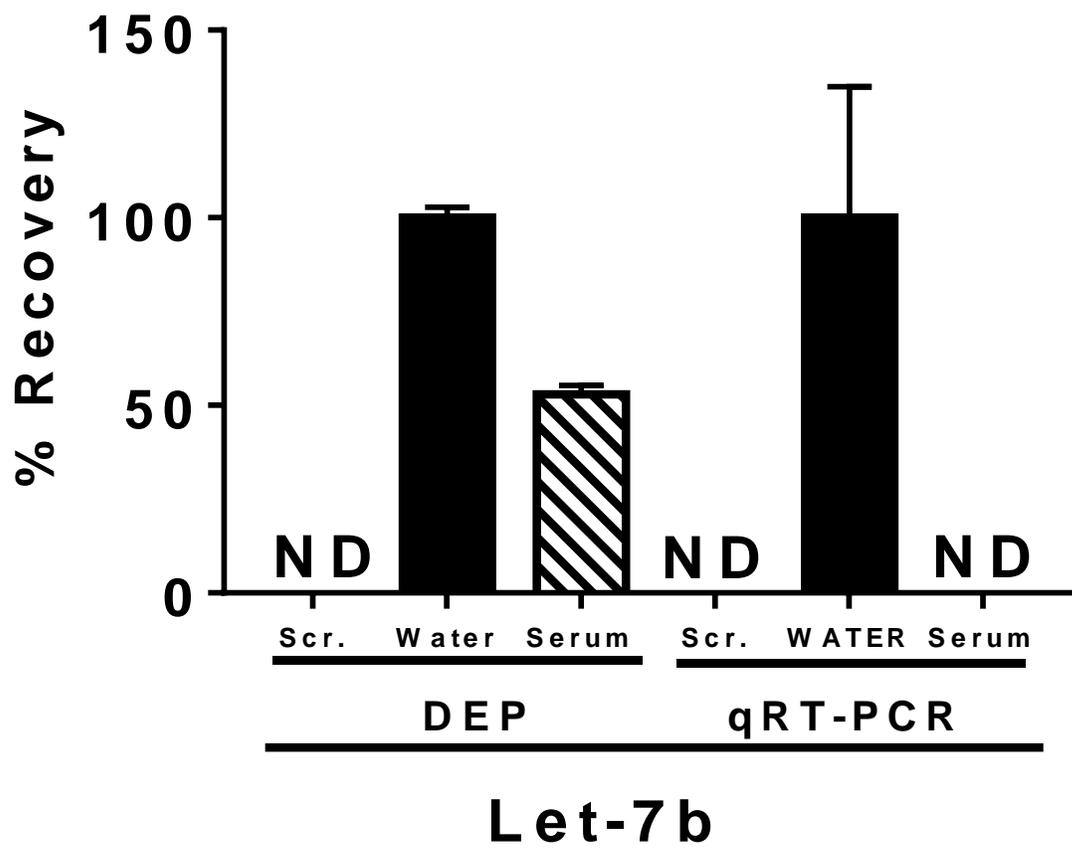
Figure 58. Scrambled versus Let-7b detection in water and serum by both iLluminate-miRNA and qRT-PCR platforms.
Scrambled miRNA (12 nM) or miRNA Let-7b (12 nM) were spiked into water or human serum. Samples were subsequently purified by column chromatography and measured by iLluminate-miRNA or qRT-PCR. Data is presented as a bar graph with % recovery means +/- SEM from 3 independent experiments. The abbreviation of "ND" stands for "not detected."
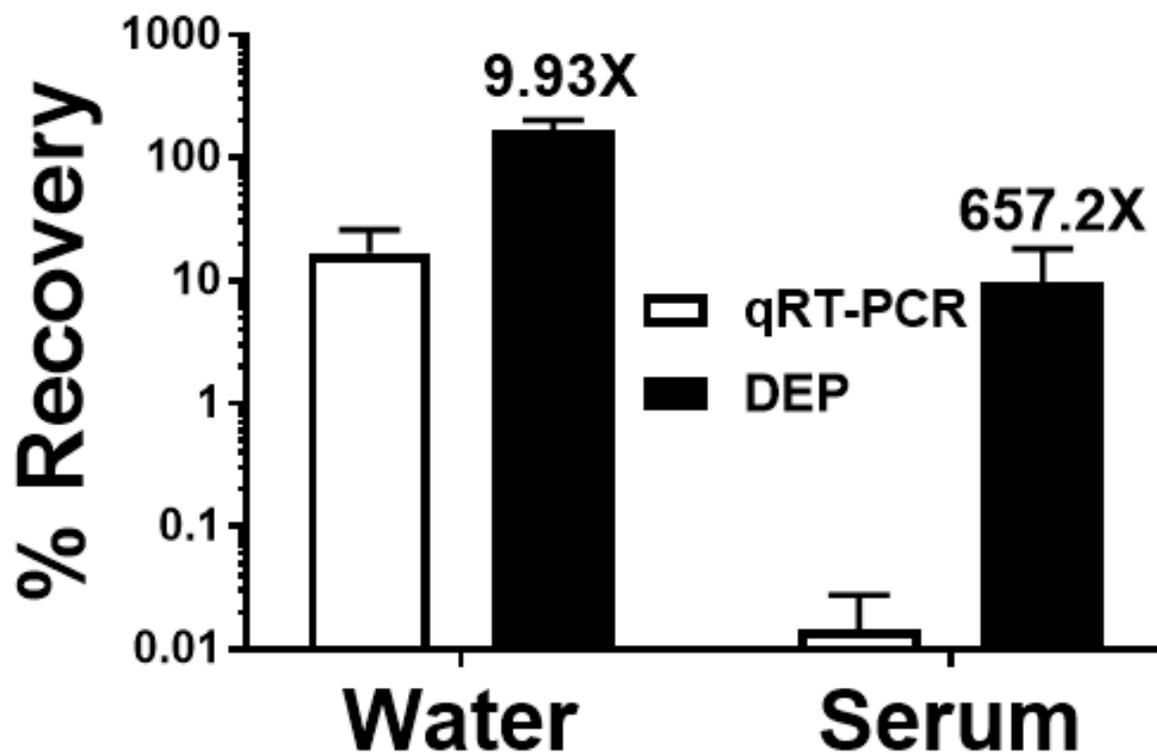
Figure 59. Direct percent recovery comparisons at 12nM in water and serum.
Direct relative comparisons of % recovery calculations at 12 nM are presented in a bar graph
+/- SEM from 3-4 independent experiments. The fold-difference in % recovery value for
iLluminate-miRNA versus qRT-PCR is placed above the appropriate bar for both water and
human serum solvents.

Table 10. Summary of iLluminate-miRNA and qRT-PCR data and from spiked-in Let-7b experiments.

Water

[Let-7b pM]	iLluminate-miRNA						qRT-PCR					
	F.I.E. Means	+/- SEM	Expected	Recovery	+/- SEM	N	Ct Means	+/- SEM	Expected	Recovery	+/- SEM	N
12000	75662143	2171322	2.083031	100*	3	3	10.39833	0.292038	100	100*	43.30659	3
3000	15425028	112101.7	0.520758	81.54687	0	3	13.68667	0.149481	25	10.23559	59.05029	3
750	13172686	124004	0.130189	278.558	0	3	16.465	0.186167	6.25	1.49194	29.2151	3
187.5	576083.7	23188.9	0.032547	48.72893	0	3	19.95	0.586349	1.5625	0.133248	88.62043	4
46.9	389066.3	4179.031	0.008141	131.569	0	3	23.32125	0.43261	0.390833	0.012877	78.10656	4
11.7	70961	3272	0.002031	96.19145	0	3	26.11875	0.990096	0.0975	0.001852	167.703	4
2.9	14164	3356	0.000503	77.46233	0	3	28.75625	0.769148	0.024167	0.000298	139.7295	4
0.732	9673	2290	0.000127	209.5814	0	3	30.21833	0.738497	0.0061	0.000108	107.1436	3
0.183	1609	334	3.18E-05	139.4465	0	3	33.70833	1.13822	0.001525	9.62E-06	186.2121	3
0.0458	638	78	7.95E-06	220.9316	0	3	36.47	1.040108	0.000382	1.42E-06	150	3
0.0114	328	35	1.98E-06	456.3222	0	3	38.74667	1.165241	0.000095	2.93E-07	186.2121	3
0	0	0	0	0	0	3	40.09667	0	0	1.15E-07	134.686	3

Serum

[Let-7b pM]	iLluminate-miRNA						qRT-PCR					
	F.I.E. Means	+/- SEM	Expected	Recovery	+/- SEM	N	Ct Means	+/- SEM	Expected	Recovery	+/- SEM	N
12000	40012795	954924.4	100	52.88*	2	3	36.945	1.6	100	1.02E-06	53.96605	3
120	5955.333	514.7032	1	0.007871	0	3	38.0275	2.6	1	4.82E-09	29.45412	4
60	3027	744	0.5	0.004001	0	3	35.97833	2.28	0.5	9.97E-09	5.806601	3
30	1011.667	277.1552	0.25	0.001337	0	3	36.97667	1.99	0.25	2.49E-09	1.161297	3
12	588.3333	131.1025	0.1	0.000778	0	3	35.86833	0.76	0.1	2.15E-09	0.086068	3
1.2	132	20	0.01	0.000174	0	3	36.05625	2.2	0.01	1.89E-10	0.085388	4
0	13.33333	3.756476	0	1.76E-05	0	3	37.423	2.3	0	0	0.023027	4

Table 11.   Comparison to predicted percent recovery to 100%.

Water				
Procedure	Mean	SEM	P value	Significance
qRT-PCR	16.85	9.106	0.001	****
iLluminate-miRNA	167.3	35.89	0.155	ns
Serum				
Procedure	Mean	SEM	P value	Significance
qRT-PCR	0.01459	0.01311	0.0001	****
iLluminate-miRNA	9.588	8.661	0.0003	***

4.4. Discussion

A major finding of this study is the validation of the iLluminate-miRNA platform in spiked-in miRNA detection from both water and human serum samples. These results demonstrated that while qRT-PCR is able to detect known microRNA concentrations in water, it was not able to accurately detect miRNA Let-7b in human serum. The iLluminate-miRNA technology on the other hand was able to detect microRNA levels in both solvents and with much greater accuracy and precision than qRT-PCR. The ability to accurately measure microRNA levels in human serum can greatly improve cancer and other disease diagnosis. The sensitivity, quickness, and low cost of this early-detection platform may allow for earlier diagnosis of cancers in the future.

Comparison of the qRT-PCR data to the predicted percent recovery shows a statistical loss of Let-7b miRNA in both water and serum sample groups. In water the percent recovered (figure 55) decreases gradually, whereas in serum the highest and lowest Let-7b starting concentrations are nearly indistinguishable. This could be associated with loss in column chromatography, but the higher percent recovery for the iLluminate-miRNA system suggests the column was able to isolate more miRNA than recovered. For the qRT-PCR experiments we see a steady decline in detection as the sample is diluted with a 0.99 R^2 value. This tell us that the

178

dilution of the microRNA samples was well completed with high accuracy. The results show nearly a 2-fold Cq change per 1 to 4 dilution confirming the doubling amplification of the target cDNA per Cq. To better visualize the data the y-axis was set to 41 – the average Cq to generate a downwards slope similar to that observed with the iLluminate-miRNA platform. Many researchers set a cutoff for Cq at 35, which was not done for this experiment. The inclusion of data below 35 allows for the visualization of the downward trend all the way to 11 fM of total let-7b.

The serum results are quite interesting for qRT-PCR and suggested no detection of the microRNA at all. There is no observable change between 100 ng and 0.01ng of spiked in let-7b. There may be numerous reasons at play, which could be resulting in this lack of detection. The human serum may contain Taq inhibitors that may be preventing amplification of the final product. The ability of the primers to anneal to the final product may be an issue, but the same sequences were used for detection for the iLluminate-miRNA platform and it was able to detect the double stranded duplex samples. The isolation was most likely not an issue, as both iLluminate-miRNA and qRT-PCR used the same samples for detection. Previous research by Chen et al. has described that the utilization of stem-loop primers may assist in the detection of microRNA's by qRT-PCR (Chen et al. 2005). This may help qRT-PCR amplification, but since the same primer sequences were used by iLluminate-miRNA for hybridization, we can be confident that the target microRNAs were found and bound by the introduced primers.

Numerous microRNA detection methods have been purposed. For example Rodríguez-Dorantes et al. published a method of miRNA analysis from urine to detect prostate cancer markers (Rodríguez-Dorantes, Salido-Guadarrama, and García-Tobilla 2014). Another method developed at Oregon State University, uses a fluorescent probe to bind to target microRNA

179

complexes and is recognized when excited with a laser (Larkey et al. 2014). Most purposed platforms, including iLluminate-miRNA utilize a fluorescently labeled complementary sequence to bind target microRNAs, but the pulldown and isolation of these targets differs. As discussed in the introduction section of this chapter, approaches include magnetic pulldowns or ELISA type secondary antibodies. This is where iLluminate-miRNA's strategy diverges from the rest. This technology is able to concentrate desired samples into "hotspots" on the TIAM array thereby allowing for fluorescence amplification due to the shape of the gold-plated electrode.

The detection capabilities of iLluminate-miRNA are seen in both water and serum samples. In the water samples, we can see the detection limits are greater than those of qRT-PCR which was reaching the 41 Cq undetectable range at lower concentrations. This did not hold true for iLluminate-miRNA which was able to detect the lower amounts. Future experiments using water controls could include lower concentrations of spiked in microRNA to determine this technology's lowest detection limit. The human serum samples greatly surpassed expectations for this platform when compared to qRT-PCR. The enzymatic assay was unable to detect even the highest amounts of let-7b, whereas the iLluminate-miRNA platform was able to detect the lowest concentration used equaling 1.2 pM. This data suggests that the iLluminate-miRNA platform may be an alternative for early cancer biomarker detection due to its ability to detect low concentrations in human serum.

Future experiments to validate the iLluminate-miRNA technique include the analysis of in-serum microRNA samples. The samples tested for these previous experiments included spiked-in microRNA, which is excellent for proof-of-concept, but not applicable in the real world. The next step would be to test endogenous levels of microRNA present in human serum samples which would allow for in vivo validation of its detection. A collaboration with medical

researchers from Valley Hospital in Ridgewood, NJ, will assist in completing this goal.

Hybridization efficiency optimization is another future goal to minimize product loss and reduce

time during the hybridization step. This involves the testing of different hybridization techniques

and the utilization of the one that allows for the formation of the most miRNA-probe duplexes.

Increases in efficiency may be achieved by modification of temperature, pH, substrate

concentration and time. One final idea is to multiplex this technology using multiple

fluorophores for detection.

5. REFERENCES

Aarts, Esther, Thomas H. A. Ederveen, Jilly Naaijen, Marcel P. Zwiers, Jos Boekhorst, Harro M. Timmerman, Sanne P. Smeekens, Mihai G. Netea, Jan K. Buitelaar, Barbara Franke, Sacha A. F. T. van Hijum, and Alejandro Arias Vasquez. 2017. 'Gut microbiome in ADHD and its relation to neural reward anticipation', *PLoS One*, 12: e0183509.

Abad, C., C. Martinez, M. G. Juarranz, A. Arranz, J. Leceta, M. Delgado, and R. P. Gomariz. 2003. 'Therapeutic effects of vasoactive intestinal peptide in the trinitrobenzene sulfonic acid mice model of Crohn's disease', *Gastroenterology*, 124: 961-71.

Abubucker, Sahar, Nicola Segata, Johannes Goll, Alyxandria M. Schubert, Jacques Izard, Brandi L. Cantarel, Beltran Rodriguez-Mueller, Jeremy Zucker, Mathangi Thiagarajan, Bernard Henrissat, Owen White, Scott T. Kelley, Barbara Methé, Patrick D. Schloss, Dirk Gevers, Makedonka Mitreva, and Curtis Huttenhower. 2012. 'Metabolic Reconstruction for Metagenomic Data and Its Application to the Human Microbiome', *PLOS Computational Biology*, 8: e1002358.

Aguilera, M., P. Vergara, and V. Martinez. 2013. 'Stress and antibiotics alter luminal and wall-adhered microbiota and enhance the local expression of visceral sensory-related systems in mice', *Neurogastroenterol Motil*, 25: e515-29.

Angel, Thomas E., Mark R. Chance, and Krzysztof Palczewski. 2009. 'Conserved waters mediate structural and functional activation of family A (rhodopsin-like) G protein-coupled receptors', *Proceedings of the National Academy of Sciences*, 106: 8555-60.

Arata, Hideyuki, Kazuo Hosokawa, and Mizuo Maeda. 2014. 'Rapid Sub-attomole MicroRNA Detection on a Portable Microfluidic Chip', *Analytical Sciences*, 30: 129-35.

Asano, Y., T. Hiramoto, R. Nishino, Y. Aiba, T. Kimura, K. Yoshihara, Y. Koga, and N. Sudo. 2012. 'Critical role of gut microbiota in the production of biologically active, free catecholamines in the gut lumen of mice', *Am J Physiol Gastrointest Liver Physiol*, 303: G1288-95.

Bäckhed, Fredrik, Hao Ding, Ting Wang, Lora V. Hooper, Gou Young Koh, Andras Nagy, Clay F. Semenkovich, and Jeffrey I. Gordon. 2004. 'The gut microbiota as an environmental factor that regulates fat storage', *Proc Natl Acad Sci U S A*, 101: 15718-23.

Bai, Z., H. Zhang, N. Li, Z. Bai, L. Zhang, Z. Xue, H. Jiang, Y. Song, and D. Zhou. 2016. 'Impact of Environmental Microbes on the Composition of the Gut Microbiota of Adult BALB/c Mice', *PLoS One*, 11: e0160568.

Baldwin, Joyce M., Gebhard F. X. Schertler, and Vinzenz M. Unger. 1997. 'An alpha-carbon template for the transmembrane helices in the rhodopsin family of G-protein-coupled receptors11Edited by R. Huber', *Journal of Molecular Biology*, 272: 144-64.

Ballesta, Jose, Stephen R Bloom, Julia M Polak, and John G Batsakis. 1985. 'Distribution and localization of regulatory peptides', *CRC Critical Reviews in Clinical Laboratory Sciences*, 22: 185-218.

Barboza, J. L., M. S. Okun, and B. Moshiree. 2015. 'The treatment of gastroparesis, constipation and small intestinal bacterial overgrowth syndrome in patients with Parkinson's disease', *Expert Opin Pharmacother*, 16: 2449-64.

Bargmann, Cornelia I. 1997. 'Olfactory receptors, vomeronasal receptors, and the organization of olfactory information', *Cell*, 90: 585-87.

Barka, E. A., P. Vatsa, L. Sanchez, N. Gaveau-Vaillant, C. Jacquard, J. P. Meier-Kolthoff, H. P. Klenk, C. Clement, Y. Ouhdouch, and G. P. van Wezel. 2016. 'Taxonomy, Physiology, and Natural Products of Actinobacteria', *Microbiol Mol Biol Rev*, 80: 1-43.

Barouei, J., Z. Bendiks, A. Martinic, D. Mishchuk, D. Heeney, Y. H. Hsieh, D. Kieffer, J. Zaragoza, R. Martin, C. Slupsky, and M. L. Marco. 2017. 'Microbiota, metabolome, and immune alterations in obese mice fed a high-fat diet containing type 2 resistant starch', *Mol Nutr Food Res*, 61.

Becker, C., M. F. Neurath, and S. Wirtz. 2015. 'The Intestinal Microbiota in Inflammatory Bowel Disease', *Ilar j*, 56: 192-204.

Bell, D. S. 2015. 'Changes seen in gut bacteria content and distribution with obesity: causation or association?', *Postgrad Med*, 127: 863-8.

Bell, G. I. 1986. 'The glucagon superfamily: precursor structure and gene organization', *Peptides*, 7 Suppl 1: 27-36.

Benach, J. L., E. Li, and M. M. McGovern. 2012. 'A microbial association with autism', *MBio*, 3.

Berry, D., C. Schwab, G. Milinovich, J. Reichert, K. Ben Mahfoudh, T. Decker, M. Engel, B. Hai, E. Hainzl, S. Heider, L. Kenner, M. Muller, I. Rauch, B. Strobl, M. Wagner, C. Schleper, T. Urich, and A. Loy. 2012. 'Phylotype-level 16S rRNA analysis reveals new bacterial indicators of health state in acute murine colitis', *Isme j*, 6: 2091-106.

Bettelli, E., Y. Carrier, W. Gao, T. Korn, T. B. Strom, M. Oukka, H. L. Weiner, and V. K. Kuchroo. 2006. 'Reciprocal developmental pathways for the generation of pathogenic effector TH17 and regulatory T cells', *Nature*, 441: 235-8.

Bevan, J. A., G. M. Buga, M. A. Moskowitz, and S. I. Said. 1986. 'In vitro evidence that vasoactive intestinal peptide is a transmitter of neuro-vasodilation in the head of the cat', *Neuroscience*, 19: 597-604.

Bhargava, P., and E. M. Mowry. 2014. 'Gut microbiome and multiple sclerosis', *Curr Neurol Neurosci Rep*, 14: 492.

Biancani, P., M. C. Beinfeld, D. H. Coy, C. Hillemeier, J. H. Walsh, and J. Behar. 1988. 'Dysfunction of the gastrointestinal tract. Vasoactive intestinal peptide in peristalsis and sphincter function', *Ann N Y Acad Sci*, 527: 546-67.

Bianconi, E., A. Piovesan, F. Facchin, A. Beraudi, R. Casadei, F. Frabetti, L. Vitale, M. C. Pelleri, S. Tassani, F. Piva, S. Perez-Amodio, P. Strippoli, and S. Canaider. 2013. 'An estimation of the number of cells in the human body', *Ann Hum Biol*, 40: 463-71.

Billington, C. K., and R. B. Penn. 2003. 'Signaling and regulation of G protein-coupled receptors in airway smooth muscle', *Respir Res*, 4: 2.

Bishop, A. E., J. M. Polak, Y. Yiangou, N. D. Christofides, and S. R. Bloom. 1984. 'The distributions of PHI and VIP in porcine gut and their co-localisation to a proportion of intrinsic ganglion cells', *Peptides*, 5: 255-9.

Bjarnadottir, T. K., D. E. Gloriam, S. H. Hellstrand, H. Kristiansson, R. Fredriksson, and H. B. Schioth. 2006. 'Comprehensive repertoire and phylogenetic analysis of the G protein-coupled receptors in human and mouse', *Genomics*, 88: 263-73.

Bjarnadóttir, Thóra K., Robert Fredriksson, Pär J. Höglund, David E. Gloriam, Malin C. Lagerström, and Helgi B. Schiöth. 2004. 'The human and mouse repertoire of the adhesion family of G-protein-coupled receptors', *Genomics*, 84: 23-33.

Blaser, M. J., and S. Falkow. 2009. 'What are the consequences of the disappearing human microbiota?', *Nat Rev Microbiol*, 7: 887-94.

Blobel, G., P. Walter, C. N. Chang, B. M. Goldman, A. H. Erickson, and V. R. Lingappa. 1979. 'Translocation of proteins across membranes: the signal hypothesis and beyond', *Symp Soc Exp Biol*, 33: 9-36.

Bockaert, J., and J. P. Pin. 1999. 'Molecular tinkering of G protein-coupled receptors: an evolutionary success', *Embo j*, 18: 1723-9.

Bohnsack, M. T., K. Czaplinski, and D. Gorlich. 2004. 'Exportin 5 is a RanGTP-dependent dsRNA-binding protein that mediates nuclear export of pre-miRNAs', *Rna*, 10: 185-91.

Borchert, G. M., W. Lanier, and B. L. Davidson. 2006. 'RNA polymerase III transcribes human microRNAs', *Nat Struct Mol Biol*, 13: 1097-101.

Borland, Gillian, Brian O. Smith, and Stephen J. Yarwood. 2009. 'EPAC proteins transduce diverse cellular actions of cAMP', *British Journal of Pharmacology*, 158: 70-86.

Boyerinas, B., S. M. Park, A. Hau, A. E. Murmann, and M. E. Peter. 2010. 'The role of let-7 in cell differentiation and cancer', *Endocr Relat Cancer*, 17: F19-36.

Brandl, K., G. Plitas, B. Schnabl, R. P. DeMatteo, and E. G. Pamer. 2007. 'MyD88-mediated signals induce the bactericidal lectin RegIII gamma and protect mice against intestinal Listeria monocytogenes infection', *J Exp Med*, 204: 1891-900.

Brandt, D. R., and E. M. Ross. 1985. 'GTPase activity of the stimulatory GTP-binding regulatory protein of adenylate cyclase, Gs. Accumulation and turnover of enzyme-nucleotide intermediates', *J Biol Chem*, 260: 266-72.

Buday, László, and Julian Downward. 1993. 'Epidermal growth factor regulates p21ras through the formation of a complex of receptor, Grb2 adapter protein, and Sos nucleotide exchange factor', *Cell*, 73: 611-20.

Burokas, A., R. D. Moloney, T. G. Dinan, and J. F. Cryan. 2015. 'Microbiota regulation of the Mammalian gut-brain axis', *Adv Appl Microbiol*, 91: 1-62.

Butun, A., M. Naziroglu, S. Demirci, O. Celik, and A. C. Uguz. 2015. 'Riboflavin and vitamin E increase brain calcium and antioxidants, and microsomal calcium-ATP-ase values in rat headache models induced by glyceryl trinitrate', *J Membr Biol*, 248: 205-13.

Calin, G. A., C. D. Dumitru, M. Shimizu, R. Bichi, S. Zupo, E. Noch, H. Aldler, S. Rattan, M. Keating, K. Rai, L. Rassenti, T. Kipps, M. Negrini, F. Bullrich, and C. M. Croce. 2002. 'Frequent deletions and down-regulation of micro- RNA genes miR15 and miR16 at 13q14 in chronic lymphocytic leukemia', *Proc Natl Acad Sci U S A*, 99: 15524-9.

Candeias, S. M., and U. S. Gaipl. 2016. 'The Immune System in Cancer Prevention, Development and Therapy', *Anticancer Agents Med Chem*, 16: 101-7.

Carvalho, A. T., C. C. Elia, H. S. de Souza, P. R. Elias, E. L. Pontes, H. P. Lukashok, F. C. de Freitas, and J. R. Lapa e Silva. 2003. 'Immunohistochemical study of intestinal eosinophils in inflammatory bowel disease', *J Clin Gastroenterol*, 36: 120-5.

Cassel, Dan, and Zvi Selinger. 1978. 'Mechanism of adenylate cyclase activation through the beta-adrenergic receptor: catecholamine-induced displacement of bound GDP by GTP', *Proceedings of the National Academy of Sciences*, 75: 4155-59.

Chao, Anne. 1984. 'Nonparametric Estimation of the Number of Classes in a Population', *Scandinavian Journal of Statistics*, 11: 265-70.

Chartrel, N., Y. Wang, A. Fournier, H. Vaudry, and J. M. Conlon. 1995. 'Frog vasoactive intestinal polypeptide and galanin: primary structures and effects on pituitary adenylate cyclase', *Endocrinology*, 136: 3079-86.

Chen, C., D. A. Ridzon, A. J. Broomer, Z. Zhou, D. H. Lee, J. T. Nguyen, M. Barbisin, N. L. Xu, V. R. Mahuvakar, M. R. Andersen, K. Q. Lao, K. J. Livak, and K. J. Guegler. 2005.

'Real-time quantification of microRNAs by stem-loop RT-PCR', *Nucleic Acids Res*, 33: e179.

Chen, J, M DeVivo, J Dingus, A Harry, J Li, J Sui, DJ Carty, JL Blank, JH Exton, RH Stoffel, and al. et. 1995. 'A region of adenylyl cyclase 2 critical for regulation by G protein beta gamma subunits', *Science*, 268: 1166-69.

Chen, Jonathan, Jennifer Martinez, Teresa A Milner, Jochen Buck, and Lonny R Levin. 2013. 'Neuronal expression of soluble adenylyl cyclase in the mammalian brain', *Brain Research*, 1518: 1-8.

Chen, W., B. Paulus, D. Shu, Wilson, and V. Chadwick. 2001. 'Increased serum levels of eotaxin in patients with inflammatory bowel disease', *Scand J Gastroenterol*, 36: 515-20.

Chen, Yanqiu, Martin J. Cann, Tatiana N. Litvin, Vadim Iourgenko, Meeghan L. Sinclair, Lonny R. Levin, and Jochen Buck. 2000. 'Soluble Adenylyl Cyclase as an Evolutionarily Conserved Bicarbonate Sensor', *Science*, 289: 625-28.

Chevalier, Claire, Ozren Stojanović, Didier J Colin, Nicolas Suarez-Zamorano, Valentina Tarallo, Christelle Veyrat-Durebex, Dorothée Rigo, Salvatore Fabbiano, Ana Stevanović, Stefanie Hagemann, Xavier Montet, Yann Seimbille, Nicola Zamboni, Siegfried Hapfelmeier, and Mirko Trajkovski. 2015. 'Gut Microbiota Orchestrates Energy Homeostasis during Cold', *Cell*, 163: 1360-74.

Choi, M. Y., E. J. Fuerst, A. Rafaeli, and R. Jurenka. 2003. 'Identification of a G protein-coupled receptor for pheromone biosynthesis activating neuropeptide from pheromone glands of the moth Helicoverpa zea', *Proc Natl Acad Sci U S A*, 100: 9721-6.

Chu, D. M., J. Ma, A. L. Prince, K. M. Antony, M. D. Seferovic, and K. M. Aagaard. 2017. 'Maturation of the infant microbiome community structure and function across multiple body sites and in relation to mode of delivery', *Nat Med*, 23: 314-26.

Clamp, Michele, Ben Fry, Mike Kamal, Xiaohui Xie, James Cuff, Michael F. Lin, Manolis Kellis, Kerstin Lindblad-Toh, and Eric S. Lander. 2007. 'Distinguishing protein-coding and noncoding genes in the human genome', *Proceedings of the National Academy of Sciences*, 104: 19428-33.

Clarke, G., S. Grenham, P. Scully, P. Fitzgerald, R. D. Moloney, F. Shanahan, T. G. Dinan, and J. F. Cryan. 2012. 'The microbiome-gut-brain axis during early life regulates the hippocampal serotonergic system in a sex-dependent manner', *Molecular Psychiatry*, 18: 666.

Clarke, G., R. M. Stilling, P. J. Kennedy, C. Stanton, J. F. Cryan, and T. G. Dinan. 2014. 'Minireview: Gut microbiota: the neglected endocrine organ', *Mol Endocrinol*, 28: 1221-38.

Clemente, Jose C., Erica C. Pehrsson, Martin J. Blaser, Kuldip Sandhu, Zhan Gao, Bin Wang, Magda Magris, Glida Hidalgo, Monica Contreras, Óscar Noya-Alarcón, Orlana Lander, Jeremy McDonald, Mike Cox, Jens Walter, Phaik Lyn Oh, Jean F. Ruiz, Selena Rodriguez, Nan Shen, Se Jin Song, Jessica Metcalf, Rob Knight, Gautam Dantas, and M. Gloria Dominguez-Bello. 2015. 'The microbiome of uncontacted Amerindians', *Science Advances*, 1.

Coleman, David E, Albert M Berghuis, Ethan Lee, Maurine E Linder, and Alfred G Gilman. 1994. 'Structures of active conformations of Gi alpha 1 and the mechanism of GTP hydrolysis', *Science*, 265: 1405-12.

Collins, S. M., M. Surette, and P. Bercik. 2012. 'The interplay between the intestinal microbiota and the brain', *Nat Rev Microbiol*, 10: 735-42.

Colwell, C. S., S. Michel, J. Itri, W. Rodriguez, J. Tam, V. Lelievre, Z. Hu, X. Liu, and J. A. Waschek. 2003. 'Disrupted circadian rhythms in VIP- and PHI-deficient mice', *Am J Physiol Regul Integr Comp Physiol*, 285: R939-49.

Conlin, V. S., X. Wu, C. Nguyen, C. Dai, B. A. Vallance, A. M. J. Buchan, L. Boyer, and K. Jacobson. 2009. 'Vasoactive intestinal peptide ameliorates intestinal barrier disruption associated with Citrobacter rodentium-induced colitis', *American Journal of Physiology-Gastrointestinal and Liver Physiology*, 297: G735-G50.

Cook, J. V., and K. A. Eidne. 1997. 'An intramolecular disulfide bond between conserved extracellular cysteines in the gonadotropin-releasing hormone receptor is essential for binding and activation', *Endocrinology*, 138: 2800-6.

Cooper, Max D., and Brantley R. Herrin. 2010. 'How did our complex immune system evolve?', *Nature Reviews Immunology*, 10: 2.

Costa, M. C., A. L. Leitao, and F. J. Enguita. 2014. 'MicroRNA profiling in plasma or serum using quantitative RT-PCR', *Methods Mol Biol*, 1182: 121-9.

Costello, E. K., C. L. Lauber, M. Hamady, N. Fierer, J. I. Gordon, and R. Knight. 2009. 'Bacterial Community Variation in Human Body Habitats Across Space and Time', *Science (New York, NY)*, 326.

Cramer, P. 2004. 'Structure and function of RNA polymerase II', *Adv Protein Chem*, 67: 1-42.

Critchfield, J. W., S. van Hemert, M. Ash, L. Mulder, and P. Ashwood. 2011. 'The potential role of probiotics in the management of childhood autism spectrum disorders', *Gastroenterol Res Pract*, 2011: 161358.

Curtis, M. M., Z. Hu, C. Klimko, S. Narayanan, R. Deberardinis, and V. Sperandio. 2014. 'The gut commensal Bacteroides thetaiotaomicron exacerbates enteric infection through modification of the metabolic landscape', *Cell Host Microbe*, 16: 759-69.

Cutz, E., W. Chan, N. S. Track, A. Goth, and S. I. Said. 1978. 'Release of vasoactive intestinal polypeptide in mast cells by histamine liberators', *Nature*, 275: 661-2.

Dahiya, Neetu, Cheryl A. Sherman-Baust, Tian-Li Wang, Ben Davidson, Ie-Ming Shih, Yongqing Zhang, William Wood, III, Kevin G. Becker, and Patrice J. Morin. 2008. 'MicroRNA Expression and Identification of Putative miRNA Targets in Ovarian Cancer', *PLoS One*, 3: e2436.

Dahlhamer, J. M., E. P. Zammitti, B. W. Ward, A. G. Wheaton, and J. B. Croft. 2016. 'Prevalence of Inflammatory Bowel Disease Among Adults Aged >/=18 Years - United States, 2015', *MMWR Morb Mortal Wkly Rep*, 65: 1166-69.

Darzi, J., G. S. Frost, and M. D. Robertson. 2011. 'Do SCFA have a role in appetite regulation?', *Proc Nutr Soc*, 70: 119-28.

Dasgupta, S., D. Erturk-Hasdemir, J. Ochoa-Reparaz, H. C. Reinecker, and D. L. Kasper. 2014. 'Plasmacytoid dendritic cells mediate anti-inflammatory responses to a gut commensal molecule via both innate and adaptive mechanisms', *Cell Host Microbe*, 15: 413-23.

Davenport, Emily R., Orna Mizrahi-Man, Katelyn Michelini, Luis B. Barreiro, Carole Ober, and Yoav Gilad. 2014. 'Seasonal Variation in Human Gut Microbiome Composition', *PLoS One*, 9: e90731.

Davenport, Emily R., Jon G. Sanders, Se Jin Song, Katherine R. Amato, Andrew G. Clark, and Rob Knight. 2017. 'The human microbiome in evolution', *BMC Biology*, 15: 127.

David, L. A., C. F. Maurice, R. N. Carmody, D. B. Gootenberg, J. E. Button, B. E. Wolfe, A. V. Ling, A. S. Devlin, Y. Varma, M. A. Fischbach, S. B. Biddinger, R. J. Dutton, and P. J.

Turnbaugh. 2014. 'Diet rapidly and reproducibly alters the human gut microbiome', *Nature*, 505: 559-63.

De Witte, C., C. Schulz, A. Smet, P. Malfertheiner, and F. Haesebrouck. 2016. 'Other Helicobacters and gastric microbiota', *Helicobacter*, 21 Suppl 1: 62-8.

Dejda, A., I. Matczak, and J. Z. Nowak. 2004. '[Peptide histidine-isoleucine and and its human analogue peptide histidine-methionine: localization, receptors and biological function]', *Postepy Hig Med Dosw (Online)*, 58: 18-26.

Delgado, M. 2003. 'VIP: a very important peptide in T helper differentiation', *Trends Immunol*, 24: 221-4.

Delgado, M., and D. Ganea. 2003. 'Vasoactive intestinal peptide prevents activated microglia-induced neurodegeneration under inflammatory conditions: potential therapeutic role in brain trauma', *Faseb j*, 17: 1922-4.

Delgado, M., E. J. Munoz-Elias, R. P. Gomariz, and D. Ganea. 1999. 'Vasoactive intestinal peptide and pituitary adenylate cyclase-activating polypeptide prevent inducible nitric oxide synthase transcription in macrophages by inhibiting NF-kappa B and IFN regulatory factor 1 activation', *J Immunol*, 162: 4685-96.

Delgado, M., W. Sun, J. Leceta, and D. Ganea. 1999. 'VIP and PACAP differentially regulate the costimulatory activity of resting and activated macrophages through the modulation of B7.1 and B7.2 expression', *J Immunol*, 163: 4213-23.

Delgado, R. M., 3rd, M. A. Nawar, A. M. Zewail, B. Kar, W. K. Vaughn, K. K. Wu, N. Aleksic, N. Sivasubramanian, K. McKay, D. L. Mann, and J. T. Willerson. 2004. 'Cyclooxygenase-2 inhibitor treatment improves left ventricular function and mortality in a murine model of doxorubicin-induced heart failure', *Circulation*, 109: 1428-33.

Denli, A. M., B. B. Tops, R. H. Plasterk, R. F. Ketting, and G. J. Hannon. 2004. 'Processing of primary microRNAs by the Microprocessor complex', *Nature*, 432: 231-5.

DeSantis, T. Z., P. Hugenholtz, N. Larsen, M. Rojas, E. L. Brodie, K. Keller, T. Huber, D. Dalevi, P. Hu, and G. L. Andersen. 2006. 'Greengenes, a chimera-checked 16S rRNA gene database and workbench compatible with ARB', *Appl Environ Microbiol*, 72: 5069-72.

Dessauer, C. W., and A. G. Gilman. 1997. 'The catalytic mechanism of mammalian adenylyl cyclase. Equilibrium binding and kinetic analysis of P-site inhibition', *J Biol Chem*, 272: 27787-95.

Dessauer, C. W., J. J. Tesmer, S. R. Sprang, and A. G. Gilman. 1998. 'Identification of a Gialpha binding site on type V adenylyl cyclase', *J Biol Chem*, 273: 25831-9.

Dey, R. D., W. A. Shannon, Jr., and S. I. Said. 1981. 'Localization of VIP-immunoreactive nerves in airways and pulmonary vessels of dogs, cat, and human subjects', *Cell Tissue Res*, 220: 231-8.

Diel, S., K. Klass, B. Wittig, and C. Kleuss. 2006. 'Gbetagamma activation site in adenylyl cyclase type II. Adenylyl cyclase type III is inhibited by Gbetagamma', *J Biol Chem*, 281: 288-94.

Dietert, R. R., J. M. Dietert, and J. C. Dewitt. 2011. 'Environmental risk factors for autism', *Emerg Health Threats J*, 4: 7111.

Dockray, Graham J. 2014. 'Gastrointestinal hormones and the dialogue between gut and brain', *The Journal of Physiology*, 592: 2927-41.

Dorsam, G. P., K. Benton, J. Failing, and S. Batra. 2011. 'Vasoactive intestinal peptide signaling axis in human leukemia', *World J Biol Chem*, 2: 146-60.

Dorsam, S. T., E. Vomhof-Dekrey, R. J. Hermann, J. S. Haring, T. Van der Steen, E. Wilkerson, G. Boskovic, J. Denvir, Y. Dementieva, D. Primerano, and G. P. Dorsam. 2010. 'Identification of the early VIP-regulated transcriptome and its associated, interactome in resting and activated murine CD4 T cells', *Mol Immunol*, 47: 1181-94.

Dotevall, G., and N. G Kock. 1968. *Absorption Studies in Regional Enterocolitis (Mb. Crohn)*.

Drews, J. 2000. 'Drug discovery: a historical perspective', *Science*, 287: 1960-4.

Du, B. H., J. Eng, J. D. Hulmes, M. Chang, Y. C. Pan, and R. S. Yalow. 1985. 'Guinea pig has a unique mammalian VIP', *Biochem Biophys Res Commun*, 128: 1093-8.

Dyer, K. D., J. M. Moser, M. Czapiga, S. J. Siegel, C. M. Percopo, and H. F. Rosenberg. 2008. 'Functionally competent eosinophils differentiated ex vivo in high purity from normal mouse bone marrow', *J Immunol*, 181: 4004-9.

Dyer, K. D., C. M. Percopo, and H. F. Rosenberg. 2009. 'Generation of eosinophils from unselected bone marrow progenitors: wild-type, TLR- and eosinophil-deficient mice', *Open Immunol J*, 2: 163-67.

Ebert, M. S., and P. A. Sharp. 2012. 'Roles for microRNAs in conferring robustness to biological processes', *Cell*, 149: 515-24.

El-Merahbi, R., M. Loffler, A. Mayer, and G. Sumara. 2015. 'The roles of peripheral serotonin in metabolic homeostasis', *FEBS Lett*, 589: 1728-34.

El-Shazly, A. E., D. Y. Begon, G. Kustermans, M. Arafa, E. Dortu, M. Henket, P. P. Lefebvre, R. Louis, and P. Delvenne. 2013. 'Novel association between vasoactive intestinal peptide and CRTH2 receptor in recruiting eosinophils: a possible biochemical mechanism for allergic eosinophilic inflammation of the airways', *J Biol Chem*, 288: 1374-84.

Elson, C. O., Y. Cong, C. T. Weaver, T. R. Schoeb, T. K. McClanahan, R. B. Fick, and R. A. Kastelein. 2007. 'Monoclonal anti-interleukin 23 reverses active colitis in a T cell-mediated model in mice', *Gastroenterology*, 132: 2359-70.

Ericsson, A. C., J. W. Davis, W. Spollen, N. Bivens, S. Givan, C. E. Hagan, M. McIntosh, and C. L. Franklin. 2015. 'Effects of vendor and genetic background on the composition of the fecal microbiota of inbred mice', *PLoS One*, 10: e0116704.

Evans, Christian C., Kathy J. LePard, Jeff W. Kwak, Mary C. Stancukas, Samantha Laskowski, Joseph Dougherty, Laura Moulton, Adam Glawe, Yunwei Wang, Vanessa Leone, Dionysios A. Antonopoulos, Dan Smith, Eugene B. Chang, and Mae J. Ciancio. 2014. 'Exercise Prevents Weight Gain and Alters the Gut Microbiota in a Mouse Model of High Fat Diet-Induced Obesity', *PLoS One*, 9: e92193.

Fabricius, D., B. Karacay, D. Shutt, W. Leverich, B. Schafer, E. Takle, D. Thedens, G. Khanna, S. Raikwar, B. Yang, M. E. Desmond, and M. S. O'Dorisio. 2011. 'Characterization of intestinal and pancreatic dysfunction in VPAC1-null mutant mouse', *Pancreas*, 40: 861-71.

Fahrenkrug, Jan. 1985. 'Evidence for common precursors but differential processing of VIP and PHM in VIP-producing tumors', *Peptides*, 6: 357-61.

Faith, Daniel P. 1992. 'Conservation evaluation and phylogenetic diversity', *Biological Conservation*, 61: 1-10.

Farrens, David L, Christian Altenbach, Ke Yang, Wayne L Hubbell, and H Gobind Khorana. 1996. 'Requirement of rigid-body motion of transmembrane helices for light activation of rhodopsin', *Science*, 274: 768-70.

Fei, N., and L. Zhao. 2013. 'An opportunistic pathogen isolated from the gut of an obese human causes obesity in germfree mice', *Isme j*, 7: 880-4.

Feldmann, M., F. M. Brennan, and R. N. Maini. 1996. 'Role of cytokines in rheumatoid arthritis', *Annu Rev Immunol*, 14: 397-440.

Fernandez-Martin, Amelia, Elena Gonzalez-Rey, Alejo Chorny, Javier Martin, David Pozo, Doina Ganea, and Mario Delgado. 2006. 'VIP Prevents Experimental Multiple Sclerosis by Downregulating Both Inflammatory and Autoimmune Components of the Disease', *Annals of the New York Academy of Sciences*, 1070: 276-81.

Ferstl, Ruth, Remo Frei, Elisa Schiavi, Patrycja Konieczna, Weronika Barcik, Mario Ziegler, Roger P. Lauener, Christophe Chassard, Christophe Lacroix, Cezmi A. Akdis, and Liam O'Mahony. 2014. 'Histamine receptor 2 is a key influence in immune responses to intestinal histamine-secreting microbes', *Journal of Allergy and Clinical Immunology*, 134: 744-46.e3.

Filardo, E. J. 2002. 'Epidermal growth factor receptor (EGFR) transactivation by estrogen via the G-protein-coupled receptor, GPR30: a novel signaling pathway with potential significance for breast cancer', *J Steroid Biochem Mol Biol*, 80: 231-8.

Finegold, S. M., D. Molitoris, Y. Song, C. Liu, M. L. Vaisanen, E. Bolte, M. McTeague, R. Sandler, H. Wexler, E. M. Marlowe, M. D. Collins, P. A. Lawson, P. Summanen, M. Baysallar, T. J. Tomzynski, E. Read, E. Johnson, R. Rolfe, P. Nasir, H. Shah, D. A. Haake, P. Manning, and A. Kaul. 2002. 'Gastrointestinal microflora studies in late-onset autism', *Clin Infect Dis*, 35: S6-s16.

Fire, Andrew Z., and Craig C. Mello. 2006. 'The Nobel Prize in Physiology or Medicine 2006', *Nobel Media AB 2014*, 2006.

Fishbein, V. A., D. H. Coy, S. J. Hocart, N. Y. Jiang, J. E. Mrozinski, Jr., S. A. Mantey, and R. T. Jensen. 1994. 'A chimeric VIP-PACAP analogue but not VIP pseudopeptides function as VIP receptor antagonists', *Peptides*, 15: 95-100.

Fransen, Floris, Elena Zagato, Elisa Mazzini, Bruno Fosso, Caterina Manzari, Sahar El Aidy, Andrea Chiavelli, Anna Maria D'Erchia, Maya K Sethi, Oliver Pabst, Marinella Marzano, Silvia Moretti, Luigina Romani, Giuseppe Penna, Graziano Pesole, and Maria Rescigno. 'BALB/c and C57BL/6 Mice Differ in Polyreactive IgA Abundance, which Impacts the Generation of Antigen-Specific IgA and Microbiota Diversity', *Immunity*, 43: 527-40.

Frase, L. L., F. A. Gaffney, L. D. Lane, J. C. Buckey, S. I. Said, C. G. Blomqvist, and G. J. Krejs. 1987. 'Cardiovascular effects of vasoactive intestinal peptide in healthy subjects', *Am J Cardiol*, 60: 1356-61.

Fredriksson, Robert, Malin C. Lagerström, Lars-Gustav Lundin, and Helgi B. Schiöth. 2003. 'The G-Protein-Coupled Receptors in the Human Genome Form Five Main Families. Phylogenetic Analysis, Paralogon Groups, and Fingerprints', *Molecular Pharmacology*, 63: 1256-72.

Frei, R., R. Ferstl, P. Konieczna, M. Ziegler, T. Simon, T. M. Rugeles, S. Mailand, T. Watanabe, R. Lauener, C. A. Akdis, and L. O'Mahony. 2013. 'Histamine receptor 2 modifies dendritic cell responses to microbial ligands', *J Allergy Clin Immunol*, 132: 194-204.

Fujimoto, W., M. Inaoki, T. Fukui, Y. Inoue, and T. Kuhara. 2005. 'Biotin deficiency in an infant fed with amino acid formula', *J Dermatol*, 32: 256-61.

Gallo, Alessia, Mayank Tandon, Ilias Alevizos, and Gabor G. Illei. 2012. 'The Majority of MicroRNAs Detectable in Serum and Saliva Is Concentrated in Exosomes', *PLoS One*, 7: e30679.

Ganea, D., R. Rodriguez, and M. Delgado. 2003. 'Vasoactive intestinal peptide and pituitary adenylate cyclase-activating polypeptide: players in innate and adaptive immunity', *Cell Mol Biol (Noisy-le-grand)*, 49: 127-42.

Garcia-Zepeda, E. A., M. E. Rothenberg, R. T. Ownbey, J. Celestin, P. Leder, and A. D. Luster. 1996. 'Human eotaxin is a specific chemoattractant for eosinophil cells and provides a new mechanism to explain tissue eosinophilia', *Nat Med*, 2: 449-56.

Gether, U., and B. K. Kobilka. 1998. 'G protein-coupled receptors. II. Mechanism of agonist activation', *J Biol Chem*, 273: 17979-82.

Ghouri, Y. A., D. M. Richards, E. F. Rahimi, J. T. Krill, K. A. Jelinek, and A. W. DuPont. 2014. 'Systematic review of randomized controlled trials of probiotics, prebiotics, and synbiotics in inflammatory bowel disease', *Clin Exp Gastroenterol*, 7: 473-87.

Gilman, A. G. 1984. 'G proteins and dual control of adenylate cyclase', *Cell*, 36: 577-9.

———. 1990. 'Regulation of adenylyl cyclase by G proteins', *Adv Second Messenger Phosphoprotein Res*, 24: 51-7.

———. 1995. 'Nobel Lecture. G proteins and regulation of adenylyl cyclase', *Biosci Rep*, 15: 65-97.

Gilman, Alfred G. 1970. 'A Protein Binding Assay for Adenosine 3′:5′-Cyclic Monophosphate', *Proc Natl Acad Sci U S A*, 67: 305-12.

Girardet, Clémence, Bruno Lebrun, Marie-Jeanne Cabirol-Pol, Catherine Tardivel, Anne-Marie François-Bellan, Denis Becquet, and Olivier Bosler. 2013. 'Brain-derived neurotrophic factor/TrkB signaling regulates daily astroglial plasticity in the suprachiasmatic nucleus: Electron-microscopic evidence in mouse', *Glia*, 61: 1172-77.

Gleich, G. J., and C. R. Adolphson. 1986. 'The eosinophilic leukocyte: structure and function', *Adv Immunol*, 39: 177-253.

Goetzl, E. J., J. K. Voice, S. Shen, G. Dorsam, Y. Kong, K. M. West, C. F. Morrison, and A. J. Harmar. 2001. 'Enhanced delayed-type hypersensitivity and diminished immediate-type hypersensitivity in mice lacking the inducible VPAC(2) receptor for vasoactive intestinal peptide', *Proc Natl Acad Sci U S A*, 98: 13854-9.

Gokbuget, D., J. A. Pereira, S. Bachofner, A. Marchais, C. Ciaudo, M. Stoffel, J. H. Schulte, and U. Suter. 2015. 'The Lin28/let-7 axis is critical for myelination in the peripheral nervous system', *Nat Commun*, 6: 8584.

Gomariz, R. P., A. Arranz, C. Abad, M. Torroba, C. Martinez, F. Rosignoli, M. Garcia-Gomez, J. Leceta, and Y. Juarranz. 2005. 'Time-course expression of Toll-like receptors 2 and 4 in inflammatory bowel disease and homeostatic effect of VIP', *J Leukoc Biol*, 78: 491-502.

Gomariz, Rosa, Monica Fuente, Angel Hernanz, and Javier Leceta. 1992. 'Occurrence of Vasoactive Intestinal Peptide (VIP) in Lymphoid Organs from Rat and Mousea', *Annals of the New York Academy of Sciences*, 650: 13-18.

Gomariz, Rosa P., Maria J. Lorenzo, Lucinda Cacicedo, Angeles Vicente, and Agustin G. Zapata. 1990. 'Demonstration of immunoreactive vasoactive intestinal peptide (IR-VIP) and somatostatin (IR-SOM) in rat thymus', *Brain, Behavior, and Immunity*, 4: 151-61.

Goodfellow, S. J., and R. J. White. 2007. 'Regulation of RNA polymerase III transcription during mammalian cell growth', *Cell Cycle*, 6: 2323-6.

Goursaud, S., N. Pineau, L. Becq-Giraudon, P. Gressens, J. M. Muller, and T. Janet. 2005. 'Human H9 cells proliferation is differently controlled by vasoactive intestinal peptide or

peptide histidine methionine: implication of a GTP-insensitive form of VPAC1 receptor', *J Neuroimmunol*, 158: 94-105.

Gozes, I. 2001. 'Neuroprotective peptide drug delivery and development: potential new therapeutics', *Trends Neurosci*, 24: 700-5.

Graul, Richard C, and Wolfgang Sadée. 2001. 'Evolutionary relationships among G protein-coupled receptors using a clustered database approach', *AAps pharmsci*, 3: 25.

Grice, E. A., and J. A. Segre. 2011. 'The skin microbiome', *Nat Rev Microbiol*, 9: 244-53.

Groneberg, D. A., J. Springer, and A. Fischer. 2001. 'Vasoactive intestinal polypeptide as mediator of asthma', *Pulm Pharmacol Ther*, 14: 391-401.

Gueimonde, M., S. Sakata, M. Kalliomaki, E. Isolauri, Y. Benno, and S. Salminen. 2006. 'Effect of maternal consumption of lactobacillus GG on transfer and establishment of fecal bifidobacterial microbiota in neonates', *J Pediatr Gastroenterol Nutr*, 42: 166-70.

Guerrero, J. M., J. C. Prieto, F. L. Elorza, R. Ramirez, and R. Goberna. 1981. 'Interaction of vasoactive intestinal peptide with human blood mononuclear cells', *Molecular and Cellular Endocrinology*, 21: 151-60.

Ha, Minju, and V. Narry Kim. 2014. 'Regulation of microRNA biogenesis', *Nature reviews Molecular cell biology*, 15: 509.

Hamann, J., E. Hartmann, and R. A. van Lier. 1996. 'Structure of the human CD97 gene: exon shuffling has generated a new type of seven-span transmembrane molecule related to the secretin receptor superfamily', *Genomics*, 32: 144-7.

Hanoune, Jacques, and Nicole Defer. 2001. 'Regulation and role of adenylyl cyclase isoforms', *Annual review of pharmacology and toxicology*, 41: 145-74.

Harayama, Hiroshi. 2013. 'Roles of intracellular cyclic AMP signal transduction in the capacitation and subsequent hyperactivation of mouse and boar spermatozoa', *Journal of Reproduction and Development*, 59: 421-30.

Harmar, A. J., H. M. Marston, S. B. Shen, C. Spratt, K. M. West, W. J. Sheward, C. F. Morrison, J. R. Dorin, H. D. Piggins, J. C. Reubi, J. S. Kelly, E. S. Maywood, and M. H. Hastings. 2002. 'The VPAC(2) receptor is essential for circadian function in the mouse suprachiasmatic nuclei', *Cell*, 109: 497-508.

Harmar, A. J., W. J. Sheward, C. F. Morrison, B. Waser, M. Gugger, and J. C. Reubi. 2004. 'Distribution of the VPAC2 receptor in peripheral tissues of the mouse', *Endocrinology*, 145: 1203-10.

Harmar, Anthony J., Jan Fahrenkrug, Illana Gozes, Marc Laburthe, Victor May, Joseph R. Pisegna, David Vaudry, Hubert Vaudry, James A. Waschek, and Sami I. Said. 2012. 'Pharmacology and functions of receptors for vasoactive intestinal peptide and pituitary adenylate cyclase-activating polypeptide: IUPHAR Review 1', *British Journal of Pharmacology*, 166: 4-17.

Hart, Marcia L., Alexandra Meyer, Philip J. Johnson, and Aaron C. Ericsson. 2015. 'Comparative Evaluation of DNA Extraction Methods from Feces of Multiple Host Species for Downstream Next-Generation Sequencing', *PLoS One*, 10: e0143334.

Hauk, V., L. Fraccaroli, E. Grasso, A. Eimon, R. Ramhorst, O. Hubscher, and C. Perez Leiros. 2014. 'Monocytes from Sjogren's syndrome patients display increased vasoactive intestinal peptide receptor 2 expression and impaired apoptotic cell phagocytosis', *Clin Exp Immunol*, 177: 662-70.

Hayes, Josie, Pier Paolo Peruzzi, and Sean Lawler. 2014. 'MicroRNAs in cancer: biomarkers, functions and therapy', *Trends Mol Med*, 20: 460-69.

191

He, Lin, and Gregory J. Hannon. 2004. 'MicroRNAs: small RNAs with a big role in gene regulation', *Nature Reviews Genetics*, 5: 522.

Henning, R. J., and D. R. Sawmiller. 2001. 'Vasoactive intestinal peptide: cardiovascular effects', *Cardiovasc Res*, 49: 27-37.

Hillenbrand, M., C. Schori, J. Schoppe, and A. Pluckthun. 2015. 'Comprehensive analysis of heterotrimeric G-protein complex diversity and their interactions with GPCRs in solution', *Proc Natl Acad Sci U S A*, 112: E1181-90.

Hoare, Sam R. J. 2005. 'Mechanisms of peptide and nonpeptide ligand binding to Class B G-protein-coupled receptors', *Drug Discovery Today*, 10: 417-27.

Hoffman, L. M., S. E. Brooks, M. R. Stein, and L. Schneck. 1994. 'Cyclic AMP causes differentiation and decreases the expression of neutral glycosphingolipids in cell cultures derived from a malignant glioma', *Biochim Biophys Acta*, 1222: 37-44.

Hollister, E. B., K. Riehle, R. A. Luna, E. M. Weidler, M. Rubio-Gonzales, T. A. Mistretta, S. Raza, H. V. Doddapaneni, G. A. Metcalf, D. M. Muzny, R. A. Gibbs, J. F. Petrosino, R. J. Shulman, and J. Versalovic. 2015. 'Structure and function of the healthy pre-adolescent pediatric gut microbiome', *Microbiome*, 3: 36.

Holscher, H. D., K. L. Faust, L. A. Czerkies, R. Litov, E. E. Ziegler, H. Lessin, T. Hatch, S. Sun, and K. A. Tappenden. 2012. 'Effects of prebiotic-containing infant formula on gastrointestinal tolerance and fecal microbiota in a randomized controlled trial', *JPEN J Parenter Enteral Nutr*, 36: 95s-105s.

Hosoya, M., C. Kimura, K. Ogi, S. Ohkubo, Y. Miyamoto, H. Kugoh, M. Shimizu, H. Onda, M. Oshimura, A. Arimura, and et al. 1992. 'Structure of the human pituitary adenylate cyclase activating polypeptide (PACAP) gene', *Biochim Biophys Acta*, 1129: 199-206.

Hot, A., and P. Miossec. 2011. 'Effects of interleukin (IL)-17A and IL-17F in human rheumatoid arthritis synoviocytes', *Ann Rheum Dis*, 70: 727-32.

Hu, W. P., J. D. Li, C. S. Colwell, and Q. Y. Zhou. 2011. 'Decreased REM sleep and altered circadian sleep regulation in mice lacking vasoactive intestinal polypeptide', *Sleep*, 34: 49-56.

Hutvagner, G., J. McLachlan, A. E. Pasquinelli, E. Balint, T. Tuschl, and P. D. Zamore. 2001. 'A cellular function for the RNA-interference enzyme Dicer in the maturation of the let-7 small temporal RNA', *Science*, 293: 834-8.

Inglese, J., L. M. Luttrell, J. A. Iniguez-Lluhi, K. Touhara, W. J. Koch, and R. J. Lefkowitz. 1994. 'Functionally active targeting domain of the beta-adrenergic receptor kinase: an inhibitor of G beta gamma-mediated stimulation of type II adenylyl cyclase', *Proc Natl Acad Sci U S A*, 91: 3637-41.

International Human Genome Sequencing, Consortium. 2001. 'Initial sequencing and analysis of the human genome', *Nature*, 409: 860.

Ishihara, Takeshi, Ryuichi Shigemoto, Kensaku Mori, Kenji Takahashi, and Shigekazu Nagata. 1992. 'Functional expression and tissue distribution of a novel receptor for vasoactive intestinal polypeptide', *Neuron*, 8: 811-19.

Iwase, T., Y. Uehara, H. Shinji, A. Tajima, H. Seo, K. Takada, T. Agata, and Y. Mizunoe. 2010. 'Staphylococcus epidermidis Esp inhibits Staphylococcus aureus biofilm formation and nasal colonization', *Nature*, 465: 346-9.

Jakobsson, H. E., T. R. Abrahamsson, M. C. Jenmalm, K. Harris, C. Quince, C. Jernberg, B. Bjorksten, L. Engstrand, and A. F. Andersson. 2014. 'Decreased gut microbiota diversity,

delayed Bacteroidetes colonisation and reduced Th1 responses in infants delivered by caesarean section', *Gut*, 63: 559-66.

Jenkins, T. A., J. C. Nguyen, K. E. Polglaze, and P. P. Bertrand. 2016. 'Influence of Tryptophan and Serotonin on Mood and Cognition with a Possible Role of the Gut-Brain Axis', *Nutrients*, 8.

Ji, I., C. Lee, Y. Song, P. M. Conn, and T. H. Ji. 2002. 'Cis- and trans-activation of hormone receptors: the LH receptor', *Mol Endocrinol*, 16: 1299-308.

Jiang, X., H. Jing, and D. Ganea. 2002. 'VIP and PACAP down-regulate CXCL10 (IP-10) and up-regulate CCL22 (MDC) in spleen cells', *J Neuroimmunol*, 133: 81-94.

Jimeno, R., R. P. Gomariz, I. Gutierrez-Canas, C. Martinez, Y. Juarranz, and J. Leceta. 2010. 'New insights into the role of VIP on the ratio of T-cell subsets during the development of autoimmune diabetes', *Immunol Cell Biol*, 88: 734-45.

Jimeno, R., J. Leceta, M. Garin, A. M. Ortiz, M. Mellado, J. M. Rodriguez-Frade, C. Martinez, S. Perez-Garcia, R. P. Gomariz, and Y. Juarranz. 2015. 'Th17 polarization of memory Th cells in early arthritis: the vasoactive intestinal peptide effect', *J Leukoc Biol*, 98: 257-69.

Johnson, Jethro S., Monica N. Opiyo, Marian Thomson, Karim Gharbi, Jonathan R. Seckl, Andreas Heger, and Karen E. Chapman. 2016. '11β-hydroxysteroid dehydrogenase-1 deficiency alters the gut microbiome response to Western diet', *J Endocrinol*, 232: 273-83.

Jonsson, M., O. Norrgard, and S. Forsgren. 2012. 'Epithelial expression of vasoactive intestinal peptide in ulcerative colitis: down-regulation in markedly inflamed colon', *Dig Dis Sci*, 57: 303-10.

Joost, P., and A. Methner. 2002. 'Phylogenetic analysis of 277 human G-protein-coupled receptors as a tool for the prediction of orphan receptor ligands', *Genome Biol*, 3: Research0063.

Jordan, F., M. Lauria, M. Scotti, T. P. Nguyen, P. Praveen, M. Morine, and C. Priami. 2015. 'Diversity of key players in the microbial ecosystems of the human body', *Sci Rep*, 5: 15920.

Kakarala, Kavita Kumari, and Kaiser Jamil. 2014. 'Sequence-structure based phylogeny of GPCR Class A Rhodopsin receptors', *Molecular Phylogenetics and Evolution*, 74: 66-96.

Kanehisa, M., M. Furumichi, M. Tanabe, Y. Sato, and K. Morishima. 2017. 'KEGG: new perspectives on genomes, pathways, diseases and drugs', *Nucleic Acids Res*, 45: D353-d61.

Kanehisa, M., and S. Goto. 2000. 'KEGG: kyoto encyclopedia of genes and genomes', *Nucleic Acids Res*, 28: 27-30.

Kanehisa, M., S. Goto, Y. Sato, M. Furumichi, and M. Tanabe. 2012. 'KEGG for integration and interpretation of large-scale molecular data sets', *Nucleic Acids Res*, 40: D109-14.

Kanehisa, M., Y. Sato, M. Kawashima, M. Furumichi, and M. Tanabe. 2016. 'KEGG as a reference resource for gene and protein annotation', *Nucleic Acids Res*, 44: D457-62.

Kasselman, L. J., N. A. Vernice, J. DeLeon, and A. B. Reiss. 2018. 'The gut microbiome and elevated cardiovascular risk in obesity and autoimmunity', *Atherosclerosis*, 271: 203-13.

Kasubuchi, M., S. Hasegawa, T. Hiramatsu, A. Ichimura, and I. Kimura. 2015. 'Dietary gut microbial metabolites, short-chain fatty acids, and host metabolic regulation', *Nutrients*, 7: 2839-49.

Kawasaki, Shinji, Tsuyoshi Mimura, Takumi Satoh, Kouji Takeda, and Youichi Niimura. 2006. 'Response of the Microaerophilic Bifidobacterium Species, B. boum and B. thermophilum, to Oxygen', *Appl Environ Microbiol*, 72: 6854-58.

Kinashi, T., and K. Katagiri. 2005. 'Regulation of immune cell adhesion and migration by regulator of adhesion and cell polarization enriched in lymphoid tissues', *Immunology*, 116: 164-71.

Kiss, Tamás. 2001. 'Small nucleolar RNA-guided post-transcriptional modification of cellular RNAs', *Embo j*, 20: 3617-22.

Kitts, P. A., D. M. Church, F. Thibaud-Nissen, J. Choi, V. Hem, V. Sapojnikov, R. G. Smith, T. Tatusova, C. Xiang, A. Zherikov, M. DiCuccio, T. D. Murphy, K. D. Pruitt, and A. Kimchi. 2016. 'Assembly: a resource for assembled genomes at NCBI', *Nucleic Acids Res*, 44: D73-80.

Kleuss, Christiane, André S Raw, Ethan Lee, Stephen R Sprang, and Alfred G Gilman. 1994. 'Mechanism of GTP hydrolysis by G-protein alpha subunits', *Proceedings of the National Academy of Sciences*, 91: 9828-31.

Kobilka, B. K. 1995. 'Amino and carboxyl terminal modifications to facilitate the production and purification of a G protein-coupled receptor', *Anal Biochem*, 231: 269-71.

Kong, H. H. 2011. 'Skin microbiome: genomics-based insights into the diversity and role of skin microbes', *Trends Mol Med*, 17: 320-8.

Kong, H. H., J. Oh, C. Deming, S. Conlan, E. A. Grice, M. A. Beatson, E. Nomicos, E. C. Polley, H. D. Komarow, P. R. Murray, M. L. Turner, and J. A. Segre. 2012. 'Temporal shifts in the skin microbiome associated with disease flares and treatment in children with atopic dermatitis', *Genome Res*, 22: 850-9.

Korkmaz, O. T., N. Tuncel, M. Tuncel, E. M. Oncu, V. Sahinturk, and M. Celik. 2010. 'Vasoactive intestinal peptide (VIP) treatment of Parkinsonian rats increases thalamic gamma-aminobutyric acid (GABA) levels and alters the release of nerve growth factor (NGF) by mast cells', *J Mol Neurosci*, 41: 278-87.

Korn, Thomas, Estelle Bettelli, Mohamed Oukka, and Vijay K. Kuchroo. 2009. 'IL-17 and Th17 Cells', *Annu Rev Immunol*, 27: 485-517.

Koval, Alexey, Vladimir Purvanov, Diane Egger-Adam, and Vladimir L. Katanaev. 2011. 'Yellow submarine of the Wnt/Frizzled signaling: Submerging from the G protein harbor to the targets', *Biochemical Pharmacology*, 82: 1311-19.

Kristensen, Bo, Birgitte Georg, and Jan Fahrenkrug. 1997. 'Cholinergic regulation of VIP gene expression in human neuroblastoma cells', *Brain Research*, 775: 99-106.

Kubinak, J. L., C. Petersen, W. Z. Stephens, R. Soto, E. Bake, R. M. O'Connell, and J. L. Round. 2015. 'MyD88 signaling in T cells directs IgA-mediated control of the microbiota to promote health', *Cell Host Microbe*, 17: 153-63.

Kuczynski, J., J. Stombaugh, W. A. Walters, A. Gonzalez, J. G. Caporaso, and R. Knight. 2012. 'Using QIIME to analyze 16S rRNA gene sequences from microbial communities', *Curr Protoc Microbiol*, Chapter 1: Unit 1E.5.

Kuhl, A. A., C. Loddenkemper, J. Westermann, and J. C. Hoffmann. 2002. 'Role of gamma delta T cells in inflammatory bowel disease', *Pathobiology*, 70: 150-5.

Kumar, Sudhir, and S. Blair Hedges. 1998. 'A molecular timescale for vertebrate evolution', *Nature*, 392: 917-20.

Kuncova, J., J. Chvojka, R. Sykora, J. Sviglerova, M. Stengl, L. Nalos, A. Krouzecky, and M. Matejovic. 2011. 'Tissue concentrations of vasoactive intestinal peptide are affected by peritonitis-induced sepsis and hemofiltration in pigs', *Physiol Res*, 60: 531-40.

Laburthe, Marc, Alain Couvineau, and Var Tan. 2007. 'Class II G protein-coupled receptors for VIP and PACAP: Structure, models of activation and pharmacology', *Peptides*, 28: 1631-39.

Lampinen, M., M. Carlson, L. D. Hakansson, and P. Venge. 2004. 'Cytokine-regulated accumulation of eosinophils in inflammatory disease', *Allergy*, 59: 793-805.

Lampinen, M., M. Carlson, P. Sangfelt, Y. Taha, M. Thorn, L. Loof, Y. Raab, and P. Venge. 2001. 'IL-5 and TNF-alpha participate in recruitment of eosinophils to intestinal mucosa in ulcerative colitis', *Dig Dis Sci*, 46: 2004-9.

Lampinen, M., A. Ronnblom, K. Amin, G. Kristjansson, F. Rorsman, P. Sangfelt, B. Safsten, M. Wagner, A. Wanders, O. Winqvist, and M. Carlson. 2005. 'Eosinophil granulocytes are activated during the remission phase of ulcerative colitis', *Gut*, 54: 1714-20.

Lange, T., S. Dimitrov, and J. Born. 2010. 'Effects of sleep and circadian rhythm on the human immune system', *Ann N Y Acad Sci*, 1193: 48-59.

Langille, Morgan G. I., Jesse Zaneveld, J. Gregory Caporaso, Daniel McDonald, Dan Knights, Joshua A. Reyes, Jose C. Clemente, Deron E. Burkepile, Rebecca L. Vega Thurber, Rob Knight, Robert G. Beiko, and Curtis Huttenhower. 2013. 'Predictive functional profiling of microbial communities using 16S rRNA marker gene sequences', *Nature Biotechnology*, 31: 814.

Larkey, Nicholas E., C. Kyle Almlie, Victoria Tran, Marianne Egan, and Sean M. Burrows. 2014. 'Detection of miRNA Using a Double-Strand Displacement Biosensor with a Self-Complementary Fluorescent Reporter', *Analytical Chemistry*, 86: 1853-63.

Larmonier, C. B., K. W. Shehab, F. K. Ghishan, and P. R. Kiela. 2015. 'T Lymphocyte Dynamics in Inflammatory Bowel Diseases: Role of the Microbiome', *Biomed Res Int*, 2015: 504638.

Lau, N. C., L. P. Lim, E. G. Weinstein, and D. P. Bartel. 2001. 'An abundant class of tiny RNAs with probable regulatory roles in Caenorhabditis elegans', *Science*, 294: 858-62.

Layden, B. T., A. R. Angueira, M. Brodsky, V. Durai, and W. L. Lowe, Jr. 2013. 'Short chain fatty acids and their receptors: new metabolic targets', *Transl Res*, 161: 131-40.

LeBlanc, J. G., C. Milani, G. S. de Giori, F. Sesma, D. van Sinderen, and M. Ventura. 2013. 'Bacteria as vitamin suppliers to their host: a gut microbiota perspective', *Curr Opin Biotechnol*, 24: 160-8.

Leceta, J., R. P. Gomariz, C. Martinez, C. Abad, D. Ganea, and M. Delgado. 2000. 'Receptors and transcriptional factors involved in the anti-inflammatory activity of VIP and PACAP', *Ann N Y Acad Sci*, 921: 92-102.

Lee, L. T., J. K. Tam, D. W. Chan, and B. K. Chow. 2009. 'Molecular cloning and mRNA distribution of pituitary adenylate cyclase-activating polypeptide (PACAP)/PACAP-related peptide in the lungfish', *Ann N Y Acad Sci*, 1163: 209-14.

Lee, R. C., R. L. Feinbaum, and V. Ambros. 1993. 'The C. elegans heterochronic gene lin-4 encodes small RNAs with antisense complementarity to lin-14', *Cell*, 75: 843-54.

Lee, Y., M. Kim, J. Han, K. H. Yeom, S. Lee, S. H. Baek, and V. N. Kim. 2004. 'MicroRNA genes are transcribed by RNA polymerase II', *Embo j*, 23: 4051-60.

Lemay, V., A. Hossain, Y. N. Osheim, A. L. Beyer, and F. Dragon. 2011. 'Identification of novel proteins associated with yeast snR30 small nucleolar RNA', *Nucleic Acids Res*, 39: 9659-70.

Ley, R. E., F. Backhed, P. Turnbaugh, C. A. Lozupone, R. D. Knight, and J. I. Gordon. 2005. 'Obesity alters gut microbial ecology', *Proc Natl Acad Sci USA*, 102.

Ley, Ruth E., Peter J. Turnbaugh, Samuel Klein, and Jeffrey I. Gordon. 2006. 'Microbial ecology: Human gut microbes associated with obesity', *Nature*, 444: 1022-23.

Li, L., and Y. Liu. 2011. 'Diverse small non-coding RNAs in RNA interference pathways', *Methods Mol Biol*, 764: 169-82.

Liang, X., F. D. Bushman, and G. A. FitzGerald. 2015. 'Rhythmicity of the intestinal microbiota is regulated by gender and the host circadian clock', *Proc Natl Acad Sci U S A*, 112: 10479-84.

Linder, Maurine E, Pamela Middleton, John R Hepler, Ronald Taussig, Alfred G Gilman, and Susanne M Mumby. 1993. 'Lipid modifications of G proteins: alpha subunits are palmitoylated', *Proceedings of the National Academy of Sciences*, 90: 3675-79.

Linder, Maurine E, Iok-Hou Pang, Robert J Duronio, Jeffrey I Gordon, Paul C Sternweis, and Alfred G Gilman. 1991. 'Lipid modifications of G protein subunits. Myristoylation of Go alpha increases its affinity for beta gamma', *Journal of Biological Chemistry*, 266: 4654-59.

Liu, Hui-Xin, Clarissa Santos Rocha, Satya Dandekar, and Yu-Jui Yvonne Wan. 2016. 'Functional analysis of the relationship between intestinal microbiota and the expression of hepatic genes and pathways during the course of liver regeneration', *Journal of hepatology*, 64: 641-50.

Liu, Weipeng, Xiaoming Zhou, and Da Xing. 2014. 'Rapid and reliable microRNA detection by stacking hybridization on electrochemiluminescent chip system', *Biosensors and Bioelectronics*, 58: 388-94.

Liu, Y. J., Y. F. Guo, L. S. Zhang, Y. F. Pei, N. Yu, P. Yu, C. J. Papasian, and H. W. Deng. 2010. 'Biological pathway-based genome-wide association analysis identified the vasoactive intestinal peptide (VIP) pathway important for obesity', *Obesity (Silver Spring)*, 18: 2339-46.

Liu, Yu, Arnold E. Ruoho, Vibha D. Rao, and James H. Hurley. 1997. 'Catalytic mechanism of the adenylyl and guanylyl cyclases: Modeling and mutational analysis', *Proceedings of the National Academy of Sciences*, 94: 13414-19.

Logothetis, D. E., Y. Kurachi, J. Galper, E. J. Neer, and D. E. Clapham. 1987. 'The beta gamma subunits of GTP-binding proteins activate the muscarinic K+ channel in heart', *Nature*, 325: 321-6.

Lomer, M. C., K. Kodjabashia, C. Hutchinson, S. M. Greenfield, R. P. Thompson, and J. J. Powell. 2004. 'Intake of dietary iron is low in patients with Crohn's disease: a case-control study', *Br J Nutr*, 91: 141-8.

Lorenzo-Díaz, Fabián, Virtu Solano-Collado, Rudi Lurz, Alicia Bravo, and Manuel Espinosa. 2012. 'Autoregulation of the Synthesis of the MobM Relaxase Encoded by the Promiscuous Plasmid pMV158', *Journal of Bacteriology*, 194: 1789-99.

Love, J. A., V. L. Go, and J. H. Szurszewski. 1988. 'Vasoactive intestinal peptide and other peptides as neuromodulators of colonic motility in the guinea pig', *Ann N Y Acad Sci*, 527: 360-8.

Lu, T. X., E. J. Lim, J. A. Besse, S. Itskovich, A. J. Plassard, P. C. Fulkerson, B. J. Aronow, and M. E. Rothenberg. 2013. 'MiR-223 deficiency increases eosinophil progenitor proliferation', *J Immunol*, 190: 1576-82.

Lucassen, E. A., H. C. van Diepen, T. Houben, S. Michel, C. S. Colwell, and J. H. Meijer. 2012. 'Role of vasoactive intestinal peptide in seasonal encoding by the suprachiasmatic nucleus clock', *Eur J Neurosci*, 35: 1466-74.

Luckey, T. D. 1972. 'Introduction to intestinal microecology', *The American Journal of Clinical Nutrition*, 25: 1292-94.

Lundberg, J. M., J. Fahrenkrug, T. Hokfelt, C. R. Martling, O. Larsson, K. Tatemoto, and A. Anggard. 1984. 'Co-existence of peptide HI (PHI) and VIP in nerves regulating blood flow and bronchial smooth muscle tone in various mammals including man', *Peptides*, 5: 593-606.

Luo, R., S. J. Jeong, Z. Jin, N. Strokes, S. Li, and X. Piao. 2011. 'G protein-coupled receptor 56 and collagen III, a receptor-ligand pair, regulates cortical development and lamination', *Proc Natl Acad Sci U S A*, 108: 12925-30.

Luttrell, Louis M, Yehia Daaka, and Robert J Lefkowitz. 1999. 'Regulation of tyrosine kinase cascades by G-protein-coupled receptors', *Current opinion in cell biology*, 11: 177-83.

Madaan, Alka, Ritu Verma, Anu T Singh, Swatantra Kumar Jain, and Manu Jaggi. 2014. 'A stepwise procedure for isolation of murine bone marrow and generation of dendritic cells', *2014*.

Makris, A., A. Piperopoulos, and I. Karmaniolou. 2014. 'Multiple sclerosis: basic knowledge and new insights in perioperative management', *J Anesth*, 28: 267-78.

Markby, David W, Rene Onrust, and Henry R Bourne. 1993. 'Separate GTP binding and GTPase activating domains of a G alpha subunit', *Science*, 262: 1895-901.

Marshall, B. J., and J. R. Warren. 1984. 'Unidentified curved bacilli in the stomach of patients with gastritis and peptic ulceration', *Lancet*, 1: 1311-5.

Martinez, C., A. M. Ortiz, Y. Juarranz, A. Lamana, I. V. Seoane, J. Leceta, R. Garcia-Vicuna, R. P. Gomariz, and I. Gonzalez-Alvaro. 2014. 'Serum levels of vasoactive intestinal peptide as a prognostic marker in early arthritis', *PLoS One*, 9: e85248.

Matranga, C., Y. Tomari, C. Shin, D. P. Bartel, and P. D. Zamore. 2005. 'Passenger-strand cleavage facilitates assembly of siRNA into Ago2-containing RNAi enzyme complexes', *Cell*, 123: 607-20.

Maudsley, S., S. A. Patel, S. S. Park, L. M. Luttrell, and B. Martin. 2012. 'Functional signaling biases in G protein-coupled receptors: Game Theory and receptor dynamics', *Mini Rev Med Chem*, 12: 831-40.

Mazmanian, S. K., C. H. Liu, A. O. Tzianabos, and D. L. Kasper. 2005. 'An immunomodulatory molecule of symbiotic bacteria directs maturation of the host immune system', *Cell*, 122: 107-18.

Mazmanian, Sarkis K., June L. Round, and Dennis L. Kasper. 2008. 'A microbial symbiosis factor prevents intestinal inflammatory disease', *Nature*, 453: 620.

Michino, Mayako, Enrique Abola, Gpcr Dock participants, Charles L. Brooks Iii, J. Scott Dixon, John Moult, and Raymond C. Stevens. 2009. 'Community-wide assessment of GPCR structure modelling and ligand docking: GPCR Dock 2008', *Nature Reviews Drug Discovery*, 8: 455.

Miescher-Rüsch, Friedrich. 1871. *Ueber die chemische Zusammensetzung der Eiterzellen*.

Mikkelsen, J. D., and J. Fahrenkrug. 1994. 'Concentrations and distribution of vasoactive intestinal peptide (VIP), peptide histidine isoleucine (PHI) and peptide histidine valine (PHV) in the cerebral cortex and the suprachiasmatic nucleus of the mouse', *Brain Res*, 656: 95-107.

Millar, Robert P., Claire L. Newton, and Antonia K. Roseweir. 2012. 'Chapter 2 - Neuroendocrine GPCR Signaling A2 - Fink, George.' in Donald W. Pfaff and Jon E. Levine (eds.), *Handbook of Neuroendocrinology* (Academic Press: San Diego).

Miller, J. E., D. Granados-Fuentes, T. Wang, L. Marpegan, T. E. Holy, and E. D. Herzog. 2014. 'Vasoactive intestinal polypeptide mediates circadian rhythms in mammalian olfactory bulb and olfaction', *J Neurosci*, 34: 6040-6.

Mir, A., M. Minguez, J. Tatay, I. Pascual, A. Pena, V. Sanchiz, P. Almela, F. Mora, and A. Benages. 2002. 'Elevated serum eotaxin levels in patients with inflammatory bowel disease', *Am J Gastroenterol*, 97: 1452-7.

Mishra, A., S. P. Hogan, J. J. Lee, P. S. Foster, and M. E. Rothenberg. 1999. 'Fundamental signals that regulate eosinophil homing to the gastrointestinal tract', *J Clin Invest*, 103: 1719-27.

Mittelbach Gary, G., F. Steiner Christopher, M. Scheiner Samuel, L. Gross Katherine, L. Reynolds Heather, B. Waide Robert, R. Willig Michael, I. Dodson Stanley, and Laura Gough. 2001. 'WHAT IS THE OBSERVED RELATIONSHIP BETWEEN SPECIES RICHNESS AND PRODUCTIVITY?', *Ecology*, 82: 2381-96.

Miyake, S., S. Kim, W. Suda, K. Oshima, M. Nakamura, T. Matsuoka, N. Chihara, A. Tomita, W. Sato, S. W. Kim, H. Morita, M. Hattori, and T. Yamamura. 2015. 'Dysbiosis in the Gut Microbiota of Patients with Multiple Sclerosis, with a Striking Depletion of Species Belonging to Clostridia XIVa and IV Clusters', *PLoS One*, 10: e0137429.

Miyata, A., A. Arimura, R. R. Dahl, N. Minamino, A. Uehara, L. Jiang, M. D. Culler, and D. H. Coy. 1989. 'Isolation of a novel 38 residue-hypothalamic polypeptide which stimulates adenylate cyclase in pituitary cells', *Biochem Biophys Res Commun*, 164: 567-74.

Miyata, A., L. Jiang, R. D. Dahl, C. Kitada, K. Kubo, M. Fujino, N. Minamino, and A. Arimura. 1990. 'Isolation of a neuropeptide corresponding to the N-terminal 27 residues of the pituitary adenylate cyclase activating polypeptide with 38 residues (PACAP38)', *Biochem Biophys Res Commun*, 170: 643-8.

Mohney, R. P., and R. E. Zigmond. 1998. 'Vasoactive intestinal peptide enhances its own expression in sympathetic neurons after injury', *J Neurosci*, 18: 5285-93.

Moodley, Y., B. Linz, Y. Yamaoka, H. M. Windsor, S. Breurec, J. Y. Wu, A. Maady, S. Bernhoft, J. M. Thiberge, S. Phuanukoonnon, G. Jobb, P. Siba, D. Y. Graham, B. J. Marshall, and M. Achtman. 2009. 'The peopling of the Pacific from a bacterial perspective', *Science*, 323: 527-30.

Moody, T. W., G. Czerwinski, N. I. Tarasova, and C. J. Michejda. 2002. 'VIP-ellipticine derivatives inhibit the growth of breast cancer cells', *Life Sci*, 71: 1005-14.

Morampudi, V., V. S. Conlin, U. Dalwadi, X. Wu, K. C. Marshall, C. Nguyen, B. A. Vallance, and K. Jacobson. 2015. 'Vasoactive intestinal peptide prevents PKCepsilon-induced intestinal epithelial barrier disruption during EPEC infection', *Am J Physiol Gastrointest Liver Physiol*, 308: G389-402.

Morimoto, J., S. J. Simpson, and F. Ponton. 2017. 'Direct and trans-generational effects of male and female gut microbiota in Drosophila melanogaster', *Biol Lett*, 13.

Mosli, M. H., J. Rivera-Nieves, and B. G. Feagan. 2014. 'T-cell trafficking and anti-adhesion strategies in inflammatory bowel disease: current and future prospects', *Drugs*, 74: 297-311.

Murphy, E. A., K. T. Velazquez, and K. M. Herbert. 2015. 'Influence of high-fat diet on gut microbiota: a driving force for chronic disease risk', *Curr Opin Clin Nutr Metab Care*, 18: 515-20.

Murthy, KS, KM Zhang, JG Jin, JR Grider, and GM Makhlouf. 1993. 'VIP-mediated G protein-coupled Ca2+ influx activates a constitutive NOS in dispersed gastric muscle cells', *American Journal of Physiology-Gastrointestinal and Liver Physiology*, 265: G660-G71.

Mutt, Viktor, and Sami I. Said. 1974. 'Structure of the Porcine Vasoactive Intestinal Octacosapeptide', *European Journal of Biochemistry*, 42: 581-89.

Muzes, G., B. Molnar, and F. Sipos. 2012. 'Regulatory T cells in inflammatory bowel diseases and colorectal cancer', *World J Gastroenterol*, 18: 5688-94.

Naor, Zvi, Outhiriaradjou Benard, and Rony Seger. 2000. 'Activation of MAPK cascades by G-protein-coupled receptors: the case of gonadotropin-releasing hormone receptor', *Trends in Endocrinology & Metabolism*, 11: 91-99.

Naseribafrouei, A., K. Hestad, E. Avershina, M. Sekelja, A. Linlokken, R. Wilson, and K. Rudi. 2014. 'Correlation between the human fecal microbiota and depression', *Neurogastroenterol Motil*, 26: 1155-62.

Natochin, M., K. G. Gasimov, and N. O. Artemyev. 2001. 'Inhibition of GDP/GTP exchange on G alpha subunits by proteins containing G-protein regulatory motifs', *Biochemistry*, 40: 5322-8.

Neer, E. J. 1976. 'The size of adenylate cyclase and guanylate cyclase from the rat renal medulla', *J Supramol Struct*, 4: 51-61.

Neufeld, K. M., N. Kang, J. Bienenstock, and J. A. Foster. 2011. 'Reduced anxiety-like behavior and central neurochemical change in germ-free mice', *Neurogastroenterology & Motility*, 23: 255-e119.

Ng, Stephanie Y. L., Billy K. C. Chow, Jun Kasamatsu, Masanori Kasahara, and Leo T. O. Lee. 2012. 'Agnathan VIP, PACAP and Their Receptors: Ancestral Origins of Today's Highly Diversified Forms', *PLoS One*, 7: e44691.

Nilsson, A. 1975. 'Structure of the vasoactive intestinal octacosapeptide from chicken intestine. The amino acid sequence', *FEBS Lett*, 60: 322-6.

Noel, Joseph P, Heidi E Hamm, and Paul B Sigler. 1993. 'The 2.2 Å crystal structure of transducin-α complexed with GTPγS', *Nature*, 366: 654.

Noguchi, Koichi, Emiko Senba, Yasuhiro Morita, Makoto Sato, and Masaya Tohyama. 1989. 'Prepro-VIP and preprotachykinin mRNAs in the rat dorsal root ganglion cells following peripheral axotomy', *Molecular Brain Research*, 6: 327-30.

Nussdorfer, Gastone G., and Ludwik K. Malendowicz. 1998. 'Role of VIP, PACAP, and related peptides in the regulation of the hypothalamo—pituitary–adrenal axis', *Peptides*, 19: 1443-67.

O'Dorisio, M. S., N. S. Hermina, T. M. O'Dorisio, and S. P. Balcerzak. 1981. 'Vasoactive intestinal polypeptide modulation of lymphocyte adenylate cyclase', *J Immunol*, 127: 2551-4.

O'Hara, Andrea J., Ling Wang, Bruce J. Dezube, William J. Harrington, Blossom Damania, and Dirk P. Dittmer. 2009. 'Tumor suppressor microRNAs are underrepresented in primary effusion lymphoma and Kaposi sarcoma', *Blood*, 113: 5938-41.

Ochoa-Reparaz, J., D. W. Mielcarz, L. E. Ditrio, A. R. Burroughs, D. M. Foreau, S. Haque-Begum, and L. H. Kasper. 2009. 'Role of gut commensal microflora in the development of experimental autoimmune encephalomyelitis', *J Immunol*, 183: 6041-50.

Odamaki, Toshitaka, Kumiko Kato, Hirosuke Sugahara, Nanami Hashikura, Sachiko Takahashi, Jin-zhong Xiao, Fumiaki Abe, and Ro Osawa. 2016. 'Age-related changes in gut microbiota composition from newborn to centenarian: a cross-sectional study', *BMC Microbiology*, 16: 90.

Offen, D., Y. Sherki, E. Melamed, M. Fridkin, D. E. Brenneman, and I. Gozes. 2000. 'Vasoactive intestinal peptide (VIP) prevents neurotoxicity in neuronal cultures: relevance to neuroprotection in Parkinson's disease', *Brain Res*, 854: 257-62.

Okada, T., O. P. Ernst, K. Palczewski, and K. P. Hofmann. 2001. 'Activation of rhodopsin: new insights from structural and biochemical studies', *Trends Biochem Sci*, 26: 318-24.

Okazaki, Kimitake, Chiharu Kimura, Takuo Kosaka, Takuya Watanabe, Shoichi Ohkubo, Kazuhiro Ogi, Chieko Kitada, Haruo Onda, and Masahiko Fujino. 1992. 'Expression of human pituitary adenylate cyclase activating polypeptide (PACAP) cDNA in CHO cells and characterization of the products', *FEBS Lett*, 298: 49-56.

Oldham, William M, and Heidi E Hamm. 2008. 'Heterotrimeric G protein activation by G-protein-coupled receptors', *Nature reviews Molecular cell biology*, 9: 60.

Otero, L. L., V. E. Ruiz, and G. I. Perez Perez. 2014. 'Helicobacter pylori: the balance between a role as colonizer and pathogen', *Best Pract Res Clin Gastroenterol*, 28: 1017-29.

Ottman, Noora, Hauke Smidt, and Clara Belzer. 2012. 'The function of our microbiota: who is out there and what do they do?', *Frontiers in Cellular and Infection Microbiology*, 2.

Overington, J. P., B. Al-Lazikani, and A. L. Hopkins. 2006. 'How many drug targets are there?', *Nat Rev Drug Discov*, 5: 993-6.

Palczewski, Krzysztof, Takashi Kumasaka, Tetsuya Hori, Craig A. Behnke, Hiroyuki Motoshima, Brian A. Fox, Isolde Le Trong, David C. Teller, Tetsuji Okada, Ronald E. Stenkamp, Masaki Yamamoto, and Masashi Miyano. 2000. 'Crystal Structure of Rhodopsin: A G Protein-Coupled Receptor', *Science*, 289: 739-45.

Palle, Connie, Bent Ottesen, and Jan Fahrenkrug. 1992. 'Peptide histidine valine (PHV) is present and biologically active in the human female genital tract', *Regulatory Peptides*, 38: 101-09.

Palmer, C., E. M. Bik, D. B. Digiulio, D. A. Relman, and P. O. Brown. 2007. 'Development of the Human Infant Intestinal Microbiota', *PLoS Biol*, 5.

Pantaloni, C, P Brabet, B Bilanges, A Dumuis, S Houssami, D Spengler, J Bockaert, and L Journot. 1996. 'Alternative splicing in the N-terminal domain of the PACAP receptor modulates receptor selectivity and relative potencies of PACAP-27 and-38 in phospholipase C activation', *J. Biol. Chem*, 271: 22146-51.

Parker, D. S., J. P. Raufman, T. L. O'Donohue, M. Bledsoe, H. Yoshida, and J. J. Pisano. 1984. 'Amino acid sequences of helospectins, new members of the glucagon superfamily, found in Gila monster venom', *J Biol Chem*, 259: 11751-5.

Patterson, C. C., G. Dahlquist, G. Soltesz, and A. Green. 2001. 'Is childhood-onset type I diabetes a wealth-related disease? An ecological analysis of European incidence rates', *Diabetologia*, 44 Suppl 3: B9-16.

Pauls, S., N. C. Foley, D. K. Foley, J. LeSauter, M. H. Hastings, E. S. Maywood, and R. Silver. 2014. 'Differential contributions of intra-cellular and inter-cellular mechanisms to the spatial and temporal architecture of the suprachiasmatic nucleus circadian circuitry in

wild-type, cryptochrome-null and vasoactive intestinal peptide receptor 2-null mutant mice', *Eur J Neurosci*, 40: 2528-40.

Peng, Yang, Jin-Jun Guo, Yan-Min Liu, and Xiao-Ling Wu. 2014. 'MicroRNA-34A inhibits the growth, invasion and metastasis of gastric cancer by targeting PDGFR and MET expression', *Biosci Rep*, 34: e00112.

Petkov, V., W. Mosgoeller, R. Ziesche, M. Raderer, L. Stiebellehner, K. Vonbank, G. C. Funk, G. Hamilton, C. Novotny, B. Burian, and L. H. Block. 2003. 'Vasoactive intestinal peptide as a new drug for treatment of primary pulmonary hypertension', *J Clin Invest*, 111: 1339-46.

Petra, A. I., S. Panagiotidou, E. Hatziagelaki, J. M. Stewart, P. Conti, and T. C. Theoharides. 2015. 'Gut-Microbiota-Brain Axis and Its Effect on Neuropsychiatric Disorders With Suspected Immune Dysregulation', *Clin Ther*, 37: 984-95.

Petter-Lane, W. 1962. 'The Provision and Use of Pathogen-free Laboratory Animals', *Proceedings of the Royal Society of Medicine*, 55: 253-63.

Pin, J. P., J. Kniazeff, C. Goudet, A. S. Bessis, J. Liu, T. Galvez, F. Acher, P. Rondard, and L. Prézeau. 2004. 'The activation mechanism of class-C G-protein coupled receptors', *Biology of the Cell*, 96: 335-42.

Pitcher, Julie A, James Inglese, Joyce B Higgins, Jeffery L Arriza, Patrick J Casey, Chong Kim, Jeffery L Benovic, Madan M Kwatra, Marc G Caron, and Robert J Lefkowitz. 1992. 'Role of beta gamma subunits of G proteins in targeting the beta-adrenergic receptor kinase to membrane-bound receptors', *Science*, 257: 1264-67.

Pull, S. L., J. M. Doherty, J. C. Mills, J. I. Gordon, and T. S. Stappenbeck. 2005. 'Activated macrophages are an adaptive element of the colonic epithelial progenitor niche necessary for regenerative responses to injury', *Proc Natl Acad Sci U S A*, 102: 99-104.

Qin, J., R. Li, J. Raes, M. Arumugam, K. S. Burgdorf, C. Manichanh, T. Nielsen, N. Pons, F. Levenez, T. Yamada, D. R. Mende, J. Li, J. Xu, S. Li, D. Li, J. Cao, B. Wang, H. Liang, H. Zheng, Y. Xie, J. Tap, P. Lepage, M. Bertalan, J. M. Batto, T. Hansen, D. Le Paslier, A. Linneberg, H. B. Nielsen, E. Pelletier, P. Renault, T. Sicheritz-Ponten, K. Turner, H. Zhu, C. Yu, S. Li, M. Jian, Y. Zhou, Y. Li, X. Zhang, S. Li, N. Qin, H. Yang, J. Wang, S. Brunak, J. Dore, F. Guarner, K. Kristiansen, O. Pedersen, J. Parkhill, J. Weissenbach, P. Bork, S. D. Ehrlich, and J. Wang. 2010. 'A human gut microbial gene catalogue established by metagenomic sequencing', *Nature*, 464: 59-65.

Quast, Christian, Elmar Pruesse, Pelin Yilmaz, Jan Gerken, Timmy Schweer, Pablo Yarza, Jörg Peplies, and Frank Oliver Glöckner. 2013. 'The SILVA ribosomal RNA gene database project: improved data processing and web-based tools', *Nucleic Acids Res*, 41: D590-D96.

Quesada, M. A., H. S. Rye, J. C. Gingrich, A. N. Glazer, and R. A. Mathies. 1991. 'High-sensitivity DNA detection with a laser-excited confocal fluorescence gel scanner', *Biotechniques*, 10: 616-25.

Rabot, S., M. Membrez, F. Blancher, B. Berger, D. Moine, L. Krause, R. Bibiloni, A. Bruneau, P. Gerard, J. Siddharth, C. L. Lauber, and C. J. Chou. 2016. 'High fat diet drives obesity regardless the composition of gut microbiota in mice', *Sci Rep*, 6: 32484.

Rakhilin, S. V., P. A. Olson, A. Nishi, N. N. Starkova, A. A. Fienberg, A. C. Nairn, D. J. Surmeier, and P. Greengard. 2004. 'A network of control mediated by regulator of calcium/calmodulin-dependent signaling', *Science*, 306: 698-701.

Rampelli, S., S. L. Schnorr, C. Consolandi, S. Turroni, M. Severgnini, C. Peano, P. Brigidi, A. N. Crittenden, A. G. Henry, and M. Candela. 2015. 'Metagenome Sequencing of the Hadza Hunter-Gatherer Gut Microbiota', *Curr Biol*, 25: 1682-93.

Rand, T. A., S. Petersen, F. Du, and X. Wang. 2005. 'Argonaute2 cleaves the anti-guide strand of siRNA during RISC activation', *Cell*, 123: 621-9.

Rangon, C. M., E. Dicou, S. Goursaud, L. Mounien, S. Jegou, T. Janet, J. M. Muller, V. Lelievre, and P. Gressens. 2006. 'Mechanisms of VIP-induced neuroprotection against neonatal excitotoxicity', *Ann N Y Acad Sci*, 1070: 512-7.

Reeves, A. E., M. J. Koenigsknecht, I. L. Bergin, and V. B. Young. 2012. 'Suppression of Clostridium difficile in the gastrointestinal tracts of germfree mice inoculated with a murine isolate from the family Lachnospiraceae', *Infect Immun*, 80: 3786-94.

Reiter, E., S. Marion, F. Robert, C. Troispoux, F. Boulay, F. Guillou, and P. Crepieux. 2001. 'Kinase-inactive G-protein-coupled receptor kinases are able to attenuate follicle-stimulating hormone-induced signaling', *Biochem Biophys Res Commun*, 282: 71-8.

Ren, J., H. Ni, M. Kim, K. L. Cooley, R. M. Valenzuela, and C. V. Asche. 2017. 'Allergies, antibiotics use, and multiple sclerosis', *Curr Med Res Opin*, 33: 1451-56.

Reubi, J. C. 2000. 'In vitro evaluation of VIP/PACAP receptors in healthy and diseased human tissues. Clinical implications', *Ann N Y Acad Sci*, 921: 1-25.

Ridlon, J. M., D. J. Kang, P. B. Hylemon, and J. S. Bajaj. 2014. 'Bile acids and the gut microbiome', *Curr Opin Gastroenterol*, 30: 332-8.

Robberecht, Patrick, Marie-Claire Woussen-Colle, Philippe De Neef, Philippe Gourlet, Louis Buscail, André Vandermeers, Marie-Claire Vandermeers-Piret, and Jean Christophe. 1991. 'The two forms of the pituitary adenylate cyclase activating polypeptide (PACAP (1–27) and PACAP (1–38)) interact with distinct receptors on rat pancreatic AR 4-2J cell membranes', *FEBS Lett*, 286: 133-36.

Robertson, B. R., J. L. O'Rourke, B. A. Neilan, P. Vandamme, S. L. On, J. G. Fox, and A. Lee. 2005. 'Mucispirillum schaedleri gen. nov., sp. nov., a spiral-shaped bacterium colonizing the mucus layer of the gastrointestinal tract of laboratory rodents', *Int J Syst Evol Microbiol*, 55: 1199-204.

Robishaw, Janet D, Murray D Smigel, and Alfred G Gilman. 1986. 'Molecular basis for two forms of the G protein that stimulates adenylate cyclase', *Journal of Biological Chemistry*, 261: 9587-90.

Rodríguez-Dorantes, Mauricio, A. Ivan Salido-Guadarrama, and Pilar García-Tobilla. 2014. 'Prostate Cancer Detection Using a Noninvasive Method for Quantifying miRNAs.' in Martha Robles-Flores (ed.), *Cancer Cell Signaling: Methods and Protocols* (Springer New York: New York, NY).

Rothberg, J. M., W. Hinz, T. M. Rearick, J. Schultz, W. Mileski, M. Davey, J. H. Leamon, K. Johnson, M. J. Milgrew, M. Edwards, J. Hoon, J. F. Simons, D. Marran, J. W. Myers, J. F. Davidson, A. Branting, J. R. Nobile, B. P. Puc, D. Light, T. A. Clark, M. Huber, J. T. Branciforte, I. B. Stoner, S. E. Cawley, M. Lyons, Y. Fu, N. Homer, M. Sedova, X. Miao, B. Reed, J. Sabina, E. Feierstein, M. Schorn, M. Alanjary, E. Dimalanta, D. Dressman, R. Kasinskas, T. Sokolsky, J. A. Fidanza, E. Namsaraev, K. J. McKernan, A. Williams, G. T. Roth, and J. Bustillo. 2011. 'An integrated semiconductor device enabling non-optical genome sequencing', *Nature*, 475: 348-52.

Rothenberg, M. E., R. Ownbey, P. D. Mehlhop, P. M. Loiselle, M. van de Rijn, J. V. Bonventre, H. C. Oettgen, P. Leder, and A. D. Luster. 1996. 'Eotaxin triggers eosinophil-selective

chemotaxis and calcium flux via a distinct receptor and induces pulmonary eosinophilia in the presence of interleukin 5 in mice', *Mol Med*, 2: 334-48.

Rutayisire, E., K. Huang, Y. Liu, and F. Tao. 2016. 'The mode of delivery affects the diversity and colonization pattern of the gut microbiota during the first year of infants' life: a systematic review', *BMC Gastroenterol*, 16: 86.

Sadelain, M. W., H. Y. Qin, J. Lauzon, and B. Singh. 1990. 'Prevention of type I diabetes in NOD mice by adjuvant immunotherapy', *Diabetes*, 39: 583-9.

Said, S. I., and V. Mutt. 1970. 'Polypeptide with broad biological activity: isolation from small intestine', *Science*, 169: 1217-8.

Said, Sami I., and Viktor Mutt. 1972. 'Isolation from Porcine-Intestinal Wall of a Vasoactive Octacosapeptide Related to Secretin and to Glucagon', *European Journal of Biochemistry*, 28: 199-204.

Samarasinghe, A. E., S. A. Hoselton, and J. M. Schuh. 2010a. 'The absence of the VPAC(2) receptor does not protect mice from Aspergillus induced allergic asthma', *Peptides*, 31: 1068-75.

———. 2010b. 'Spatio-temporal localization of vasoactive intestinal peptide and neutral endopeptidase in allergic murine lungs', *Regul Pept*, 164: 151-7.

Sampson, T. R., and S. K. Mazmanian. 2015. 'Control of brain development, function, and behavior by the microbiome', *Cell Host Microbe*, 17: 565-76.

Sands, W. A., H. D. Woolson, G. R. Milne, C. Rutherford, and T. M. Palmer. 2006. 'Exchange protein activated by cyclic AMP (Epac)-mediated induction of suppressor of cytokine signaling 3 (SOCS-3) in vascular endothelial cells', *Mol Cell Biol*, 26: 6333-46.

Sanger, F., G. M. Air, B. G. Barrell, N. L. Brown, A. R. Coulson, C. A. Fiddes, C. A. Hutchison, P. M. Slocombe, and M. Smith. 1977. 'Nucleotide sequence of bacteriophage phi X174 DNA', *Nature*, 265: 687-95.

Sanger, F., and A. R. Coulson. 1978. 'The use of thin acrylamide gels for DNA sequencing', *FEBS Lett*, 87: 107-10.

Sanger, F., S. Nicklen, and A. R. Coulson. 1977. 'DNA sequencing with chain-terminating inhibitors', *Proc Natl Acad Sci U S A*, 74: 5463-7.

Savage, D. C. 1977. 'Microbial ecology of the gastrointestinal tract', *Annu Rev Microbiol*, 31.

Schei, K., E. Avershina, T. Oien, K. Rudi, T. Follestad, S. Salamati, and R. A. Odegard. 2017. 'Early gut mycobiota and mother-offspring transfer', *Microbiome*, 5: 107.

Scher, J. U., and S. B. Abramson. 2011. 'The microbiome and rheumatoid arthritis', *Nat Rev Rheumatol*, 7: 569-78.

Schmidt, M., C. Sand, K. H. Jakobs, M. C. Michel, and P. A. Weernink. 2007. 'Epac and the cardiovascular system', *Curr Opin Pharmacol*, 7: 193-200.

Schnorr, S. L., M. Candela, S. Rampelli, M. Centanni, C. Consolandi, G. Basaglia, S. Turroni, E. Biagi, C. Peano, M. Severgnini, J. Fiori, R. Gotti, G. De Bellis, D. Luiselli, P. Brigidi, A. Mabulla, F. Marlowe, A. G. Henry, and A. N. Crittenden. 2014. 'Gut microbiome of the Hadza hunter-gatherers', *Nat Commun*, 5: 3654.

Schratzberger, P., A. Geiseler, S. Dunzendorfer, N. Reinisch, C. M. Kahler, and C. J. Wiedermann. 1998. 'Similar involvement of VIP receptor type I and type II in lymphocyte chemotaxis', *J Neuroimmunol*, 87: 73-81.

Schroeder, A., D. H. Loh, M. C. Jordan, K. P. Roos, and C. S. Colwell. 2011. 'Circadian regulation of cardiovascular function: a role for vasoactive intestinal peptide', *Am J Physiol Heart Circ Physiol*, 300: H241-50.

Schulte, Gunnar, and Vítězslav Bryja. 2007. 'The Frizzled family of unconventional G-protein-coupled receptors', *Trends in Pharmacological Sciences*, 28: 518-25.

Schussler, P., M. Kluge, A. Yassouridis, M. Dresler, M. Uhr, and A. Steiger. 2012. 'Ghrelin levels increase after pictures showing food', *Obesity (Silver Spring)*, 20: 1212-7.

Schwarz, D. S., G. Hutvagner, T. Du, Z. Xu, N. Aronin, and P. D. Zamore. 2003. 'Asymmetry in the assembly of the RNAi enzyme complex', *Cell*, 115: 199-208.

Segata, N. 2015. 'Gut Microbiome: Westernization and the Disappearance of Intestinal Diversity', *Curr Biol*, 25: R611-3.

Segata, N., J. Izard, L. Waldron, D. Gevers, L. Miropolsky, W. S. Garrett, and C. Huttenhower. 2011. 'Metagenomic biomarker discovery and explanation', *Genome Biol*, 12: R60.

Segre, Gino V., and Steven R. Goldring. 1993. 'Receptors for secretin, calcitonin, parathyroid hormone (PTH)/PTH-related peptide, vasoactive intestinal peptide, glucagonlike peptide 1, growth hormone-releasing hormone, and glucagon belong to a newly discovered G-protein-linked receptor family', *Trends in Endocrinology & Metabolism*, 4: 309-14.

Seifert, Roland, Andrea Strasser, Erich H. Schneider, Detlef Neumann, Stefan Dove, and Armin Buschauer. 2013. 'Molecular and cellular analysis of human histamine receptor subtypes', *Trends in Pharmacological Sciences*, 34: 10.1016/j.tips.2012.11.001.

Sender, Ron, Shai Fuchs, and Ron Milo. 2016. 'Revised estimates for the number of human and bacteria cells in the body', *bioRxiv*.

Sethupathy, P., B. Corda, and A. G. Hatzigeorgiou. 2006. 'TarBase: A comprehensive database of experimentally supported animal microRNA targets', *Rna*, 12: 192-7.

Shajib, M. S., and W. I. Khan. 2015. 'The role of serotonin and its receptors in activation of immune responses and inflammation', *Acta Physiol (Oxf)*, 213: 561-74.

Shannon, C. E. 1948. 'A Mathematical Theory of Communication', *Bell System Technical Journal*, 27: 379-423.

Sharon, G., D. Segal, I. Zilber-Rosenberg, and E. Rosenberg. 2011. 'Symbiotic bacteria are responsible for diet-induced mating preference in Drosophila melanogaster, providing support for the hologenome concept of evolution', *Gut Microbes*, 2: 190-2.

Sheehan, D., C. Moran, and F. Shanahan. 2015. 'The microbiota in inflammatory bowel disease', *J Gastroenterol*, 50: 495-507.

Sheh, A., and J. G. Fox. 2013. 'The role of the gastrointestinal microbiome in Helicobacter pylori pathogenesis', *Gut Microbes*, 4: 505-31.

Shen, S., C. Spratt, W. J. Sheward, I. Kallo, K. West, C. F. Morrison, C. W. Coen, H. M. Marston, and A. J. Harmar. 2000. 'Overexpression of the human VPAC2 receptor in the suprachiasmatic nucleus alters the circadian phenotype of mice', *Proc Natl Acad Sci U S A*, 97: 11575-80.

Shin, H., Z. Pei, K. A. Martinez, 2nd, J. I. Rivera-Vinas, K. Mendez, H. Cavallin, and M. G. Dominguez-Bello. 2015. 'The first microbial environment of infants born by C-section: the operating room microbes', *Microbiome*, 3: 59.

Shivers, B. D., T. J. Gorcs, P. E. Gottschall, and A. Arimura. 1991. 'Two high affinity binding sites for pituitary adenylate cyclase-activating polypeptide have different tissue distributions', *Endocrinology*, 128: 3055-65.

Shu, Ye, and Philip J. Scarpace. 1994. *Forskolin Binding Sites and G-Protein Immunoreactivity in Rat Hearts During Aging*.

Shuryak, I., V. Y. Matrosova, E. K. Gaidamakova, R. Tkavc, O. Grichenko, P. Klimenkova, R. P. Volpe, and M. J. Daly. 2017. 'Microbial cells can cooperate to resist high-level chronic ionizing radiation', *PLoS One*, 12: e0189261.

Singh, B., N. Qin, and G. Reid. 2015. 'Microbiome Regulation of Autoimmune, Gut and Liver Associated Diseases', *Inflamm Allergy Drug Targets*, 14: 84-93.

Sitkauskiene, B., A. K. Johansson, S. Sergejeva, S. Lundin, M. Sjostrand, and J. Lotvall. 2004. 'Regulation of bone marrow and airway CD34+ eosinophils by interleukin-5', *Am J Respir Cell Mol Biol*, 30: 367-78.

Smalley, S. G., P. A. Barrow, and N. Foster. 2009. 'Immunomodulation of innate immune responses by vasoactive intestinal peptide (VIP): its therapeutic potential in inflammatory disease', *Clin Exp Immunol*, 157: 225-34.

Smids, C., C. S. Horjus Talabur Horje, J. Drylewicz, B. Roosenboom, M. J. M. Groenen, E. van Koolwijk, E. G. van Lochem, and P. J. Wahab. 2018. 'Intestinal T Cell Profiling in Inflammatory Bowel Disease: Linking T Cell Subsets to Disease Activity and Disease Course', *J Crohns Colitis*, 12: 465-75.

Sprang, Stephen R. 1997. 'G protein mechanisms: insights from structural analysis', *Annual review of biochemistry*, 66: 639-78.

Sprent, J., E. K. Gao, O. Kanagawa, and S. R. Webb. 1988. 'T-cell selection in the thymus', *Princess Takamatsu Symp*, 19: 127-36.

Stahlhut, C., and F. J. Slack. 2013. 'MicroRNAs and the cancer phenotype: profiling, signatures and clinical implications', *Genome Med*, 5: 111.

Stiefel, U., M. A. Tima, and M. M. Nerandzic. 2015. 'Metallo-beta-lactamase-producing bacteroides species can shield other members of the gut microbiota from antibiotics', *Antimicrob Agents Chemother*, 59: 650-3.

Stork, P. J., and J. M. Schmitt. 2002. 'Crosstalk between cAMP and MAP kinase signaling in the regulation of cell proliferation', *Trends Cell Biol*, 12: 258-66.

'Structure, function and diversity of the healthy human microbiome'. 2012. *Nature*, 486: 207-14.

Sturm, E. M., K. D. Dyer, C. M. Percopo, A. Heinemann, and H. F. Rosenberg. 2013. 'Chemotaxis of bone marrow derived eosinophils in vivo: a novel method to explore receptor-dependent trafficking in the mouse', *Eur J Immunol*, 43: 2217-28.

Summers, Monica A., M. Sue O'Dorisio, Mary O. Cox, Maria Lara-Marquez, and Edward J. Goetzl. 2003. 'A Lymphocyte-Generated Fragment of Vasoactive Intestinal Peptide with VPAC1 Agonist Activity and VPAC2 Antagonist Effects', *Journal of Pharmacology and Experimental Therapeutics*, 306: 638-45.

Szema, A. M., S. A. Hamidi, A. Koller, and D. W. Martin. 2011. 'Vasoactive Intestinal Peptide Knockout (VIP KO) mouse model of sulfite-sensitive asthma: up-regulation of novel lung carbonyl reductase', *BMC Immunol*, 12: 66.

Szema, A. M., S. A. Hamidi, S. Lyubsky, K. G. Dickman, S. Mathew, T. Abdel-Razek, J. J. Chen, J. A. Waschek, and S. I. Said. 2006. 'Mice lacking the VIP gene show airway hyperresponsiveness and airway inflammation, partially reversible by VIP', *Am J Physiol Lung Cell Mol Physiol*, 291: L880-6.

Takamizawa, Junichi, Hiroyuki Konishi, Kiyoshi Yanagisawa, Shuta Tomida, Hirotaka Osada, Hideki Endoh, Tomoko Harano, Yasushi Yatabe, Masato Nagino, Yuji Nimura, Tetsuya Mitsudomi, and Takashi Takahashi. 2004. 'Reduced Expression of the let-7 MicroRNAs in Human Lung Cancers in Association with Shortened Postoperative Survival', *Cancer Research*, 64: 3753-56.

Takei, Yoshio. 2016. 'Chapter 18 - Secretin (Pituitary Adenylate Cyclase-Activating Polypeptide) Family.' in, *Handbook of Hormones* (Academic Press: San Diego).

Tam, Janice K. V., Leo T. O. Lee, and Billy K. C. Chow. 2007. 'PACAP-related peptide (PRP)—Molecular evolution and potential functions', *Peptides*, 28: 1920-29.

Tang, WJ, and AG Gilman. 1991. 'Type-specific regulation of adenylyl cyclase by G protein beta gamma subunits', *Science*, 254: 1500-03.

———. 1995. 'Construction of a soluble adenylyl cyclase activated by Gs alpha and forskolin', *Science*, 268: 1769-72.

Thaiss, C. A., N. Zmora, M. Levy, and E. Elinav. 2016. 'The microbiome and innate immunity', *Nature*, 535: 65-74.

Thevelein, J. M., and J. H. de Winde. 1999. 'Novel sensing mechanisms and targets for the cAMP-protein kinase A pathway in the yeast Saccharomyces cerevisiae', *Mol Microbiol*, 33: 904-18.

Thwaites, D. T., J. Young, M. C. Thorndyke, and R. Dimaline. 1989. 'The isolation and chemical characterization of a novel vasoactive intestinal peptide-related peptide from a teleost fish, the cod, Gadus morhua', *Biochimica et Biophysica Acta (BBA) - Protein Structure and Molecular Enzymology*, 999: 217-20.

Tilg, H., and A. R. Moschen. 2014. 'Microbiota and diabetes: an evolving relationship', *Gut*, 63: 1513-21.

Tito, Raúl Y., Simone Macmil, Graham Wiley, Fares Najar, Lauren Cleeland, Chunmei Qu, Ping Wang, Frederic Romagne, Sylvain Leonard, Agustín Jiménez Ruiz, Karl Reinhard, Bruce A. Roe, and Cecil M. Lewis, Jr. 2008. 'Phylotyping and Functional Analysis of Two Ancient Human Microbiomes', *PLoS One*, 3: e3703.

Tomas, Julie, Céline Mulet, Azadeh Saffarian, Jean-Baptiste Cavin, Robert Ducroc, Béatrice Regnault, Chek Kun Tan, Kalina Duszka, Rémy Burcelin, Walter Wahli, Philippe J. Sansonetti, and Thierry Pédron. 2016. 'High-fat diet modifies the PPAR-γ pathway leading to disruption of microbial and physiological ecosystem in murine small intestine', *Proceedings of the National Academy of Sciences*, 113: E5934-E43.

Tong, L., H. Xue, L. Xiong, J. Xiao, and Y. Zhou. 2015. 'Improved RT-PCR Assay to Quantitate the Pri-, Pre-, and Mature microRNAs with Higher Efficiency and Accuracy', *Mol Biotechnol*, 57: 939-46.

Tremaroli, V., and F. Backhed. 2012. 'Functional interactions between the gut microbiota and host metabolism', *Nature*, 489: 242-9.

Tremlett, H., D. W. Fadrosh, A. A. Faruqi, F. Zhu, J. Hart, S. Roalstad, J. Graves, S. Lynch, and E. Waubant. 2016. 'Gut microbiota in early pediatric multiple sclerosis: a case-control study', *Eur J Neurol*, 23: 1308-21.

Trumpp-Kallmeyer, S., B. Chini, B. Mouillac, C. Barberis, J. Hoflack, and M. Hibert. 1995. 'Towards understanding the role of the first extracellular loop for the binding of peptide hormones to G-protein coupled receptors', *Pharm Acta Helv*, 70: 255-62.

Trumpp-Kallmeyer, S., J. Hoflack, A. Bruinvels, and M. Hibert. 1992. 'Modeling of G-protein-coupled receptors: application to dopamine, adrenaline, serotonin, acetylcholine, and mammalian opsin receptors', *J Med Chem*, 35: 3448-62.

Tsukada, T., S. J. Horovitch, M. R. Montminy, G. Mandel, and R. H. Goodman. 1985. 'Structure of the human vasoactive intestinal polypeptide gene', *Dna*, 4: 293-300.

Turner, J. T., S. B. Jones, and D. B. Bylund. 1986. 'A fragment of vasoactive intestinal peptide, VIP(10-28), is an antagonist of VIP in the colon carcinoma cell line, HT29', *Peptides*, 7: 849-54.

Ulrich, C. D., 2nd, M. Holtmann, and L. J. Miller. 1998. 'Secretin and vasoactive intestinal peptide receptors: members of a unique family of G protein-coupled receptors', *Gastroenterology*, 114: 382-97.

Ulucan, C., X. Wang, E. Baljinnyam, Y. Bai, S. Okumura, M. Sato, S. Minamisawa, S. Hirotani, and Y. Ishikawa. 2007. 'Developmental changes in gene expression of Epac and its upregulation in myocardial hypertrophy', *Am J Physiol Heart Circ Physiol*, 293: H1662-72.

Unger, Vinzenz M, Paul A Hargrave, Joyce M Baldwin, and Gebhard FX Schertler. 1997. 'Arrangement of rhodopsin transmembrane α-helices', *Nature*, 389: 203.

Usdin, T. B., T. I. Bonner, and E. Mezey. 1994. 'Two receptors for vasoactive intestinal polypeptide with similar specificity and complementary distributions', *Endocrinology*, 135: 2662-80.

V. D. Steen, Travis, Manpreet Bains, Wanjara Steve, Bisnett Brittany, Laney Caleb, Huber Ben, T. Dorsam Sheri, M. Schuh Jane, and P. Dorsam Glenn. 2016. 'VIP Signaling Fails to Alter Gene Expression but Induces Different [cAMP]i Responses in Human Malignant Hut-78 and Molt-4 T Cell Lines; Implications for Different G-protein Coupling for VIP Receptors', *Immunology, Endocrine & Metabolic Agents in Medicinal Chemistry*, 16: 178-98.

Vaishampayan, Parag A., Jennifer V. Kuehl, Jeffrey L. Froula, Jenna L. Morgan, Howard Ochman, and M. Pilar Francino. 2010. 'Comparative Metagenomics and Population Dynamics of the Gut Microbiota in Mother and Infant', *Genome Biology and Evolution*, 2: 53-66.

Valberg, L. S., P. R. Flanagan, A. Kertesz, and D. C. Bondy. 1986. 'Zinc absorption in inflammatory bowel disease', *Dig Dis Sci*, 31: 724-31.

van Biesen, T., B. E. Hawes, D. K. Luttrell, K. M. Krueger, K. Touhara, E. Porfiri, M. Sakaue, L. M. Luttrell, and R. J. Lefkowitz. 1995. 'Receptor-tyrosine-kinase- and G beta gamma-mediated MAP kinase activation by a common signalling pathway', *Nature*, 376: 781-4.

Vandenplas, Yvan, Irina Zakharova, and Yulia Dmitrieva. 2015. 'Oligosaccharides in infant formula: more evidence to validate the role of prebiotics', *British Journal of Nutrition*, 113: 1339-44.

Velmanickam, L., M. Fondakowski, I. T. Lima, Jr., and D. Nawarathna. 2017. 'Integrated dielectrophoretic and surface plasmonic platform for million-fold improvement in the detection of fluorescent events', *Biomicrofluidics*, 11: 044115.

Velmanickam, L., D. Laudenbach, and D. Nawarathna. 2016. 'Dielectrophoretic label-free immunoassay for rare-analyte quantification in biological samples', *Phys Rev E*, 94: 042408.

Venter, J. Craig, Mark D. Adams, Eugene W. Myers, Peter W. Li, Richard J. Mural, Granger G. Sutton, Hamilton O. Smith, Mark Yandell, Cheryl A. Evans, Robert A. Holt, Jeannine D. Gocayne, Peter Amanatides, Richard M. Ballew, Daniel H. Huson, Jennifer Russo Wortman, Qing Zhang, Chinnappa D. Kodira, Xiangqun H. Zheng, Lin Chen, Marian Skupski, Gangadharan Subramanian, Paul D. Thomas, Jinghui Zhang, George L. Gabor Miklos, Catherine Nelson, Samuel Broder, Andrew G. Clark, Joe Nadeau, Victor A. McKusick, Norton Zinder, Arnold J. Levine, Richard J. Roberts, Mel Simon, Carolyn

Slayman, Michael Hunkapiller, Randall Bolanos, Arthur Delcher, Ian Dew, Daniel Fasulo, Michael Flanigan, Liliana Florea, Aaron Halpern, Sridhar Hannenhalli, Saul Kravitz, Samuel Levy, Clark Mobarry, Knut Reinert, Karin Remington, Jane Abu-Threideh, Ellen Beasley, Kendra Biddick, Vivien Bonazzi, Rhonda Brandon, Michele Cargill, Ishwar Chandramouliswaran, Rosane Charlab, Kabir Chaturvedi, Zuoming Deng, Valentina Di Francesco, Patrick Dunn, Karen Eilbeck, Carlos Evangelista, Andrei E. Gabrielian, Weiniu Gan, Wangmao Ge, Fangcheng Gong, Zhiping Gu, Ping Guan, Thomas J. Heiman, Maureen E. Higgins, Rui-Ru Ji, Zhaoxi Ke, Karen A. Ketchum, Zhongwu Lai, Yiding Lei, Zhenya Li, Jiayin Li, Yong Liang, Xiaoying Lin, Fu Lu, Gennady V. Merkulov, Natalia Milshina, Helen M. Moore, Ashwinikumar K Naik, Vaibhav A. Narayan, Beena Neelam, Deborah Nusskern, Douglas B. Rusch, Steven Salzberg, Wei Shao, Bixiong Shue, Jingtao Sun, Zhen Yuan Wang, Aihui Wang, Xin Wang, Jian Wang, Ming-Hui Wei, Ron Wides, Chunlin Xiao, Chunhua Yan, Alison Yao, Jane Ye, Ming Zhan, Weiqing Zhang, Hongyu Zhang, Qi Zhao, Liansheng Zheng, Fei Zhong, Wenyan Zhong, Shiaoping C. Zhu, Shaying Zhao, Dennis Gilbert, Suzanna Baumhueter, Gene Spier, Christine Carter, Anibal Cravchik, Trevor Woodage, Feroze Ali, Huijin An, Aderonke Awe, Danita Baldwin, Holly Baden, Mary Barnstead, Ian Barrow, Karen Beeson, Dana Busam, Amy Carver, Angela Center, Ming Lai Cheng, Liz Curry, Steve Danaher, Lionel Davenport, Raymond Desilets, Susanne Dietz, Kristina Dodson, Lisa Doup, Steven Ferriera, Neha Garg, Andres Gluecksmann, Brit Hart, Jason Haynes, Charles Haynes, Cheryl Heiner, Suzanne Hladun, Damon Hostin, Jarrett Houck, Timothy Howland, Chinyere Ibegwam, Jeffery Johnson, Francis Kalush, Lesley Kline, Shashi Koduru, Amy Love, Felecia Mann, David May, Steven McCawley, Tina McIntosh, Ivy McMullen, Mee Moy, Linda Moy, Brian Murphy, Keith Nelson, Cynthia Pfannkoch, Eric Pratts, Vinita Puri, Hina Qureshi, Matthew Reardon, Robert Rodriguez, Yu-Hui Rogers, Deanna Romblad, Bob Ruhfel, Richard Scott, Cynthia Sitter, Michelle Smallwood, Erin Stewart, Renee Strong, Ellen Suh, Reginald Thomas, Ni Ni Tint, Sukyee Tse, Claire Vech, Gary Wang, Jeremy Wetter, Sherita Williams, Monica Williams, Sandra Windsor, Emily Winn-Deen, Keriellen Wolfe, Jayshree Zaveri, Karena Zaveri, Josep F. Abril, Roderic Guigó, Michael J. Campbell, Kimmen V. Sjolander, Brian Karlak, Anish Kejariwal, Huaiyu Mi, Betty Lazareva, Thomas Hatton, Apurva Narechania, Karen Diemer, Anushya Muruganujan, Nan Guo, Shinji Sato, Vineet Bafna, Sorin Istrail, Ross Lippert, Russell Schwartz, Brian Walenz, Shibu Yooseph, David Allen, Anand Basu, James Baxendale, Louis Blick, Marcelo Caminha, John Carnes-Stine, Parris Caulk, Yen-Hui Chiang, My Coyne, Carl Dahlke, Anne Deslattes Mays, Maria Dombroski, Michael Donnelly, Dale Ely, Shiva Esparham, Carl Fosler, Harold Gire, Stephen Glanowski, Kenneth Glasser, Anna Glodek, Mark Gorokhov, Ken Graham, Barry Gropman, Michael Harris, Jeremy Heil, Scott Henderson, Jeffrey Hoover, Donald Jennings, Catherine Jordan, James Jordan, John Kasha, Leonid Kagan, Cheryl Kraft, Alexander Levitsky, Mark Lewis, Xiangjun Liu, John Lopez, Daniel Ma, William Majoros, Joe McDaniel, Sean Murphy, Matthew Newman, Trung Nguyen, Ngoc Nguyen, Marc Nodell, Sue Pan, Jim Peck, Marshall Peterson, William Rowe, Robert Sanders, John Scott, Michael Simpson, Thomas Smith, Arlan Sprague, Timothy Stockwell, Russell Turner, Eli Venter, Mei Wang, Meiyuan Wen, David Wu, Mitchell Wu, Ashley Xia, Ali Zandieh, and Xiaohong Zhu. 2001. 'The Sequence of the Human Genome', *Science*, 291: 1304-51.

Vertongen, P., S. N. Schiffmann, P. Gourlet, and P. Robberecht. 1998. 'Autoradiographic visualization of the receptor subclasses for vasoactive intestinal polypeptide (VIP) in rat brain', *Ann N Y Acad Sci*, 865: 412-5.

Viazis, N., J. Vlachogiannakos, O. Georgiou, M. Rodias, D. Georgiadis, V. Papastamopoulos, I. G. Baraboutis, D. G. Karamanolis, and A. Skoutelis. 2010. 'Course of inflammatory bowel disease in patients infected with human immunodeficiency virus', *Inflamm Bowel Dis*, 16: 507-11.

Voice, J. K., C. Grinninger, Y. Kong, Y. Bangale, S. Paul, and E. J. Goetzl. 2003. 'Roles of vasoactive intestinal peptide (VIP) in the expression of different immune phenotypes by wild-type mice and T cell-targeted type II VIP receptor transgenic mice', *J Immunol*, 170: 308-14.

Voigt, R. M., K. C. Summa, C. B. Forsyth, S. J. Green, P. Engen, A. Naqib, M. H. Vitaterna, F. W. Turek, and A. Keshavarzian. 2016. 'The Circadian Clock Mutation Promotes Intestinal Dysbiosis', *Alcohol Clin Exp Res*, 40: 335-47.

Vomhof-DeKrey, E. E., and G. P. Dorsam. 2008. 'Stimulatory and suppressive signal transduction regulates vasoactive intestinal peptide receptor-1 (VPAC-1) in primary mouse CD4 T cells', *Brain Behav Immun*, 22: 1024-31.

Vosko, A., H. C. van Diepen, D. Kuljis, A. M. Chiu, D. Heyer, H. Terra, E. Carpenter, S. Michel, J. H. Meijer, and C. S. Colwell. 2015. 'Role of vasoactive intestinal peptide in the light input to the circadian system', *Eur J Neurosci*, 42: 1839-48.

Vu, J. P., M. Larauche, M. Flores, L. Luong, J. Norris, S. Oh, L. J. Liang, J. Waschek, J. R. Pisegna, and P. M. Germano. 2015. 'Regulation of Appetite, Body Composition, and Metabolic Hormones by Vasoactive Intestinal Polypeptide (VIP)', *J Mol Neurosci*, 56: 377-87.

Vu, J. P., M. Million, M. Larauche, L. Luong, J. Norris, J. A. Waschek, C. Pothoulakis, J. R. Pisegna, and P. M. Germano. 2014. 'Inhibition of vasoactive intestinal polypeptide (VIP) induces resistance to dextran sodium sulfate (DSS)-induced colitis in mice', *J Mol Neurosci*, 52: 37-47.

Walter, Jens, and Ruth Ley. 2011. 'The Human Gut Microbiome: Ecology and Recent Evolutionary Changes', *Annual Review of Microbiology*, 65: 411-29.

Walters, W. A., J. G. Caporaso, C. L. Lauber, D. Berg-Lyons, N. Fierer, and R. Knight. 2011. 'PrimerProspector: de novo design and taxonomic analysis of barcoded polymerase chain reaction primers', *Bioinformatics*, 27: 1159-61.

Wang, Mei, Siv Ahrné, Bengt Jeppsson, and Göran Molin. 2005. 'Comparison of bacterial diversity along the human intestinal tract by direct cloning and sequencing of 16S rRNA genes', *FEMS Microbiology Ecology*, 54: 219-31.

Wang, X., S. P. Heazlewood, D. O. Krause, and T. H. J. Florin. 2003. 'Molecular characterization of the microbial species that colonize human ileal and colonic mucosa by using 16S rDNA sequence analysis', *Journal of Applied Microbiology*, 95: 508-20.

Wang, Y., and J. M. Conlon. 1993. 'Neuroendocrine peptides (NPY, GRP, VIP, somatostatin) from the brain and stomach of the alligator', *Peptides*, 14: 573-9.

Wassenaar, T. M., and P. Panigrahi. 2014. 'Is a foetus developing in a sterile environment?', *Lett Appl Microbiol*, 59: 572-9.

Watson, J. D., and F. H. Crick. 1953. 'The structure of DNA', *Cold Spring Harb Symp Quant Biol*, 18: 123-31.

Wen, L., R. E. Ley, P. Y. Volchkov, P. B. Stranges, L. Avanesyan, A. C. Stonebraker, C. Hu, F. S. Wong, G. L. Szot, J. A. Bluestone, J. I. Gordon, and A. V. Chervonsky. 2008. 'Innate immunity and intestinal microbiota in the development of Type 1 diabetes', *Nature*, 455: 1109-13.

Wershil, B. K., C. W. Turck, S. P. Sreedharan, J. Yang, S. An, S. J. Galli, and E. J. Goetzl. 1993. 'Variants of vasoactive intestinal peptide in mouse mast cells and rat basophilic leukemia cells', *Cell Immunol*, 151: 369-78.

Whipps JM, Lewis K, Cooke RC. 1988. 'Mycoparasitism and plant disease control', *Fungi in Biological Control Systems*: 161–87.

Whisnant, R E, A G Gilman, and C W Dessauer. 1996. 'Interaction of the two cytosolic domains of mammalian adenylyl cyclase', *Proceedings of the National Academy of Sciences*, 93: 6621-25.

Whitman, W. B., D. C. Coleman, and W. J. Wiebe. 1998. 'Prokaryotes: the unseen majority', *Proc Natl Acad Sci U S A*, 95: 6578-83.

Whittaker, R. H. 1960. 'Vegetation of the Siskiyou Mountains, Oregon and California', *Ecological Monographs*, 30: 279-338.

———. 1972. 'Evolution and Measurement of Species Diversity', *Taxon*, 21: 213-51.

Wittpoth, C., K. Scholich, Y. Yigzaw, T. M. Stringfield, and T. B. Patel. 1999. 'Regions on adenylyl cyclase that are necessary for inhibition of activity by beta gamma and G(ialpha) subunits of heterotrimeric G proteins', *Proc Natl Acad Sci U S A*, 96: 9551-6.

Wolf, S. A., J. Fisher, I. Bechmann, B. Steiner, E. Kwidzinski, and R. Nitsch. 2002. 'Neuroprotection by T-cells depends on their subtype and activation state', *J Neuroimmunol*, 133: 72-80.

Wu, Huixian, Chong Wang, Karen J. Gregory, Gye Won Han, Hyekyung P. Cho, Yan Xia, Colleen M. Niswender, Vsevolod Katrich, Jens Meiler, Vadim Cherezov, P. Jeffrey Conn, and Raymond C. Stevens. 2014. 'Structure of a Class C GPCR Metabotropic Glutamate Receptor 1 Bound to an Allosteric Modulator', *Science*, 344: 58-64.

Wu, L., L. H. Nguyen, K. Zhou, T. Y. de Soysa, L. Li, J. B. Miller, J. Tian, J. Locker, S. Zhang, G. Shinoda, M. T. Seligson, L. R. Zeitels, A. Acharya, S. C. Wang, J. T. Mendell, X. He, J. Nishino, S. J. Morrison, D. J. Siegwart, G. Q. Daley, N. Shyh-Chang, and H. Zhu. 2015. 'Precise let-7 expression levels balance organ regeneration against tumor suppression', *Elife*, 4: e09431.

Wu, R. 1972. 'Nucleotide sequence analysis of DNA', *Nat New Biol*, 236: 198-200.

Wu, X., V. S. Conlin, V. Morampudi, N. R. Ryz, Y. Nasser, G. Bhinder, K. S. Bergstrom, H. B. Yu, C. C. Waterhouse, A. M. Buchan, O. E. Popescu, W. T. Gibson, J. A. Waschek, B. A. Vallance, and K. Jacobson. 2015. 'Vasoactive intestinal polypeptide promotes intestinal barrier homeostasis and protection against colitis in mice', *PLoS One*, 10: e0125225.

Xi, Y., G. Wu, T. Ai, N. Cheng, J. M. Kalisnik, J. Sun, S. Abbasi, D. Yang, C. Fan, X. Yuan, S. Wang, M. Elayda, I. D. Gregoric, B. K. Kantharia, S. F. Lin, and J. Cheng. 2013. 'Ionic mechanisms underlying the effects of vasoactive intestinal polypeptide on canine atrial myocardium', *Circ Arrhythm Electrophysiol*, 6: 976-83.

Xia, M., G. O. Gaufo, Q. Wang, S. P. Sreedharan, and E. J. Goetzl. 1996. 'Transduction of specific inhibition of HuT 78 human T cell chemotaxis by type I vasoactive intestinal peptide receptors', *J Immunol*, 157: 1132-8.

Xie, Z., C. Chang, and Z. Zhou. 2014. 'Molecular mechanisms in autoimmune type 1 diabetes: a critical review', *Clin Rev Allergy Immunol*, 47: 174-92.

Xu, W., M. Li, J. F. Ding, J. D. Gu, and Z. H. Luo. 2014. 'Bacteria dominate the ammonia-oxidizing community in a hydrothermal vent site at the Mid-Atlantic Ridge of the South Atlantic Ocean', *Appl Microbiol Biotechnol*, 98: 7993-8004.

Yan, S. Z., D. Hahn, Z. H. Huang, and W. J. Tang. 1996. 'Two cytoplasmic domains of mammalian adenylyl cyclase form a Gs alpha- and forskolin-activated enzyme in vitro', *J Biol Chem*, 271: 10941-5.

Yan, S. Z., Z. H. Huang, V. D. Rao, J. H. Hurley, and W. J. Tang. 1997. 'Three discrete regions of mammalian adenylyl cyclase form a site for Gsalpha activation', *J Biol Chem*, 272: 18849-54.

Yeh, Y. Y., H. G. Ozer, A. M. Lehman, K. Maddocks, L. Yu, A. J. Johnson, and J. C. Byrd. 2015. 'Characterization of CLL exosomes reveals a distinct microRNA signature and enhanced secretion by activation of BCR signaling', *Blood*, 125: 3297-305.

Yi, Rui, Yi Qin, Ian G. Macara, and Bryan R. Cullen. 2003. 'Exportin-5 mediates the nuclear export of pre-microRNAs and short hairpin RNAs', *Genes & Development*, 17: 3011-16.

Yoshimoto, T., K. Takeda, T. Tanaka, K. Ohkusu, S. Kashiwamura, H. Okamura, S. Akira, and K. Nakanishi. 1998. 'IL-12 up-regulates IL-18 receptor expression on T cells, Th1 cells, and B cells: synergism with IL-18 for IFN-gamma production', *J Immunol*, 161: 3400-7.

Yoshizawa, H., Y. Morishita, M. Watanabe, K. Ishibashi, S. Muto, E. Kusano, and D. Nagata. 2015. 'TGF-beta(1)-siRNA delivery with nanoparticles inhibits peritoneal fibrosis', *Gene Ther*, 22: 333-40.

You, S., J. L. Silsby, J. Farris, D. N. Foster, and M. E. el Halawani. 1995. 'Tissue-specific alternative splicing of turkey preprovasoactive intestinal peptide messenger ribonucleic acid, its regulation, and correlation with prolactin secretion', *Endocrinology*, 136: 2602-10.

Youngblood, Ben, J. Scott Hale, Haydn T. Kissick, Eunseon Ahn, Xiaojin Xu, Andreas Wieland, Koichi Araki, Erin E. West, Hazem E. Ghoneim, Yiping Fan, Pranay Dogra, Carl W. Davis, Bogumila T. Konieczny, Rustom Antia, Xiaodong Cheng, and Rafi Ahmed. 2017. 'Effector CD8 T cells dedifferentiate into long-lived memory cells', *Nature*, 552: 404.

Yuasa, M., T. Matsui, S. Ando, Y. Ishii, H. Sawamura, S. Ebara, and T. Watanabe. 2013. 'Consumption of a low-carbohydrate and high-fat diet (the ketogenic diet) exaggerates biotin deficiency in mice', *Nutrition*, 29: 1266-70.

Zackular, Joseph P., Nielson T. Baxter, Kathryn D. Iverson, William D. Sadler, Joseph F. Petrosino, Grace Y. Chen, and Patrick D. Schloss. 2013. 'The Gut Microbiome Modulates Colon Tumorigenesis', *MBio*, 4.

Zarrinpar, Amir, Amandine Chaix, Shibu Yooseph, and Satchidananda Panda. 2014. 'Diet and Feeding Pattern Affect the Diurnal Dynamics of the Gut Microbiome', *Cell Metabolism*, 20: 1006-17.

Zavilgelsky, G. B., S. K. Abilev, V. V. Sukhodolets, and S. I. Ahmad. 1998. 'Isolation and analysis of UV and radio-resistant bacteria from Chernobyl', *J Photochem Photobiol B*, 43: 152-7.

Zenewicz, Lauren A., Andrey Antov, and Richard A. Flavell. 2009. 'CD4 T-cell differentiation and inflammatory bowel disease', *Trends Mol Med*, 15: 199-207.

Zeng, Y., R. Yi, and B. R. Cullen. 2003. 'MicroRNAs and small interfering RNAs can inhibit mRNA expression by similar mechanisms', *Proc Natl Acad Sci U S A*, 100: 9779-84.

Zhang, Gongyi, Yu Liu, Arnold E Ruoho, and James H Hurley. 1997. 'Structure of the adenylyl cyclase catalytic core', *Nature*, 386: 247.

Zhang, H., F. A. Kolb, V. Brondani, E. Billy, and W. Filipowicz. 2002. 'Human Dicer preferentially cleaves dsRNAs at their termini without a requirement for ATP', *Embo j*, 21: 5875-85.

Zilber-Rosenberg, I., and E. Rosenberg. 2008. 'Role of microorganisms in the evolution of animals and plants: the hologenome theory of evolution', *FEMS Microbiol Rev*, 32: 723-35.

Zimmermann, G., D. Zhou, and R. Taussig. 1998. 'Genetic selection of mammalian adenylyl cyclases insensitive to stimulation by Gsalpha', *J Biol Chem*, 273: 6968-75.

APPENDIX. NUMERICAL DATA AND TAXONOMIC TREE EXPANSION

Table A1. VIP Strains at the phylum taxonomic level.

Taxonomy	Male			Female		
	WT	HET	KO	WT	HET	KO
Actinobacteria	0%	0%	0%	0%	0%	0%
Bacteroidetes	63%	44%	66%	53%	47%	68%
Chlamydiae	0%	0%	0%	0%	0%	0%
Cyanobacteria	0%	0%	0%	0%	0%	0%
Deferribacteres	7%	7%	3%	4%	6%	0%
Firmicutes	22%	42%	15%	36%	42%	13%
Proteobacteria	6%	4%	16%	4%	4%	17%
Saccharibacteria	1%	1%	0%	1%	1%	0%
Tenericutes	1%	1%	0%	1%	1%	0%
Verrucomicrobia	1%	0%	0%	0%	0%	1%

Table A2. VIP Strains at the class taxonomic level.

Taxonomy	Male			Female		
	WT	HET	KO	WT	HET	KO
Actinobacteria	0%	0%	0%	0%	0%	0%
Coriobacteriia	0%	0%	0%	0%	0%	0%
Bacteroidia	63%	44%	66%	53%	47%	68%
Chlamydiae	0%	0%	0%	0%	0%	0%
Chloroplast	0%	0%	0%	0%	0%	0%
Melainabacteria	0%	0%	0%	0%	0%	0%
Deferribacteres	7%	7%	3%	4%	6%	0%
Bacilli	0%	0%	1%	0%	0%	1%
Clostridia	21%	42%	14%	36%	42%	12%
Erysipelotrichia	0%	0%	0%	0%	0%	0%
Alphaproteobacteria	0%	0%	0%	0%	0%	0%
Betaproteobacteria	4%	1%	5%	2%	2%	4%
Deltaproteobacteria	1%	1%	1%	1%	1%	1%
Epsilonproteobacteria	1%	2%	9%	1%	2%	9%
Gammaproteobacteria	0%	0%	0%	0%	0%	3%
Saccharibacteria; Unknown Class	1%	1%	0%	1%	1%	0%
Mollicutes	1%	1%	0%	1%	1%	0%
Verrucomicrobiae	1%	0%	0%	0%	0%	1%

Table A3. VIP Strains at the order taxonomic level.

Taxonomy	**Male**			**Female**		
	WT	HET	KO	WT	HET	KO
Bifidobacteriales	0.00%	0.00%	0.20%	0.00%	0.00%	0.10%
Coriobacteriales	0.00%	0.00%	0.00%	0.00%	0.00%	0.00%
Bacteroidales	62.80%	44.40%	66.30%	53.40%	46.70%	68.30%
Chlamydiales	0.30%	0.10%	0.10%	0.30%	0.20%	0.30%
Chloroplast;Ambiguous_taxa	0.00%	0.00%	0.00%	0.00%	0.00%	0.00%
Gossypium arboreum	0.00%	0.00%	0.00%	0.00%	0.00%	0.00%
Gastranaerophilales	0.10%	0.10%	0.00%	0.10%	0.00%	0.10%
Deferribacterales	6.50%	7.20%	2.80%	4.30%	5.70%	0.40%
Lactobacillales	0.30%	0.10%	0.80%	0.10%	0.10%	0.70%
Clostridiales	21.40%	41.80%	13.60%	36.00%	41.70%	12.20%
Erysipelotrichales	0.20%	0.10%	0.30%	0.10%	0.20%	0.40%
Rhodospirillales	0.20%	0.00%	0.00%	0.00%	0.00%	0.00%
Burkholderiales	4.10%	1.40%	5.20%	2.00%	1.70%	4.30%
Desulfovibrionales	0.70%	0.90%	1.00%	0.90%	1.10%	0.80%
Campylobacterales	1.10%	2.10%	9.20%	0.80%	1.50%	8.50%
Enterobacteriales	0.20%	0.00%	0.10%	0.00%	0.00%	3.10%
Saccharibacteria; Unknown Order	0.70%	1.30%	0.20%	1.20%	0.70%	0.00%
Anaeroplasmatales	0.80%	0.30%	0.00%	0.50%	0.40%	0.00%
Mollicutes RF9	0.10%	0.10%	0.10%	0.20%	0.10%	0.00%
Verrucomicrobiales	0.50%	0.00%	0.20%	0.00%	0.00%	0.70%

Table A4. VIP Strains at the family taxonomic level.

Taxonomy	Male			Female		
	WT	HET	KO	WT	HET	KO
Bifidobacteriaceae	0.00%	0.00%	0.20%	0.00%	0.00%	0.10%
Coriobacteriaceae	0.00%	0.00%	0.00%	0.00%	0.00%	0.00%
Bacteroidaceae	16.80%	4.70%	31.90%	6.30%	7.30%	35.80%
Bacteroidales S24-7 group	28.90%	25.30%	12.80%	32.00%	25.50%	13.20%
Porphyromonadaceae	6.30%	0.70%	16.30%	1.10%	2.00%	16.30%
Prevotellaceae	0.80%	1.50%	2.00%	1.30%	0.90%	1.90%
Rikenellaceae	10.10%	12.10%	3.20%	12.70%	11.00%	1.20%
Chlamydiaceae	0.30%	0.10%	0.10%	0.30%	0.20%	0.30%
Chloroplast;Ambiguous_taxa	0.00%	0.00%	0.00%	0.00%	0.00%	0.00%
Gossypium arboreum	0.00%	0.00%	0.00%	0.00%	0.00%	0.00%
Gastranaerophilales; uncultured bacterium	0.10%	0.10%	0.00%	0.10%	0.00%	0.10%
Deferribacteraceae	6.50%	7.20%	2.80%	4.30%	5.70%	0.40%
Lactobacillaceae	0.20%	0.10%	0.50%	0.10%	0.00%	0.50%
Lactobacillales; uncultured	0.10%	0.00%	0.20%	0.00%	0.00%	0.20%
Christensenellaceae	0.00%	0.00%	0.00%	0.00%	0.00%	0.00%
Clostridiaceae 1	0.10%	0.00%	0.00%	0.10%	0.10%	0.00%
Clostridiales vadinBB60 group	0.50%	0.70%	0.00%	0.40%	1.40%	0.00%
Family XIII	0.00%	0.00%	0.00%	0.00%	0.00%	0.00%
Lachnospiraceae	16.00%	31.70%	11.30%	27.60%	31.90%	10.50%
Peptococcaceae	0.20%	0.20%	0.10%	0.30%	0.30%	0.10%
Peptostreptococcaceae	0.00%	0.00%	0.20%	0.00%	0.00%	0.20%
Ruminococcaceae	4.60%	9.10%	1.90%	7.60%	8.00%	1.50%
Erysipelotrichaceae	0.20%	0.10%	0.30%	0.10%	0.20%	0.40%
Rhodospirillaceae	0.20%	0.00%	0.00%	0.00%	0.00%	0.00%
Alcaligenaceae	4.10%	1.40%	5.20%	2.00%	1.70%	4.30%
Desulfovibrionaceae	0.70%	0.90%	1.00%	0.90%	1.10%	0.80%
Helicobacteraceae	1.10%	2.10%	9.20%	0.80%	1.50%	8.50%
Enterobacteriaceae	0.20%	0.00%	0.10%	0.00%	0.00%	3.10%
Saccharibacteria; Unknown Family	0.70%	1.30%	0.20%	1.20%	0.70%	0.00%
Anaeroplasmataceae	0.80%	0.30%	0.00%	0.50%	0.40%	0.00%
Mollicutes RF9; uncultured bacterium	0.10%	0.10%	0.10%	0.20%	0.10%	0.00%
Verrucomicrobiaceae	0.50%	0.00%	0.20%	0.00%	0.00%	0.70%

Table A5. VIP Strains at the genus taxonomic level.

Taxonomy	Male			Female		
	WT	HET	KO	WT	HET	KO
Bifidobacterium	0.00%	0.00%	0.20%	0.00%	0.00%	0.10%
Coriobacteriaceae UCG-002	0.00%	0.00%	0.00%	0.00%	0.00%	0.00%
Bacteroides	16.80%	4.70%	31.90%	6.30%	7.30%	35.80%
Bacteroidales S24-7 group; Ambiguous_taxa	0.50%	0.40%	0.10%	0.40%	0.30%	0.10%
Bacteroidales S24-7 group; uncultured Bacteroidales	2.20%	1.70%	0.40%	2.40%	1.90%	0.60%
Bacteroidales S24-7 group; uncultured bacterium	26.30%	23.20%	12.30%	29.10%	23.20%	12.40%
Bacteroidales S24-7 group; unidentified	0.00%	0.00%	0.00%	0.10%	0.20%	0.00%
Parabacteroides	4.80%	0.30%	7.70%	0.30%	0.50%	7.40%
Porphyromonadaceae; uncultured	1.40%	0.40%	8.60%	0.70%	1.50%	8.80%
Alloprevotella	0.50%	1.00%	0.70%	0.50%	0.50%	1.80%
Prevotella 9	0.00%	0.00%	0.00%	0.00%	0.30%	0.00%
Prevotellaceae NK3B31 group	0.10%	0.10%	1.00%	0.20%	0.00%	0.10%
Prevotellaceae UCG-001	0.20%	0.40%	0.30%	0.60%	0.20%	0.10%
Alistipes	9.60%	11.70%	3.20%	12.20%	10.30%	1.10%
Rikenellaceae RC9 gut group	0.50%	0.40%	0.00%	0.60%	0.70%	0.10%
Chlamydia	0.30%	0.10%	0.10%	0.30%	0.20%	0.30%
Chloroplast;Ambiguous_taxa	0.00%	0.00%	0.00%	0.00%	0.00%	0.00%
Gossypium arboreum	0.00%	0.00%	0.00%	0.00%	0.00%	0.00%
Gastranaerophilales; uncultured bacterium	0.10%	0.10%	0.00%	0.10%	0.00%	0.10%
Mucispirillum	6.50%	7.20%	2.80%	4.30%	5.70%	0.40%
Lactobacillus	0.20%	0.10%	0.50%	0.10%	0.00%	0.50%
Lactobacillales; uncultured bacterium	0.10%	0.00%	0.20%	0.00%	0.00%	0.20%
Christensenellaceae; uncultured	0.00%	0.00%	0.00%	0.00%	0.00%	0.00%
Candidatus Arthromitus	0.10%	0.00%	0.00%	0.10%	0.10%	0.00%
Clostridiales vadinBB60 group;Ambiguous_taxa	0.40%	0.60%	0.00%	0.30%	1.20%	0.00%
Clostridiales vadinBB60 group; uncultured bacterium	0.10%	0.10%	0.00%	0.10%	0.30%	0.00%
Family XIII UCG-001	0.00%	0.00%	0.00%	0.00%	0.00%	0.00%
[Eubacterium] nodatum group	0.00%	0.00%	0.00%	0.00%	0.00%	0.00%
Acetatifactor	0.00%	0.00%	0.00%	0.00%	0.00%	0.00%
Anaerosporobacter	0.00%	0.00%	0.00%	0.00%	0.00%	0.00%
Anaerostipes	0.00%	0.00%	0.40%	0.00%	0.00%	0.20%
Blautia	0.40%	0.60%	1.50%	0.70%	0.80%	0.30%
Coprococcus 1	0.10%	0.20%	0.10%	0.20%	0.10%	0.10%
Lachnoclostridium	0.20%	0.30%	1.20%	0.30%	0.20%	1.70%

Table A5. VIP Strains at the genus taxonomic level (continued).

Taxonomy	Male			Female		
	WT	HET	KO	WT	HET	KO
Lachnospiraceae FCS020 group	0.00%	0.00%	0.00%	0.00%	0.00%	0.00%
Lachnospiraceae NK4A136 group	7.60%	17.20%	3.20%	16.50%	15.10%	3.20%
Lachnospiraceae UCG-001	0.10%	0.30%	0.20%	0.20%	0.20%	0.20%
Lachnospiraceae UCG-004	0.00%	0.00%	0.00%	0.00%	0.00%	0.00%
Lachnospiraceae UCG-006	0.10%	0.10%	0.00%	0.10%	0.00%	0.00%
Lachnospiraceae UCG-008	0.80%	3.50%	0.30%	2.70%	5.60%	0.20%
Marvinbryantia	0.10%	0.20%	0.00%	0.10%	0.20%	0.10%
Roseburia	1.20%	1.30%	2.20%	0.40%	1.60%	2.00%
Tyzzerella	0.00%	0.00%	0.00%	0.00%	0.00%	0.00%
[Eubacterium] oxidoreducens group	0.00%	0.20%	0.00%	0.10%	0.10%	0.00%
[Eubacterium] xylanophilum group	0.10%	0.10%	0.10%	0.00%	0.10%	0.00%
Lachnospiraceae; mouse gut metagenome	0.10%	0.20%	0.00%	0.10%	0.10%	0.00%
Lachnospiraceae; uncultured	5.10%	7.50%	2.00%	5.90%	7.60%	2.60%
Peptococcus	0.00%	0.00%	0.00%	0.00%	0.00%	0.00%
Peptococcaceae; uncultured	0.10%	0.20%	0.10%	0.30%	0.20%	0.00%
Peptoclostridium	0.00%	0.00%	0.20%	0.00%	0.00%	0.20%
Anaerotruncus	0.60%	0.90%	0.50%	0.60%	1.00%	0.50%
Butyricicoccus	0.30%	0.50%	0.10%	0.50%	0.40%	0.10%
Flavonifractor	0.00%	0.00%	0.10%	0.00%	0.00%	0.00%
Oscillibacter	0.60%	1.40%	0.20%	0.90%	1.20%	0.20%
Ruminiclostridium	0.60%	1.90%	0.10%	1.20%	1.20%	0.10%
Ruminiclostridium 5	0.10%	0.10%	0.00%	0.20%	0.20%	0.00%
Ruminiclostridium 6	0.10%	0.30%	0.00%	0.30%	0.20%	0.00%
Ruminiclostridium 9	0.80%	1.40%	0.20%	1.40%	1.50%	0.20%
Ruminococcaceae NK4A214 group	0.00%	0.10%	0.00%	0.10%	0.00%	0.00%
Ruminococcaceae UCG-003	0.00%	0.00%	0.00%	0.00%	0.00%	0.00%
Ruminococcaceae UCG-009	0.00%	0.10%	0.00%	0.10%	0.10%	0.00%
Ruminococcaceae UCG-014	0.20%	0.70%	0.20%	0.60%	0.40%	0.00%
Ruminococcus 1	0.10%	0.20%	0.00%	0.20%	0.20%	0.00%
[Eubacterium] coprostanoli genes group	0.10%	0.00%	0.00%	0.00%	0.00%	0.00%
Ruminococcaceae; uncultured	1.00%	1.50%	0.40%	1.60%	1.70%	0.20%
Erysipelatoclostridium	0.00%	0.00%	0.10%	0.00%	0.10%	0.10%
Faecalibaculum	0.00%	0.00%	0.00%	0.10%	0.00%	0.20%
[Clostridium] innocuum group	0.00%	0.00%	0.10%	0.00%	0.00%	0.00%
Erysipelotrichaceae; uncultured	0.00%	0.00%	0.00%	0.00%	0.10%	0.00%
Erysipelotrichaceae; uncultured bacterium	0.00%	0.00%	0.00%	0.00%	0.00%	0.00%
Rhodospirillaceae; uncultured	0.20%	0.00%	0.00%	0.00%	0.00%	0.00%

Table A5. VIP Strains at the genus taxonomic level (continued).

Taxonomy	**Male**			**Female**		
	WT	HET	KO	WT	HET	KO
Parasutterella	4.10%	1.40%	5.20%	2.00%	1.70%	4.30%
Bilophila	0.10%	0.10%	0.00%	0.10%	0.10%	0.00%
Desulfovibrio	0.60%	0.70%	1.00%	0.90%	0.90%	0.80%
Helicobacter	1.10%	2.10%	9.20%	0.80%	1.50%	8.50%
Escherichia-Shigella	0.00%	0.00%	0.00%	0.00%	0.00%	0.30%
Raoultella	0.00%	0.00%	0.00%	0.00%	0.00%	0.10%
Serratia	0.20%	0.00%	0.10%	0.00%	0.00%	2.70%
Saccharimonas	0.70%	1.30%	0.20%	1.20%	0.70%	0.00%
Anaeroplasma	0.80%	0.30%	0.00%	0.50%	0.40%	0.00%
Mollicutes RF9; uncultured bacterium	0.10%	0.10%	0.10%	0.20%	0.10%	0.00%
Akkermansia	0.50%	0.00%	0.20%	0.00%	0.00%	0.70%

Class Level Taxonomy
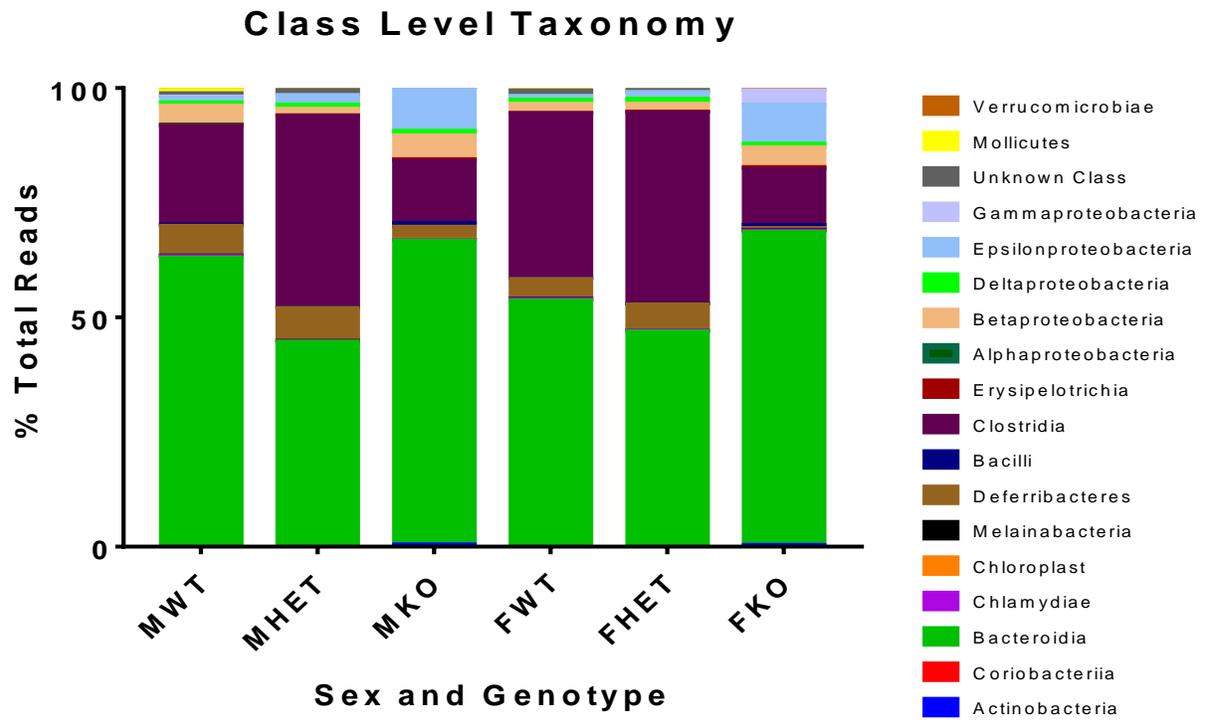
Figure A1.   Changes at the class level in VIP strains.
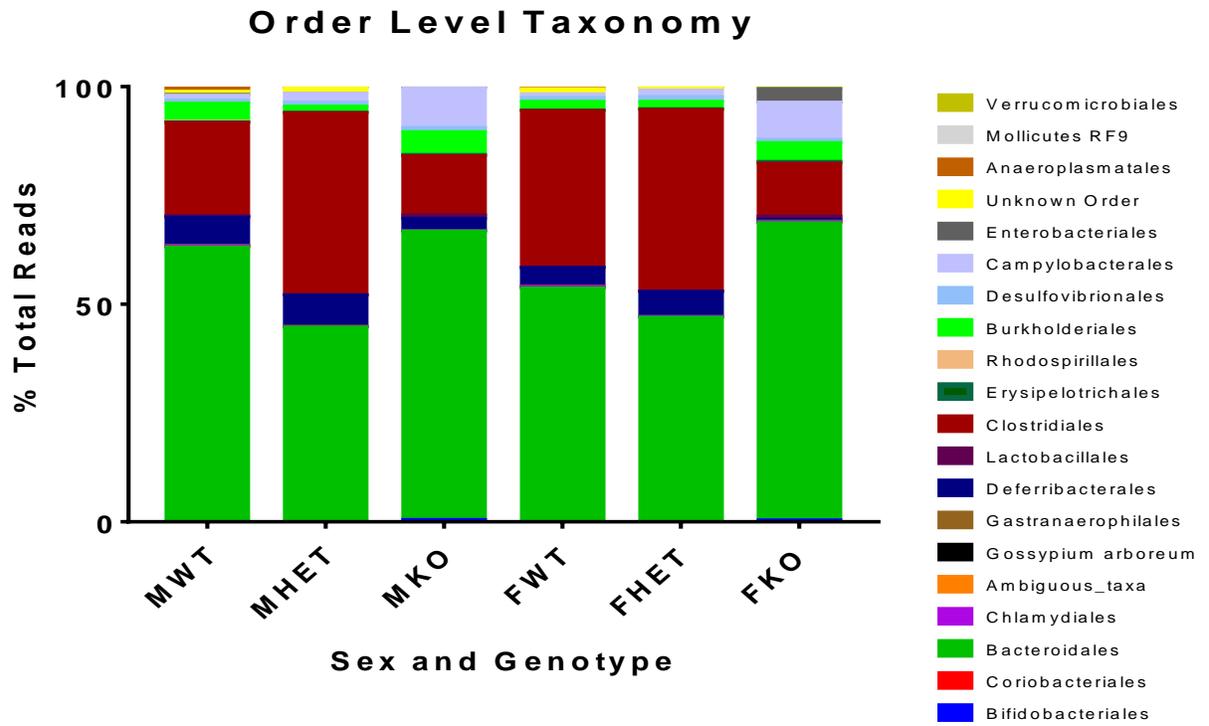
Figure A2.   VIP male and female order level taxonomic changes.
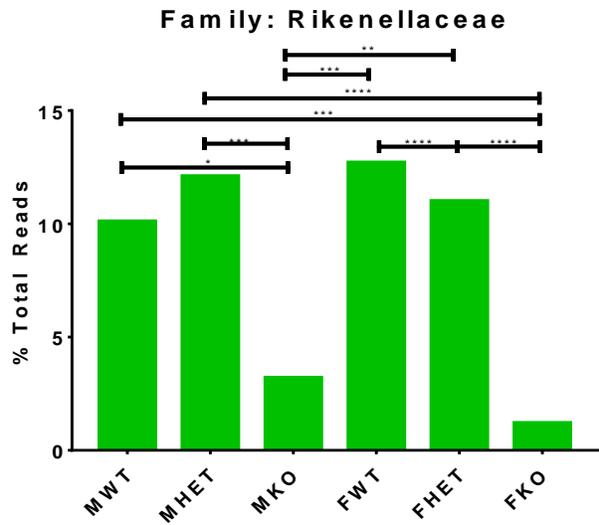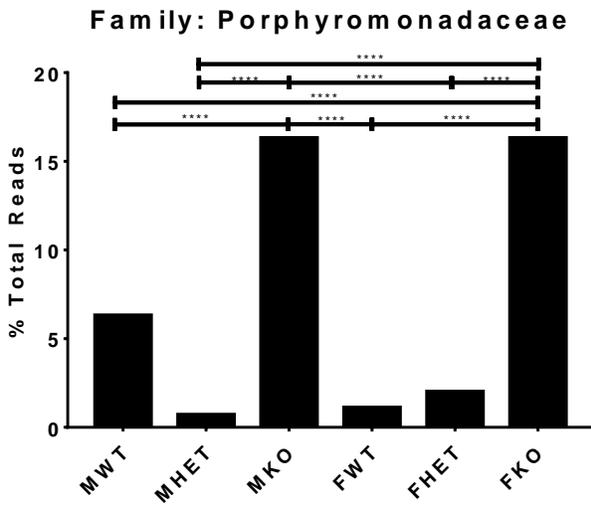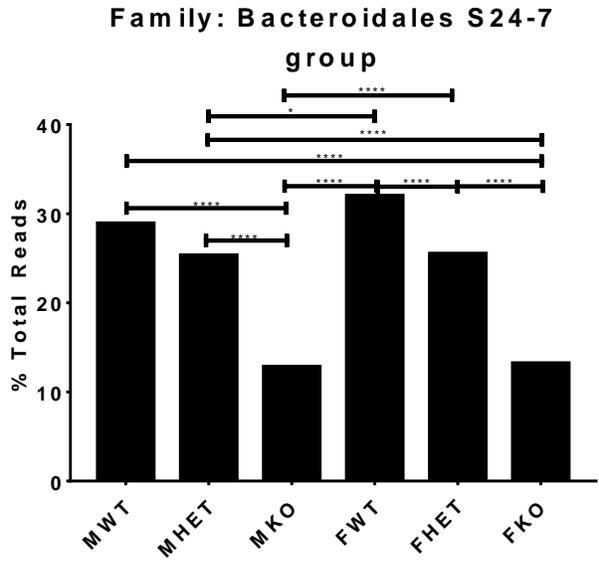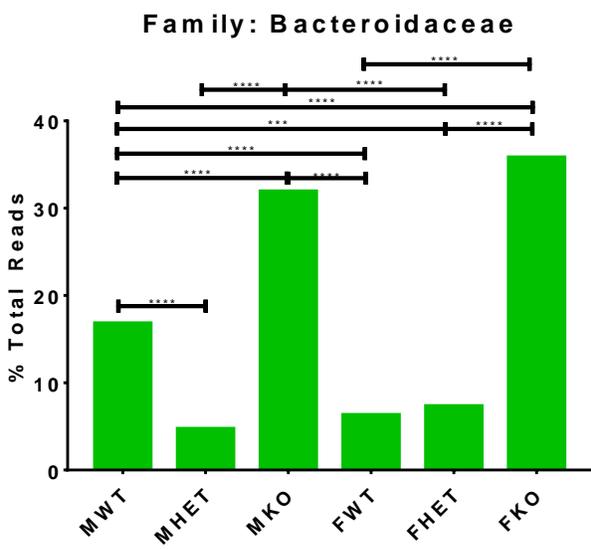
Figure A3. Changes in abundance between individual bacterial families.
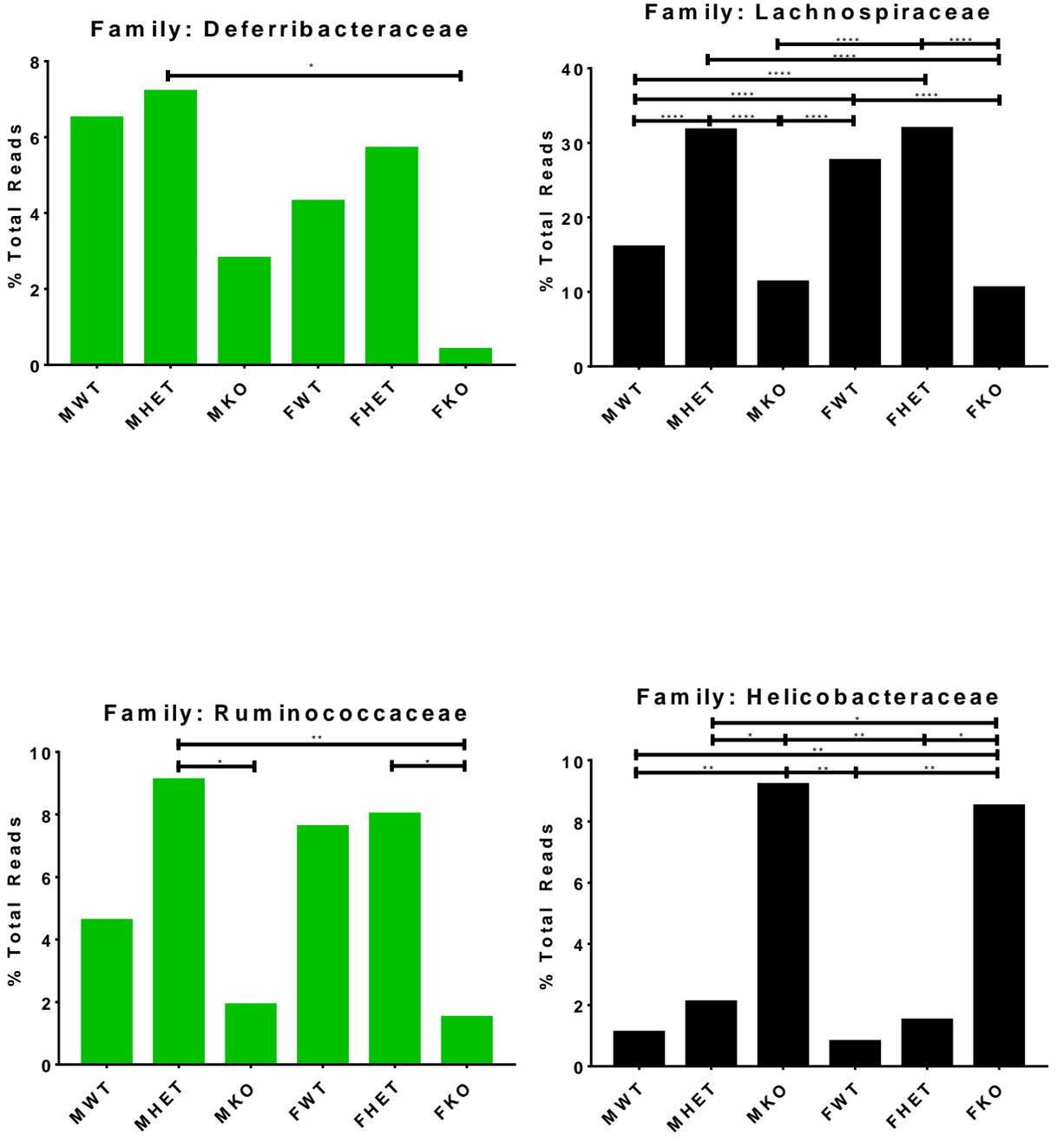
Figure A3.   Changes in abundance between individual bacterial families (continued).